Understanding the Corrosivity of the Flowback Fluid Following an Acid Job

Benjamin David Pickles

Submitted in accordance with the requirements for the degree of
Doctor of Philosophy

The University of Leeds
Institute of Functional Surfaces
School of Mechanical Engineering

August 2017

The candidate confirms that the work submitted is his/her own and that appropriate credit has been given where reference has been made to the work of others.

This copy has been supplied on the understanding that it is copyright material and that no quotation from the thesis may be published without proper acknowledgement.

The right of Benjamin David Pickles to be identified as Author of this work has been asserted by him in accordance with the Copyright, Designs and Patents Act 1988.

Acknowledgements

Abstract

Acid stimulation is a widely established technique to prolong the life of oilfield wells and generate increased levels of hydrocarbon production. High strength acids are injected into formations to facilitate the dissolution of fines in the vicinity of the wellbore and/or create channels in the reservoir itself to improve permeability. The majority of previous acidizing research has focused on the ability of chemical inhibitors to protect the downhole assets during this injection process. Very little research has studied the corrosivity of the fluid which flows back once production restarts following an acid job. After the acid has been shut in the wellbore, production restarts and there exists a period over which unreacted acid is transported through the production pipeline along with the process fluid. The concentration of acid (and any remaining inhibitor) then gradually declines over time until normal production resumes. Such a process is termed 'acid flow-back' and can be particularly detrimental to the integrity of production pipelines.

This thesis addresses the corrosion process associated with the flowback fluid following an acid stimulation procedure. By testing a range of solutions with much lower acid concentrations than the injected acid it was hoped that the corrosivity of the flowback fluid could be better characterised. However, established mass loss and short term electrochemical tests were found to be inadequate for characterising the flowback process. This research offers a new perspective on how to quantify the corrosivity of the flow-back fluid using a continuous flow cell integrated with *in-situ* electrochemistry and capable of operating at temperatures of up to 80°C. It was observed that if the acid and inhibitor concentration of the solution is diluted to between 100-1,000 times less than the injected acid/inhibitor concentration then the corrosivity of the solution is significantly higher than that of the injected acid. Two clear peaks in the corrosion rate of the steel were observed during the flowback process. The first peak was found to be controlled by a critical inhibitor concentration and the second peak was controlled by a critical solution H^+ concentration.

Unlike previous methodologies, the new test methodology is able to profile the full flowback process in a single test. This has significant cost and time saving implications for testing specific flowback profiles encountered following different acid jobs.

Table of Contents

List of Tables

List of Figures

Chapter 1 Introduction and Research Project Background

1.1 Project Background

Acid injection is one of the oldest well stimulation techniques still currently in use, with the first acid treatment estimated to have performed as early as 1895 [1]. The primary aim of an acid job is always to increase production from a well by increasing the near wellbore permeability [2, 3].

The issues associated with injecting high strength acids through the steel production tubulars should not be understated. If the expensive steel assets found downhole are not able to be sufficiently protected from the injected acids, then many acid jobs would not be performed [4]. High concentrations of highly efficient inhibitors are injected with the high strength acids. These inhibitors are specifically designed to work at very low pH and are able to reduce the corrosion rates on the steel tubulars to acceptable values. This inhibited acid is typically injected through a coiled tubing string which is run through the production tubing in order to protect it from the acid [5].

It is clear that great care and significant expense is taken to protect the expensive downhole steel assets from the injected acids. Once the acid has been injected it is shut in the well for several hours before production restarts [6]. The reacted acid is then produced through the expensive production tubing under the assumption that the flowback fluid is no longer corrosive. This assumption is based on the belief that all of the injected acid has reacted with the formation and/or any scales found around the wellbore [7].

1.2 Why Perform Acid Jobs?

The aim of any acid job is always the same; to improve hydrocarbon production from the reservoir by increasing the near wellbore permeability. If the acid job is performed correctly it can result in the hydrocarbon production increasing significantly. Figure 1.1 shows how an acid job can almost double the production from a well; expressed as barrels of oil produced per day (BPD). The injection of acids into hydrocarbon reservoirs can increase the permeability in two ways [1].

1. *Matrix Acidizing* is used to remove near wellbore damage. The acid is intended to enlarge pore spaces and dissolve scales plugging these spaces. Removal of this wellbore damage can lead to a drastic increase in permeability and hence the production rate. This is particularly useful for increasing the life of older reservoirs with increased scale problems due to an increase in the water cut [1].

2. *Acid Fracturing* involves injecting the acid at a pressure high enough to open fractures in the formation. The acid then dissolves the walls of the fracture creating etched fracture faces. When the pressure is released and the fracture closes these etched fracture faces do not seal together. This results in highly conductive flow channels remaining open after the treatment [1].
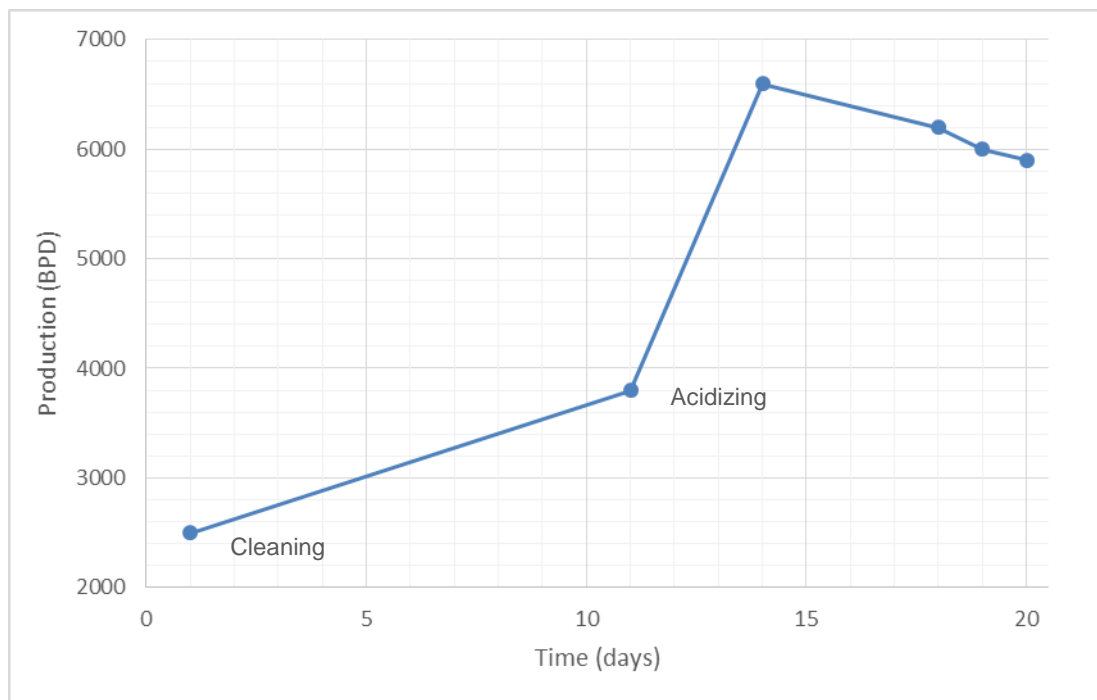
Figure 1.1 Increase in production (expressed in barrels per day) before and after performing an acid job on a well in the field. Data adapted from Valdes, et al. [6].

1.2.1 Controlling the Corrosion Rate

Both techniques have significant corrosion implications on the expensive downhole steel assets. Acidizing corrosion inhibitors are incredibly important for protecting the expensive downhole tubulars. The choice of the acid treatment itself can in some cases be governed by the most economical means of controlling the corrosion rate, as the corrosion inhibitors typically

constitute a significant portion of the total cost of an acid job [1]. A range of acids are used based on the formation and scales encountered. For example; a mixture of hydrochloric and hydrofluoric acid is typically used to stimulate sandstone formations (in order to ensure the dissolution of silicate materials) [8, 9]. The inhibitors therefore have to be chosen for each acid job and they are usually complex mixtures of organic compounds that are designed to be highly efficient in low pH solutions.

1.2.2 Corrosivity of the Flowback Fluid

The flowback fluid is complex in nature and can be difficult to characterise. The corrosivity of the fluid which flows back following an acid job is dependent on several factors (including but not limited to the pH, inhibitor concentration, CO_2 concentration and shut in time). Unfortunately, characterising the flowback fluid is made increasingly difficult by the fact that no two reservoirs produce the same flowback profile. For example, it has been shown that the pH of the flowback fluid can be between 0-3 [7, 10, 11] or that the acid can be fully neutralised prior to production restarting [12].

Despite several publications indicating the potential dangers of the flowback fluid [13-15], almost all of the previous research has focused on the corrosivity of the injected high strength acid containing high concentrations of inhibitor. Laboratory tests of these inhibitors have found them to be highly efficient in reducing the corrosion rate of the injected acid. However, once production restarts following the acid job a complex mixture of unspent acid, spent acid and formation brine with an unknown quantity of inhibitor flows back through the production tubing. Figure 1.2 shows an example of the acid concentration of the flowback fluid once the well is reopened following an acid job.

Figure 1.2 suggests that it may take as long as 21 hours for all of the injected acid to be fully produced and the production fluid return to pre-acid job acid concentrations. It is unknown how corrosive this flowback fluid may potentially be and if any inhibitors are still present in the solution. If inhibitor is still present then it is unknown if it is able to effectively inhibit the unreacted acid at the increased pH of the flowback fluid.
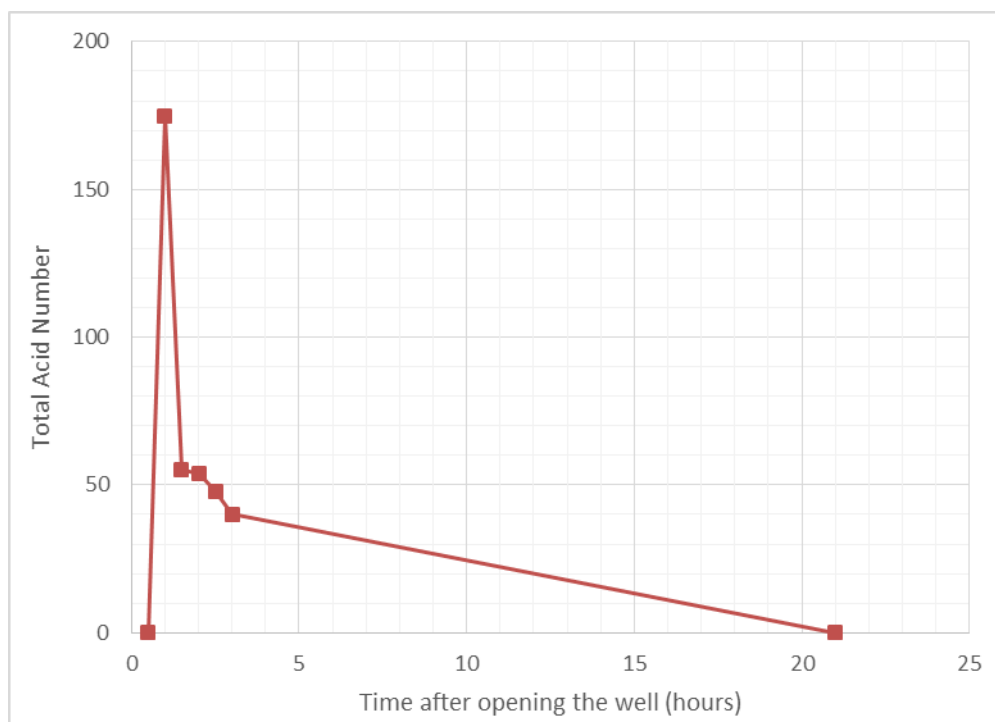
Figure 1.2 Example of the acid concentration (expressed as the total acid number) of the flowback fluid once production restarts following an acid job. Data adapted from Valdes, et al. [6].

1.3 Protecting Downhole Tubing During Acid Jobs

As mentioned previously, a large portion of the cost of an acid job can be on the inhibitors used to protect the steel tubulars [1]. In order to further protect the expensive production tubing strings a coiled tubing string is typically used to inject the acid into the formation. This price of this coiled tubing varies between jobs as the it relies upon the steel grade and the diameter and length of the tubing required [16]. Typically each string will be used for a number of jobs (based on the individual policy of each service company) before being replaced by a new coiled tubing string. This highlights how seriously the corrosivity of the injection fluid is taken and the significant costs and lengths operators go to in order to ensure that downhole assets are adequately protected.

Once the acid has been injected, production restarts and the flowback fluid is produced through the expensive production tubing. A typical assumption used in the field is that the flowback fluid does not pose a threat to the production tubing. This is due to the volume of injected acid being calculated in order to

completely react in the wellbore [1]. Therefore, based on this assumption, it is deemed acceptable to allow the flowback fluid from an acid job to be produced through the production tubing.

There has only been a minimal amount of research work aimed at understanding the corrosivity of the flowback fluid. The small amount of research performed has tended to find that the flowback fluid replicated in the laboratory poses a similar corrosion threat to the injected high strength acids [13-15]. It is therefore surprising that in much of the published literature a greater effort has not been made to characterise the flowback fluid corrosivity and any future problems which may arise by allowing it to flow back through the production tubing.

1.3.1 The Cost of Protecting the Production Tubing

A significant portion of the cost of an acid job is in protecting the production tubing [4]. This is due to the loss of production which arises from a failed production tubing string. If the production tubing fails this represents significant cost implications for the reservoir because without a viable production tubing string the well has to be closed until the compromised string can be fished from the well. A new production tubing string has to then be run at significant cost. Meanwhile, the operator has lost revenue as the well has not been producing whilst the tubing string is replaced (this can take several days).

Due to the potential cost implications arising from damage to the downhole tubulars, considerable expense is encountered when protecting the production tubing from the injected acid. If the flowback fluid following an acid job is produced through the production tubing it is important to understand how this might potentially damage the tubing string. Not taking into account the damage caused by the flowback fluid could potentially lead to significant costs to the operator if the production tubing string fails.

1.4 Objectives

The main objective of the project is to understand the corrosivity of the fluid which flows back once production restarts following an acid job. Little to no

research has been performed testing the corrosivity of solutions containing HCl concentrations much lower than the concentrations at which the HCl is injected (several orders of magnitude smaller). By significantly reducing the acid and inhibitor concentration of test solutions it was hoped that an understanding could be gained as to how the corrosivity of the flowback fluid changes once production restarts following an acid job. The intention of these tests was to understand how the flowback fluid may corrode the expensive production tubing strings used in the field. Therefore the overall objective of the work can be summarised in the following statement.

- To understand the corrosivity of the fluid which flows back following an acid job.

Initial tests were performed using pre-existing test methodologies designed to measure the corrosion rates of the injected acids. It soon became apparent that these methodologies could only provide a limited understanding of the flowback process. In order to understand the corrosivity of the flowback fluid the experimental objectives were as follows.

- To develop a new test methodology capable of more accurately modelling the flowback process following an acid job. The new test methodology should ideally model the entire flowback process in a single test.
- Validate the corrosion rates measured with the new test methodology using the corrosion rate data obtained from pre-existing closed vessel test methodologies.

Chapter 2 Fundamentals of Corrosion and Acid Corrosion

2.1 Fundamentals of Corrosion

2.1.1 Introduction

The deterioration of metals (i.e. corrosion) is a huge global problem with an estimated annual cost of US$2.5 trillion in 2013 [17]. At the time this was estimated to be as high as 3.4% of the global gross domestic product (GDP) [17]. As discussed in Section 1.3.1 a significant portion of the cost of an acid job is spent on protecting the expensive metal tubing from deterioration as a result of corrosion. Therefore it is vital to discuss the fundamental electrochemistry of aqueous corrosion and also the electrochemical techniques that can be used to monitor the rates at which metals are corroding.

2.1.2 The Principles and Thermodynamics of Aqueous Corrosion

Put simply, corrosion is the conversion of metals to a lower energy form and this change in energy of the system is the driving force for the corrosion process [18]. Whether or not a particular reaction will occur is defined by the thermodynamics of the reaction. In addition to determining whether or not corrosion can occur, it is the thermodynamics of a reaction which also predict the stable corrosion products that will form [18]. Therefore thermodynamics is at the heart of all corrosion processes.

A metal in contact with a solution will always move towards the lowest free energy state as this is the most stable state for a set of reactants. A system is only said to be at equilibrium once it reaches this state of lowest free energy. Only once it reaches equilibrium can it be said that the system is stable and there is no longer a driving force for change from that state [18]. Metals placed in aqueous solutions are rarely at equilibrium and will try to lower their energy by reacting to form products which are thermodynamically more stable [19]. Equation 2.1 shows the relationship between the free energy (ΔG) and the electrochemical potential (E) of a system. Where n represents the number of electrons in the reaction and Faraday's constant is represented by F [18].

$$\Delta G = -nFE \qquad (2.1)$$

When a system is at equilibrium the free energy change (ΔG) and the driving force (the electrochemical potential, E) are equal to zero. If the change in free energy is greater than zero (or the difference in the electrode potential is less than zero) then corrosion occurs through the removal of metal atoms from the surface and the production of metal ions in the solution [18]. This change in free energy (ΔG) at a given temperature is defined by Equation 2.2. Which relates the free energy (ΔG) to the free energy at standard conditions of 273.15K and 1atm (G^0), the universal gas constant (R, equal to 8.314 J/K/mol), the temperature (T), and the concentrations/pressures of the multiplied product or reactant series ($a_{products}$ and $a_{reactants}$) [19].

$$\Delta G = \Delta G^0 - RT \times ln\frac{a_{products}}{a_{reactants}} \qquad (2.2)$$

Using Equation 2.2, the electrochemical potential (E) can be determined under non-standard conditions through the use of the Nernst Equation (Equation 2.3) [19]. Which relates the potential difference at non-standard conditions (E) to the standard cell potential (E^0), the universal gas constant (R), the temperature (T), the number of moles of electrons transferred in the cell reaction (n), the Faraday constant (F) and the concentrations/pressures of the product or reactant series ($a_{products}$ and $a_{reactants}$) [19].

$$E = E^0 - \frac{RT}{nF}ln\frac{a_{products}}{a_{reactants}} \qquad (2.3)$$

2.1.2.1 The Butler-Volmer Equation

The Nernst equation (Equation 2.3) cannot be used to calculate the rate at which a material is corroding. In order to calculate the rate of corrosion a relationship for calculating the corrosion current (i_{corr}) is required. The Butler-Volmer equation is derived from the simultaneous cathodic and anodic reactions, each of which depends upon the surface overpotential and the concentration of reactants [20]. The net rate of reaction (r) is provided in Equation 2.4 and is equal to the difference between the rate of the forward and the backward reaction.

$$r = \frac{i_n}{nF} = k_a C_R\, e^{\left[\frac{(1-\beta)nF}{RT}V\right]} - k_c C_O e^{\left[\frac{-\beta nF}{RT}V\right]} \tag{2.4}$$

The terms in Equation 2.4 that have not been previously defined represent the rate constants of the anodic and cathodic reactions (k_a and k_c) and the concentrations of the anodic and cathodic reactants (C_R and C_O). β is a symmetry factor defined as the fraction of the activation energy barrier that is affected by the activation voltage loss [21]. The factor used in the second term (β) represents the fraction of the applied potential (V) that promotes the cathodic reaction. The fraction of the applied potential (V) that promotes the anodic reaction ($1-\beta$) is found in the first term of Equation 2.4. The symmetry factor (β) is explained through the use of a potential energy diagram showing the potential energy curve for an applied potential (Figure 2.1) [20].
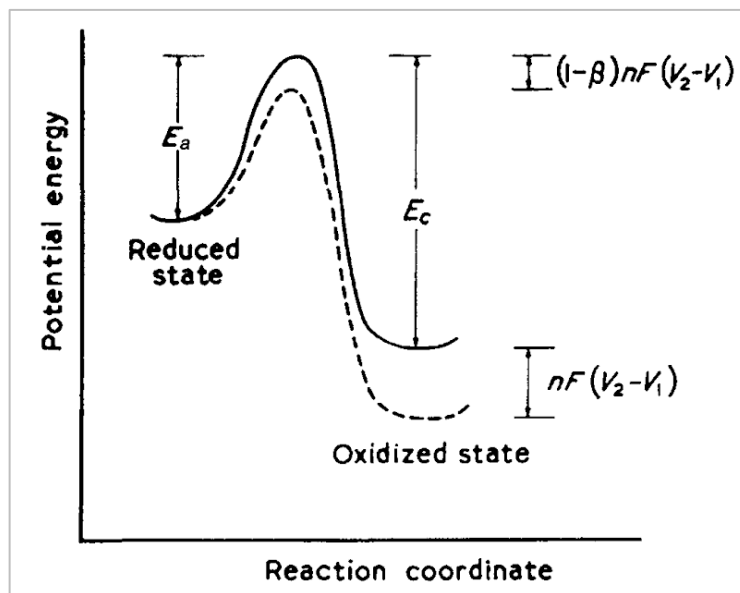
Figure 2.1 The elementary charge step shown on a potential-energy diagram. The solid curve represents the potential-energy curve for an applied voltage (V_1) and the dashed line represents the potential-energy curve for an applied voltage (V_2) where $V_2 > V_1$. The anodic and cathodic activation energies (E_a and E_c) are also shown [20].

Figure 2.1 compares the potential-energy curve for two different applied potentials (V_1 and V_2). The potential V_2 is greater than the potential V_1 and this results in the reaction being driven anodically. There is also a change of the energy of the reduced state relative to the oxidized state (shown on Figure 2.1). As a result of this change in the applied potential the activation energy increases in the cathodic direction (E_c) and decreases in the anodic direction

($\underline{E_a}$). The new cathodic (E_{c2}) and anodic (E_{a2}) activation energies are provided in Equation 2.5 and 2.6 respectively [20].

$$E_{c2} = E_{c1} + \beta nF(V_2 - V_1) \tag{2.5}$$

$$E_{a2} = E_{a1} - (1 - \beta)nF(V_2 - V_1) \tag{2.6}$$

Equation 2.5 and 2.6 can now be used to replace the exponential terms in Equation 2.4. The net rate of reaction is equal to zero when the rate of the forward reaction equals the rate of the backward reaction allowing Equation 2.4 to be rewritten as Equation 2.7. U is the value of the potential difference at which the net rate of reaction is zero [20].

$$k_a C_R e^{\left[\frac{(1-\beta)nFU}{RT}\right]} = k_c C_O e^{\left[\frac{-\beta nFU}{RT}\right]} \tag{2.7}$$

Equation 2.7 can then be rearranged to give Equation 2.8 which is a form of the Nernst equation (Equation 2.3) [20].

$$U = \frac{RT}{nF} \ln \frac{k_c C_O}{k_a C_R} \tag{2.8}$$

At the equilibrium potential, the surface overpotential (η_s) is given by Equation 2.9 [20].

$$\eta_s = V - U \tag{2.9}$$

Equation 2.8 and 2.9 can then be substituted into Equation 2.4 to produce Equation 2.10.

$$\frac{i_n}{nF} = k_a C_R e^{\left[\frac{(1-\beta)nF}{RT}\eta_s + (1-\beta)\ln\frac{k_c C_O}{k_a C_R}\right]} - k_c C_O e^{\left[\frac{-\beta nF}{RT}\eta_s - \beta\ln\frac{k_c C_O}{k_a C_R}\right]} \tag{2.10}$$

Equation 2.10 can be further simplified using Equation 2.9 and the definition of the exchange current density (i_0) defined in Equation 2.11. This simplified equation is shown in Equation 2.12 [20].

$$i_0 = nF k_a^{\beta} k_c^{1-\beta} C_R^{\beta} C_O^{1-\beta} \tag{2.11}$$

$$i_n = i_0 \left[e^{\left[\frac{(1-\beta)nF}{RT} \eta_s \right]} - e^{\left[-\frac{\beta nF}{RT} \eta_s \right]} \right] \tag{2.12}$$

Equation 2.12 is known as the Butler-Volmer equation. This can be written in the form shown in Equation 2.13 which provides a relationship between the corrosion potential and the applied current density (it should be noted that this is the case for a corroding electrode in the absence of parallel reduction-oxidation reactions). The relationship shown in Equation 2.13 is dependent upon the presence of both a single charge transfer controlled anodic and cathodic reaction [22-24].

$$i = i_{corr} \times e^{\left(\frac{\alpha nF\eta}{RT} \right)} - e^{\left(\frac{-(1-\alpha)nF\eta}{RT} \right)} \tag{2.13}$$

Equation 2.13 relates the external current density as a result of an applied potential (i) to the corrosion current density (i_{corr}) when the electrode is at open circuit potential (OCP). The additional term α is a coefficient with a value between 0-1 [23]. Equation 2.9 can be used to rewrite Equation 2.13 without the test electrode overpotential term (η). Equation 2.14 presents an experimentally observed relationship between the applied current (i) and the potential for a corroding electrode (E_{corr}) in relation to the anodic and cathodic Tafel constants (β_a and β_c) [22].

$$i = i_{corr} \times e^{\left(\frac{2.3(E-E_{corr})}{\beta_a} \right)} - e^{\left(\frac{2.3(E-E_{corr})}{\beta_c} \right)} \tag{2.14}$$

The Tafel constants are provided by the slopes of polarisation curves in the anodic and cathodic Tafel regimes (shown in Figure 2.3). Equation 2.15 shows

how the anodic and cathodic Tafel values are calculated using the polarization curves [22].

$$\beta_a, \beta_c = \frac{\partial E}{\partial \log i} \qquad (2.15)$$

This relationship forms the basis of using the polarisation resistance (R_p) to calculate the corrosion rate [22]. This is discussed in greater detail in Section 2.2.2.

2.1.3 Electrochemical Corrosion Reactions

Equation 2.16 shows the anodic reaction which occurs when metal atoms are oxidised and leave the metal lattice (*M*) as ions [19, 23].

$$M \rightarrow M^+ + e^- \qquad (2.16)$$

The produced electrons (e^-) shown in Equation 2.16 create an excess of electrons at the metal surface. These produced electrons are then transferred to electrochemically active species which are dissolved in the electrolyte. The reduction of these electrochemically active species (found in the electrolyte) is referred to as the cathodic reaction. In order for metallic corrosion to be sustained, both the anodic and cathodic reactions must be present. This is illustrated by the anodic and cathodic half reactions for the corrosion of iron (*Fe*) shown in Equation 2.17 and 2.18 respectively [23].

$$Fe \rightarrow Fe^{2+} + 2e^- \qquad (2.17)$$

$$2H^+ + 2e^- \rightarrow H_2 \qquad (2.18)$$

Equation 2.17 illustrates that an iron atom (*Fe*) at the metal surface produces 2 free electrons (e^-) and an iron ion (Fe^{2+}). The produced electrons (e^-) are then consumed in the cathodic half reaction (Equation 2.18) through the reduction of hydrogen ions (H^+) to hydrogen (H_2). The overall corrosion

reaction is shown in Equation 2.19 and is the summation of both half reactions (Equation 2.17 and 2.18) [23].

$$Fe + 2H^+ \rightarrow Fe^{2+} + H_2 \qquad\qquad (2.19)$$

2.2 Measuring the Corrosion Rate

Several electrochemical methods can be used to measure the rate at which a metal is corroding in an electrolyte. The direct current (DC) techniques used in this work; Linear Polarisation Resistance (LPR) and Tafel polarisation are discussed in turn. Even when a metal is corroding, and therefore has a corrosion current (i_{corr}), no measurable external current will flow. Only through the application of an external potential to a test electrode can the electrical current response be measured [23]. The applied potential and the corresponding current can then be used to determine the magnitude of a corrosion current (i_{corr}) which can then in turn be used to calculate a corrosion rate.

2.2.1 The 3 Electrode Cell

A typical electrochemical test cell is shown in Figure 2.2. The cell consists of a working, counter and reference electrode connected to a potentiostat. The aim of the cell is to find the rate at which the working electrode is corroding. The reference electrode provides a fixed reference point for corrosion measurements and should be made from a material with a known and stable open circuit potential (OCP) [23].

The potentiostat is able to polarise the working electrode away from its OCP to a potential value determined by the potentiostat. The counter electrode maintains electrode electrical neutrality by concurrently withdrawing electrical current (which is supplied by the potentiostat) to the counter electrode (and vice-versa) [23].

A variety of corrosion behaviours can be determined from the relationship between the applied potential and the measured current response. This includes determining whether or not a metal will passivate, if pitting corrosion

will occur or if a coating will provide corrosion protection [23]. The application of the three electrode cell and the electrochemical fundamentals discussed in Section 2.1.2 are used to calculate the rate at which the working electrode is corroding.
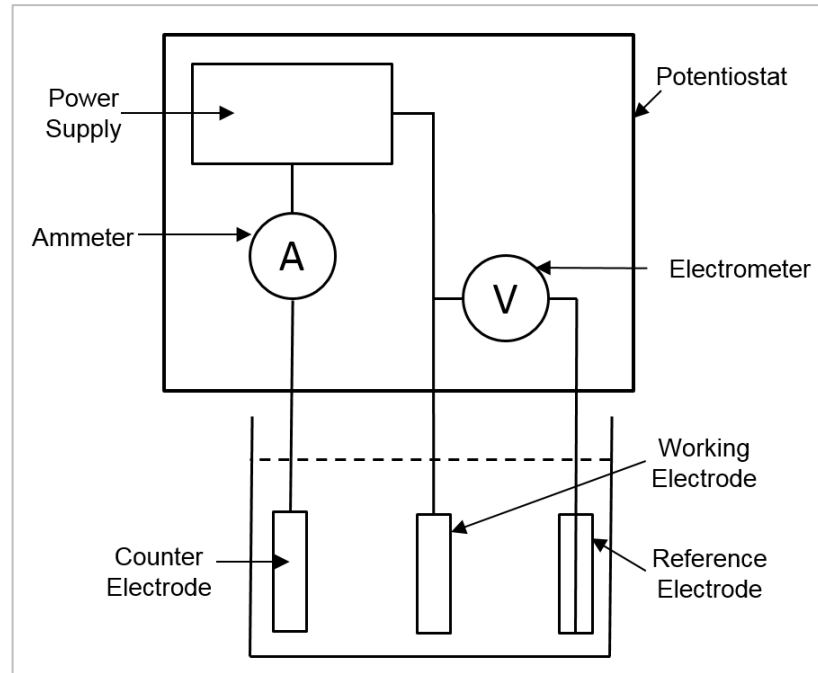
Figure 2.2 The 3 electrode cell consisting of a working, reference and counter electrode connected to a potentiostat [23].

2.2.2 Linear Polarisation Resistance

Through the application of a small potential (typically between ±10mV and ±20mV from E_{corr}) a linear relationship is observed between the applied voltage and the measured current response (as shown in Figure 2.3).

The gradient of this linear line at small applied potentials gives the polarisation resistance (R_p). Stern and Geary simplified Equation 2.13 for the application of these small overpotentials [25]. The Maclaurin series expansion is shown in Equation 2.20 [26].

$$e^x = 1 + x + \frac{x^2}{2!} + \frac{x^3}{3!} \text{....}$$

(2.20)
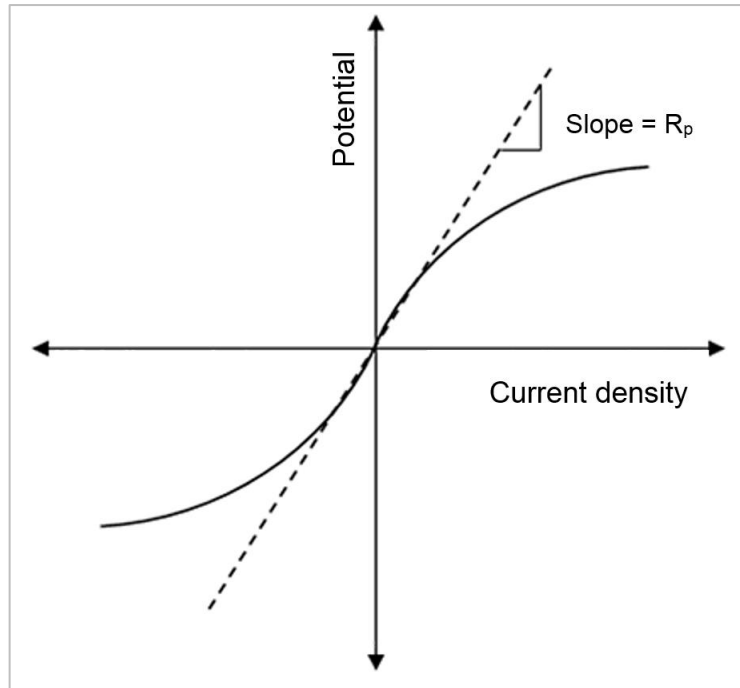
Figure 2.3 An example of the region over which the relationship between the applied potential and measured current response is linear [27].

By applying this series expansion to Equation 2.14 (and by neglecting the higher terms) the relationship can be simplified to Equation 2.21. Whereby the polarisation resistance (R_p) is the gradient of the linear polarisation plot over small applied potentials (as can be seen in Figure 2.3) [22].

$$R_p = \frac{\Delta E}{\Delta I} = \frac{1}{2.303 i_{corr}} \times \frac{\beta_a \beta_c}{\beta_a + \beta_c} \qquad (2.21)$$

Equation 2.21 can then be rearranged to give an expression which allows the corrosion current (i_{corr}) to be calculated (Equation 2.22). The corrosion current (i_{corr}) found using Equation 2.22 can then be used to calculate the corrosion rate (using Equation 2.23).

$$i_{corr} = \frac{1}{2.303 R_P} \times \frac{\beta_a \beta_c}{\beta_a + \beta_c} \qquad (2.22)$$

As the sample is only polarised between 5-20mV of the corrosion potential (E_{corr}) the technique is non-destructive and allows several corrosion rate measurements to be taken over the duration of a test on a single sample.

However, it is important to note that in order to calculate accurate corrosion rates the Tafel constants (β_a and β_c) must be known.

2.2.3 Tafel Plots

Tafel plots are generated by polarising the sample both anodically and cathodically by as much as 1V (as recommended by ASTM standard G5 [28]). The measured current response is then plotted on a logarithmic scale, an example of which is shown in Figure 2.4.
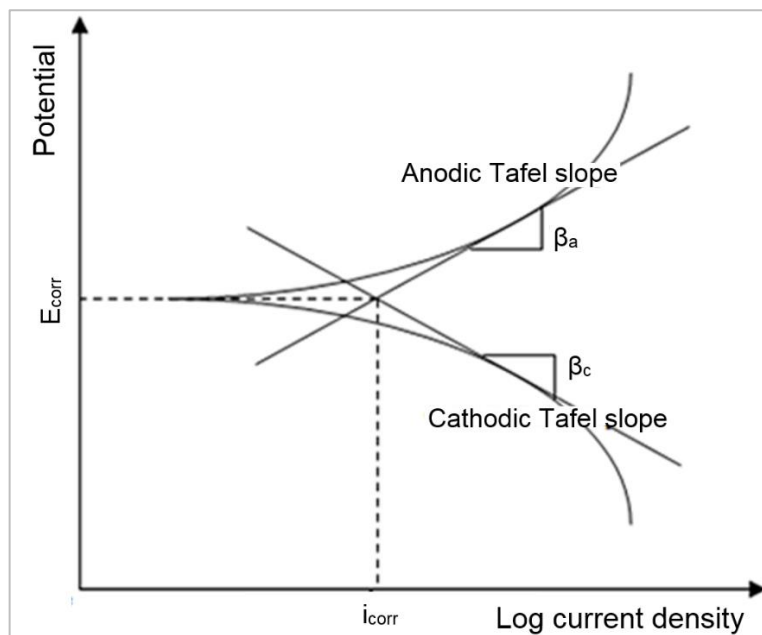
Figure 2.4 An example Tafel plot showing how the corrosion current (i_{corr}) and the anodic and cathodic Tafel slopes can be determined [27].

The main limitation of using Tafel plots to measure the corrosion rate is that the technique is destructive to the working electrode, due to the large applied potentials. If several corrosion rate measurements are required on a single sample then finding the polarisation resistance (R_p) by applying much smaller potentials is a more suitable technique for observing how the corrosion rate varies overtime (as outlined in Section 2.1.4.2).

Tafel slopes can be drawn onto the linear parts of each polarisation plot shown in Figure 2.4. The anodic and cathodic Tafel constants (β_a and β_c) can then be used to calculate the corrosion current (i_{corr}) using the polarisation resistance (R_p) as shown in Equation 2.22. Alternatively, the corrosion current,

i_{corr}, is the intersection of the anodic and cathodic extrapolations at OCP (as illustrated in Figure 2.4). The corrosion current (i_{corr}) can then be used to calculate the corrosion rate using Equation 2.23. Where K is a constant representing several terms, EW is the equivalent weight of the metal and ρ is the metal density [23].

$$Corrosion\ Rate = \frac{i_{corr} \times K \times EW}{\rho} \tag{2.23}$$

2.2.4 Extrapolating the Tafel Slopes

When a large enough potential is applied to move the sample away from the corrosion potential, the applied current density reflects the kinetics of either the anodic or cathodic reaction (depending upon the applied potential). Extrapolation of the linear portion of the polarisation curve (as illustrated in Figure 2.4) provides important information which can be used to calculate the rate at which the sample is corroding [29].

- The gradient of the linear extrapolation of the anodic and cathodic polarisation plots provide the anodic (β_a) and cathodic (β_c) Tafel constants.
- The intersection of the two linear extrapolations provides the corrosion current (i_{corr}), which can be used to calculate the corrosion rate using Equation 2.23.

It is important to note that non-linear polarisation curves (when plotted on a graph of log current vs. potential) are not true Tafel slopes. Therefore Tafel slopes should only been drawn on linear regions of polarisation curves and should not be drawn at a tangent to a non-linear curve [30].

2.2.4.1 Limitations of Tafel Slopes

In order for the Tafel extrapolation method to be a valid for determining the corrosion rate the following must be true [31].

1. The anodic or cathodic Tafel region must be well defined and at least one of the polarisation curves must be under activation control. It is preferable for both the anodic and cathodic branches of the polarisation curves to be under activation control [31].

2. There must be no significant localised corrosion. The corrosion must be general and without any preferential attack of the metal along grain boundaries. Individual metal grains can become dislodged from the metal surface. The metal loss from this effect is not taken into account by the Tafel method, leading to an underestimation of the corrosion rate [32, 33].

3. The potential applied when obtaining the Tafel slopes must not result in any additional anodic or cathodic reactions. This means that the anodic and cathodic reactions that occur during the polarisation must be the same reactions that occur at the corrosion potential [31].

In order to limit the analysis issues, the polarisation curve should be linear over at least one decade of current density and the extrapolation of the Tafel slope should start 50-100mV away from the corrosion potential [29]. Both rules should be used in order to improve the accuracy of the manual Tafel slope extrapolations. Interpreting the polarisation data is not always straight forward and due to the manual extrapolation of the Tafel slopes there is always some ambiguity in where the slopes should be drawn on the polarisation curves. An additional issue rises from the fact that the system must be steady state, i.e. corroding at a rate which does not change with time. However, a universal rule for when a system has reached steady state does not exist and indeed in many systems may never be truly achieved (merely approached) [29].

The most widely used method for determining when a system has reached steady state is through the monitoring of the corrosion potential (E_{corr}) over time and establishing that it has not changed over a given potential range for a given period of time. Kelly, et al. [29] recommend a change of less than 5mV in E_{corr} over a time period of 10 minutes as a suitable criteria for the system reaching steady state. Due to the issues outlined in this section corrosion rates calculated using Tafel extrapolation should always be compared to values found from mass loss tests if possible [29].

2.2.5 Polarisation Behaviour

The hypothetical Tafel plot displayed in Figure 2.4 will be observed provided the corrosion is activation controlled. If the corrosion rate is activation controlled then the conditions are typically far removed from the reversible potentials for any of the reactions and therefore the kinetics exhibited in Figure

2.4 suggest that mass transport limitations are not significant [24]. In contrast Figure 2.5 illustrates the effect of different reaction kinetics on the cathodic Tafel polarisation [24]. When the cathodic reactant is limited then the mass transport is of primary importance and the maximum corrosion rate is a function of the limiting current density (i_{lim}) of the cathodic reactant as shown in Equation 2.24 [24].

$$i_{corr} = i_{lim} \tag{2.24}$$
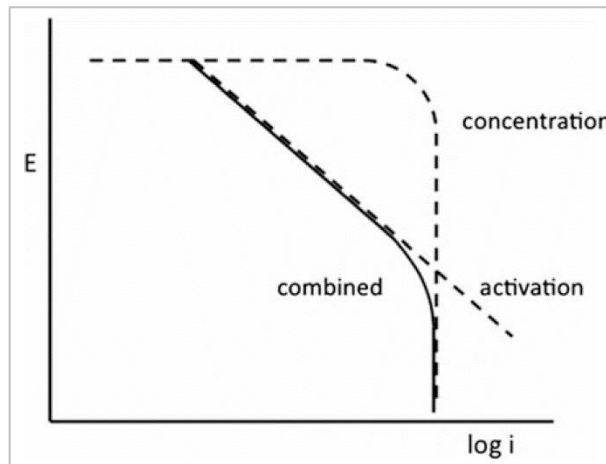
Figure 2.5 Comparison between cathodic polarisation behaviour when the reaction kinetics are either concentration controlled, activation controlled or a combination of the two [24].

This is of particular importance to the results presented in this thesis as the rate of the mass transport of protons to an iron surface limits the rate of corrosion in dilute hydrochloric acid solutions [24]. The Tafel extrapolation of cathodic polarisation data can be difficult under these conditions as the Tafel region may not be extensive [34]. As the gradient of the cathodic Tafel slope tends towards values significantly larger than the anodic Tafel slope (as shown by the concentration controlled Tafel extrapolation on Figure 2.5), Equation 2.22 can be simplified to give Equation 2.25 [35, 36].

$$i_{corr} = \frac{\beta_a}{2.303R_P} \tag{2.25}$$

Equation 2.25 can then be used to calculate the corrosion current (i_{corr}) when the cathodic Tafel constant cannot be reliably calculated as the reaction is diffusion controlled. The calculated corrosion current can then be used to calculate the corrosion rate of the sample (Equation 2.23). It should be noted that the use of both the anodic and cathodic regions is preferred, however the corrosion rate can be determined through the use of a single polarisation curve.

2.3 Acid Corrosion

2.3.1 Introduction

As discussed in Section 1.2 high molarity acid is injected into hydrocarbon reservoirs with the intention being to increase near wellbore permeability by dissolving built up scales and/or the formation itself [1]. The acid is injected through carbon steel coiled tubing strings; it then reacts in the wellbore, before it is produced through the production tubing. Therefore there are three acid reactions which take place over the duration of the acid job.

1. The corrosion caused by the high strength acid (containing high concentrations of inhibitor) on the steel coiled tubing string.
2. The reaction between the acid and the wellbore scales or the formation itself. The most typical reaction encountered in the field is between hydrochloric acid and calcium carbonate.
3. The corrosion caused by the diluted acid which flows back following the acid job (containing little to no inhibitor [14]) on the production tubing.

The reaction between the acid once it has been injected (with wellbore scales or the carbonate formation) will be discussed briefly. The reaction between the acid and the steel tubulars is then discussed with a focus upon the potential metal loss from both the coiled tubing string (during injection) and the production tubing (during flowback).

2.3.2 Acid Carbonate Reactions

As discussed in Section 1.2, there are two reasons why acid is injected into a reservoir. In sandstone formations, acid is typically injected to remove scales which are reducing the near wellbore permeability. In carbonate reservoirs, where the acid is able to react with the reservoir rock, acid is injected at

overpressure to open fractures in the formation. The acid then etches flow channels into these fractures, these etched channels increase the permeability as they leave flow channels through the formation once the fractures are closed [1]. In the field there are many different types of acid job performed in a wide range of different formations and a wide variety of acids are used to dissolve an even wider range of minerals found in each individual reservoir [4].

A commonly performed acid job is the injection of high strength hydrochloric acid to remove calcium carbonate scale from around the wellbore [1]. This procedure is commonplace in older production wells which have seen drastically increased water cut. However newly drilled wells can also show significant drop off in production after producing for relatively short times, as shown in Figure 2.6 [6]. One of the main issues associated with producing more formation fluids (or injection fluids) is that they can lead to a significant decrease in production from a reservoir. Formation water often causes scaling problems around the wellbore due to the high mineral content of the fluid. This scale drastically reduces the near wellbore permeability which leads to significantly decreased production [37].
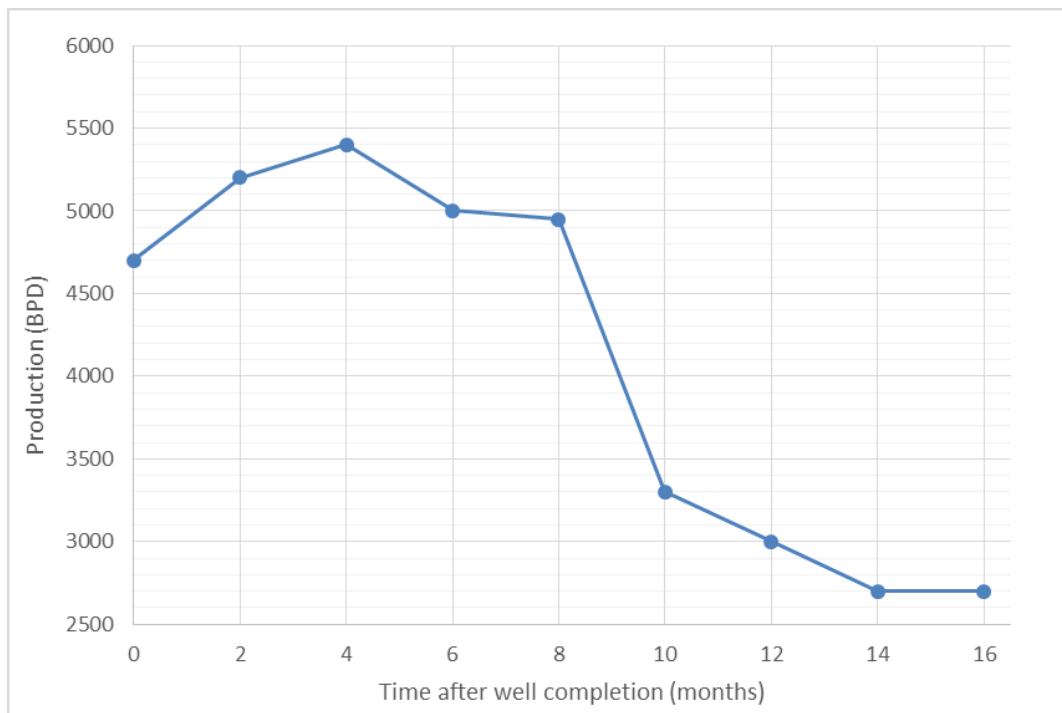
Figure 2.6 Production from an oil well over the first 16 months after well completion. Data adapted from Valdes, et al. [6].

As the aim of the project is to understand the corrosion implications of the flowback fluid, understanding all possible acid/mineral reactions that could take place in a reservoir is beyond the scope of this project. However, it is important to consider the primary chemical reaction associated with the most commonly performed acid job; the removal of calcium carbonate using hydrochloric acid, and how this reaction effects the composition of the flowback fluid. The reaction between hydrochloric acid (*HCl*) and calcium carbonate (*CaCO₃*) is shown in Equation 2.26 [1].

$$2HCl + CaCO_3 \rightleftarrows H_2O + CO_2 + CaCl_2 \qquad (2.26)$$
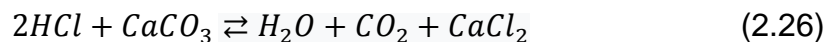
This reaction states that 2 molecules of hydrochloric acid react with a single molecule of calcium carbonate to produce a molecule of water (*H₂O*), carbon dioxide (*CO₂*) and calcium chloride (*CaCl₂*). When planning an acid job it is vital to understand the reaction kinetics and the time required for the acid to react with the calcium carbonate in order to ensure the acid job is successful [1]. However, in terms of flowback following an acid job, fully discussing all of the reaction kinetics is again beyond the scope of this project.

Equation 2.26 is important for understanding the flowback fluid as it shows that the amount of water, carbon dioxide and calcium chloride is directly related to the amount of HCl that has reacted in the wellbore. The acid concentration of the flowback fluid measured in the field (Figure 1.2) shows that the acid concentration of the solution decreases over time once production restarts [6]. This suggests that initially partially unreacted acid flows back and the acid concentration decreases over time as more spent acid and formation fluids are produced.

Therefore, Equation 2.26 suggests that the carbon dioxide (*CO₂*) and calcium chloride (*CaCl₂*) concentration of the solution will increase over time once production restarts and more reacted acid is produced. This is important when considering the solution chemistry of the flowback fluid as the amount of carbon dioxide and calcium chloride in the flowback is directly related to the amount of reacted HCl. This further highlights the complex chemistry of the fluid which is produced once production restarts following an acid job.

2.3.3 Acid Steel Reactions

As mentioned previously, a large range of different acids are used to stimulate oil and gas wells. The acids are chosen based on the scale and formation type and the quantity of acid pumped will vary between each job performed. It is beyond the scope of this work to discuss all of the possible acid concentrations and acid mixtures used in the field. Therefore, once again the commonly performed acidizing job involving the injection of hydrochloric acid to remove calcium carbonate scales is considered.

In order to fully understand the inhibition of hydrochloric acid it is first vital to understand the reaction between the acid and the carbon steel tubulars. When iron is placed in high strength hydrochloric acid a rapid reaction occurs where the iron is attacked and hydrogen gas is evolved, meaning that hydrochloric acid is very corrosive to most of the metals and alloys found in the field [38]. Figure 2.7 shows the electrolytic cells set up on the metal surface due to acid corrosion. At the anodic sites metallic iron goes into the solution (Equation 2.17) whilst at the cathodic sites electrons are consumed (Equation 2.18). These electrons reduce hydrogen ions to molecular hydrogen and then gaseous hydrogen (H_2) [1].
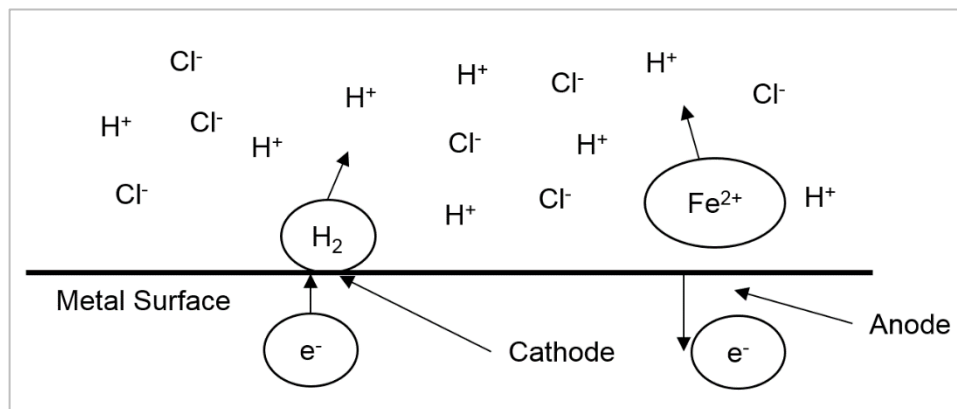
Figure 2.7 The electrolytic cells created on the metal surface as a result of acid corrosion [1].

This rapid evolution of hydrogen is described in Equation 2.17 and 2.18 [39]. If the acid contains dissolved oxygen (no effort is made to remove oxygen from the acid injected in the field) then the anodic reaction remains the same (Equation 2.17) and the cathodic reaction is shown by Equation 2.27. The overall reaction due to dissolved oxygen is shown in Equation 2.28 [19].

$$O_2 + 4H^+ + 4e^- \rightarrow 2H_2O \qquad (2.27)$$

$$2Fe + O_2 + 4H^+ \rightarrow 2Fe^{2+} + 2H_2O \qquad (2.28)$$
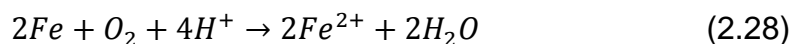
It has been found that the corrosion of metals by acids is increased by the presence of dissolved oxygen. However at high acid concentrations the effect of oxygen is not significant because the oxidizing action is dominated by the corrosivity of the acid itself [39].

2.4 Inhibiting the Corrosion of Steel

In order for an inhibitor to effectively reduce the corrosion rate of steels in acid solutions it must reduce the reaction rate at either the anode, the cathode or both. The degree to which the electrochemically active sites are blocked by the inhibitor dictates its ability to decrease the corrosion rate [40].

2.4.1 Inhibiting the Cathodic or Anodic Reaction

It is important to understand how inhibitors are able to reduce the corrosion rate through inhibiting either the anodic and/or cathodic reactions. It is common for mixtures of inhibitors to be used in commercially available formulations. It is important to note that an extensive list of compounds are used to inhibit corrosion rates of metals. The selection of a particular inhibitor for a particular environment depends on several factors including the pH, temperature and type of alloy used [41].

Inhibitor mechanisms are complex and it is not possible to predict a chemical compounds overall performance despite certain principles being common to many inhibitor compounds. Despite this complexity, inhibitors can be broadly classified as either anodic, cathodic or mixed type inhibitors [41].

2.4.1.1 Anodic Inhibitors

Anodic inhibitors usually form protective films on a metal surface that limit the anodic reaction [42]. The addition of anodic inhibitors can affect the anodic

reaction in two potential ways; they can either lower the rate or influence the reaction mechanism of the anodic reaction [43].

In the anodic reaction (Equation 2.17) iron is oxidised and forms ferrous ions in the anodic reaction. These ferrous ions are soluble in acid solutions. Anodic inhibitors share electrons from the inhibitor molecule with the anodic sites on the metal surface. The anodic reaction is therefore prevented due to the established bond between the inhibitor and the metal surface [4]. Anodic inhibitors therefore shift the corrosion potential (E_{corr}) in the anodic direction (known as ennobling) [43, 44]. It is important to note that anodic inhibitors can lead to intense local attack if they are not present in sufficient quantities. This results in the formation of small anodic areas on the metal surface [42].

2.4.1.2 Cathodic Inhibitors

As with anodic inhibitors, cathodic inhibitors can affect the cathodic reaction by either lowering the rate of reaction or influencing the reaction mechanism [43]. In general cathodic inhibitors tend to form a visible film on the metal and are not considered to be as effective as anodic inhibitors [41, 42]. However unlike anodic inhibitors, an insufficient concentration of cathodic inhibitor does not lead to pitting corrosion. The reduced inhibitor concentration simply leads to a decrease in corrosion rate over the entire metal surface [41].

At the cathode, hydrogen ions are reduced to hydrogen atoms (Equation 2.18). These hydrogen atoms then combine to form hydrogen (H_2) which desorbs from the metal surface as a gas. Cathodic inhibitors attach to the cathodic area of the metal surface through electrostatic attraction. This forms a protective film that inhibits the corrosion rate by preventing ions diffusing to or from the iron surface [4, 40]. It is important to note that it is possible for a number of materials to be reduced at the cathodic sites and that hydrogen evolution is not the only possible cathodic reaction (known as a depolarized cathode reaction). The most common depolarizer is dissolved oxygen (heavy metal ions and organic molecules can also act as depolarizers), however the principles of inhibition do not change [43]. Cathodic inhibitors are able to create a negative shift in potential, producing a new corrosion potential (E_{corr}). Therefore a new corrosion current (i_{corr}) is produced which is lower than the previous value (the relationship between E_{corr} and i_{corr} is discussed in greater detail in Section 2.1.2) [43].

2.4.2 Mechanistic Explanation of Acidizing Inhibitors

It is important to consider the mechanisms of the inhibitors commonly used in acidizing jobs. Organic film forming inhibitors are discussed, with a particular emphasis on the inhibition mechanisms of the inhibitor used in this work; propargyl alcohol (PA). The organic corrosion inhibitors used in reducing acidizing corrosion are able to form protective films on the surface of the steel. In general this is due to the inhibitor possessing three criteria; conjugated double or triple bonds and aromatic rings, electronegative atoms and a high degree of planarity [45]. Once the inhibitor has been adsorbed onto the metal surface it is able to affect the corrosion reaction in several ways [46].

1. The inhibitor makes a physical barrier preventing the diffusion of corrosion products to and from the steel surface.
2. The inhibitor can also directly block the anodic or cathodic sites (discussed in greater detail in Section 2.4.1).
3. It may interact with the intermediate to the corrosion reaction which has adsorbed onto the surface.
4. The inhibitor may change the electrical double layer which develops at the interface between the solution and the metal. This can in turn lead to a change in the rate of the corrosion reaction.

2.4.3 Inhibitor Effectiveness

The ability of the inhibitor to adsorb onto the steel surface determines the effectiveness of the inhibitor. This is true for both cathodic and anodic type inhibitors. Typically increasing the concentration of inhibitor has little effect on reducing the corrosion rate of the acid. This is provided that a minimum amount of inhibitor is present to form an adsorbed monolayer [4]. Inhibitor effectiveness can be controlled by many factors (discussed in greater detail in Section 3.2) but temperature is the most important limiting factor. Increasing the temperature increases the rate of the acid corrosion reaction and can also reduce the ability of some inhibitors to adsorb onto the steel surface [4].

Chapter 3 Literature Review

3.1 Introduction

Acid injection is a long established technique for increasing production from hydrocarbon reservoirs [1], and as would be expected the literature is extensive regarding how to optimise acid jobs [1, 8, 47-63] and protect the downhole steel assets from the high strength injected acids [5, 15, 46, 64-86].

Understandably the main focus of the previous research tends to be the study of the efficiency of various newly developed inhibitor compounds added to high concentration acids (designed to replicate acid injection). However the focus of this work is directed towards the corrosion implications of the flowback fluid once production restarts following an acid job. Unfortunately there has been very little focus on the inhibitor efficiency at concentrations less than the values used during acid injection or in solutions with a pH greater than 0 (representative of the flowback fluid). Therefore the aim of the literature review will be to understand the flowback fluid composition and focus on the studies which have attempted to replicate the flowback process in the laboratory. The test methodologies used to test the corrosivity of injected acids are discussed in order to further understand how best to test the corrosivity of the flowback fluid.

The established technique for testing inhibitor efficiencies is to place a mass loss coupon, cut from tubing grade steel, in injection strength acid (containing a known quantity of inhibitor) [13, 68, 71, 78, 85, 87-101]. The inhibitor efficiency is then typically found by comparing the mass loss from the coupon both with and without inhibitor present [71, 78, 87-90, 92-99]. The other commonly used technique for measuring the corrosion rate is through the use of electrochemistry. Typically a small sample is cut from the tubing and encased in a holder or resin/plastic before being placed in the inhibited acid. A potentiostat and 3 electrode-cell is then used to perform a variety of electrochemical measurements on the sample [64, 74, 78, 87-89, 91-93, 99-103]. The literature review aims to look at previously used experimental techniques with the outcome being to attempt to use or modify these previous methodologies to more accurately replicate what is seen in the field once production resumes following an acid job.

3.2 Acid Reaction Rates and Inhibition

In the field there are several parameters which can affect the rate of reaction of the acid and as a result its corrosivity. All acids used for well stimulation require a corrosion inhibitor in order to help to minimise the corrosion damage caused to the steel assets found downhole [1]. The injected acids can also lead to both hydrogen and chloride stress cracking [45]. This section will focus primarily on film forming corrosion inhibitors (in particular propargyl alcohol) and the studies which have focused on the ability of propargyl alcohol (PA) to reduce the corrosion rate and also techniques used to measure the protective inhibitor film.

3.2.1 Parameters Influencing the Acid Steel Reaction

Several factors can influence the rate of the acid steel reaction described in the previous section. The degree to which each parameter affects the rate of reaction varies between parameters and the significance of each parameter can vary depending on whether the injected acid or the flowback fluid is being considered.

3.2.1.1 Acid Type and Concentration

Injected acids can typically be characterised as either mineral acids, dilute organic acids, powdered organic acids, hybrid acid systems or retarded acid systems [1]. Hydrochloric acid is used almost exclusively in carbonaceous formations whilst a hydrochloric-hydrofluoric (HCl-HF) acid mixture is used almost entirely for stimulating sandstone formations. Organic acids, due to their lower corrosivity, are used primarily in jobs which require long contact times between the acid and the tubulars. Powdered acids and acid mixtures have limited uses and are typically only used when the common acid systems are not suitable [1]. Each acid will be injected at different concentrations depending on the nature of each individual acid job. For example, HCl can be injected at strengths between 5-15%. Whilst HCl-HF mixtures can vary between 12% HCl with 3% HF and 9% HCl with 6% HF [1].

Due to the large range of acid types, mixtures and concentrations used in the field, the corrosivity of each acid job should be considered individually based on the acid type and molarity. The acid concentration of the flowback fluid compared to the injected acid can also vary between each individual acid job.

This is due to the amount of acid that reacts with the formation varying between each acid job (as discussed in Section 3.6).

3.2.1.2 Oxygen

When injecting acids into oil and gas reservoirs no effort is made to remove oxygen from the injected acid solution [85]. Once in the wellbore the oxygen present in the injected acid will be drastically reduced and the amount of carbon dioxide in contact with the solution will drastically increase [14]. The reservoir will contain carbon dioxide and there is also a large amount produced from the reaction between the acid and the carbonates in the formation (as discussed in Section 2.3.2).

Whitman and Russel [39] found that when steel is placed in contact with acid solutions the presence of oxygen can play an important role in the rate of corrosion. However this trend was only seen at temperatures less than 50°C, at higher temperatures the oxygen is less important due to the lower oxygen solubility at higher temperatures. The more rapid increase in corrosion with hydrogen gas evolution also makes the presence of oxygen much less significant [39]. The downhole temperatures in the wellbore are considerably higher than 50°C, therefore the effect of oxygen can be said to be minimal when compared to the corrosivity of the hydrochloric acid solution.

3.2.1.3 Aqueous Salts

Once production restarts following an acid job the flowback fluid will consist of a mixture of acid and formation fluids (hydrocarbons and formation waters). The salinity as well as the relative concentrations of the dissolved species can vary between formation waters [104], several examples of which are shown in Table 3.1. However the major cation in oilfield brines is sodium (Na^+) and the major anion is chloride (Cl^-) (as can be seen from the fluid compositions in Table 3.1). Other dissolved solids (e.g. calcium, magnesium, bromide and potassium) may or may not be present and the concentration can vary significantly between each oilfield [4, 105]. Harned and Brumbaugh [106] found that the activity of HCl is influenced by the presence and concentration of aqueous salts. Therefore it is important to understand how the increased aqueous salt concentration of the flowback fluid effects the activity of the HCl in the flowback fluid.

Fluid Component (mg/L)	Seawater	Miller (North Sea)	Mahakam Basin (Indonesia)	Offshore Louisiana (Gulf of Mexico)
Na	10,760	28,800	2,329	29,600
Cl	19,350	47,680	2,817	48,250
K	399	1,820	43	144
Mg	1,290	115	86	620
Ca	411	1,060	132	2,080
Sr	8	110	-	49
Ba	0.021	1,030	-	33
Fe	0.034	10	-	8.6
SO_4	2,700	7	190	21
HCO_3	142	2,070	2,935	226

Table 3.1 Example formation water compositions from a range of sedimentary basins around the world [104, 107, 108]. The composition of seawater is provided for comparison [109].

Several authors [110-112] have shown that the pH of HCl is lowered through the addition of NaCl (therefore increasing the activity coefficient of the HCl). McCarty and Vitz [111] and Lewis and Randall [112] demonstrated that for strong HCl concentrations (0.98M to 11.9M) the activity coefficient of HCl increases dramatically, reaching 42.4 at 11.9M concentration. This therefore makes calculating the true pH of the flowback fluid difficult as the pH relates to the log of the activity of H^+, not the log of concentration. For example, McCarty and Vitz [111], found that if the HCl concentration is reduced significantly to 0.01M then the actual pH is 2.04 (not 2.00, the value calculated from the H^+ concentration).

The discrepancy between the actual pH and the value calculated from the H^+ concentration becomes less significant as the HCl concentration of the flowback fluid is diluted. This is an important point when considering the flowback fluid (acid diluted with formation brines). Although the discrepancy between the H^+ concentration and effective concentration is minimal for flowback fluids it is unknown what the actual difference is between the values.

Therefore, throughout the thesis, the corrosivity is discussed as a function of log(H⁺) and this value is not the true pH of the solution. All pH values quoted throughout the thesis are approximations calculated using the H^+ concentration of the solution.

3.2.1.4 Temperature

Increasing the temperature increases the rate of almost all chemical reactions [38]. However the exact relationship between the rate of reaction and the temperature of the acid is complex and varies based on each individual acid. The relationship between temperature and reaction rate of HCl will be considered as it is the most commonly used stimulation fluid. The relationship between the reaction rate and temperature of each acid used in the field is beyond the scope of this work.
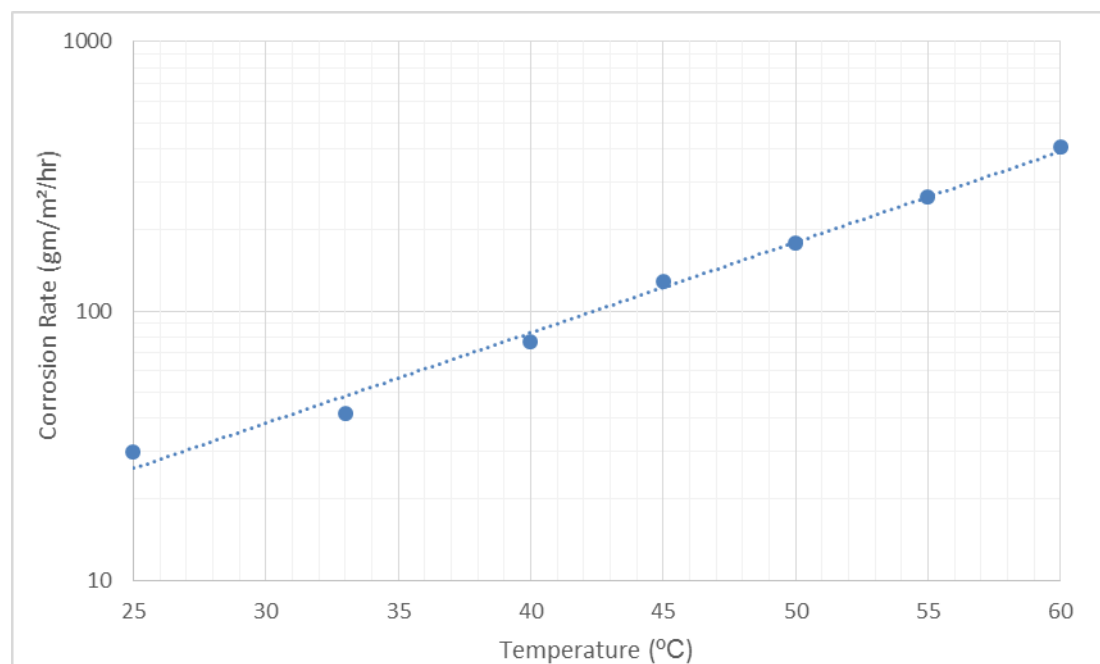
Figure 3.1 The effect of increasing temperature on the corrosion rate of mild steel in 5.5M HCl. The corrosion rate is plotted on a logarithmic scale. Data adapted from Mathur and Vasudevan [113].

Figure 3.1 shows the relationship between temperature and corrosion rate on mild steel in 5.5M HCl found by Mathur and Vasudevan [113]. Figure 3.1 shows that a logarithmic relationship exists between the temperature and the corrosion rate (indicated by the linear trend line). The work by Mathur and Vasudevan [113] found that over this temperature range the corrosion rate

increased exponentially with temperature. This highlights how important the temperature is when considering the corrosivity of both the injected acids and the flowback fluids.

3.2.1.5 Flow Velocity

As HCl is the most commonly used acid in the field it will once again be used to understand the relationship between corrosivity and flow regime. Several publications have found that the flow velocity has very little effect on the corrosion rate of carbon steel samples in injection strength HCl (0.5-4M) [76, 114, 115]. The corrosion rate does not increase with increasing flow velocity because the corrosion of low carbon steel in strong HCl (at elevated temperatures) is generally under activation control. The corrosion rate is therefore independent of the rate of transport of corrosion species as the corrosion rate is controlled by charge transfer [114].

3.2.2 Acidizing Corrosion Inhibitors

Organic compounds, in particular acetylenic alcohols, are used almost exclusively for inhibiting acidic media used in well stimulation jobs [45]. In order for an acidizing corrosion inhibitor to be effective it must meet the following criteria [45].

1. The inhibitor must be able to significantly reduce the rate of corrosion between the acid and steel.
2. It must be stable in solutions with high acid concentrations (very low pH) and at high bottom hole static temperature (BHST).
3. Acidizing corrosion inhibitors are injected in high concentrations compared to other corrosion inhibitors. For this reason they have to be very cost effective.
4. Depending on the local environmental requirements some inhibitors may not be suitable due to their toxicity. For this reason green inhibitors are more desirable (although unfortunately they often do not inhibit the corrosion rate as well as 'non-green' inhibitors).

The efficiency of a particular corrosion inhibitor depends on several variables. The characteristics of the protective film are incredibly important and they depend primarily upon the inhibitor molecules chemical structure. The size and shape of the inhibitor molecule also dictates the inhibitor efficiency, as does the electrical potential of the metal [46].

The efficiency of the inhibitor is also affected by variables specific to each well. The temperature can have a significant impact on the inhibitor efficiency as can the exposure time [46]. The acid velocity is also important as it can reduce inhibitor efficiency (through physical removal of protective inhibitor films) [114, 116]. It is clear that the development of an effective inhibitor is therefore complex and is made difficult due to the large number of factors which may affect its performance (temperature, concentration, compatibility and solubility considerations) [117].

3.2.3 Acetylenic Alcohols as Corrosion Inhibitors

Acetylenic alcohols readily adsorb on metal surfaces and polymerise to form a protective polymeric inhibitor film [70, 75, 83, 117-119]. They contain oxygen in the head group along with a linkage which is unsaturated and it is the oxygen compound which then polymerises on the metal surface forming the protective inhibitor film which inhibits the corrosion rate [45]. This protective inhibitor film can be incredibly complex and have multiple layers. This is illustrated in Figure 3.2 which shows the interaction, proposed by Tedeschi [117], between methyl butynol, hexynol and the iron surface.
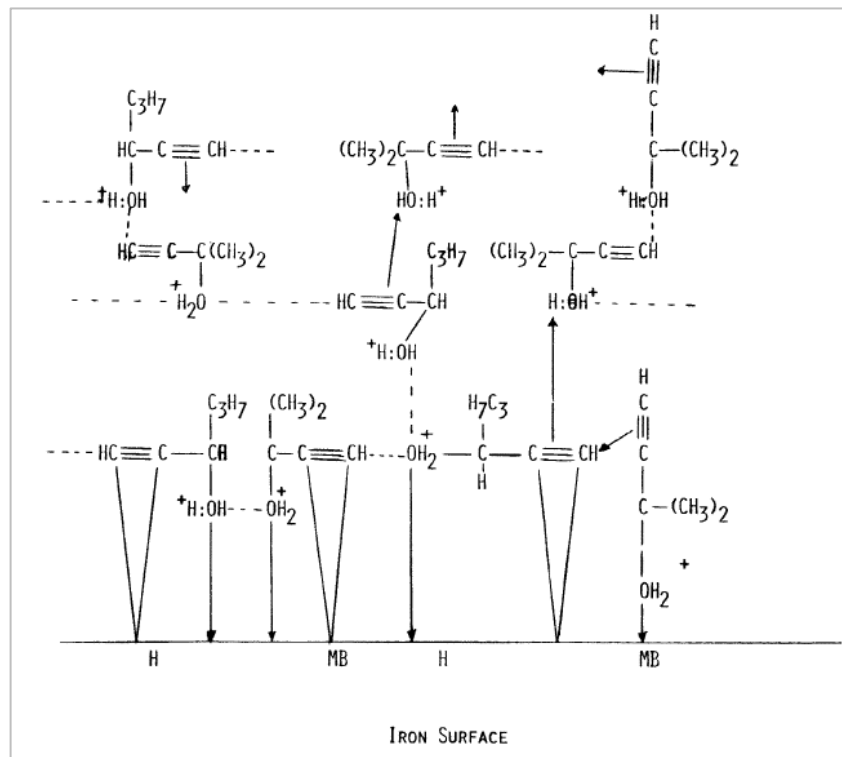
Figure 3.2 The multilayer inhibitor film formed by methyl butynol and hexynol proposed by Tedeschi [117].

The chemical structure of three additional acetylenic alcohols are shown in Figure 3.3. The acetylenic alcohols react to form oligomers at high temperatures. The oligomers then form protective films on the surface of the steel [120]. The triple bond is thought to be central to the inhibitive effect of the acetylenic alcohol [121].
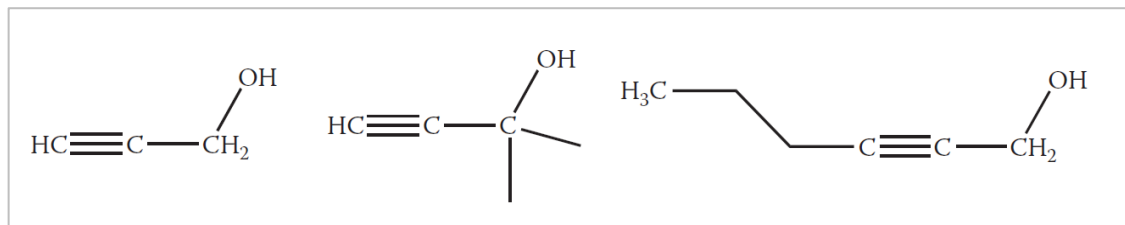
Figure 3.3 Chemical structures of (from left to right): propargyl alcohol, 2-methyl-3-butynol and 1-hexyn-3-ol [45].

It is thought that the inhibitive effect of acetylinic alcohols can be divided into two steps. The first step is chemi-sorption of acetylinic derivatives on the metal surface to form an allyl alcohol. This is then followed by polymerisation on the active metal surface which forms the protective film [85]. It is believed that this first stage takes place in the HCl through hydrogenation of the PA as shown in Equation 3.1 [122].

$$CH \equiv CCH_2OH + 2H^+ + 2e^- \rightarrow CH_2 = CHCH_2OH \qquad (3.1)$$
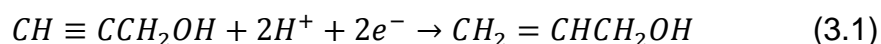
It has been suggested that the compound shown in Equation 3.1 then polymerises on the steel surface in HCl through dehydration, as shown in Equation 3.2 [123].

$$CH_2 = CHCH_2OH \rightarrow CH_2 = C = CH_2 + H_2O \qquad (3.2)$$
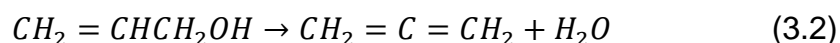
This shows that the reaction is catalysed by the HCl solution as H^+ ions are required to form the allyl alcohol (Equation 3.1) which then dehydrates (Equation 3.2) before forming the protective polymer film.

3.2.3.1 Mechanistic Explanation of Propargyl Alcohol

The inhibition mechanisms of PA are complex. It is understood that PA inhibits both the anodic and cathodic reactions and an extensive review of the available literature suggests that the inhibition mechanism should be divided into two steps [83, 86, 122-126]. The first step is the chemi-sorption of acetylenic derivatives on the surface of the metal. This is then followed by the formation of the protective film as the intermediate products polymerise on the surface of the metal.

It has been proposed that the low pH of the acid supports the surface catalysed polymerisation reaction [122]. High concentrations of inhibitor are always injected with the high strength acids as it has been shown that insufficient inhibitor in the bulk solution can be detrimental to steel tubulars. This is due to the protective inhibitor film degrading if the inhibitor concentration falls below a critical level [76, 123]. However, it should be noted that once production restarts and the fluid composition changes dramatically it is unknown how the PA functions. Due to the low pH supporting the surface catalysed polymerisation reaction, the increase in solution pH during flowback is of particular significance. To summarise the PA inhibitor is most effective when at a high concentration and low pH and inhibitor mechanisms have been proposed under these conditions [83, 86, 122-126]. However, how the flowback fluid (low PA concentration and high pH) affects the inhibition mechanism of PA has not been studied.

3.2.3.2 The Acetylenic Alcohol Inhibitor Mechanism

As discussed in Section 2.4, there are several ways in which inhibitors can protect steel from the high strength injected acids. It is widely acknowledged in literature that the electron donor capacity of the triple bond is vital to the inhibition properties of acetylenic alcohols [85, 117, 121, 127]. However it is also thought that the availability of electrons is influenced by substituent groups.

The effect that substituting each of these groups had on the corrosion rate was studied by Foster, Oakes and Kucera [121]. They first found the corrosivity of an acidic solution containing propargyl alcohol. They then repeated the experiment with a range of compounds, each of which removed

or replaced part of the propargyl alcohol molecule. The aim of the study being to find out how each part of the propargyl alcohol molecule contributed to the availability of electrons. The methane hydrogen (number 1 on Figure 3.4) was replaced with a range of elements and substituents (chlorine, iodine, hydroxymethyl and chloromethyl). This resulted in an increased corrosion rate and hence none of these compounds were found to be as good as propargyl alcohol at reducing the corrosion rate [121].

The triple bond (number 2 on Figure 3.4) was reduced through saturating the acetylenic bond by hydrogenation. Removing the triple bond resulted in the corrosion rate being as high as when the solution was uninhibited. This shows that the triple bond is essential for inhibition. Number 3 on Figure 3.4 represents the α-hydrogens. Replacement of one hydrogen atom with an alkyl group resulted in a significant increase in the corrosion rate (3-7 times greater depending on the alkyl group). Replacing both hydrogen atoms with alkyl groups lead to an even greater increase in corrosion rate (up to 50 times) [121].
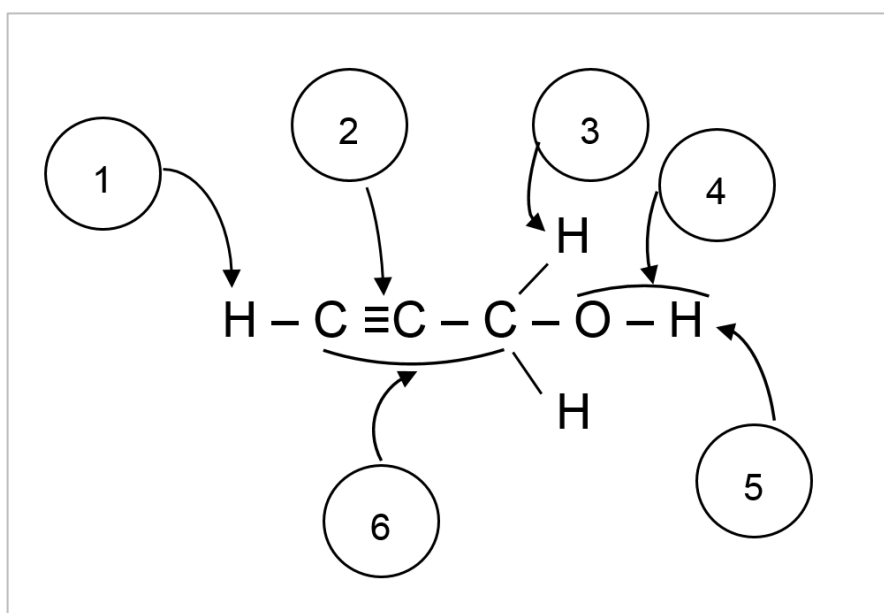
Figure 3.4 Chemical structure of propargyl alcohol provided by Foster, Oakes and Kucera [121]. Each component has been numbered 1-6 and is discussed in the text.

The hydroxyl group (number 4 on Figure 3.4) was replaced with a range of compounds (thiol (–C–SH), amidogen (–C–NH$_2$) and chlorine) and all were

found to be poor inhibitors which were a lot worse at inhibiting the acid than the propargyl alcohol. The alcoholic hydrogen (number 5 on Figure 3.4) was replaced with compounds of various lengths. The results showed that the longer the compound the higher the corrosion rate observed and hence inhibitor efficiency decreases with increasing compound length [121].

The final part of the propargyl alcohol which was altered and tested was the effect of the chain length. An additional methylene group (CH_2) was added to the compound (Equation 3.3).

$$H - C \equiv C - CH_2 - \boldsymbol{CH_2} - OH \qquad (3.3)$$
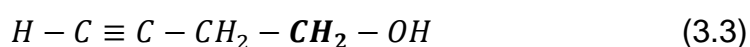
Increasing the distance of the triple bond from the hydroxyl group leads to a decrease in the inhibitors ability to reduce the rate of corrosion. This is expected as the electronegative hydroxyl group is now further from the triple bond [121]. The work by Foster, Oakes and Kucera [121] shows that each of the components highlighted in Figure 3.4 contributes to the propargyl alcohols ability to inhibit the corrosion rate of the injected acid.

3.2.3.3 Addition of Species to Improve Inhibitor Film Formation

The ability of an acetylenic alcohol to form protective films can be enhanced through the addition of other chemicals. Addition of these intensifiers can lead to improved efficiency as the ability of the inhibitor to form a protective surface layer is enhanced [128]. Elemental iodine, quaternary ammonium surfactants and amines (such as hexamethylenetetramine) can all improve the performance of the inhibitor [129]. A relatively new corrosion inhibitor has been developed which is made from the reaction of propargyl alcohol and iodine. 2,3-di-iodo-2-propen-l-ol, used in excess propargyl alcohol, provides a stable form of iodine. This form of iodide does not appear to degrade with time unlike when elemental iodine is added [130].

Research has been conducted looking at the ability of inhibitor blends to reduce the rate of corrosion of steel in acid. Mild steel mass loss coupons were placed in 10% HCl for 4 hours. A range of corrosion inhibitors (alkynols and acetylenic alcohols) were then tested individually. They were then mixed

together at ratios of either 1:5 or 1:50 of alkynols to acetylenic alcohols. Tedeschi [117] found that secondary alkynols (such as 1-hexyn-3-ol and 4-ethyl-1-octyn-3-ol) mixed with tertiary acetylenic alcohols (methyl pentynol and propargyl alcohol) resulted in superior inhibitor performances compared to either single component at concentrations equal to those used in the mixture. The most effective inhibitor was a mixture of the acetylenic alcohol 3-methyl-1-pentyn-3-ol with an alkynol (either ethyl octynol or octynol) at a ratio of 5 to 1 respectively. The corrosion rate when the inhibitor mixture was used was 339 times more effective than when the 3-methyl-1-pentyn-3-ol was used alone [117]. The addition of such intensifiers can lead to a significant increase in inhibitor efficiency.

3.2.3.4 Measuring the Inhibitor Film Thickness

The ability to measure the thickness of protective films is very desirable as it can lead to a better understanding of the conditions required for optimum film formation. Optical profiling has been used to measure the thickness of batch corrosion inhibitor films obtained under various conditions [131].

A thicker film tends to mean better corrosion inhibition as a thick film is better able to prevent the mass transfer of corrosive species to and from the metal surface. However the results of work conducted by Menendez, Bojes and Lerbscher [131] found that film thickness is not a critical parameter in determining the batch inhibitor performance when the thickness was found using specialist software. Instead it was found that the determining factors in predicting the inhibitor field performance are surface coverage and inhibitor film uniformity [131]. It is important to note that this work was not performed in acidic media, rather it is a general observation relating to film forming inhibitors.

In contrast, Poling [132] studied the infrared spectra of propargyl alcohol surface films formed on iron and steel mirrors and found that as the protective polymer coatings were increased in thickness from 20 to 100Å the corrosion protection increased significantly (Figure 3.5).
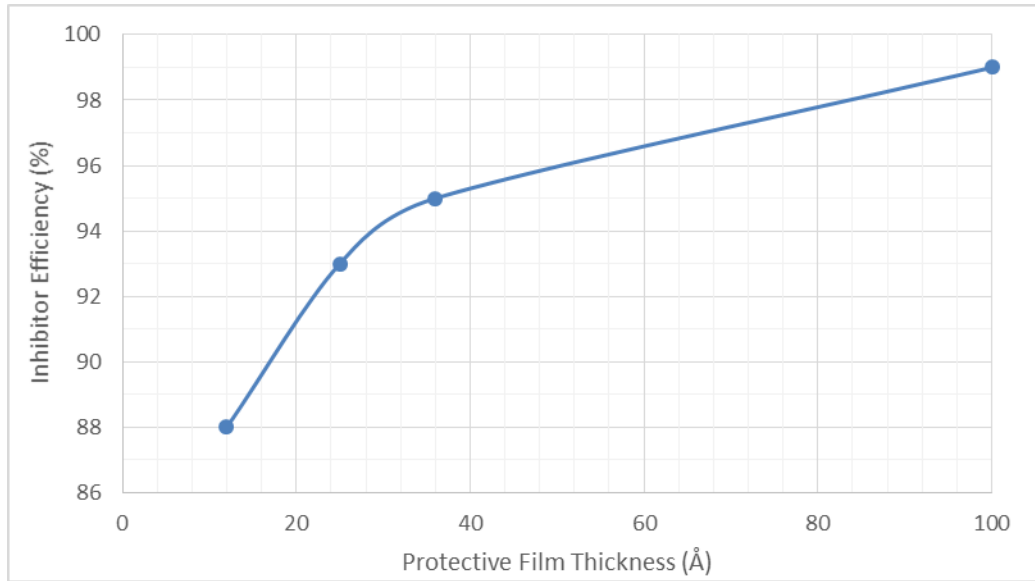
Figure 3.5 The relationship between PA film thickness and inhibitor
efficiency when tests were performed on steel coupons placed in 3.3M
HCl (containing 0.087M PA) at 65⁰C. Data adapted from Poling [132].

Poling [132] made several important observations regarding the formation of polymer films, their thickness and their ability to protect the steel.

1. Both the thickness and the composition of the polymer film control the protectiveness of the film.
2. The formed polymer films were found to contain several polar species, these included hydroxyl and carbonyl groups. Increased carbonyl content was found to decrease film protectiveness.
3. The availability of oxygen results in a thicker but crucially less protective film. The thicker film was found to have a significantly higher carbonyl content.

3.2.4 Other Acid Additives

As well as corrosion inhibitors a range of other chemicals are also added to the acid before it is injected in the field. A brief outline of several of the most common additives is provided.

3.2.4.1 Surfactants

Surfactants are added to the acid in order to demulsify the acid and the oil and reduce interfacial tension. They also alter formation wettability and help to reduce the clean-up time by preventing the formation of undesirable sludge.

Caution must be taken when adding surfactants to the solution as they may not be compatible with the corrosion inhibitor [1, 45].

3.2.4.2 Mutual Solvents

A mutual solvent is a material which has appreciable solubility in both oil and water. The exact nature of the mutual solvent and how it works are beyond the scope of this project, it should however be noted that mutual solvents are useful in acid jobs for the following reasons [1].

1. They reduce interfacial tension between oil and water.
2. Mutual solvents are able to remove oil-wetting materials as they act as a detergent. This is important as it allows these surfaces to become water wet allowing the acid to perform its desired task.
3. They are able to act as a solvent which can solubilize oil in water.
4. They are able to improve the action of surfactants and emulsifiers in contact with formation materials.

3.2.4.3 Diverting Agents

Diverting agents are used to divert the flow of the acid without damaging the formation. They are typically resins or solid organic acids. The purpose of diverting agents is to allow large production areas to be divided into several treatment stages. This is achieved through the combined use of diverting agents and other techniques to separate liquid stages [1, 45].

3.2.4.4 Emulsifiers

In some jobs the acid is emulsified in oil to increase the acid penetration. The emulsion will usually break when it reaches the reservoir temperature thus releasing the acid into the formation [45].

3.3 Mass Loss Experiments

Mass loss experiments are commonly used for studying the tubing metal losses associated with acid jobs [68, 71, 78, 85, 87-95, 97-101]. The mass loss methodology is relatively simple and there are several benefits to performing mass loss experiments. Mass loss measurements allow the corrosion rate to be easily calculated and the coupons themselves can provide

additional data as they allow any pitting corrosion to be observed and analysed [1].

3.3.1 Mass Loss Coupon Methodology

The general experimental procedure for mass loss measurements is similar for all of the previous experimental work [13, 68, 71, 78, 85, 87-95, 97-101]. A sample (of known surface area) is cut from the tubing grade steel which is being tested. The sample is placed in a known volume of acid and inhibitor at a desired temperature, ranging from room temperature [88-92, 103] to above 100°C (at pressures above 1atm) [13, 93-96], and the corrosion rate calculated from the mass loss of the coupon. The experiment is usually repeated without inhibitor present, this allows the inhibitor efficiency to be calculated from the two corrosion rates [71, 78, 87-90, 92-99]. Figure 3.6 shows a typical experimental set-up used by Metcalf and Allen [94] to perform mass loss measurements. This particular closed test vessel is capable of withstanding high pressures (up to 10,000psi). The vessel is designed to withstand such high pressure to allow experiments to be performed at temperatures over 100°C (the approximate boiling point of HCl). At this temperature the pressure in the vessel can be as high as 3,000psi due to both the vapour pressure and the expansion of gas [94].
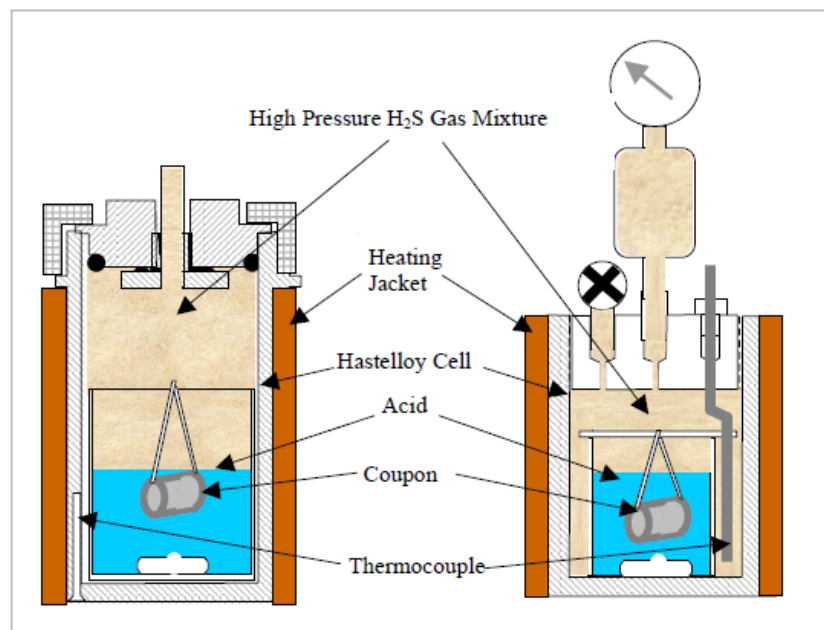
Figure 3.6 Test vessels used by Metcalf and Allen [94] to measure the mass loss from coupons placed in acid at temperatures above 100°C. The cell on the left is currently used (and allows higher pressures), the cell on the right was used in previous work.

3.3.2 Experimental Results

Previous experimental work has often consisted of simple mass loss tests used to calculate the efficiency of potential new acidizing corrosion inhibitors, although some previously published work has not used inhibitors. Khadom et al. [98] studied the effect of temperature and concentration on the corrosion rate of carbon steel in hydrochloric acid. It was found that the corrosion rate increased with increasing acid concentration and temperature as would be expected [98]. This is important to note for the injection of the hydrochloric acid into the reservoir but tells us little with regards to the corrosivity of the fluid which flows back following an acid job, other than that flowback fluid corrosivity will also increase with temperature.

Closed vessel mass loss tests are typically used to test the ability of new compounds to inhibit high strength acids (intended to replicate the injection process). For example, mass loss tests were used by Yadav, Kumar and Yadav [88] to test the ability of two newly synthesised amino acid compounds to reduce the corrosion rate of N80 grade steel in 15% HCl solution. The two compounds; acetamidoleucine and benzamidoleucine were found to be 82% and 90% efficient respectively at concentrations of 150ppm. Although both compounds are able to significantly reduce the corrosion rate of the acid it is still not higher than the efficiency of propargyl alcohol at the same concentration and experimental conditions (>95% efficiency) [93, 133].
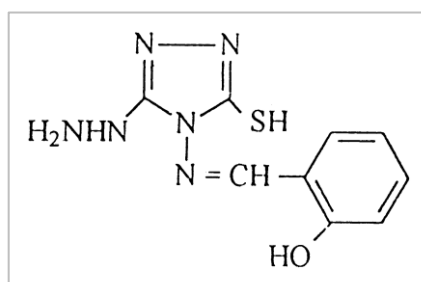
Figure 3.7 Example of a newly developed inhibitor tested by Quraishi and Jamal [93] using the mass loss test methodology. The inhibitor, SAHMT, is triazole based (4-salisylidineamino-3-hydrazino-5-mercapto-1,2,4-triazole).

The mass loss methodology was also used to test a new inhibitor developed by Quraishi and Jamal [93] which was then compared to the efficiency of propargyl alcohol. A triazole based inhibitor (referred to as SAHMT) was

synthesised which contained both a hydrazine and azomethine group in the same molecule (as can be seen in Figure 3.7).

Once again the inhibitor tested was not able to match the high efficiency of propargyl alcohol. The highest efficiency obtained by the new triazole based inhibitor was 91.6% compared to an efficiency of 99% for propargyl alcohol at the same very high inhibitor concentration of 5,000ppm (0.5% by volume). A comparison between the efficiency of the two inhibitors at a range of different concentrations is shown in Figure 3.8 [93]. This once again highlights that the majority of the previously conducted research has focused on the ability of a newly synthesised inhibitor to reduce the corrosivity of the injected acid.
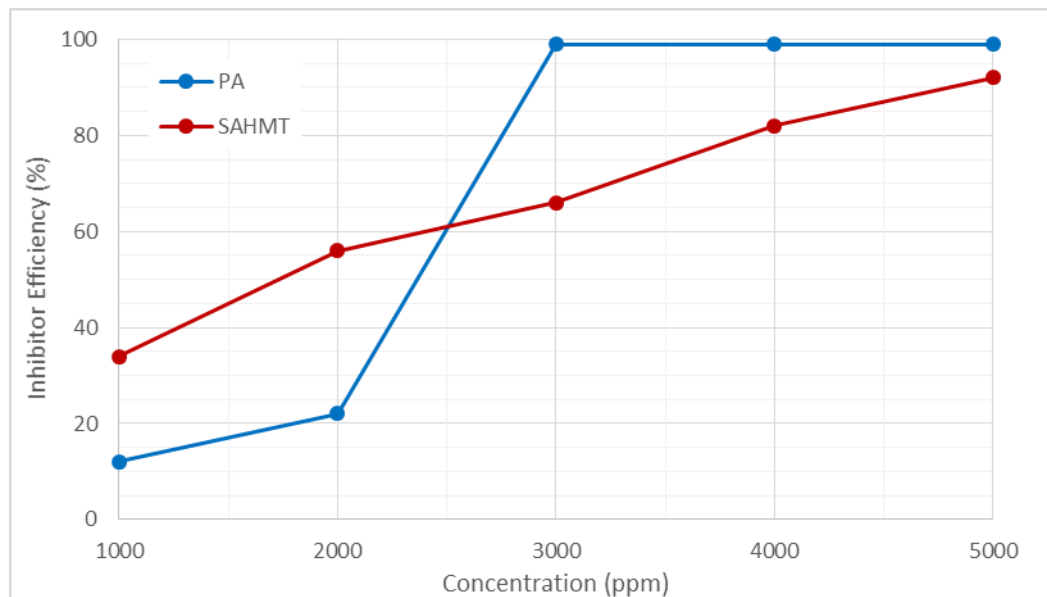
Figure 3.8 Inhibitor efficiency when a mild steel weight loss coupon was exposed to boiling 15% HCl containing different concentrations of PA and a newly developed inhibitor (SAHMT) for 0.5 hours. Data adapted from Quraishi and Jamal [93].

Metcalf, Delorey and Allen [94] drew direct comparisons between the corrosion rates calculated in the laboratory and those obtained in the field. The material deterioration of actual coiled tubing, which has been used for two acid jobs in the field was checked visually for any damage. Some examples of the damage observed on the coiled tubing strings are shown in Figure 3.9 [94]. Samples were also cut from the tubing and pickled to remove any rust or scale. The corrosion rate was then calculated by measuring the wall thickness of the tubing and comparing this value to its thickness prior to the job.

The laboratory tests were simple mass loss measurements using the high pressure cell shown in Figure 3.6 [94]. The results showed that it is possible to predict the increased corrosion rates (which were observed on the tubing samples) with good correlation between the field data and laboratory corrosion tests under simulated downhole pressure, temperature and hydrogen sulphide (H_2S) contact. It was found that if the acid is to be sufficiently inhibited under adverse conditions (high pressure, temperature and H_2S concentrations) then the inhibitor concentration must be increased [94].
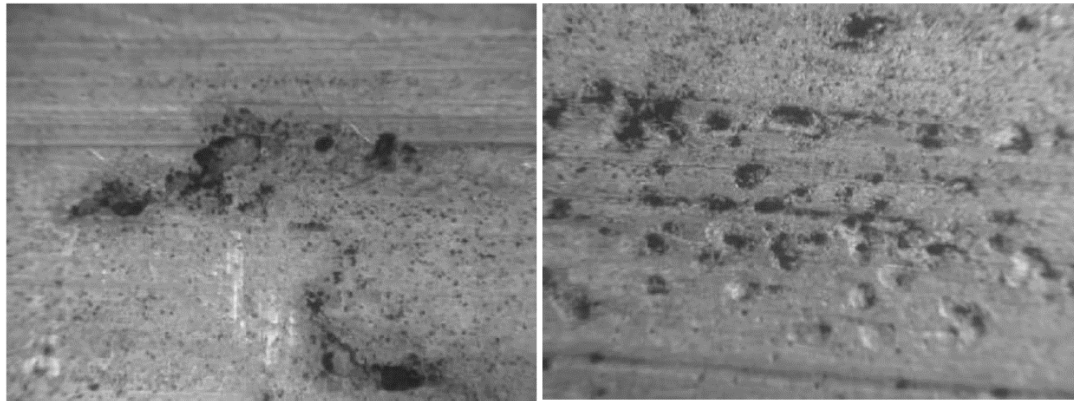
Figure 3.9 Photographs of sections of a coiled tubing string used for multiple acid jobs in a field containing hydrogen sulphide (H_2S) [94].

A large number of additional mass loss tests have been performed in previous studies. The closed vessel mass loss tests are used to test newly developed inhibitors in the hope that they can be more efficient than the industry standard film forming inhibitors. Unfortunately these tests do not consider the corrosivity of the flowback fluid, where the HCl and PA concentrations have both been significantly diluted. The mass loss test methodology must be performed in a solution with a fixed chemistry, therefore it is unable to replicate the progressively changing solution chemistry encountered once production restarts following an acid job.

3.3.3 Testing the Corrosivity of the Flowback Fluid using Mass Loss Techniques

Work conducted by Morgenthaler, Rhodes and Wheaton [7] recognised the potential corrosivity of the fluid which is produced following an acid job. The experimental work performed related to a specific case (the Auger project) located in the deep-water Gulf of Mexico. The injection of hydrochloric and

hydrofluoric acid mixtures were required in order to remove finely divided silica and alumina-silicate minerals from around the wellbore. This is a not an uncommon practice as wellbore impairments can often be caused by the materials injected with the drilling or completion fluids [7]. It is important to analyse the test methodology used and the rationale behind the work as this is one of the few studies which uses mass loss tests to understand the corrosivity of the flowback fluid.

The reasoning behind the work stems from the problems encountered in the Auger project; mainly that the reservoir sandstones were completely unconsolidated and contained no carbonate minerals. This resulted in the injected acid not being able to spend significantly prior to production being restarted [7]. The operator was therefore understandably concerned about the corrosivity of the fluid which would be produced once production was restarted. Field data from this particular case indicated that as much as 80% of the acid which is injected in the acid job is diluted by a factor of approximately two before being produced back once production restarts [7].

In order to try to replicate this flowback fluid in the laboratory a variety of synthetic laboratory brines were prepared which all varied in acid, inhibitor and mineral concentrations. Both active (N80) and passive (S13Cr and 22Cr) tubing materials were used to make the mass loss coupons that were then tested in one primary acid mixture (7.5% HCl/1.5% HF). A large test matrix was then developed which looked at the corrosion rates on the three different materials in the presence of three different inhibitors (no information is given on the inhibitor chemistries or concentrations). Between 12-192g/L of clays were also added in order to produce the 'spent acid' and attempt to more accurately replicate what is seen in the field [7]. Table 3.2 shows the 8 tests performed on N80 steel.

The outcomes of the work were very limited as the experimental work was tailored to this one specific sandstone reservoir located in the Gulf of Mexico. The results found that spent acids are highly corrosive to low-alloy steel, martensitic stainless steels and duplex stainless steels. However the acid and clay/silica mineral concentrations used to 'spend' the acid were intended to replicate one specific acid job making generalisations regarding the corrosivity of the flowback fluid in more conventional acid jobs very difficult to ascertain.

HCl Conc. (%)	HF Conc. (%)	Mineral Mass (g/L)	Inhibitor
7.5	1.5	12	None
7.5	1.5	192	None
7.5	1.5	12	A
7.5	1.5	96	A
7.5	1.5	12	B
7.5	1.5	192	B
7.5	1.5	12	C
7.5	1.5	192	C

Table 3.2 Test matrix used by Morgenthaler, Rhodes and Wheaton [7] to test the corrosivity of spent acid on N80 steel.

Although the solutions tested were titled 'spent acid' they still contained as much as 7.5% HCl and 0.75% HF. However, this concentration is likely to decrease due to the mineral loading used in each test and it is therefore important to note that the degree of acid spending due to the mineral addition is unclear. Unfortunately the work does not mention at what concentration the acids are injected in this particular field. However they do mention that field data shows that the injected acid is produced back diluted by a factor of 2. Several publications [1, 4, 134] on designing successful acid treatments cite that hydrochloric and hydrofluoric acid are injected at a range of concentrations and that HCl and HF concentrations of 15% and 3% respectively, represent acid concentrations used in a typical acid job.

Therefore the spent acid used in this work is designed to replicate the flowing back of acid which is unlikely to have significantly spent and is likely to still have a very low pH (depending upon the reaction of the acid with the added minerals). This is significant to note, as although the work is one of the few published datasets on the corrosion implications of the 'spent acid', the solutions tested may potentially be highly acidic and would still be considered 'live' acid by personnel in the field [7]. The main outcome of the work was simply that the depletion of any chemical inhibitors added and the dilution of the injected acid are both significant factors when analysing the corrosivity of spent acid.

Seth, Evans and Gabrysch [71] developed a new inhibitor package for use in acid jobs. They decided to use a basic mass loss methodology (similar to the methodologies discussed previously). The inhibitor package (no details are provided other than that it contains a newly developed corrosion inhibitor intensifier) was tested in two solutions intended to replicate the injected acids; 15% HCl and 13.5% HCl with 1.5% HF [71]. The inhibitor was also tested in spent acid, prepared following the methodology provided by Morgenthaler, Rhodes and Wheaton [7] which they used to replicate the sandstone reservoirs encountered in the Gulf of Mexico (the composition of this solution has been discussed). They also added significant amounts of aluminium and chloride ions and a reduced inhibitor concentration (to replicate adsorption onto the reservoir rock). The full spent acid composition used by Seth, Evans and Gabrysch [71] is shown in Table 3.3.

Chemical	Concentration
Hydrochloric Acid	5%
Hydrofluoric Acid	1%
Aluminium Chloride Hexahydrate	325 pptg
Ammonium Chloride	208 pptg
Corrosion Inhibitor	5 gptg
Surface Tension Reducer	1 gptg
Non Emulsifier	1 gptg
Iron Control	7.5 pptg
Mutual Solvent	25 gptg

Table 3.3 Fluid composition used by Seth, Evans and Gabrysch [71] to replicate spent acid. The concentrations are in oilfield units of pounds per thousand gallons (pptg) and gallons per thousand gallons (gptg).

Although an effort was made by Seth, Evans and Gabrysch [71] to understand how the new inhibitor package would behave in the flowback fluid the same limitations discussed previously still exist. The rationale behind preparing the spent acid in the same way as Seth, Evans and Gabrysch is unfortunately flawed for any scenario other than that outlined in their work. Seth, Evans and Gabrysch [71] have used the field data from the previous work and concluded

that the flowback fluid from acid jobs is 80% of the injected acid produced back with a dilution factor of 2. This is however only the case for the acid job in the Auger project (discussed previously). It is safe to assume that the vast majority of acid jobs will not be conducted in reservoirs with this type of geology. The main rationale behind performing acid jobs is to dissolve either the formation rock or scale build ups around the wellbore [1, 62, 135, 136]. It is therefore safe to assume that the bulk of acid jobs performed are not comparable to the Auger field which was completely unconsolidated and contained no carbonate minerals. Consequently, it is extremely unlikely that for the vast majority of acid jobs, the flowback fluid will contain such a high acid concentration that is produced for such a significant length of time.

Further tests were performed by Hernandez et al. [13] again using the technique for replicating spent acid suggested by Morgenthaler, Rhodes and Wheaton [7]. The aim of the work was to understand the material degradation risk for a range of over 30 alloys which are found in the flow path of the fluids produced following an acid job. The flowback fluid tested is once again specific to acid jobs performed in the Gulf of Mexico (as discussed previously) and two spent acid compositions were tested (shown in Table 3.4). Mass loss tests were performed in both fresh and spent acids. The spent acid was produced by passing the fresh acid through a column of mineral particles from the Gulf of Mexico formations (where the acid jobs are being performed). Inhibitor was not added to the spent acid as it was reasoned that no inhibitor is found in the flowback fluid as it will have adsorbed onto the formation minerals [13].

	Condition	Acetic Acid (%)	HF (%)	HCl (%)	Inhibitor Conc. (%)	Average pH
Spent Acid 1	Fresh	10	1	0	0.02	3.5
	Spent	10	1	0	N/A	3.5
Spent Acid 2	Fresh	10	1	9	0.01	1
	Spent	10	1	9	N/A	1

Table 3.4 Composition of acids used by Hernandez et al. [13] to test the corrosivity of the flowback fluid from acid jobs performed in the Gulf of Mexico.

Mass loss tests were performed using coupons made from a large range of alloys that were exposed to the acid for 3 days at a range of different temperatures (4-135°C). The different temperatures were intended to replicate the conditions found in four main system areas; downhole (93-135°C), subsea (60-93°C), topsides (24-38°C) and shut-in (4°C) [13].

It was found that for both of the spent acid compositions (shown in Table 3.4) both active (X65 and X70) and passive (13Cr and F6NM) materials were found to have a high risk of failure due to corrosion. It is therefore recommended that before production restarts following an acid job the carbon steel flowlines should be protected with a batch treatment of corrosion inhibitor. It is also suggested that a batch treatment should be performed after the flowback and higher corrosion inhibitor concentrations should be used until normal flowback resumes [13]. Again, the results are very limited to specific fields in the Gulf of Mexico where the injected acid only partially reacts with the formation before production restarts. However, the results once again highlight that the flowback fluid can pose a significant risk to both active and passive materials and precautions should be taken to protect expensive steel tubulars.

3.3.4 Acidizing Inhibitor Comparison

As discussed in Section 3.3.2 and 3.3.3, there are have been a large number of mass loss experiments testing a variety of different inhibitors in a range of different acids (mainly injection strength, but some attempting to replicate flowback). Ideally it would be useful to draw comparisons between the different inhibitors tested and their efficiencies at a range of different inhibitor and acid concentrations. Unfortunately the number of experimental variables between each of the tests means that a direct comparison between the different inhibitors is not possible. Any attempt at comparing them would not provide a better understanding of the efficiency of different acidizing inhibitors. The key parameters which vary between each test can be summarised as follows.

1. Temperature (ranging from room temperature to >100ºC).
2. Pressure (ranging from atmospheric pressure to 3,000psi).
3. Acid composition and concentration.
4. Steel grade (both active and passive materials are used).
5. Exposure time (this can vary from 0.5-72 hours) [13, 93].

3.4 Electrochemical Experiments

Electrochemical tests are typically performed to complement the corrosion rates measured using mass loss tests (typically achieved through polarisation plots of the inhibitors, impedance measurements or by monitoring how the potential of the sample varies over the duration of the test) [66, 69, 78, 88-93, 95, 99, 128, 137, 138]. These closed vessel electrochemistry tests tend to use a potentiostat and three electrode cell to help characterise existing or newly developed acidizing inhibitors [66, 69, 74, 88, 89, 93, 95, 102, 128, 137-139]. Corrosion rates are typically obtained from the mass loss tests and the most commonly performed electrochemical tests are anodic and cathodic polarisation tests. The anodic and cathodic polarisation curves provide an understanding as to how the inhibitor inhibits the corrosion rate, i.e. does it inhibit the anodic reaction, the cathodic reaction or both reactions [74].

3.4.1 Previous Experimental Results

Much of the previously conducted research work involved using electrochemical measurements to test inhibitors in solutions designed to replicate the injection process. Again, the focus of the tests was not on finding the corrosivity of the fluid which flows back following an acid job. High acid and inhibitor concentrations were studied and the tests performed varied in the extent to which they were able to effectively replicate the injection process. For example, two publications contained results from electrochemical experiments that tested inhibitor efficiencies at room temperature [88, 93].

Yadav, Kumar and Yadav [88] placed N80 samples in 15% HCl at two temperatures (25°C to 60°C). They tested the inhibition properties of two synthesised amino acid compounds (acetamidoleucine and benzamidoleucine). They conducted tests using both mass loss coupons and electrochemistry samples. Polarisation studies were performed using a standard 3 electrode cell consisting of; a working electrode (N80 samples with an area of $1cm^2$), counter electrode (platinum) and reference electrode (saturated calomel). The polarisation curves for each of the inhibitors tested, acetamidoleucine and benzamidoleucine (at three different concentrations) are shown in Figure 3.10 and 3.11 respectively [88]. A sweep rate of 10mV/s was used but the applied potential is not provided (however Figure 3.10 suggests that the applied potential was approximately ±100mV).
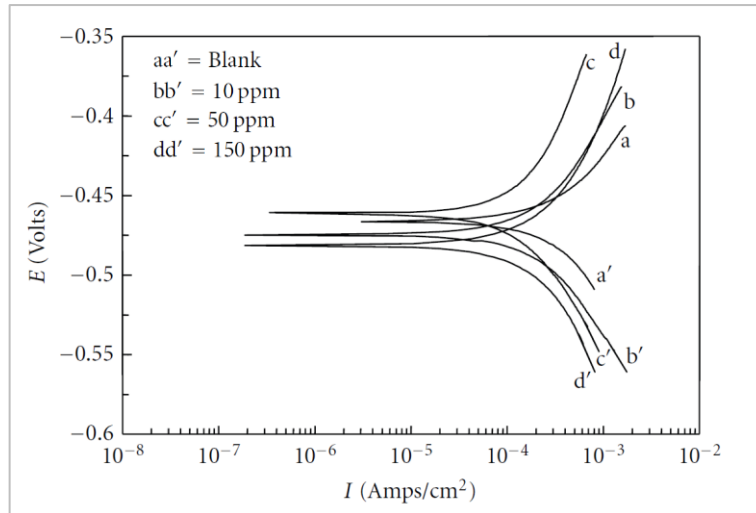
Figure 3.10 Potentiodynamic polarisation curves when N80 steel is placed in 4M HCl in the absence and presence of different concentrations (10-150ppm) of a newly developed inhibitor; acetamidoleucine [88].
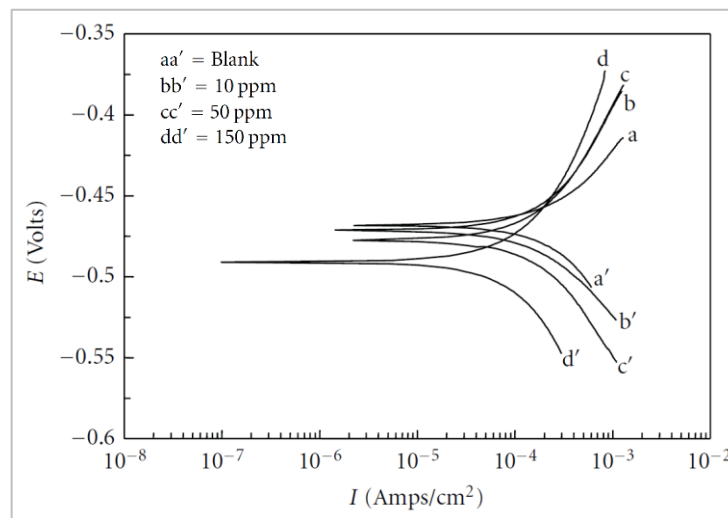
Figure 3.11 Potentiodynamic polarisation curves when N80 steel is placed in 4M HCl in the absence and presence of different concentrations (10-150ppm) of a newly developed inhibitor; benzamidoleucine [88].

The polarisation curves obtained (Figure 3.10 and 3.11) revealed that both of the inhibitors tested were mixed type inhibitors (as they inhibited both the anodic and the cathodic currents) [88]. As previously discussed in Section 3.3.2, Quraishi and Jamal [93] used mass loss coupons to test the efficiency of a newly synthesised corrosion inhibitor (which they called SAHMT). They also used 1cm^2 mild steel samples to test the efficiency of the newly developed inhibitor in 15% hydrochloric acid. Propargyl alcohol was tested at

the same concentration and experimental conditions so that a comparison could be drawn between the two inhibitors.

The polarisation curves obtained in the presence of four different SAHMT concentrations are shown in Figure 3.12. The SAHMT was found to be a mixed type inhibitor which inhibits corrosion through adsorbing onto the steel [93]. The highest efficiency obtained by the new triazole based inhibitor was 86% compared to an efficiency of 98% for propargyl alcohol at the same concentration. Direct correlation with the mass loss test is difficult as much higher inhibitor concentrations were used in the mass loss experiments [93].
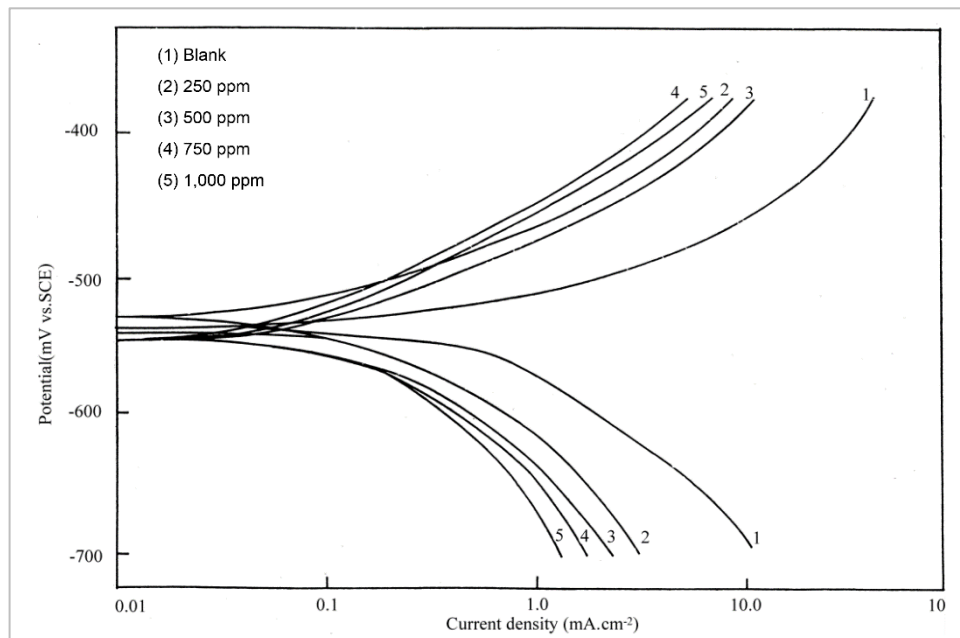
Figure 3.12 Potentiodynamic polarization curves found in the presence of different concentrations (250-1000ppm) of a newly developed inhibitor (SAHMT) created by Quraishi and Jamal [93]. Tests were performed on N-80 steel in 4M HCl at five inhibitor concentrations.

From the previous work conducted there have been no novel techniques or methodologies developed to perform the electrochemical measurements. The sample is simply cut from the tubing and placed in a specially designed holder [85] or it is embedded in a fixing material [93] before being placed in the acid. This test methodology has been found to be sufficient for testing the corrosivity of fixed concentration acid solutions intended to replicate the injection process.

3.4.2 Testing the Corrosivity of the Flowback Fluid using Electrochemical Techniques

Again, much of the research work previously conducted has focused on the ability of newly developed inhibitors to reduce the corrosion rates on tubulars during the injection with little consideration of the flowback fluid. However Huizinga and Liek [14] identified that severe damage can be caused from locally initiated acid attack in back-produced spent acid.

The research performed by Huizinga and Liek [14], and one further study by Al-Mutairi et al [15] which used the same test methodology, are the only studies which have attempted to replicate a full acid treatment (injection and flowback) using electrochemical techniques. This required testing the solution encountered at the start of the job (where high strength acid containing high concentrations of inhibitor is injected) to the point at which normal production is resumed (referred to as sweet production brines). It is important to understand both the composition of the 'spent acid' and how a full acidizing cycle was replicated in the laboratory by these authors [14, 15].

Before analysing the test methodology and spent acid composition it is important to first gain an understanding for the rationale behind the work. The problem encountered relates entirely to 13% chromium steel tubing (13Cr). The work makes no reference to the acid being injected through a coiled tubing string, therefore the 13Cr production tubing was exposed to the high strength injected acids. In addition to surviving acid stimulation treatments, the steel tubulars used are intended to be corrosion resistant in the presence of carbon dioxide and chloride containing waters (encountered during normal production). Unfortunately, very little detail is provided regarding the exact nature of the corrosion encountered in the field or the rates at which the tubulars were found to be corroding. Huizinga and Liek [14] simply state that the following problems were encountered.

- It was found that in a number of gas producing wells corrosive attack had occurred following the acid jobs. No other data is provided other than that calliper surveys were used to indicate that this attack had taken place.
- Localized attack was observed during the onshore inspection. These were noted to differ from normal stainless steel pitting as these pits

were wider and appeared in streaks. No images of the localized attack or any method of quantifying these localised attacks is provided.

In order to understand why this 'localised attack' and 'corrosive attack' occurred on the 13Cr tubulars it was decided by Huizinga and Liek that the corrosivity of the solutions listed in Table 3.5 should be tested. Because the well tubulars were all made from expensive 13Cr stainless steel the focus of the work was on the passivation behaviour of the 13Cr steel in each of the different solutions.

Acid	Compound	Quantity	pH	Chlorine Conc. (g/L)
A	Aqueous HCl	0.1M	1	154
	$CaCl_2$	234g/L		
B	Aqueous citric acid	2.5 wt.%	1	150
	$CaCl_2$	234g/L		

Table 3.5 Composition of artificial spent acid used by Huizinga and Liek [14] to test the ability of 13Cr steel to repassivate following an acid job.

The aim of the work was to gain an understanding of the ability of the 13Cr tubing to repassivate following exposure to an acid job [14]. An example of the polarisation data obtained by Huizinga and Liek [14] is shown in Figure 3.13. The test was performed in spent acid A (the composition of which can be seen in Table 3.5) at 80°C and it was purged with CO_2.

The research performed by Huizinga and Liek [14] focused entirely on passive materials with no tests performed using active materials. As the focus of this research project is on the behaviour of active materials during flowback from an acid job, the main interest of the paper produced by Huizinga and Liek [14] is the test methodology and the composition of the spent acid they used in the tests. In contrast to the research conducted by Seth, Evans and Gabrysch [71] the composition of the artificial spent acid used in there tests was more representative of a 'normal' acid job. Unlike the very specific case analysed by Seth, Evans and Gabrysch (in which an unconsolidated sandstone reservoir was replicated as discussed in Section 3.3.3), the artificial spent acid

in this work was at a much lower concentration than the injected acid. The artificial spent acid used contained 0.1M of HCl (0.375% HCl) [14], twenty times less acidic than the 2M HCl (7.5% HCl) solution tested by Seth, Evans and Gabrysch [71]. However, it is important to note that the 0.1M HCl solution still has a very low pH of 1.
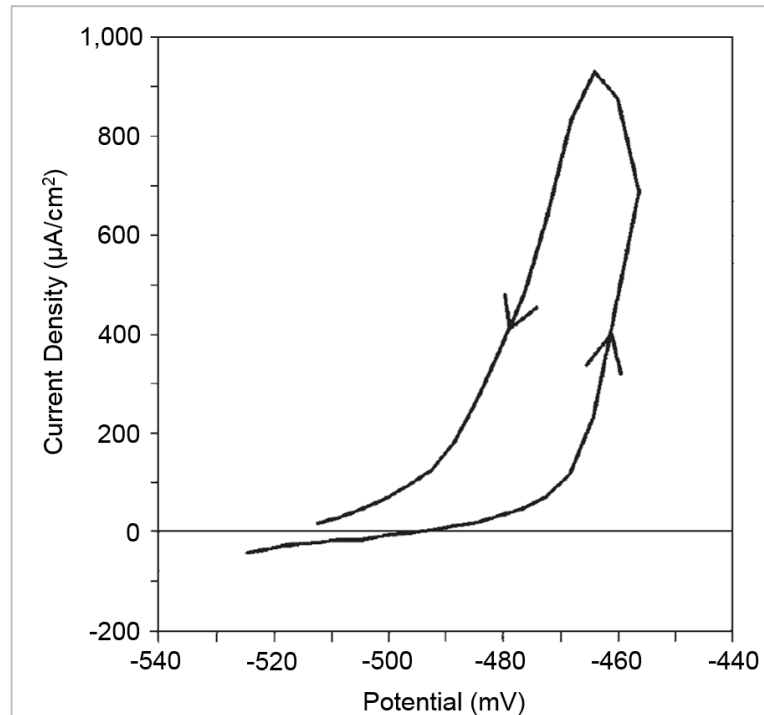
Figure 3.13 Polarisation curve obtained when 13Cr steel was placed in spent acid by Huizinga and Liek [14]. The test was performed at 80°C and the solution was purged with CO_2.

Table 3.5 shows the composition of the two artificial spent acids which were tested by Huizinga and Liek [14]; two artificial spent acids were produced by dissolving 150g of calcium chloride in hydrochloric acid and citric acid respectively. The concentrations of each acid shown in Table 3.5, were chosen as they gave a pH of 1. The rationale behind choosing this pH is briefly discussed and was chosen because a pH of approximately 1 is encountered in the spent acid due to the acid dissolving the rock [14]. An important point to note, and one which is highlighted by the author of the work is that the composition of the flowback fluid will change with time once production resumes following an acid job [14]. This instantly highlights the limitations of attempting to replicate the flowback fluid using a solution with fixed chemistry.

It is also important to analyse the electrochemical techniques employed by Huizinga and Liek [14] to study the spent acid. Tafel analysis was performed on the 13Cr steel samples by using a potentiostat to scan ±200mV from the open circuit potential (OCP) at a rate of 0.2mV/s. Samples were also polarised ±15mV from OCP in order to find the polarisation resistance (R_p). The corrosion rate was then calculated using a Stern-Geary constant calculated from the Tafel analysis [14]. Figure 3.14 shows the corrosion rates calculated using this method when 13Cr was placed in each of the spent acid compositions shown in Table 3.5 at a range of different temperatures.
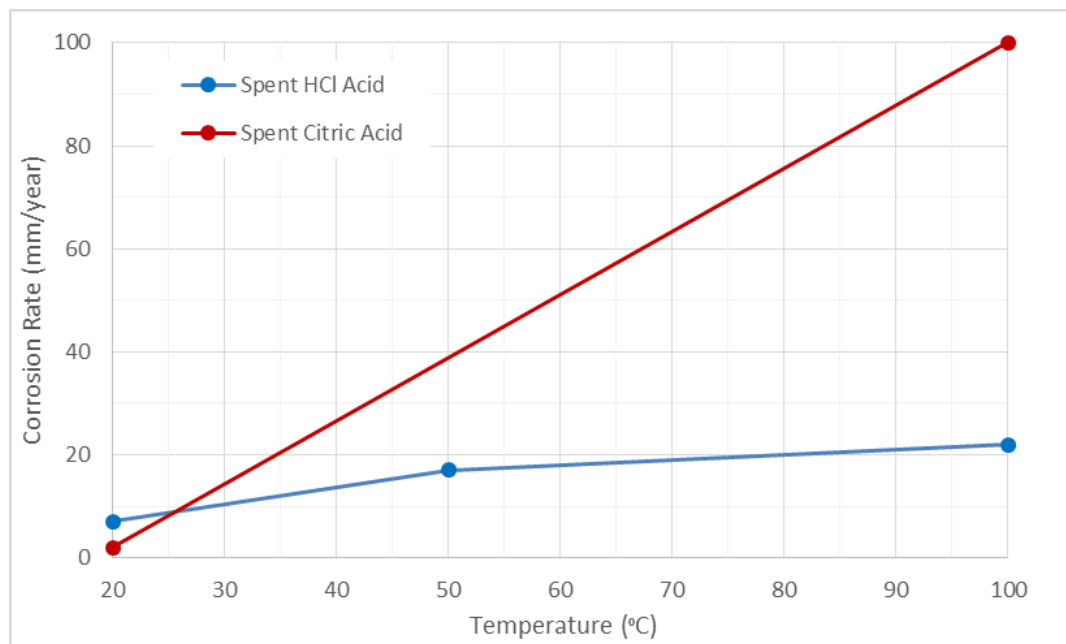
Figure 3.14 The corrosion rates calculated when 13Cr samples were placed in spent HCl and spent Citric acid solutions at a range of temperatures. Data adapted from Huizinga and Liek [14].

3.5 Testing the Corrosivity of the Flowback Fluid using Field Analysis

Al-Mutairi et al. [15] used a two channelled approach to analyse the corrosivity of flowback fluid; mass loss tests and direct analysis of well flowback fluids. In the work the authors mention that they tested mass loss coupons in the laboratory although no results from these tests are presented. The research is important as it is possibly the only published literature which has provided extensive flowback data from a large number of wells. The author mentions that over 30 wells were thoroughly examined before presenting the results

from four wells which are discussed in the paper. The reasons for choosing these wells is not discussed however the information shown in Table 3.6 is provided about each of the wells (denoted A, B, C and D) [15].

Variable	A	B	C	D
Tubing Length (ft)	10,040	8,802	8,940	10.466
Tubing Grade	C-95	C-95	SCr-13	SCr-13
Liner Length (ft)	2,870	3,318	3,090	1,434
Liner Grade	C-95	C-95	Cr-13	Cr-13
Injected HCl Conc. (wt.%)	Emulsified 28	15	Gelled 15	Gelled 15
Injected Formic Acid Conc. (wt.%)	N.A.	9	9	9
Acid Volume (gals)	10,000	10,000	10,000	10,000
Overflush Volume (gals)	15,157	16,000	45,070	39,277
Soaking Time (hours)	<1	<1	<1	≈2

Table 3.6 Key parameters of the four wells (A, B, C and D) examined by Al-Mutairi et al. [15].

The flowback fluid from the four wells was examined and the following seven parameters were recorded [15].

1. HCl concentration (%)
2. Total iron concentration (mg/L)
3. Calcium ion concentration (mg/L)
4. Magnesium ion concentration (mg/L)
5. Chlorine ion concentration (mg/L)
6. Manganese concentration (mg/L)
7. pH

Each of the above parameters was measured for between 2.5 and 16 hours once production restarted following the acid injection. The most important

parameter when discussing the corrosivity of the flowback fluid is clearly the HCl concentration of the solution (which is directly related to the solution pH). The data provided gives the pH of the flowback fluid for all four of the wells discussed. For all four wells the lowest pH measured is 0 and this value is recorded within the first 30 minutes of production restarting [15]. The HCl concentration of the solution is only given for two of the wells. The injected acid was 28wt% HCl and the HCl concertation of the flowback fluid reaches a maximum of 16wt% in one well and 0.6wt% in the second well [15]. The high HCl concentration and low pH values again indicate that the flowback fluid can still be very corrosive, this highlights the potential danger to the production tubing once production resumes following an acid job.

Another important parameter to examine is the iron content in each of the wells. Both wells for which the HCl concentration data is available show a strong correlation between the total iron concentration of the flowback fluid and the HCl concentration. Well A, which had the highest hydrochloric acid concentration (16wt%), had a maximum total iron concentration of 20,000mg/L which was recorded at a similar time to when the HCl concentration was also at a maximum (this is shown in Figure 3.15) [15].
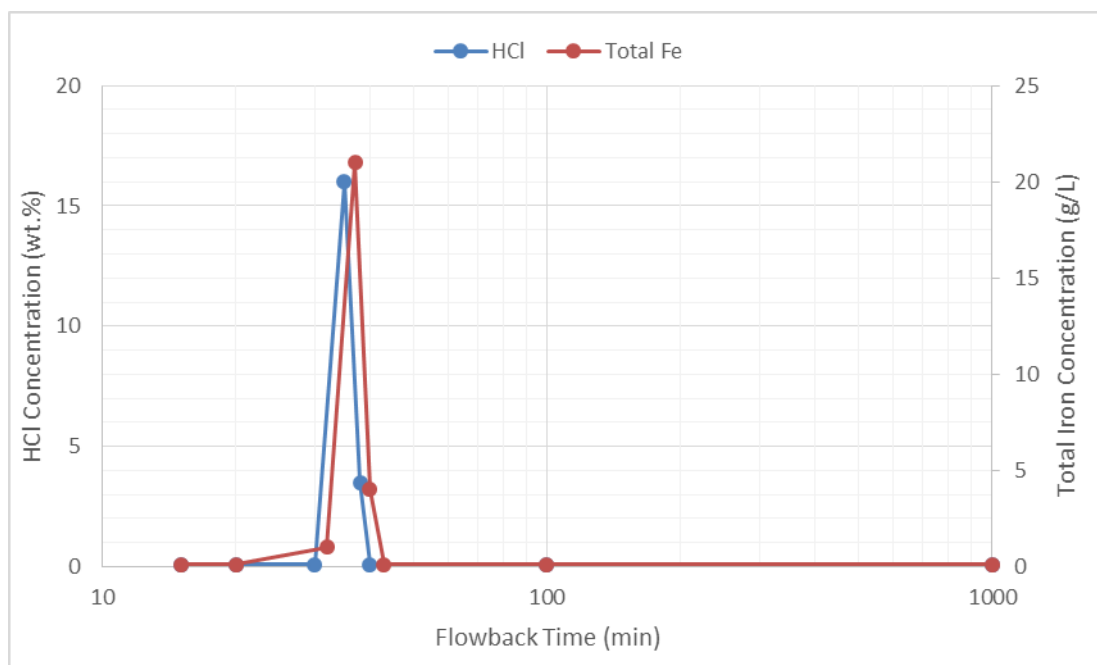
Figure 3.15 Example of the HCl and total iron concentration of the flowback fluid following an acid job from a deep carbonate reservoir. Data adapted from Al-Mutairi et al. [15].

Al-Mutairi et al. [15] state that the most important observation from the work is that the well flowback samples contain high levels of iron. The authors then go on to list the following three potential sources of the high iron levels.

1. Fluids and rocks already present in the reservoir.
2. Injected acids.
3. Well tubulars.

With such high total iron concentrations in the flowback fluid it is vital to understand the reasons for this peak when considering the corrosion implications on the production tubing. Al-Mutairi et al. [15] state that XRD was used to show that the formation rock contained no sources of iron. The authors were also confident that stringent quality control procedures were followed prior to the acid being injected which included the use of clean storage tanks and mixing the acid with field water that contained no more than 2mg/L of total iron [15]. Therefore it was concluded that the source of the iron in the flowback fluid is the live acid present in the flowback samples tested. This is further validated through analysis of the manganese levels in the flowback fluid. All wells that were completed with low-carbon steels showed a high concentration of manganese coinciding with the measured spike in total iron concentration [15].

Unfortunately the research performed by Al-Mutairi et al. is specific to a single carbonate reservoir located in Saudi Arabia, this makes it difficult to draw generalisations regarding the flowback fluid corrosivity. However, as this is the only published data showing direct measurements of total iron taken from the field the work by Al-Mutairi et al. is further validation regarding the potential corrosivity of the flowback fluid from acid jobs.

3.6 Flowback Fluid Composition

The fluid which flows back following an acid job is incredibly complex with ion and mineral concentrations varying with time. The flowback fluid usually contains varying concentrations of the following [15, 140, 141].

1. **Chlorides** – The concentration may be as high as between 50,000 to 70,000 ppm in acid flowback. This number then falls as the well cleans up and normal production resumes. Chlorides are usually stable up to the limit of chloride solubility.

2. **Iron** – Due to the corrosive nature of the acid (even with inhibitor present) large amounts of iron can be found in the solution (up to 70,000ppm if the acid concentration is still high). As the acid spends and its strength decreases the iron will begin to precipitate out of the solution. An example of the iron concentration measured in the field once production restarts following an acid job is shown in Figure 3.16 [6]. The example profile is taken from a field which was completed with 22Cr steel and highlights that high concentrations of iron can still be found in the flowback fluid despite expensive tubing grade steels being used. The significance of iron in the flowback fluid is discussed in greater detail in Section 3.6.2.
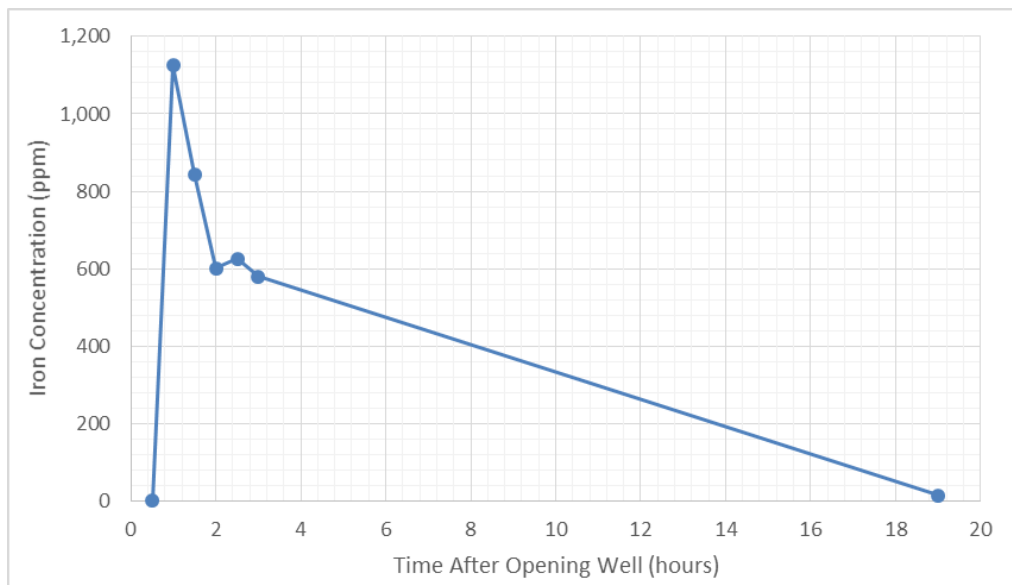
Figure 3.16 Iron concentration measured in the field, the samples were taken once production restarted following an acid job. Data adapted from Valdes et al. [6].

3. **Calcium** – The concentration of calcium ions in the flowback fluid is a direct indicator as to the amount of carbonate minerals in the formation that the acid has consumed. Therefore measuring calcium can be a direct indication of how successful an acid job has been at dissolving carbonates in the wellbore. The calcium concentration will peak and then decrease as the pH rises over the duration of the flowback process. This is due to less calcium being stable in the acid causing the excess to precipitate. This precipitation can lead to the formation of problematic calcium scales uphole. The significance of calcium in the flowback fluid is discussed in Section 3.6.2.

4. **Silicate and Aluminium** – Sandstone formations can contain as much as 10% clay. This clay lines the walls of sandstone pore spaces (Figure 3.17). Dissolution of these clays can lead to silicate and aluminium being present in the acid backflow and if the pH becomes greater than 2.5 alumino-silicate precipitation can occur.
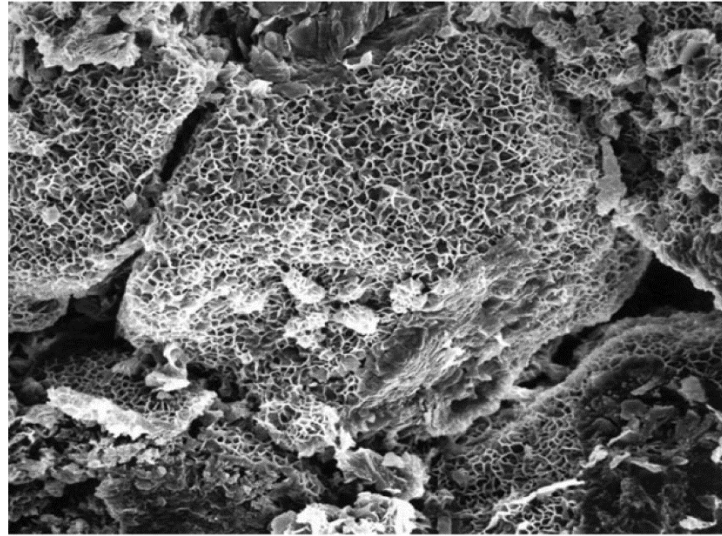
Figure 3.17 Photomicrograph image of a pore space in a sandstone formation which is lined with clay [141].

5. **Corrosion inhibitor** –The inhibitor reacts by adsorbing onto the metal surface of the tubing during injection (and thus protects the tubing from the highly corrosive acid). It is also thought to react with the formation rocks although the exact mechanism is not fully discussed in literature [140]. This contributes to the flowback fluid containing very little to no unreacted inhibitor which is able to protect the tubing string during flowback.

6. **Undissolved solids** –It is unlikely that the entire formation is made from acid soluble rocks. If 1,000 gallons of 15% HCl is injected then this will dissolve 1,840lbs of calcium carbonate; this could then free up to 500lb of fines (non-acid soluble particles). The undissolved solids can seed emulsions and scale if left in the well and are typically recovered through the use of a high energy flowback which helps to clean the well [140].

Following an acid job the well is produced at the same rate as before the treatment. The production rate can be increased once all of the spent acid has been returned or reduced to a water cut of zero. Figure 1.2 shows a typical example of the amount of acid (expressed as total acid number) which flows back once the well is opened following an acid job [6]. The decrease in acidity of the produced fluids indicates that there is a progressive dilution of the injected acid into the fluid present in the formation [6]. The last fluid to flow back from an acidizing job is also the fluid which has been in the formation for the longest time and should in theory be completely spent [140].

3.6.1 Replicating Flowback Fluid in the Laboratory

As discussed in Section 3.3.3 and 3.4.2 several previous studies have attempted to replicate the flowback fluid for use in laboratory tests [7, 14, 71]. The solution compositions have all been discussed and tests were performed in solutions of fixed chemistry. The solution chemistry is changing over the duration of the flowback [14]. This means that the information that be gained from any tests performed in a solution of fixed chemistry and HCl concentration is severely limited. Replicating the flowback from acid jobs can be problematic as every field will have a different flowback profile. However, it is illogical to suggest that the flowback fluid is of a fixed chemistry over the entire duration of the flowback process. Therefore, it can be said that no test performed at a fixed acid concentration replicates the solution which flows back once production restarts following an acid job.

3.6.2 The Importance of Iron and Calcium in Flowback

When discussing flowback fluid and the potential corrosion implications associated with the flowback it is vital to consider both its calcium and its iron content. Depending on the nature of the reservoir rock and the scale removed the calcium and iron contents can vary greatly. The corrosion implications and the relationship between the two ions is discussed in this section.

3.6.2.1 The Importance of Iron in Flowback

The relationship between the iron content and the pH of the flowback fluid is complex. The iron content of the flowback fluid is dependent on several factors. The purpose of the injected acid is of course to improve the permeability around the wellbore through the dissolution of scales around the

wellbore. However the acid also readily dissolves the iron scale in the pipes and will also attack any iron containing minerals in the formation [142].

The iron in the flowback fluid can be from several sources.

1. Before the acid even reaches the formation there is the possibility for it to dissolve rust in storage tanks [143, 144].
2. Upon injection the acid can dissolve any corrosion products in the tubing. These corrosion products found in injection tubing contain a mixture of Fe (II) and Fe (III) [143].
3. The formation brine itself may contain iron whilst sandstone reservoirs in particular can contain large quantities of iron containing minerals [143].

The iron will then remain in the acid and will not begin to precipitate out until the pH of the flowback fluid begins to rise and the iron loses it solubility. The effect of temperature on Fe (III) solubility as pH increases was studied by Taylor, Nasr-El-Din and Al-Alawi [143], and the results are shown in Figure 3.18.
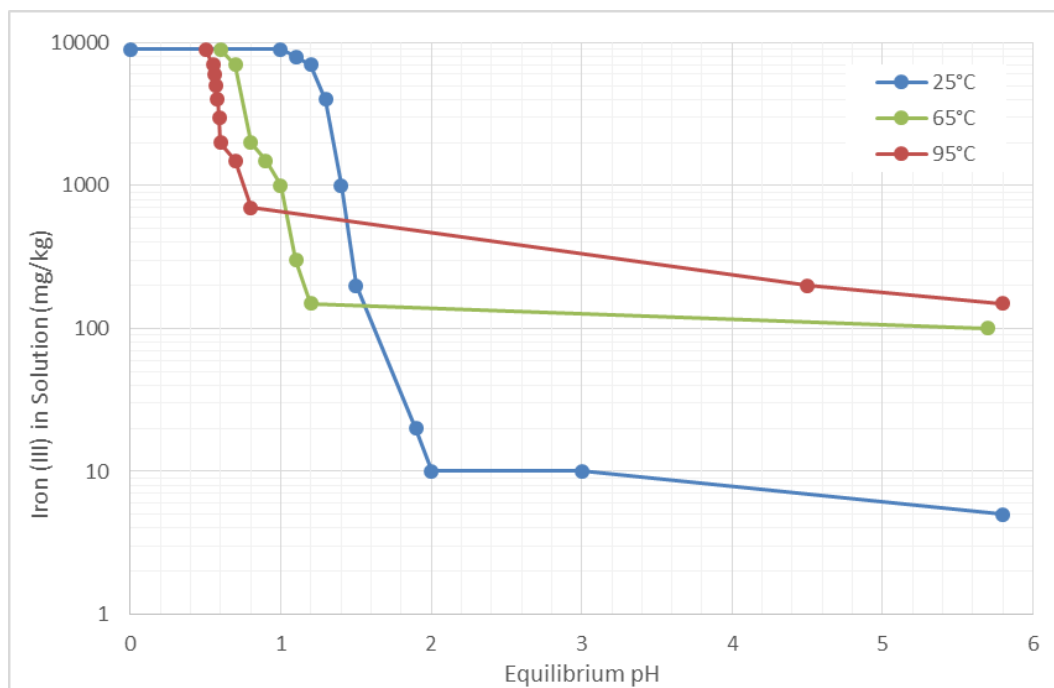
Figure 3.18 Study on the effect of pH and temperature on the solubility of Fe (III) (10,000mg/kg initial concentration). Data adapted from Taylor, Nasr-El-Din and Al-Alawi [143].

The iron content of the flowback fluid is frequently observed to be between 1,000-5,000ppm [142] but has been recorded as high as 25,000ppm [145]. In addition to the range of possible iron concentrations the scenario is further complicated by the relationship between iron (II) and iron (III). The iron exists in spent acid in both of these ionic states with iron (II) usually dominant under anaerobic conditions [142].

This highlights the main difficulty encountered when trying to replicate the iron content of the flowback fluid in the laboratory. Both the type of iron ion present (Fe (II) and Fe (III)) in addition to the concentration of each ion vary drastically in each individual acid job and are dependent on a large number of factors.

3.6.2.2 The Importance of Calcium in Flowback

As previously discussed calcium carbonate dissolution is a direct indicator as to how successful an acid job has been [140]. The calcium concentration during flowback will peak and then decrease as the pH rises and calcium carbonate begins to precipitate out of the solution. With regards to the aims of this work the focus of the calcium concentration should be on its corrosion implications during the flowback process. Previous work performed by Zhao et al. [146] found that the presence of calcium resulted in a corrosion rate decrease in the short term but had no effect on the corrosion rate in longer term experiments.

It is important to note that the calcium concentration of the flowback fluid will vary once production restarts following an acid job. However the corrosion implications of any calcium present in the flowback fluid are going to be minimal in comparison to the high corrosion rates associated with the injected hydrochloric acid. However, it is unknown what effect any calcium in the flowback fluid may have upon the efficiency of any remaining inhibitor.

3.6.2.3 The Ratio between Iron and Calcium in Flowback

When production is resumed the flowback fluid will always contain some quantity of iron and calcium. However the ratio between the two ions can vary greatly depending primarily on the nature of the reservoir which is being treated. For sandstone reservoirs the iron content in the flowback fluid is typically between 30 to 50 times higher than the calcium content. The

difference in ratio is due to the iron content of the sandstone and the amount of carbonate scale in the reservoir [140].

In carbonate reservoirs the ratio of iron to calcium is reversed, with the calcium content typically being over 100 times greater than the iron content. This is of course due to the calcium content of the formation rocks (which also typically contain very little to no iron naturally). Therefore almost all of the iron content present in the flowback fluid is due to the acid reacting with either the downhole steel assets or with corrosion products present on these assets [140].

Again this highlights the difficulty in replicating the ratio between the calcium and iron contents of the flowback fluid in the laboratory as the ratio can change drastically depending on the formation geology and the nature of the acid job.

3.7 Problem Areas and Gaps in Previous Research Work

The existing methodologies are designed to replicate the injection of high strength acids containing high inhibitor concentrations. Due to the high corrosion rates associated with high temperature and pressure acids the primary test methodology tends to be relatively simple mass loss tests. There are some limitations with using these existing methodologies to test injection strength acids, primarily related to the recommended acid volume to metal surface area ratio. However, when attempting to understand how the corrosivity of the flowback fluid changes once production restarts, using this mass loss methodology becomes very problematic. The mass loss tests require the test solution to remain fixed over the duration of the test but the solution chemistry is constantly changing during flowback from an acid job. In order to replicate the flowback process a methodology which can measure the corrosivity over the duration of the flowback process is required.

3.7.1 Acid Injection

In virtually all previous experimental work, the acid volume to metal surface area ratio is much lower than that recommended by the American Society for Testing and Materials [71, 85, 87, 88, 93, 94, 97, 98]. For example in the paper by Metcalf the ratio of acid volume to sample surface area was 33ml/in^2 for

the mass loss experiments [94]. This was chosen as it followed the testing guidelines established by the API-NACE subcommittee on acid corrosion testing [94]. However the American Society for Testing and Materials standard G31 recommends a volume to surface area ratio of 0.4L/cm^2 (2.58L/in^2) [85]. This acid volume to surface area ratio is much lower than that recommended in the standard and this was the case with all previous research which was studied [71, 85, 87, 88, 93, 94, 97, 98]. The acid volume is simply too large to be both practically and economically viable.

One way to overcome this problem would be through the use of a much smaller mass loss coupon. However, a smaller mass loss coupon would provide less accurate results which will lead to doubts on the validity of any tests performed. The mass loss tests therefore do not accurately represent acid jobs in the field whereby the tubing is in constant contact with fresh acid. In the mass loss experiments the acid is spending over the course of the experiment. This results in the acid becoming less corrosive with time and as a result the corrosion rate may be grossly underestimated from the mass loss results [85].

There are many variables to consider when attempting to replicate the injection of acid in laboratory tests. The acid composition, volume, temperature and pressure all vary between each acid job and are selected based on a variety of factors (formation geology, reason for acid job, etc.). Also, the ASTM G31 standard [147] recommended volume to surface area ratio is unfeasibly large for most mass loss tests [85]. This has resulted in each service company using their own acid volume to steel surface area ratio alongside their own testing procedures. This is likely to result in each company obtaining different results which in turn results in inhibitors being ranked in different orders of efficiency from company to company [148].

3.7.2 Acid Flowback

The corrosion rate and the inhibitor efficiency in the flowback fluid depends on a large number of variables. In acid jobs the corrosion rate is affected by the rate of both inhibitor spending and acid spending as well as the amount of carbon dioxide, calcium, oxygen and the bottom hole static temperature (BHST). The challenge is to simplify these parameters whilst still replicating (as near as possible) the conditions seen in the field [97]. There are many

experimental parameters (as shown in Table 3.7) which can affect the corrosion rate of a steel sample [149]. It is important to note the wide range of variables and which ones are relevant when attempting to replicate flowback in acidizing laboratory tests.

Parameter	Comments
Temperature	-
Carbon Dioxide (CO_2)	Consumed and has to be replenished
High Hydrogen Sulfide (H_2S)	Consumed and has to be replenished
Steel Composition	Use the same batch of steel as used in the field if possible
pH	Depending on the buffering capacity of the water
Low Hydrogen Sulfide (H_2S) (ppm)	Consumed and has to be replenished, low concentrations are difficult to control
Acetic Acid	Consumed, sensitive to pH, low concentrations are difficult to control
Flow Rate and Regime	Scale up problems
Oil Properties	Large differences between model oils, stabilized oil and live oil
Iron (Fe^{2+}) Concentration	Produced and has to be removed
Calcium (Ca^{2+}), Strontium (Sr^{2+}), Barium (Ba^{2+}) Concentrations	Consumed and has to be replenished
Steel Surface Properties	Mill scale, rust, corrosion films

Table 3.7 – Parameters which effect the corrosion rate of samples used in lab experiments proposed by Dugstad et al. [149].

The parameters from Table 3.7 which are most relevant to an experiment replicating flowback from an acidizing job are outlined below [149].

1. Temperature.

2. CO_2 concentration (acid reacting with calcium carbonate produces large amounts of CO_2).
3. Flow rate and regime (important for transfer of corrosion products to and from the surface of the steel and also the removal of any inhibitor films).
4. Fluid chemistry; the concentration of calcium and the pH are particularly relevant to acidizing jobs as the two parameters both increase over the duration of the flowback.

The majority of previous work has looked at the corrosion of steel samples in high concentration hydrochloric acids and the small amount of research which has been performed to test the flowback fluid is severely limited due to the experimental methodology used (as discussed in Section 3.3.3). Therefore a large gap exists in the understanding of the corrosivity of acid jobs. A substantial amount of the cost of acid job is spent on protecting well production tubing strings from the injected acid (through the use of expensive coiled tubing strings and inhibitors). It is therefore incredibly surprising that the flowback fluid from an acid job is produced through the production tubing with no real understanding regarding the corrosivity of this flowback fluid. The flowback fluid is very complex in nature and it could have serious corrosion implications on the coiled tubing due in part to how the inhibitor spends and the higher corrosion rates associated with this inhibitor spending. At present the corrosion implications are virtually unknown as almost no research has been conducted which has attempted to fully replicate the flowback process. This is possibly due to the difficulty in replicating the flowback process in a laboratory; as the solution chemistry is constantly changing from the moment production restarts to the point normal production is resumed. In order to achieve this a new test methodology would be almost essential, as the pre-existing test methodologies are not suitable for measuring the corrosivity of a solution with a constantly changing chemistry.

In conclusion, a large gap exists in acidizing corrosion research. In the field, flowback from acid jobs is produced through the expensive production tubing based solely on the assumption that the injected acid has either fully reacted with the formation or the flowback fluid is not corrosive enough to significantly corrode the tubing. However, the few authors who have studied flowback fluids have all found this to not be the case.

Chapter 4 Closed Vessel Experiment Methodology

4.1 Introduction

In order to gain an understanding as to how the corrosivity of the flowback fluid changes following an acid job a range of different test methodologies were used. This chapter outlines the material selection and sample preparation (which was the same across all tests). It then outlines the methodologies used for the closed vessel mass loss and electrochemistry tests. Finally, the newly developed closed vessel dilution test methodology is discussed.

4.2 Tubing Grade Steel Selection

As previously discussed coiled tubing strings are typically run through the production tubing and the acid is injected through them in order to protect the expensive production tubing from the highly corrosive acid. The tubing strings are chosen based upon the minimum yield strength required. For example HS80 a commonly used coiled tubing material has a minimum yield strength of 80,000psi [150].

There are many different coiled tubing grade steels which could be used in this work. However it was decided that just one tubing grade would be used in all tests for two main reasons.

1. A large amount of mass loss tests were performed. If several tubing grades had been tested the number of acid and inhibitor concentrations studied would have been drastically reduced.
2. The main focus of the work is to understand the effect of changing solution acidity and inhibitor concentration. By focusing on one tubing grade steel, it allows much easier direct comparison between all of the mass loss, electrochemistry and flow cell tests.

In order to validate that similar corrosion behaviour is observed for of a range of different tubing grade steels a series of initial mass loss tests were performed. These tests looked at the corrosivity of different HCl concentration solutions on three commonly used grades of coiled tubing.

4.2.1 HS80, HS90 and HS110 Comparison

The three tubing grade steels chosen to be tested were HS80, HS90 and HS110. All three are low carbon steels with a similar composition and microstructure. The steels vary in the amount of nickel, manganese and chromium each grade contains [85].

As an example, HS80 low carbon steel has the following composition 0.1-0.15% C, 0.6-0.9% Mn, <0.03% P, <0.005% S, 0.3-0.5% Si, 0.45-0.7% Cr, <0.4 Cu% and <0.25% Ni. HS80 has a ferrite/pearlite microstructure (the microstructure can be seen in Figure 4.1) with ferrite grain sizes between 5-10µm [85]. Due to the similarities between the three tubing grades it was hoped that they would exhibit similar corrosion rates when placed in different acid/brine mixtures.
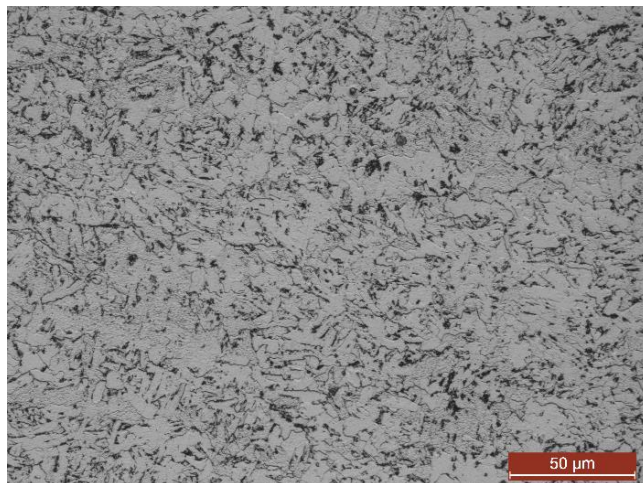
Figure 4.1 HS80 microstructure imaged by an optical microscope. The steel was etched using a 2% Nital solution.

4.3 Solution Composition

As discussed in Section 3.6, the flowback fluid chemistry is complex and constantly changing over the duration of the flowback. The HCl and PA concentration is known during injection to the reservoir (high strength HCl with a high inhibitor concentration). 1L of 4M HCl containing 540µL of PA (0.05wt.%) is used to replicate the injection strength acid. The HCl concentration of the flowback fluid is significantly less than the concentration of the injected acid. The 4M HCl solution was diluted with 4M sodium chloride

(NaCl) brine in order to give lower molarity solutions. The NaCl concentration of 4M was chosen in order to keep the chlorine concentration the same as the 4M HCl. This keeps the chlorine concentration of the solution constant for all tests. It was desirable to limit the number of variables in order to better understand how the solution corrosivity varies as the HCl and PA are diluted.

The 4M NaCl brine was produced by dissolving 234g/L of laboratory grade NaCl in distilled water. All tests were performed in 1L of solution and Table 4.1 shows the volumes of HCl, NaCl brine and PA used to make 1L of solution for each different HCl concentration tested. The inhibitor concentration of the solution is always relative to the acid concentration. Therefore the PA concentration in all tests is 0.05wt.% relative to the HCl concentration of the solution. As discussed in Section 3.6.2 the calcium and iron concentrations of the flowback fluid can vary greatly between individual acid jobs. Therefore, it was decided not to add iron and calcium to the solution as the aim of the initial tests is to understand how the corrosivity of the flowback fluid changes as the HCl and PA concentrations are diluted.

HCl Concentration (M)	Volume of 4M HCl (L)	Volume of 4M NaCl solution (L)	PA Volume (μL)
4	1	0	540
2	0.5	0.5	270
0.6	0.15	0.85	81
0.4	0.1	0.9	54
0.2	0.05	0.95	27
0.04	0.01	0.99	5.4
4×10^{-3}	1×10^{-3}	0.999	0.54
4×10^{-4}	1×10^{-4}	0.9999	0.054

Table 4.1 Solution composition for all HCl concentrations tested using the closed vessel test methodologies. All tests contain 0.05wt.% PA relative to the HCl concentration.

4.4 Mass Loss Methodology

4.4.1 Sample Preparation

Mass loss coupons were cut from sheets of tubing grade steels to give a surface area of 29±3cm² as shown in Figure 4.2. This area was chosen based on dimensions used in previous acidizing work [5, 85]. Prior to each test the mass loss coupons were wet-ground using 1200 grit silicon carbide paper, degreased with acetone, rinsed with distilled water and dried gently with compressed air.
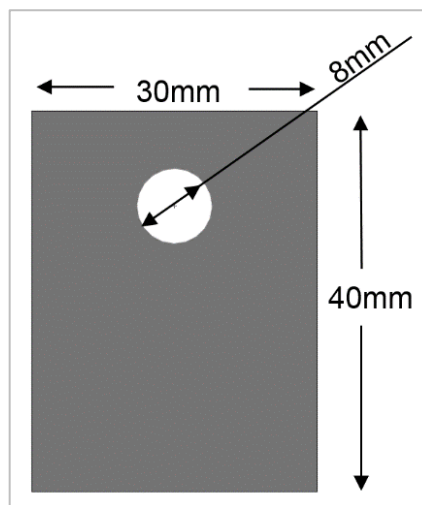
Figure 4.2 HS80 coupons used in the mass loss tests. The coupons were cut to a thickness of 4mm.

4.4.2 Test Outline

The experimental set-up is shown and annotated in Figure 4.3. For each mass loss experiment, the sample was placed in a glass beaker (with a sealed lid and a condenser) which contained 1L of a fixed concentration of HCl, NaCl brine and PA, the glass lid was specifically chosen as it had five ports. This allowed the electrochemistry and weight loss tests to be performed in the same vessel. The five ports are labelled in Figure 4.3 and were used for the following.

1. Condenser.
2. Temperature probe.
3. Bubbling CO_2 or N_2 if required.
4. Inserting electrochemistry and/or mass loss samples.
5. Combined counter and reference electrode.

For any tests where one or more ports were not required a glass stopper was used to seal it for the duration of the test. Each test solution was prepared using the volumes of HCl, NaCl brine and PA (the required volume was added using a pipette through port 4) shown in Table 4.1.

Before immersion of the test coupon, the solution was heated to 80°C using a hotplate (8) with a built in temperature controller (6) and stirred with a magnetic stirrer bar (7). The mass loss coupon dimensions were found using a set of Vernier calipers and an electronic balance was used to find the mass of the sample prior to it being placed in the solution. Throughout the experiment, the test solution was continuously stirred using the magnetic stirrer bar (7) to agitate the solution (caution was taken to prevent hydrodynamic effects on the steel surface).
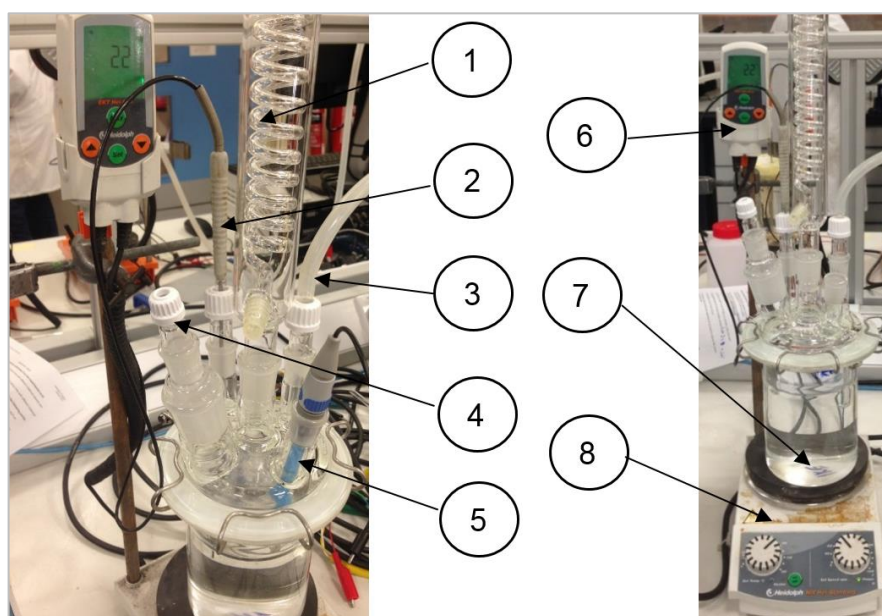
Figure 4.3 Experimental set-up for the mass loss and electrochemistry tests. Each component is labelled and discussed in the text.

No effort was made to remove dissolved oxygen from the solution and experiments were primarily performed for 3 hours but tests were also performed at shorter and longer exposure times (between 0.5-24 hours). An exposure time of 3 hours was used in several previous studies [5, 79, 99, 151] as it meets the recommendation made by ASTM G31 [147]. The standard recommends that the exposure time (in hours) should be equal to 2000 dived

by the corrosion rate in mils per year (mpy). A corrosion rate of 20mm/year (788mpy) provides a recommended test time of 3 hours (to the nearest hour).

At the end of each experiment, the sample was removed from the test solution, rinsed with distilled water and acetone and then dried gently with compressed air. The sample was then re-weighed. The determined mass loss was converted into a corrosion rate based on the dimensions of the sample prior to exposure to the test solution (Equation 4.1).

Tests were performed at the range of HCl concentrations shown in Table 4.1 with no inhibitor present and also in the presence of propargyl alcohol (PA) inhibitor. Further tests were performed where the PA concentration was varied from 5×10^{-3}-0.05wt.%. An important aspect to note here is that the PA concentration was again kept relative to the HCl concentration of the test solution in each experiment i.e. the PA concentration remained proportional to the total acid concentration of the system for all experiments. All inhibitor and HCl concentrations tested and the PA volumes added to the 1L test solution are shown in Table 4.2

PA Concentration (wt.%)	PA Volume (µL)			
	4M	2M	0.6M	0.2M
0.05	540	270	81	54
0.02	216	108	32.4	21.6
0.01	108	54	16.2	10.8
5×10^{-3}	54	27	8.1	5.4

Table 4.2 PA volume (µL) added to each different HCl and PA concentration tested. All tests contain 0.05wt.% PA relative to the HCl concentration.

4.4.3 Calculating the Corrosion Rate from Mass Loss Results

As mentioned previously the mass loss coupons were measured and weighed prior to each test being performed and then weighed after the exposure. The sample surface area, exposure time and mass loss were used to calculate the average corrosion rate of the sample over the 3 hour test. The corrosion rate can be calculated using Equation 4.1 [34].

$$Corrosion\ Rate = \frac{W \times k}{A \times T \times D} \qquad\qquad (4.1)$$

The corrosion rate is calculated from the mass loss (W) in grams, the sample area (A) in cm^2, the exposure time (T) in hours and the density (D) in g/cm^3. The density (D) of carbon steel is 7.8g/cm^3 [152] and in order to calculate a corrosion rate in mm/year a constant (k) of 8.76x10^4 is used in Equation 4.1 [34].

4.5 Electrochemistry Methodology

In addition to the weight loss tests, electrochemistry samples were also used to measure the corrosion rates associated with different HCl concentrations containing 0.05wt.% PA (again always relative to the HCl concentration). The test conditions, experimental set-up (shown in Figure 4.3) and solution preparation were identical to the mass loss tests. A mass loss coupon and two electrochemistry samples (with an exposed surface area of 1 cm² each) were used in the tests. The mass loss coupon was added to maintain approximately the same surface area to volume ratio as the mass loss tests.

The square samples used for the electrochemistry tests were cut to a size of 10mm x 10mm from HS80 tubing grade steel sheets. An electrical connection was achieved by soldering a copper wire to the one side of the specimen (Figure 4.4(a)) before mounting the samples in a non-conducting resin. The samples (shown in Figure 4.4(b)) were again wet-ground with 1200 grit silicon carbide abrasive paper, degreased with acetone, rinsed with distilled water and dried with compressed air prior to insertion into the glass cell.

In conjunction with the two working carbon steel working electrodes, a 4M Ag/AgCl reference electrode was used alongside a platinum counter electrode to form a standard three-electrode cell.
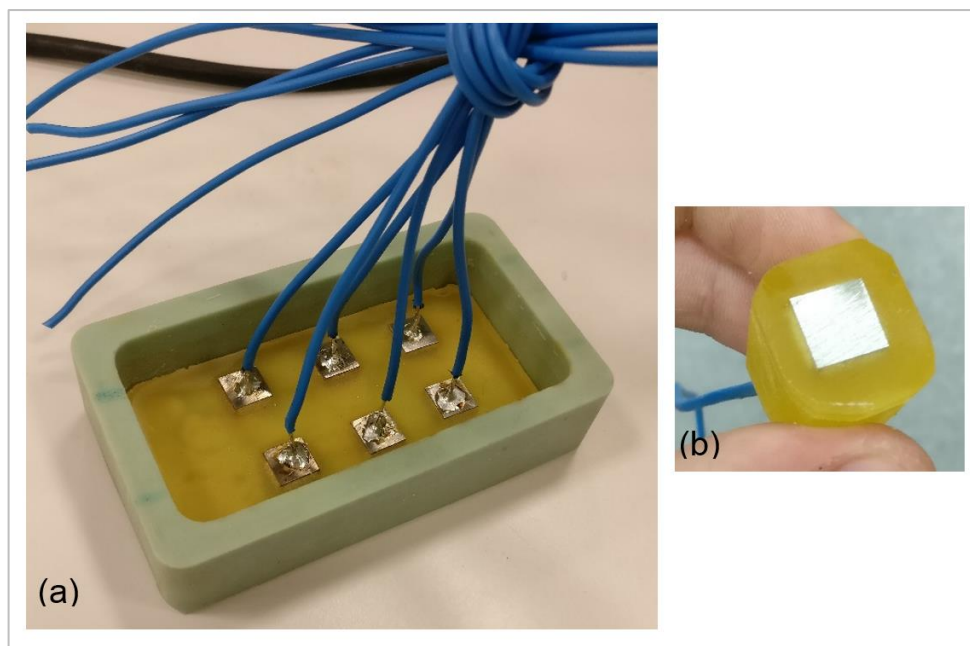
Figure 4.4 (a) Preparation of electrochemistry samples; 6 samples are shown with wires soldered to the back of each. (b) Electrochemistry sample after being wet ground using 1200 grit paper.

4.5.1 Fixed HCl Concentration Test Methodology

A variety of electrochemical tests were performed in order to understand how the corrosivity of the flowback fluid changes as the HCl concentration is reduced. In order to accurately calculate the corrosion rate, the charge transfer resistance (R_{ct}, found from LPR measurements), Tafel constants and solution resistance values had to be found for each of the different HCl concentrations tested.

The open circuit potential (OCP) of the samples was followed and allowed to stabilise for the first five minutes after which Linear Polarization Resistance (LPR) measurements were performed on each of the samples in turn i.e. performing sequential measurements on each sample. Each working electrode was polarised ±10 mV from the OCP at a scan rate of 0.25 mV/s. LPR measurements were performed on each sample every 15 minutes over the duration of the 3 hour test. The open circuit potential of the sample was measured between each of the LPR measurements.

At the end of each test AC impedance measurements were performed on each sample in order to determine the solution resistance. In addition,

cathodic and anodic Tafel polarisation plots were generated by polarising from the OCP to either ±250 mV at a scan rate of 0.5 mV/s. The cathodic sweep was generated first and the potential was scanned from OCP to -250mV, before switching to the second electrochemical sample to scan from OCP to +250mV, in order to generate the anodic Tafel. The solution resistance value and the measured anodic and cathodic Tafel slopes were used in conjunction with the polarisation resistance to determine the corrosion rates over each 3 hour experiment (as discussed in Section 2.2).

4.5.2 Calculating the Corrosion Rate from Electrochemical Results

Each 3 hour test provides all of the data required to calculate the corrosion rate of the sample using the corrosion theory outlined in Section 2.2.

4.5.2.1 The Solution Resistance and Tafel Constants

At the end of each test a potential of -250mV was applied to one of the two electrochemistry samples and the current response recorded in order to find the cathodic polarisation curve. A potential of +250mV was then applied to the second sample to give the anodic polarisation curve. The solution resistance (R_S, measured using AC impedance at the end of each test) and the current (I) measured in the polarisation tests was used to correct the voltage using Equation 4.2 [153].

$$V_{Corrected} = V - (I \times R_S) \tag{4.2}$$

The measured current (I) was plotted on a logarithmic scale against the corrected potential ($V_{corrected}$). The gradient of the linear regions of the anodic and cathodic polarisation plots provide the anodic and cathodic Tafel values (β_a and β_c) required to calculate the corrosion rate from the LPR measurements.

4.5.2.2 LPR Measurements and Calculating the Corrosion Rate

By applying a potential of ±10 mV from the OCP the polarisation resistance (R_p) can be found throughout the 3 hour tests. This value can then be used to

find the charge transfer resistance (R_{ct}) by subtracting the solution resistance (R_s), as shown in Equation 4.3.

$$R_p = R_{ct} + R_s \qquad (4.3)$$

The charge transfer resistance (R_{ct}) was then used to calculate the corrosion current density (i_{corr}) using Equation 4.4 [25].

$$i_{corr} = \frac{1}{2.303 R_{ct}} \times \frac{\beta_a \beta_c}{\beta_a + \beta_c} \qquad (4.4)$$

The corrosion current density (i_{corr}) in Amps/cm^2, was then used to calculate the corrosion rate (mm/year) using Equation 4.5.

$$Corrosion\ Rate = \frac{i_{corr} \times K \times EW}{d \times A} \qquad (4.5)$$

If the units shown in Table 4.3 are used for each value in Equation 4.5 then a constant (K) of 3,272 can be applied to provide a corrosion rate in mm/year [154, 155].

Symbol	Name	Unit	Value
i_{corr}	Corrosion Current	Amps	-
K	Constant	mm/(amp.cm.year)	3,272
EW	Equivalent Weight	grams/equivalent	27.92 [156]
d	Density	grams/cm^3	7.87 [156]
A	Sample Area	cm^2	1

Table 4.3 Values and units for each parameter shown in Equation 4.5 and used to calculate the corrosion rate of the carbon steel samples.

4.5.3 Dilution Test Methodology

In order to replicate the entire flowback dilution process in a single test a new test methodology was developed. A HS80 electrochemistry sample and a mass loss coupon (to maintain the acid to volume ratio) were placed in 1L of 4M HCl (containing 0.05wt.% PA). A peristaltic pump was used to deliver a controlled flow rate of 4M NaCl solution from the 10L container into the 1L vessel, resulting in a decrease in the HCl and PA concentration as a function of time. At the same time, an identical peristaltic pump was used to transfer the solution from the 1L vessel and into a waste container at an identical flow rate. Tygon tubing was used to transfer both solutions between vessels and to the waste container (the tubing was tested for chemical compatibility with 80ºC 4M HCl). Every effort was made to ensure that the flowrate remained constant throughout the duration of the experiment. This included using two identical peristaltic pumps with identical peristaltic tubing. Despite these efforts the maximum error in the flowrate throughout the dilution test was found to be ±5%. The flowrate was calibrated at the start of every test to ensure that the flowrate for both pumps was set to the required rate. At the end of every test the pump was tested to measure any potential fluctuation in the flowrate. The maximum change in flowrate from all tests performed was calculated at 5% (a 15ml/min starting pump rate was found to be pumping at rate of ~15.7ml/min at the end of the test).

It is vital to note that although the CO_2 concentration of the flowback fluid is a factor of significant importance, no CO_2 was bubbled in any experiments. The intention of the tests was to first gain an understanding as to how the HCl and PA concentration of the flowback fluid effects the corrosion rate of the steel tubulars. By bubbling varying quantities of CO_2 over the duration of the flowback experiments it further complicates the comparison between the HCl and PA. Initially a model chemistry was desired and these first dilution tests are intended to model the flowback process rather than simulating the true flowback environment. Potential tests involving a more realistic solution chemistry (to provide a more realistic representation of the flowback fluid) are discussed in greater detail in Section 9.4 (Future Work).

Figure 4.5 provides a schematic representation of the complete setup, the mass loss and electrochemistry sample were both placed in the 1L beaker. The 1L beaker was placed on a hotplate and heated to 80°C throughout the

duration of the test. A magnetic stirrer was used to ensure adequate mixing of the HCl and NaCl brine and caution was taken to prevent hydrodynamic effects on the steel surface. The NaCl solution was not heated prior to being pumped into the 1L vessel as it was found that at the flowrate tested (10ml/min), the dilution rate was not fast enough to cause any noticeable temperature drop of the solution throughout the test.
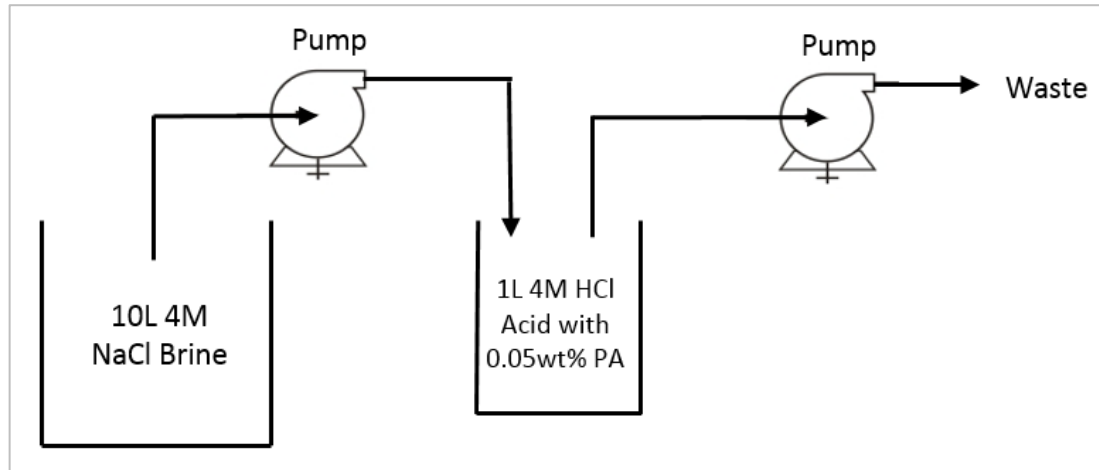
Figure 4.5 Schematic of the complete dilution test experimental setup. The HS80 samples were placed in the beaker containing the 4M HCl which was then diluted with 4M NaCl brine.

In order to ensure that the full dilution profile was captured the working electrode was polarised ±10 mV from the OCP at a scan rate of 0.25 mV/s every 5 minutes over the duration of the dilution test. The open circuit potential was recorded in-between each measurement. The R_p values, found from each of the LPR measurements performed throughout the duration of the dilution test, were used to calculate R_{ct} using Equation 4.3. The solution resistance value was found to range from 0.6-1.3Ω.cm^2 across all HCl concentrations tested and an average value of 1Ω.cm^2 was subtracted from the polarisation resistance (R_p) to calculate the charge transfer resistance (R_{ct}). The corrosion current density (i_{corr}) was then calculated from the R_{ct} values found throughout the duration of the dilution test. A range of Stern-Geary coefficients (maximum, minimum and average values) were used to calculate i_{corr} (Equation 4.3) and this is discussed in greater detail in Section 5.2.3. Each value of i_{corr} was used to calculate the corrosion rate (Equation 4.4). This allows the corrosion rate of the sample to be found throughout the duration of the entire dilution process when a range of different Stern-Geary coefficients are used.

4.5.3.1 Control of Dilution rates

As discussed in Section 3.6, the rate of dilution of the acid concentration of the flowback fluid depends upon the production rate and the quantity of unreacted acid existing in the wellbore. Figure 1.2 is a typical example of an acid flow-back profile measured in the field from Valdes et al. [6]. The aim of the dilution tests is to create an acid dilution profile similar to Figure 1.2 (a comparison between this profile and experimental flowrates is provided in Figure 4.8).

Within this particular system it is possible to control the rate of dilution of the 4M HCl by varying the speed of the two peristaltic pumps. Figure 4.6 and 4.7 show several dilution rates which can be achieved by varying the flow rate between 1 and 20ml/min, the dilution rate is expressed by Equation 4.6 where the acid molarity at a given time (C_t) is calculated from the initial acid molarity (C_0), the time in hours (t), the initial solution volume in litres (V) and the volumetric flow rate (Q) in L/s. Equation 4.6 shows the general dilution equation for a system with a fixed fluid volume [157].

$$C_t = C_0 e^{-\frac{Qt}{V}}$$

(4.6)

In order for the equation to be valid for a given system the following assumptions must be made.

1. The H^+ molarity of the dilution solution (4M NaCl brine) is significantly smaller than that of the diluted fluid (4M HCl).
2. Prefect mixing must occur in the second vessel (shown on Figure 4.5).

In order to understand which of the dilution rates shown in Figure 4.6 best represents the flowback profile from acid jobs in the field, a comparison between the four dilution rates and the profile provided by Valdes et al. [6] is shown in Figure 4.8. The profile provided by Valdes et al. provides six data points recorded once the production restarts. The first point recorded 0.5 hours after opening the well contained no acid. Therefore in order to allow for a better comparison the first point at which acid flows back is considered time 0. This allows the rate of dilution of the flowback fluid to be better compared to the four calculated dilution rates. Figure 4.8 shows that a similar dilution

profile, to that provided by Valdes et al. [6], is achieved when the solution is diluted at a rate of between 10-20ml/min.
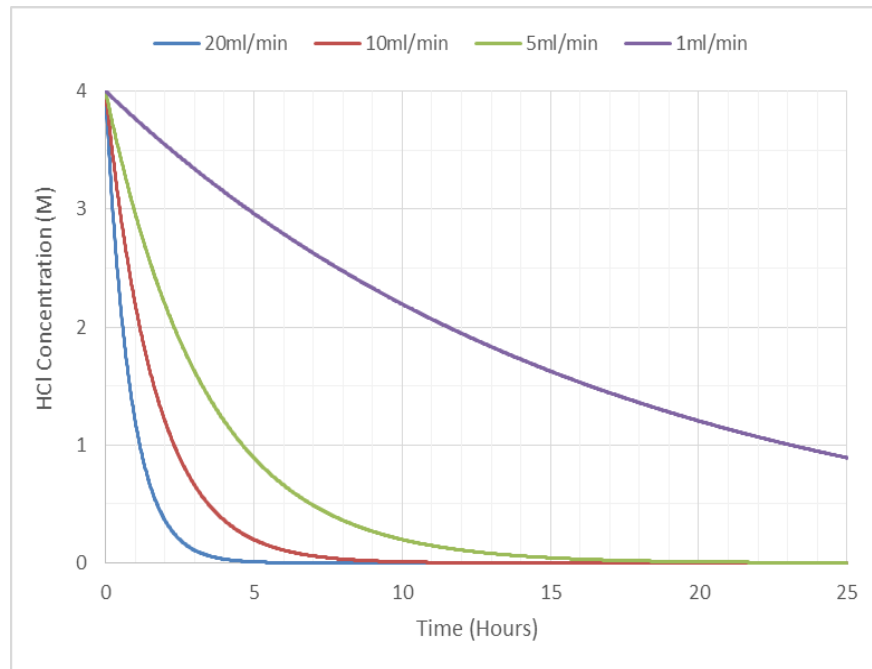
Figure 4.6 Concentration of HCl as a function of time for four flow rates on a linear concentration scale.
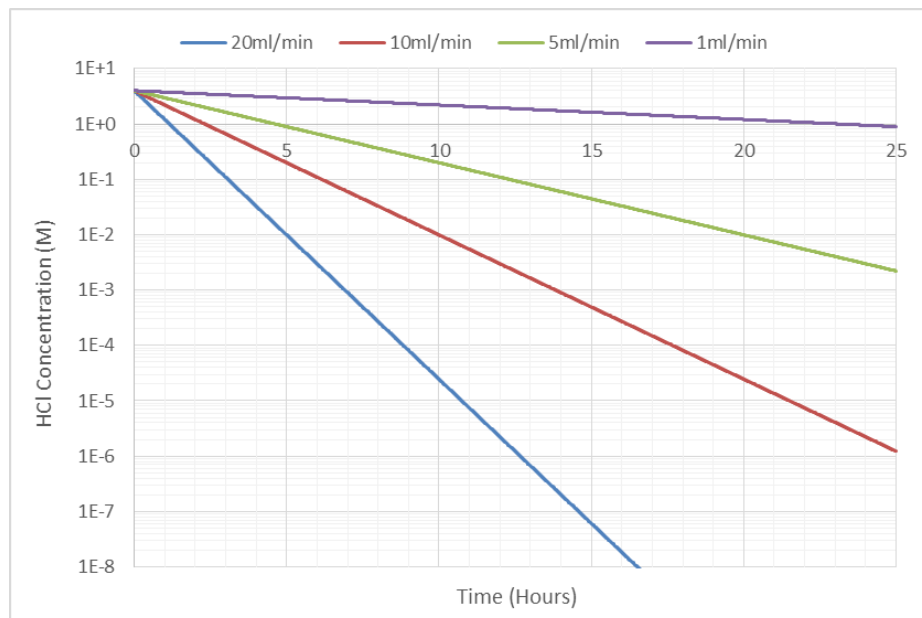
Figure 4.7 Concentration of HCl as a function of time for four flow rates on a log concentration scale.
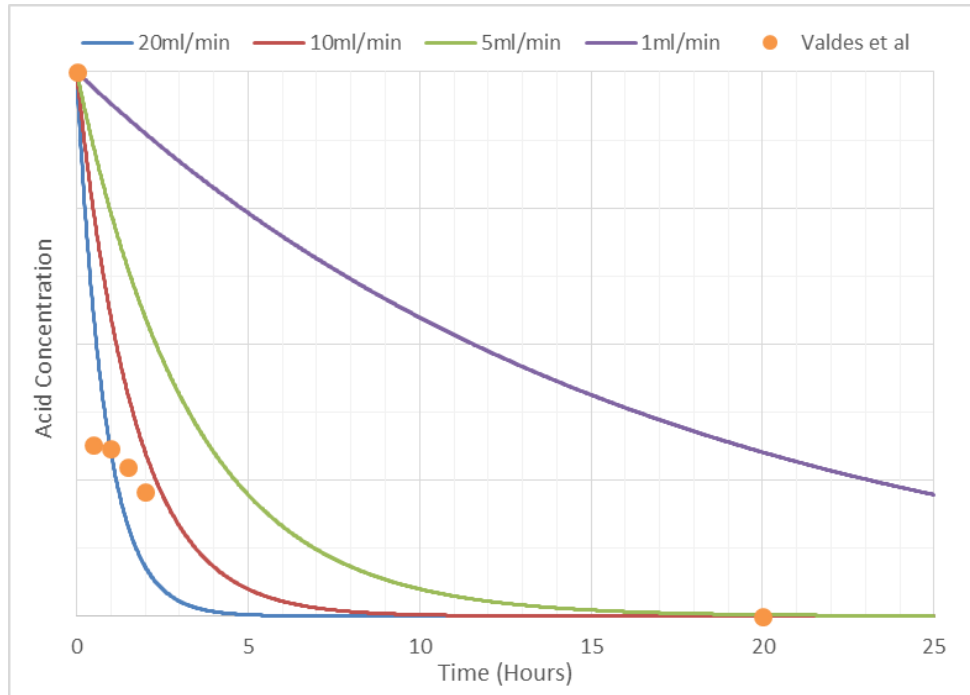
Figure 4.8 Comparison between the four potential dilution test profiles and the flowback profile from the field from Valdes et al. [6].

4.6 Surface Analysis Techniques

4.6.1 Surface Profilometry

An NPFLEX 3D interferometer was used to obtain the surface profiles of samples exposed to 4M HCl (with and without the addition of PA) for a range of different exposure times. For each sample three separate areas of 3mm by 3mm were analysed in order to provide a better representation of the surface roughness of the sample.

The three areas scanned on each sample are shown in Figure 4.9. An area of 0.5mm by 0.5mm along the edge of the sample was excluded from the scans. The software package, Vision 64, was used to determine the average surface roughness and produce both 2D and 3D profiles of the samples.
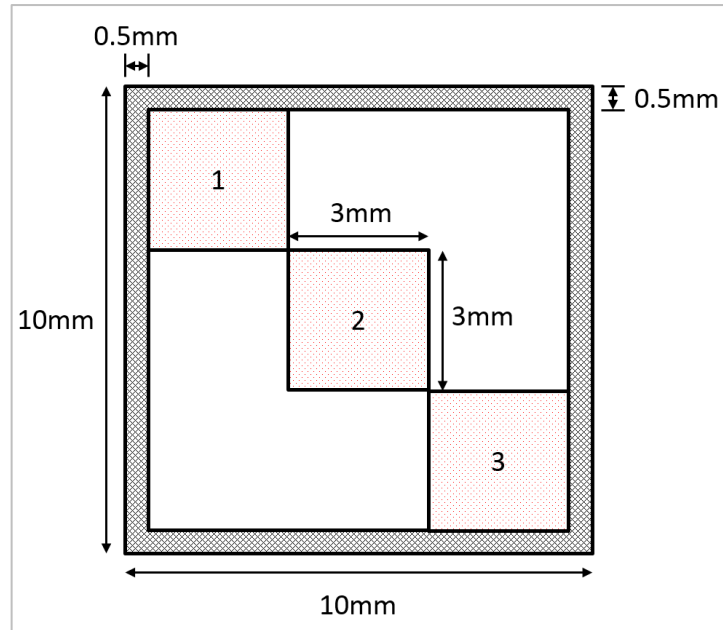
Figure 4.9 The location of the 3mm by 3mm areas (shown in red) on the HS80 samples that were analysed using the NPFLEX 3D interferometer. The area at the edge of the sample which was excluded from the scans is also shown.

4.6.2 Scanning Electron Microscopy (SEM)

A Carl Zeiss EVO MA15 scanning electron microscope was used to obtain topographic images of steel surfaces which were exposed to 4M HCl (with and without the addition of PA) for a range of different exposure times. All images were acquired using secondary electrons (at 20kV) at magnifications of 1,000 or 6,000 and a working distance of 9mm.

4.6.3 X-Ray Diffraction (XRD)

A Pananalytical X'pert multipurpose diffractometer (MPD) was used to study the material composition of samples exposed to 4M HCl but with and without PA inhibitor present. The measurements were performed using dual copper radiations (with 10 x 10mm programmable divergence slits) at a voltage of 40kV and a 40mA intensity. All scans were carried out in continuous mode in the angular region of $2\theta = 0\text{-}50^{\circ}$. The software package HighScore Plus was used for phase identification.

Chapter 5
Closed Vessel Mass Loss and Electrochemistry Results

A variety of mass loss and electrochemical tests were performed in closed beakers using the test methodologies discussed in Section 4.4 and 4.5. The aim was to understand how the corrosivity of the flowback fluid changes over time once production restarts following an acid job. The HCl and PA concentration of the flowback fluid were varied in order to replicate the dilution of the injected acid associated with the flowback process.

5.1 Mass Loss Results

5.1.1 Introduction

This chapter outlines a series of tests that were performed using the mass loss test methodology (Section 4.4) to test different molarity HCl solutions at varying inhibitor concentrations.

All mass loss tests were performed twice and the average value is presented in all of the results in this chapter, the scatter bands shown represent the maximum and minimum corrosion rates measured.

5.1.2 Corrosion Rates of Different HCl Concentrations on Different Tubing Grade Steels

As discussed in Section 4.2 there are several different coiled tubing grade steels which could be used in the mass loss and electrochemistry tests, however it was decided that just one tubing grade would be used in all tests. This was again in order to limit the number of experimental variables used throughout the work.

In order to validate that similar corrosion behaviour is seen for all tubing grade steels a series of mass loss tests were performed looking at the corrosivity of different HCl concentrations on three different grades of carbon steel tubing. As discussed in Section 4.2, HS80, HS90 and HS110 are three coiled tubing grade carbon steels used in acid jobs.

Each sample was exposed to four different HCl concentrations for 3 hours and the mass loss test procedure outlined in Section 4.4 was followed. Figure 5.1 shows the corrosion rates obtained from mass loss coupons made from each of the three tubing grade materials (HS80, HS90 and HS110).
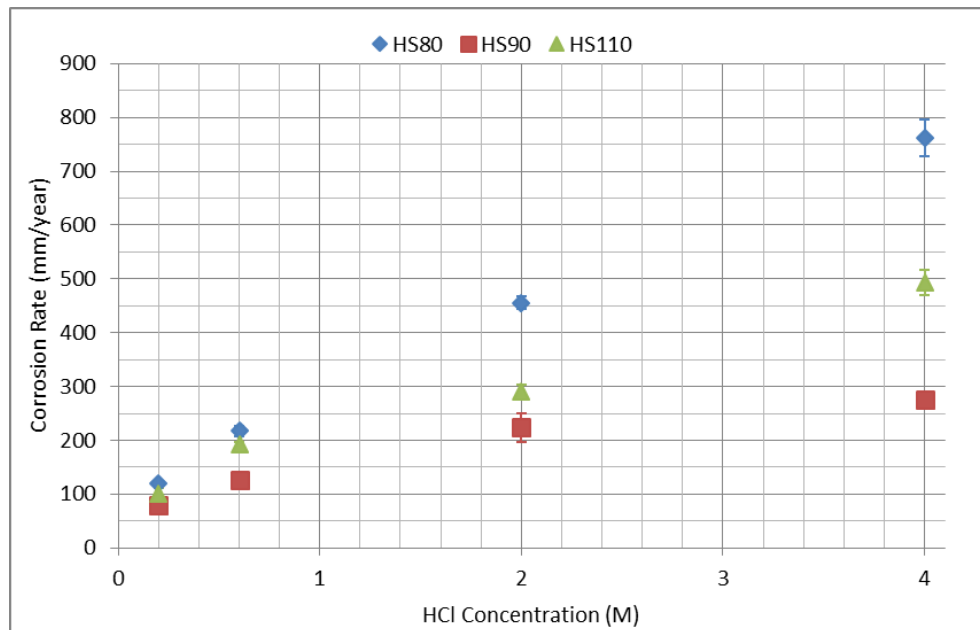
Figure 5.1 The corrosion rates obtained when mass loss coupons made from each of the three coiled tubing grade materials were placed in four different HCl concentration solutions (diluted with 4M NaCl brine) for 3 hours at 80°C. The scatter bands represent the maximum and minimum recorded corrosion rates across all 3 hour mass loss tests in each environment.

5.1.3 HS80 Corrosion Rates from a Greater Range of HCl Concentrations

Mass loss tests were performed using HS80 coupons at HCl concentrations less than 0.2M. This gives an understanding of the corrosivity of low molarity HCl solutions (without inhibitor present) encountered during flowback. Corrosion rates found from solutions containing from 4M to 4×10^{-4}M HCl are shown in Figure 5.2.
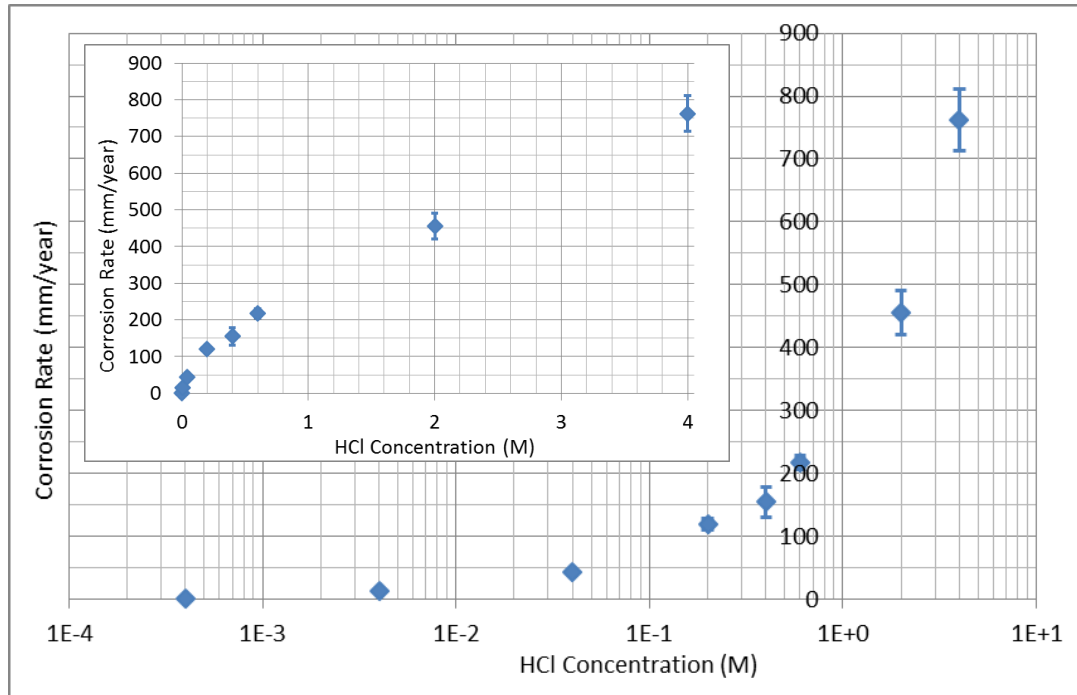
Figure 5.2 Corrosion rates found from HS80 mass loss coupons placed in a range of HCl solutions at 80°C for 3 hours. The HCl concentration is shown when plotted on both a linear and a log scale. The scatter bands represent the maximum and minimum recorded corrosion rates across all 3 hour mass loss tests in each environment. The HCl was diluted using 4M NaCl brine.

5.1.4 Effect of Propargyl Alcohol on HS80 Corrosion Rates in Hydrochloric Acid

All acids are injected with high concentrations of film-forming inhibitors, for all of these tests PA was used (as discussed in Section 4.3). These inhibitors protect the coiled tubing string from the high strength hydrochloric acid which is being injected into the reservoir. In order to gain a greater understanding of the corrosivity of the flowback fluid a range of inhibitor concentrations were tested. However it was important to first establish the corrosion rates associated with a high PA concentration of 0.05wt.%. This is a concentration which would typically be used when injecting the acid into the reservoir. In order to understand how the corrosion rate changes as the HCl molarity of the solution is reduced to very low values, mass loss tests were performed at the HCl concentrations shown in Table 4.1. All tests contained 0.05wt.% PA relative to the HCl concentration of the solution and the inhibitor volume in each test is also shown in Table 4.1. The corrosion rates at all molarities tested are shown in Figure 5.3 and 5.4 when the HCl concentration is plotted on a linear and a log scale respectively.
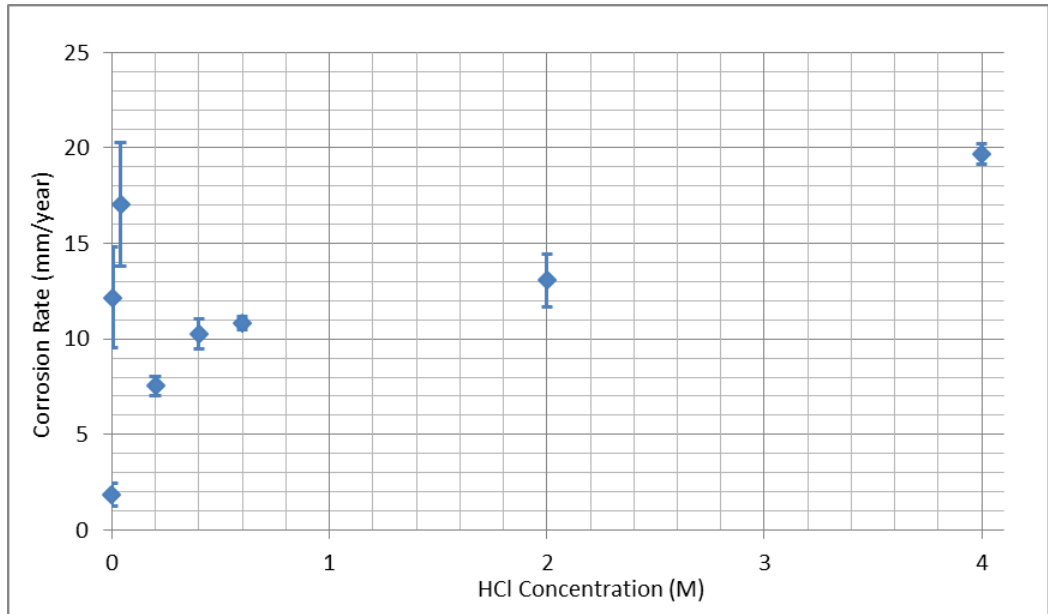
Figure 5.3 The corrosion rates obtained when HS80 mass loss coupons
were placed in different HCl molarity solutions (diluted using 4M NaCl
brine), all containing 0.05wt.% PA, for 3 hours at 80°C. The scatter
bands represent the maximum and minimum recorded corrosion rates
across all 3 hour mass loss tests in each environment. The HCl
concentration has been plotted on a linear scale.
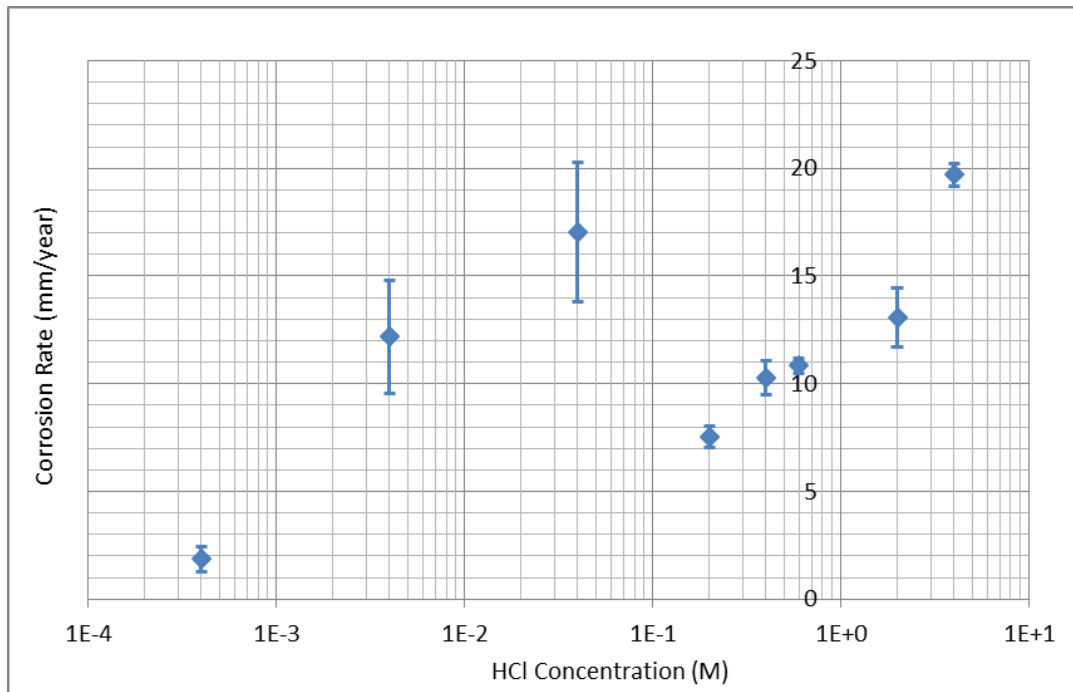
Figure 5.4 Corrosion rates found from 3 hour mass loss tests performed at
80°C in a range of different HCl concentrations (diluted using 4M NaCl
brine) with 0.05wt.% PA. The scatter bands represent the maximum
and minimum recorded corrosion rates across all 3 hour mass loss
tests in each environment. The HCl concentration has been plotted on
a log scale.

5.1.5 Effect of Varying Inhibitor Concentration on Corrosion Rate of HS80

In order to understand how the corrosion rate changes as the PA concentration is reduced three additional inhibitor concentrations were tested; 0.02wt.%, 0.01wt.% and 5×10^{-3}wt.% (relative to the HCl concentration of the solution). Figure 5.5 shows the corrosion rates for each of these four inhibitor concentrations at four different HCl concentration solutions.
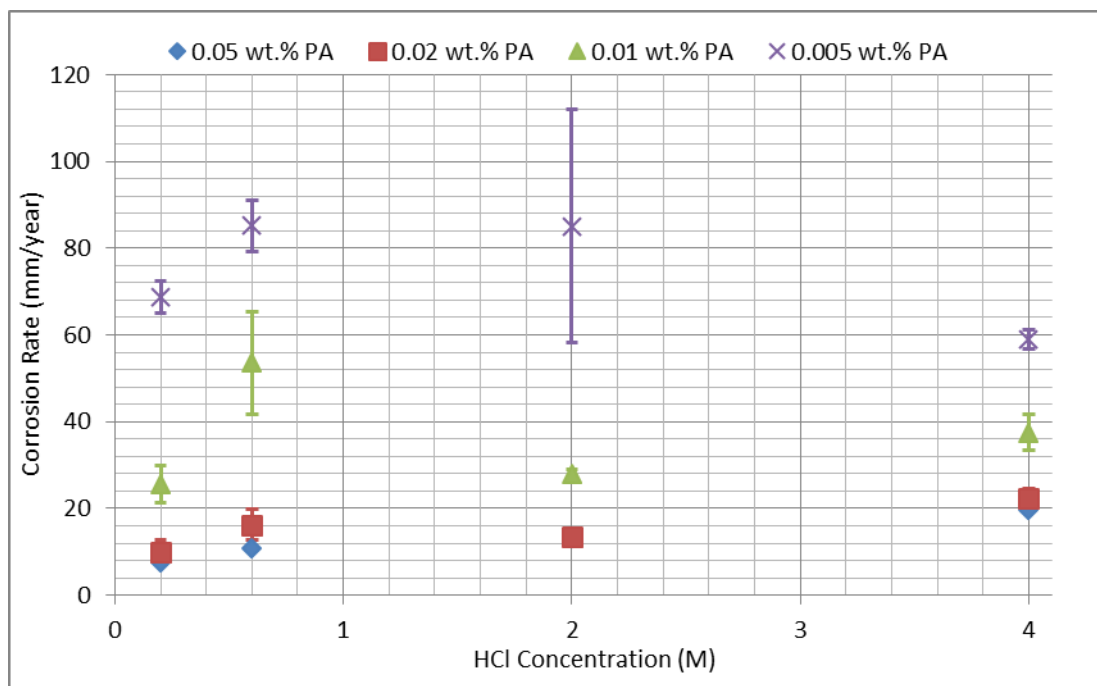
Figure 5.5 The corrosion rates obtained when HS80 mass loss coupons were placed in HCl solutions (ranging from 4M-0.2M) at four different PA concentrations (0.05-5×10^{-3}wt.%) at 80°C for 3 hours. The scatter bands represent the maximum and minimum recorded corrosion rates across all 3 hour mass loss tests in each environment. The HCl was diluted using 4M NaCl brine.

5.1.6 Effect of Varying Sample Exposure Time on the Corrosion Rate of HS80

With regards to the mass loss tests the number of different variables and therefore how much information can be gained is limited. The main three variables are the HCl concentration, inhibitor concentration and the exposure time. The 3 hour tests provide an average corrosion rate over the duration of the 3 hour test with no appreciation of how this corrosion rate may vary with time. In order to gain a greater understanding of how the corrosion rate changes throughout the mass loss tests the sample exposure time was

decreased. A high PA concentration of 0.05wt.% was chosen as this gave the most consistent results when the coupon was placed in all four of the different molarity HCl solutions. The aim of varying the exposure time was to gain an understanding of how the corrosion rate changes over the first 0.5, 1 and 3 hours of the mass loss test. Figure 5.6 shows how the corrosion rate changes with exposure time.
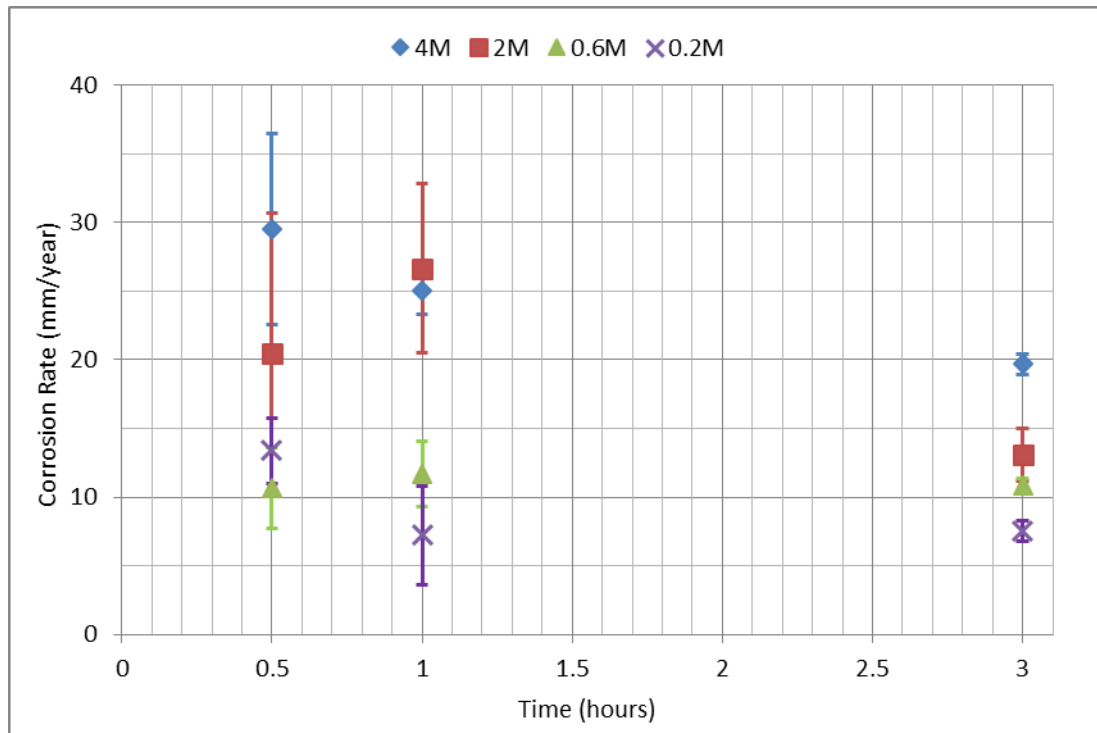
Figure 5.6 The corrosion rates obtained from HS80 mass loss coupons exposed to four HCl concentrations (all containing 0.05wt.% PA) at 80°C for three different exposure times. The scatter bands represent the maximum and minimum recorded corrosion rates across all mass loss tests in each environment.

In order to further understand how the corrosion rate changes with exposure time, mass loss coupons were placed in 4M HCl (containing 0.05wt.% PA) for exposure times longer than 3 hours. Figure 5.7 shows the corrosion rates calculated from these longer exposures. The shorter exposure times of 0.5 and 1 hour (shown in Figure 5.6) are also plotted on Figure 5.7. The corrosion rates found for exposures longer than 3 hours showed very little variation. Therefore no further HCl or PA concentrations were tested at these longer exposure times.
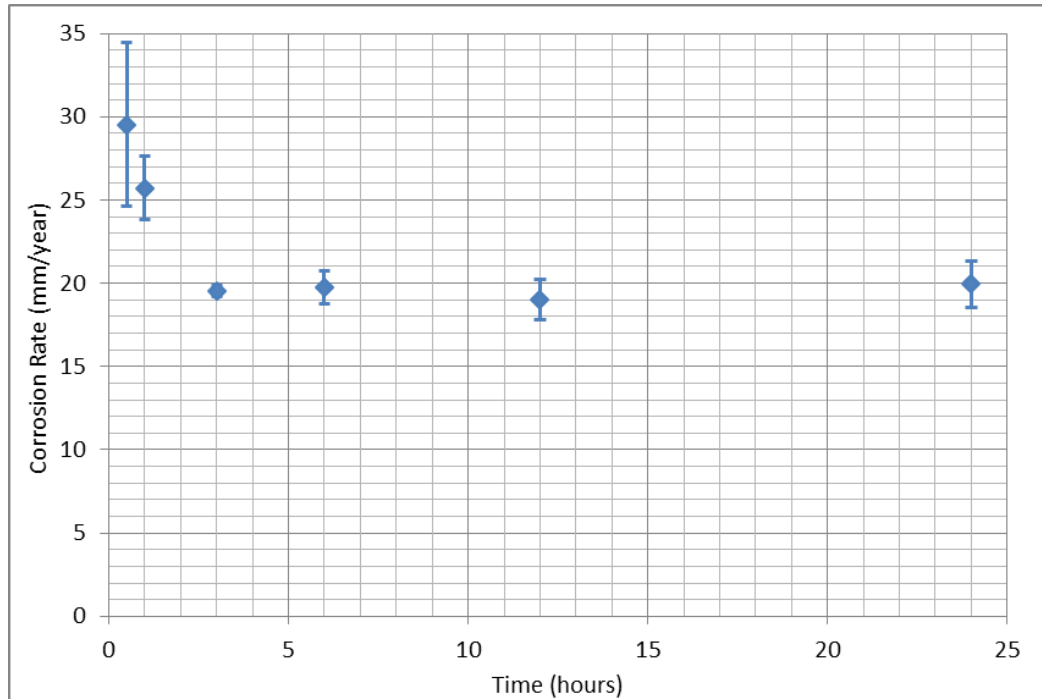
Figure 5.7 The corrosion rates obtained from HS80 mass loss coupons
exposed to 4M HCl (containing 0.05wt.% PA) at 80°C for six different
exposure times (0.5-24 hours). The scatter bands represent the
maximum and minimum recorded corrosion rates across all mass loss
tests in each environment.

5.1.7 Post Test SEM Images

5.1.7.1 Effect of Sample Exposure Time

Samples were placed in 4M HCl (containing 0.05wt.% PA) before being
removed after 3, 6, 12 and 24 hours. The detailed methodology is provided in
Section 4.6.2. The SEM images taken of these samples after exposure to the
4M HCl are shown in Figures 5.8-5.11.

Figure 5.8 shows a comparison between a sample exposed to 4M HCl both
with and without the addition of PA. Figures 5.9-5.11 show samples exposed
to 4M HCl (containing 0.05wt.% PA) for longer exposure times.
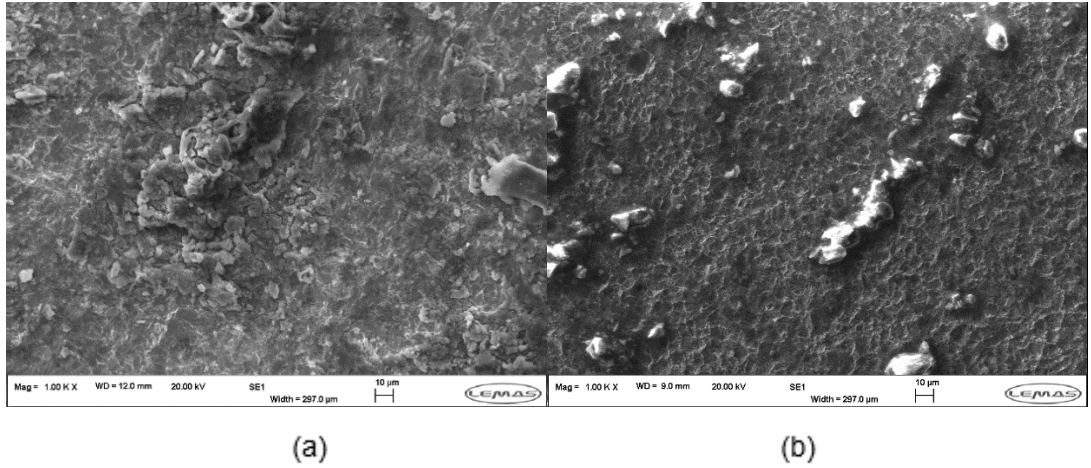
Figure 5.8 SEM images of a sample exposed to uninhibited 4M HCl (a) and a sample exposed to 4M HCl, containing 0.05wt.% PA (b) for 3 hours.
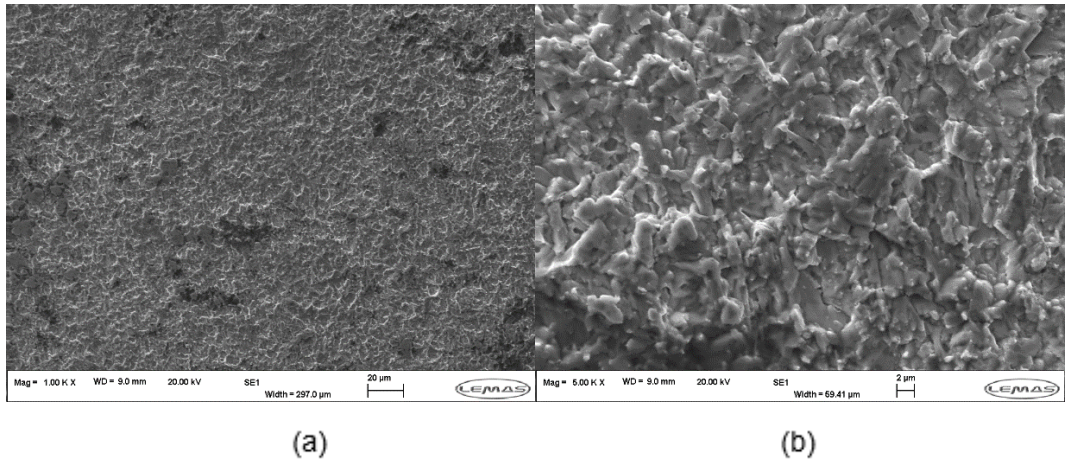
Figure 5.9 SEM images of a sample exposed to 4M HCl, containing 0.05wt.% PA, for 6 hours at magnifications of 1,000 (a) and 5,000 (b).
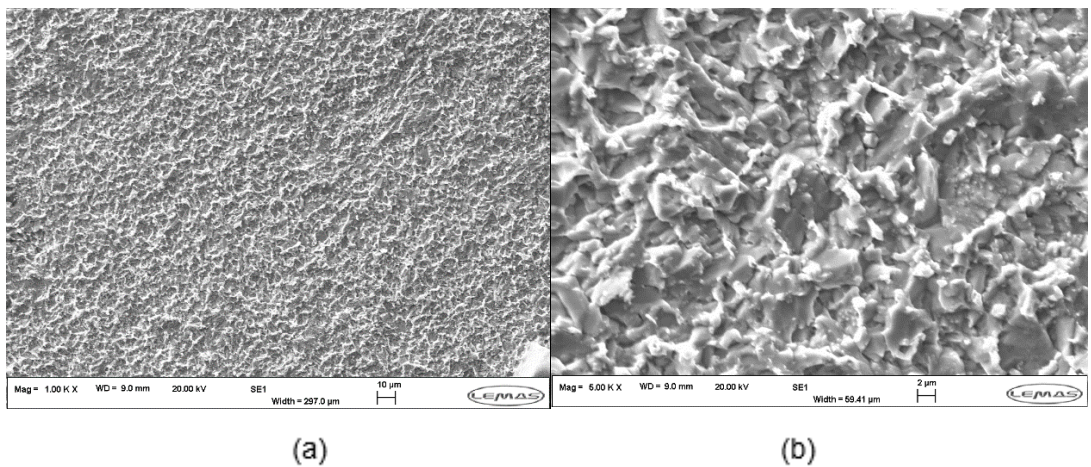
Figure 5.10 SEM images of a sample exposed to 4M HCl, containing 0.05wt.% PA, for 12 hours at magnifications of 1,000 (a) and 5,000 (b).
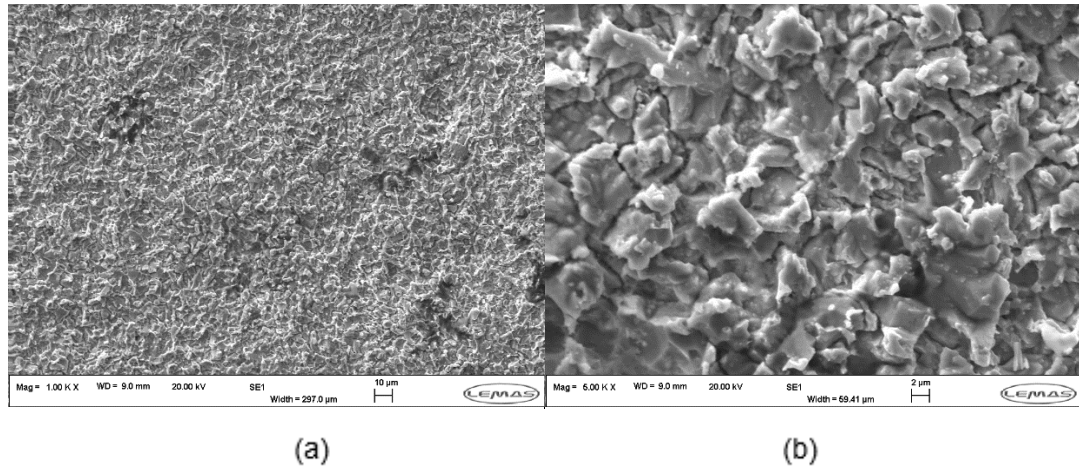
Figure 5.11 SEM images of a sample exposed to 4M HCl, containing 0.05wt.% PA, for 24 hours at magnifications of 1,000 (a) and 5,000 (b).

5.1.8 Post Test White Light Interferometry

A NPFLEX 3D interferometer was used to profile samples which had been exposed to 4M HCl (containing 0.05wt.% PA) for a range of exposure times. For each sample three separate 3mm by 3mm areas were analysed (as described in Section 4.6.1). One of these 3mm by 3mm areas (labelled number 2 on Figure 4.9) is provided for each of the exposure times along with the X and Y profiles across the centre of these areas in Figure 5.12-5.15.
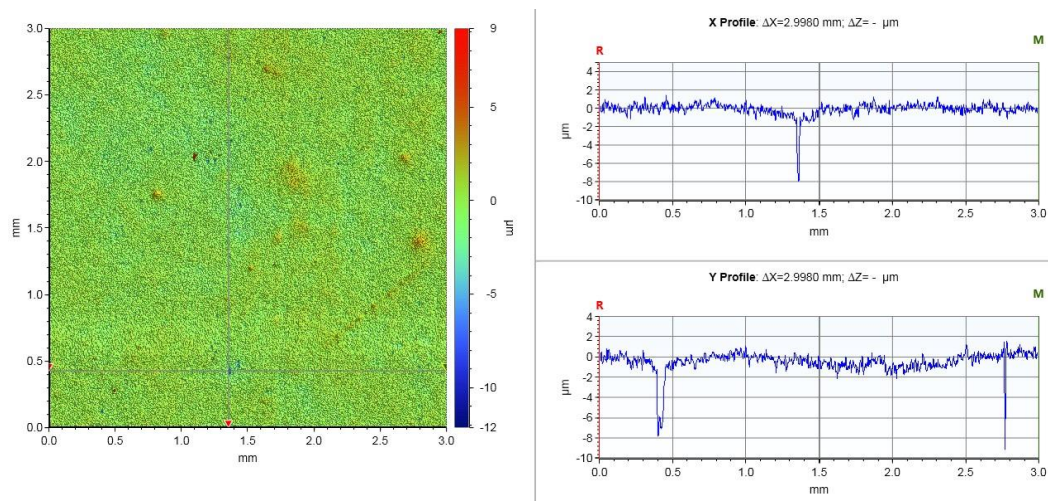
Figure 5.12 Surface profile of a sample exposed to 4M HCl, containing 0.05wt.% PA, for 3 hours.
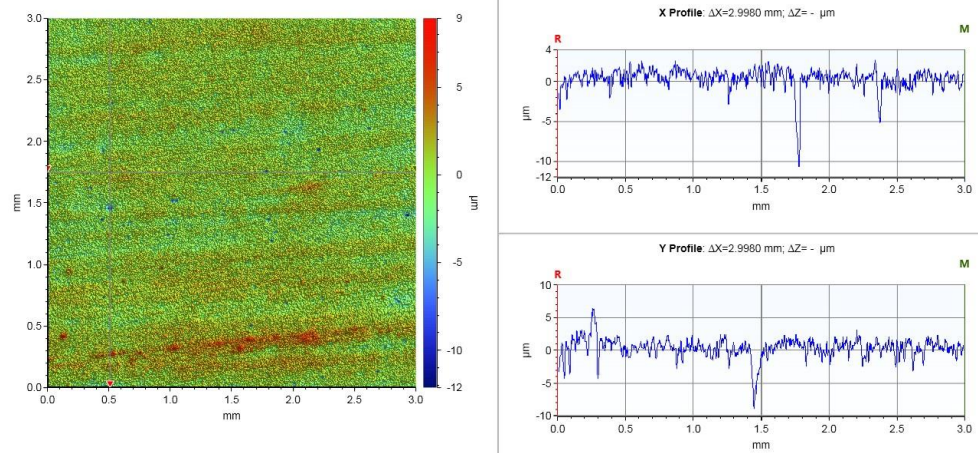
Figure 5.13 Surface profile of a sample exposed to 4M HCl, containing 0.05wt.% PA, for 6 hours.
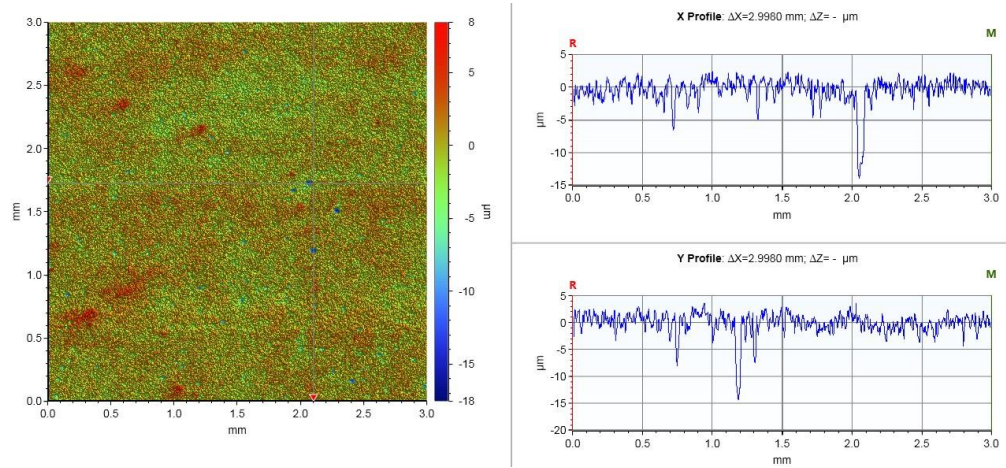
Figure 5.14 Surface profile of a sample exposed to 4M HCl, containing 0.05wt.% PA, for 12 hours.
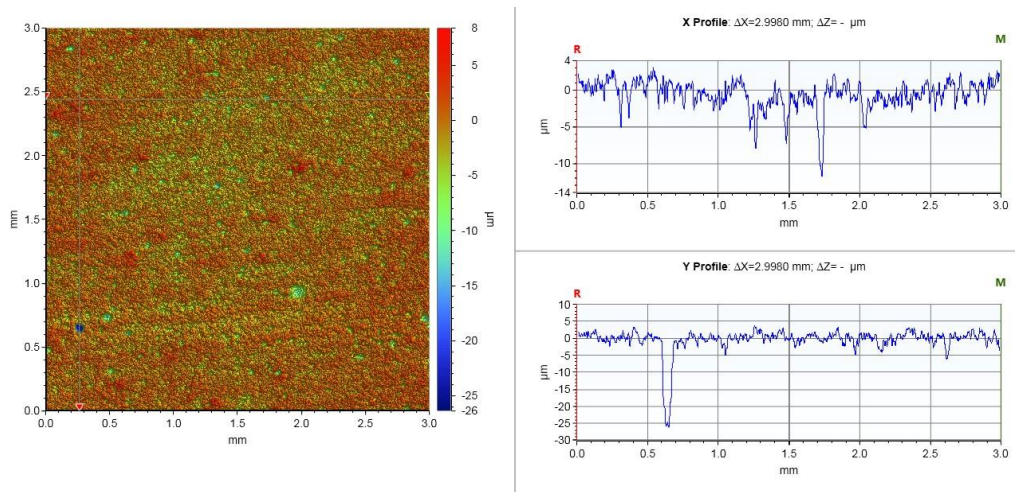
Figure 5.15 Surface profile of a sample exposed to 4M HCl, containing 0.05wt.% PA, for 24 hours.

5.1.8.1 Localised Corrosion Rates

The localised pitting rates were calculated for each of the exposure times shown in Figures 5.12-5.15. Figure 5.16 shows the variation in localised corrosion rate as the exposure time to the 4M HCl (containing 0.05wt.% PA) increases. The localised corrosion rate was calculated using the average localised depth of the top 10 deepest pits.
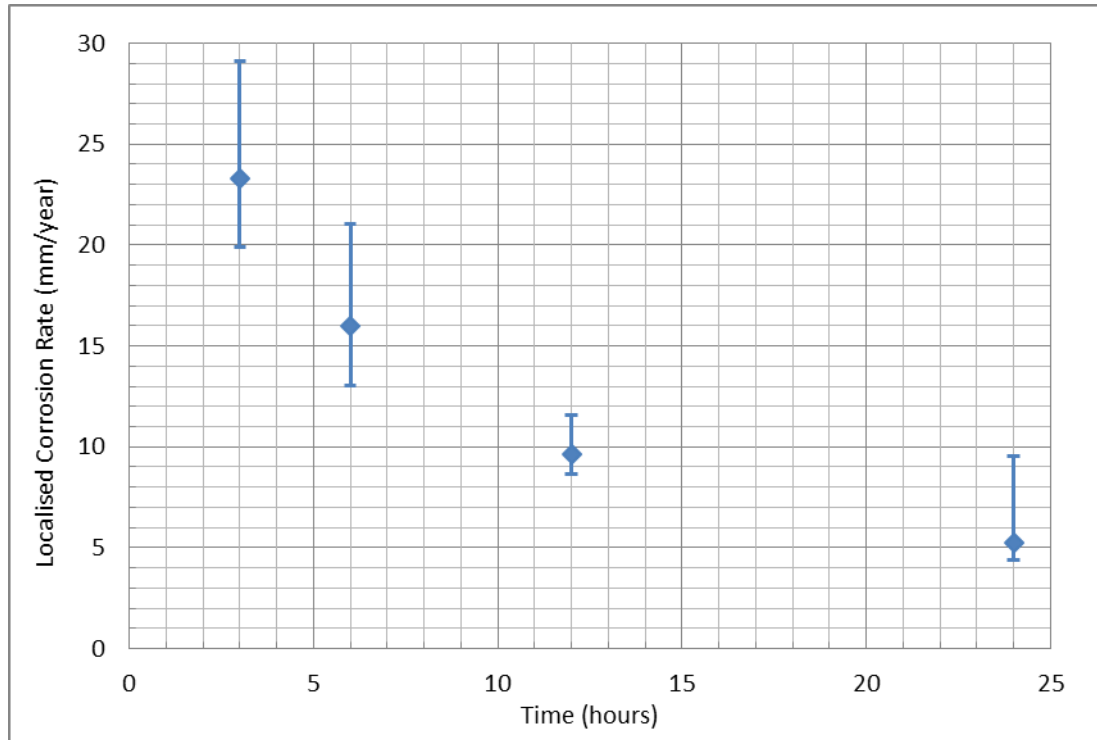
Figure 5.16 Localised corrosion rates for samples exposed to 4M HCl, containing 0.05wt.% PA, for different exposure times. All tests were performed at 80°C. The scatter bands represent the maximum and minimum measured pits (from the top 10 deepest pits).

5.1.9 X-Ray Diffraction

X-Ray diffraction (XRD) was performed on samples exposed to 4M HCl for 3 hours with and without 0.05wt.% PA present (Figure 5.17-5.18). The X-ray diffraction was performed to validate that no corrosion products formed on the steel surface once the sample had been removed from the HCl. Further details regarding the XRD methodology are provided in Section 4.6.3.
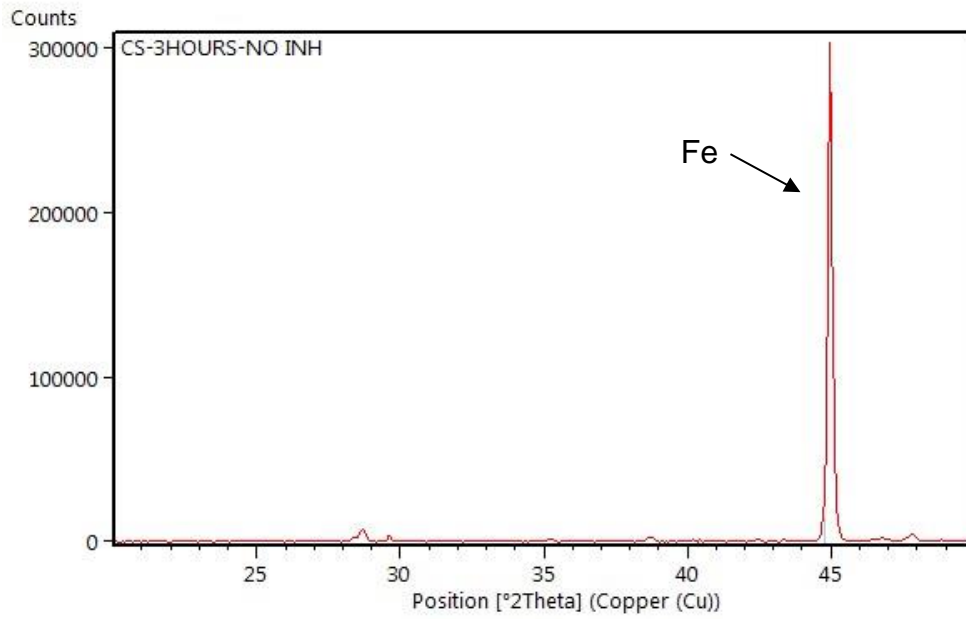
Figure 5.17 Results from X-Ray Diffraction performed on a sample after 3 hours of exposure to 4M HCl, the iron (Fe) peak has been labelled.
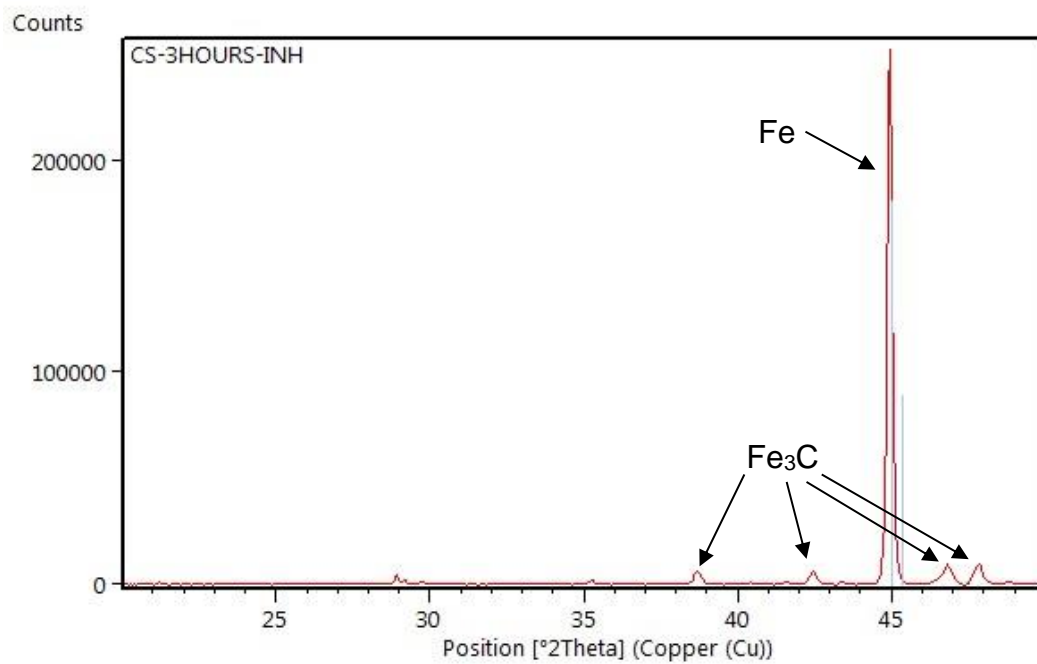
Figure 5.18 Results from X-Ray Diffraction performed on a sample after 3 hours of exposure to 4M HCl containing 0.05wt.% PA, the iron (Fe) and iron carbide (Fe_3C) peaks have been labelled.

5.2 Mass Loss Advantages and Limitations

5.2.1 Introduction

The mass loss results presented in Section 5.1 are incredibly useful for gaining an initial understanding as to how both the HCl and PA concentrations of a solution affect the corrosion rate of carbon steel tubulars. There are several benefits to using mass loss coupons to calculate the corrosivity of HCl solutions. It is however vital to acknowledge the limitations of the mass loss methodology and the results obtained from each of these tests and recognise how these limitations may potentially be overcome through the use of other techniques to measure the corrosion rate of the steel sample.

5.2.2 Benefits of Mass Loss Tests

There are several benefits to using the mass loss coupons over electrochemistry and it is vital to first outline these before discussing the limitations of the technique.

1. Unlike electrochemical techniques, corrosion rates found from mass loss coupons do not require the correct Tafel constants to be found in order to calculate the correct corrosion rate. This is important when considering that the tests performed are in a wide range of different HCl molarities and it is possible that the Tafel slopes may change as the HCl concentration of the solution is diluted.

2. In addition to the above point it is also possible that the Tafel slopes may change over the course of the test. Even for short 3 hour tests the solution chemistry is constantly changing as inhibitor and HCl react at an unknown rate over the duration of the tests.

3. Based on the potential fluctuation of the Tafel slope values, the mass loss measurements can be said to be the only methodology that provides definitive corrosion rates.

5.2.3 Mass Loss Limitations

Mass loss tests are intended to test the corrosivity of solutions with a fixed HCl and PA concentration for a given exposure time. This is not a problem when testing the corrosivity of the injected HCl, which is injected at a fixed HCl and PA concentration. Unfortunately when considering flowback from an acid job this is no longer the case as the solution chemistry is constantly changing over time.

5.2.3.1 Test Length Limitations

As discussed in Section 4.4, mass loss tests should be performed for a length of time based upon the corrosion rate of the sample, as per the recommendations of ASTM G31 [147]. Longer term tests can cause potential problems with acid spending over time. As soon as the coupon comes into contact with the HCl the molarity of the solution reduces as the H^+ reacts. Therefore concerns should be raised over the true molarity of solutions over longer duration tests. As discussed in Section 3.6 it can be up to 20 hours before the acid content of the flowback fluid returns to the levels seen prior to the acid job being performed, much longer than standard mass loss tests.

Mass loss tests provide an average corrosion rate calculated over the duration of the test. Therefore mass loss tests give no appreciation as to how the corrosion rate of the sample varies over the duration of the test. In order to try understand how the corrosivity of a solution changes over time a large number of mass loss tests would have to be performed at a range of different exposure times.

5.2.3.2 Limitations of Changing Solution Molarity

One of the main difficulties of trying to accurately replicate the flowback process is the fact that in the field the chemistry of the flowback fluid is constantly changing. As discussed in Section 3.6, once production resumes following an acid job large quantities of unspent acid can potentially flow back. The flowback fluid composition changes drastically as more formation fluid and spent acid is produced and the solution molarity reduces over time. The concentration of other species (carbon dioxide, calcium, etc.) also increase over the duration of the flowback.

It is impossible to monitor how the corrosivity of the flowback fluid changes using the mass loss methodology. The nature of the tests means that the sample must be placed in a solution of fixed chemistry for the duration of the mass loss test. Therefore, in order to fully replicate the flowback process using the mass loss methodology an impractical number of tests would have to be performed at a very large number of HCl concentrations. These tests would also fail to take into account the effect that exposing the sample to the initial high molarity flowback fluid has upon the tubing. This initial exposure to a

solution with a high HCl concentration is almost certainly going to have corrosion implications upon the steel tubulars. This is missed by the mass loss tests performed at lower HCl molarities.

5.2.4 Use of Mass Loss to Validate Electrochemical Corrosion Rates

There are clearly both advantages and disadvantages to using mass loss tests to analyse the corrosivity of flowback fluid. Therefore the most comprehensive way to characterise the flowback fluid is to perform both mass loss and electrochemical measurements and use the two techniques to complement each another. The mass loss corrosion rates are of huge importance in confirming the validity of the electrochemical measurements. Once the correct Tafel constants have been applied at each different HCl molarity they should show high agreement with the mass loss results presented in Section 5.1. This will help to validate the corrosion rates found using electrochemistry. If the corrosion rates found from the electrochemistry are not supported by the mass loss results then the ability of this technique to find the corrosivity of the flowback fluid should be questioned.

5.3 Closed Vessel and Dilution Test Real Time Electrochemistry Results

5.3.1 Introduction

This section outlines a series of electrochemical tests which were performed in order to give a greater understanding (and to allow direct comparison with the mass loss results) of the corrosivity of flowback fluids. All electrochemical tests were performed in the presence of inhibitor. A range of acid molarities and exposure times were tested at a PA concentration of 0.05wt.%. A new dilution test methodology, as outlined in Section 4.5.3, was used to more accurately replicate the changing HCl concentration observed throughout flowback following an acid job. All corrosion rate measurements were performed on separate samples and the corrosion rate results presented in this section are the average values calculated from the two tests with the error bar showing the maximum and minimum corrosion rate.

5.3.2 Tafel Slope and Solution Resistance Measurements

In order to be able to calculate the corrosion rates of samples placed in a range of different HCl molarity solutions it is first vital to gain an understanding as to how the anodic and cathodic Tafel constants change as the HCl concentration of the solution is varied. In order to correct the results from the anodic and cathodic polarisation tests the solution resistance (as discussed in Section 4.5) was found at the end of each test.

5.3.2.1 Solution Resistance Values

Solution resistance values were found using the test methodology outlined in Section 4.5. The solution resistance value was found to range from 0.6-1.3Ω.cm^2 across all HCl concentrations tested (4M to 4×10^{-4}M). The solution resistance was compensated for in all polarisation tests.

5.3.2.2 Anodic and Cathodic Tafel Slope Measurements

Table 5.1 presents the Tafel constants and the calculated Stern-Geary coefficients (as outlined in Section 4.5) for solutions containing 8 different HCl concentrations (with 0.05wt.% PA relative to the HCl concentration).

HCl Concentration (M)	β_a (mV/decade)	β_c (mV/decade)	Stern-Geary Coefficient
4	35	210	13.0
2	40	200	14.5
0.6	45	180	15.7
0.4	50	150	16.3
0.2	40	110	12.8
0.04	60	110	16.9
4×10^{-3}	30	-	13.0
4×10^{-4}	30	-	13.0

Table 5.1 Anodic and cathodic Tafel constants and the calculated Stern-Geary coefficient for 8 different HCl molarities.

The Tafel constants shown in Table 5.1 were found from the polarisation plots presented in Figure 5.19. The anodic and cathodic polarisation tests were performed on separate samples after 3 hours of exposure to the solution (full details of the experimental methodology can be found in Section 4.5). The polarisation data was corrected for the solution resistance values as outlined in Section 4.5.2. Figure 5.20 shows an example of how the β_a and β_c values were calculated.
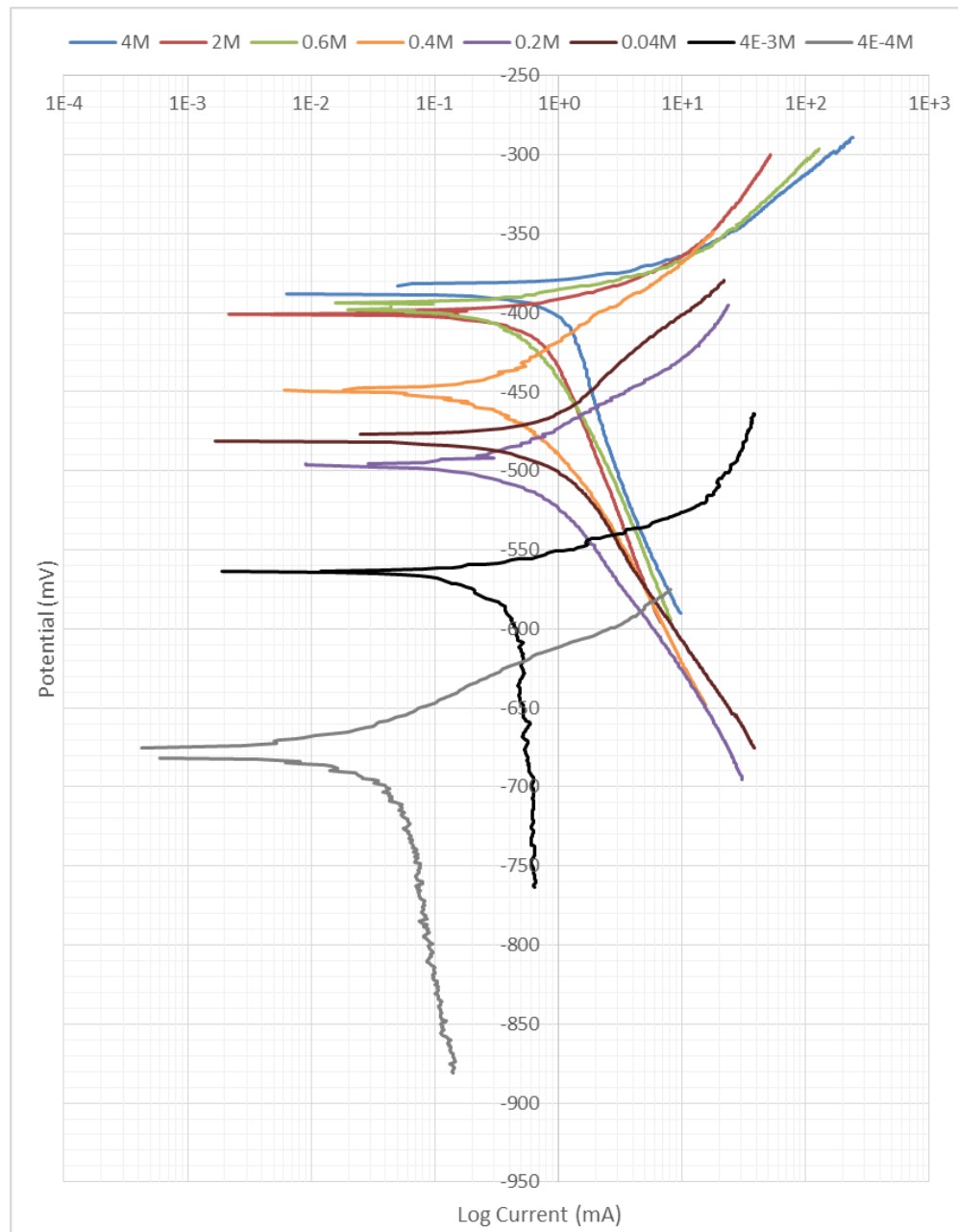
Figure 5.19 Anodic and cathodic polarisation test results performed in solutions containing from 4M to 4x10^{-4}M HCl (diluted using 4M NaCl brine) and 0.05wt.% PA (relative to the HCl concentration) at 80°C.
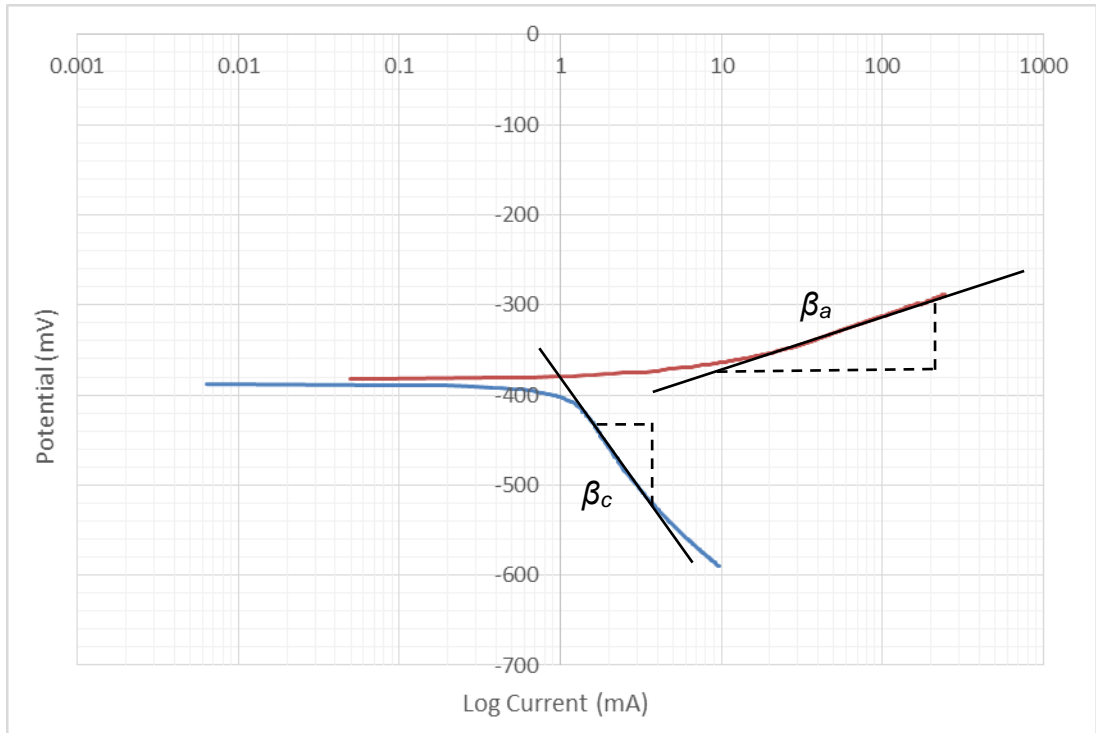
Figure 5.20 Example anodic (red) and cathodic (blue) Tafel slopes from the polarisation test performed in 4M HCl solution with 0.05wt.% PA (relative to the HCl concentration) at 80°C.

Figure 5.19 suggests that the cathodic polarisation is diffusion limited for the two lowest HCl concentrations ($4x10^{-3}$ and $4x10^{-4}$M). As discussed in Section 2.2.5, the rate of the mass transport of protons to an iron surface limits the rate of corrosion in dilute hydrochloric acid solutions [24]. This can be seen by the cathodic polarisation curves measured in the most dilute HCl solutions. Due to the gradient of the cathodic Tafel slope tending towards values significantly larger than the anodic slope, the Stern-Geary coefficient at these HCl concentrations is calculated using just the anodic Tafel constant (β_a), as shown in Equation 2.25 [35, 36].

Figure 5.21 shows that a range of different Tafel slopes could have potentially been used based on the anodic and cathodic polarisation data for the tests performed in 4M HCl (containing 0.05wt.% PA). Therefore a range of possible Stern-Geary coefficients can potentially be calculated for each of the HCl concentrations tested. The Stern-Geary coefficients shown in Table 5.1 are found from the average of the maximum and minimum possible Stern-Geary coefficients. Therefore for each HCl concentration tested there is a maximum and minimum Stern-Geary coefficient which could potentially be used to calculate the corrosion rate. The maximum possible Stern-Geary coefficient

was found from polarisation tests performed in 0.04M HCl. By using the maximum possible anodic (65mV/decade) and cathodic (155 mV/decade) Tafel slopes at this HCl concentration the maximum possible Stern-Geary coefficient from all possible tests can be calculated (19.9). The minimum possible Stern-Geary coefficient was measured in the test performed in 0.2M HCl. Similarly, the minimum possible anodic (35 mV/decade) and cathodic (95 mV/decade) Tafel slopes at this HCl concentration are used to find the minimum possible Stern-Geary coefficient (11.1). These values are used throughout the thesis to provide the maximum and minimum possible corrosion rates in tests where the HCl concentration of the solution changes throughout the test.
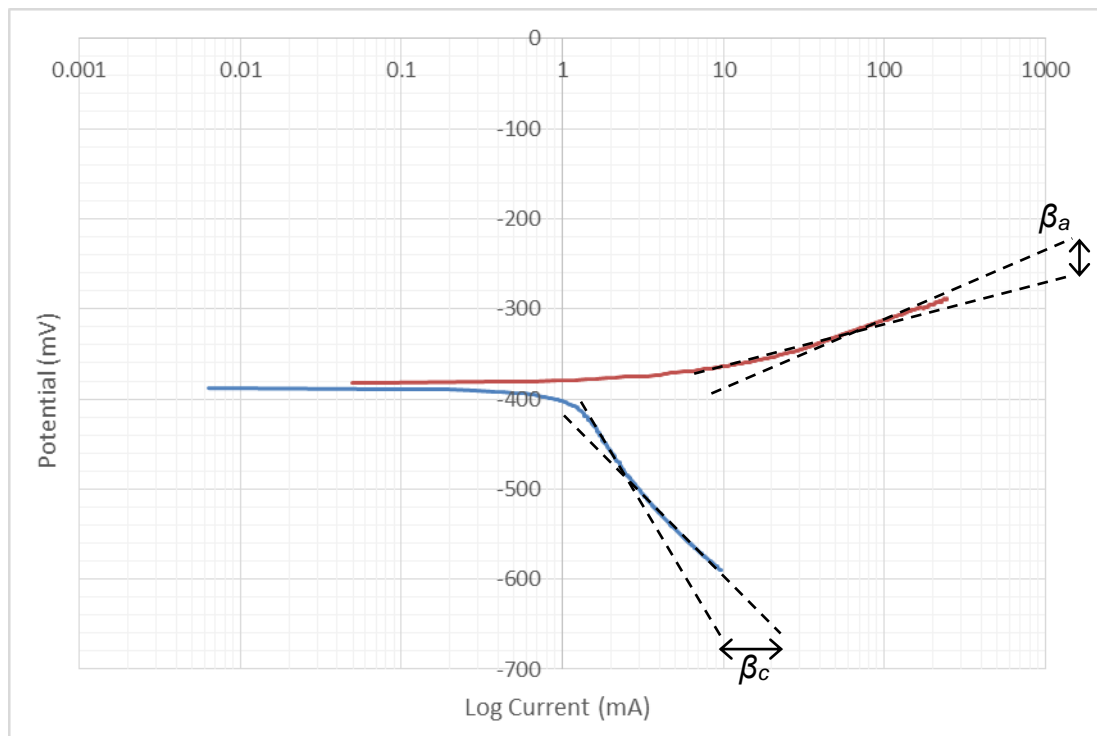
Figure 5.21 Example anodic (red) and cathodic (blue) Tafel slopes from the polarisation test performed in 4M HCl solution with 0.05wt.% PA (relative to the HCl concentration) at 80°C. The dashed lines show the range of possible Tafel slopes which could be drawn.

5.3.3 Variation of Tafel Constants over Time

Another potential issue with calculating the corrosion rate from the charge transfer resistance (R_{ct}) arises from the Stern-Geary coefficients changing throughout the duration of longer term tests. In order to better understand how the Tafel plots change over time, anodic and cathodic polarisation tests were

performed at the end of 6, 12 and 24 hours exposure to 4M HCl containing 0.05wt.% PA. Each test was performed separately and the anodic and cathodic polarisation tests were performed on a separate sample. This provides an important understanding as to how the Tafel constants change over the duration of longer term tests. The Tafel constants were found from the polarisation plots presented in Figure 5.22. Again, the polarisation data was corrected for the solution resistance. Table 5.2 displays the Tafel constants and the calculated Stern-Geary coefficients for the different exposure times. The variation in Stern-Geary coefficient for exposure times between 3-24 hours is minimal (12-13.9). However this variation further emphasises the cautions that should be taken when calculating corrosion rates from tests longer than 3 hours.
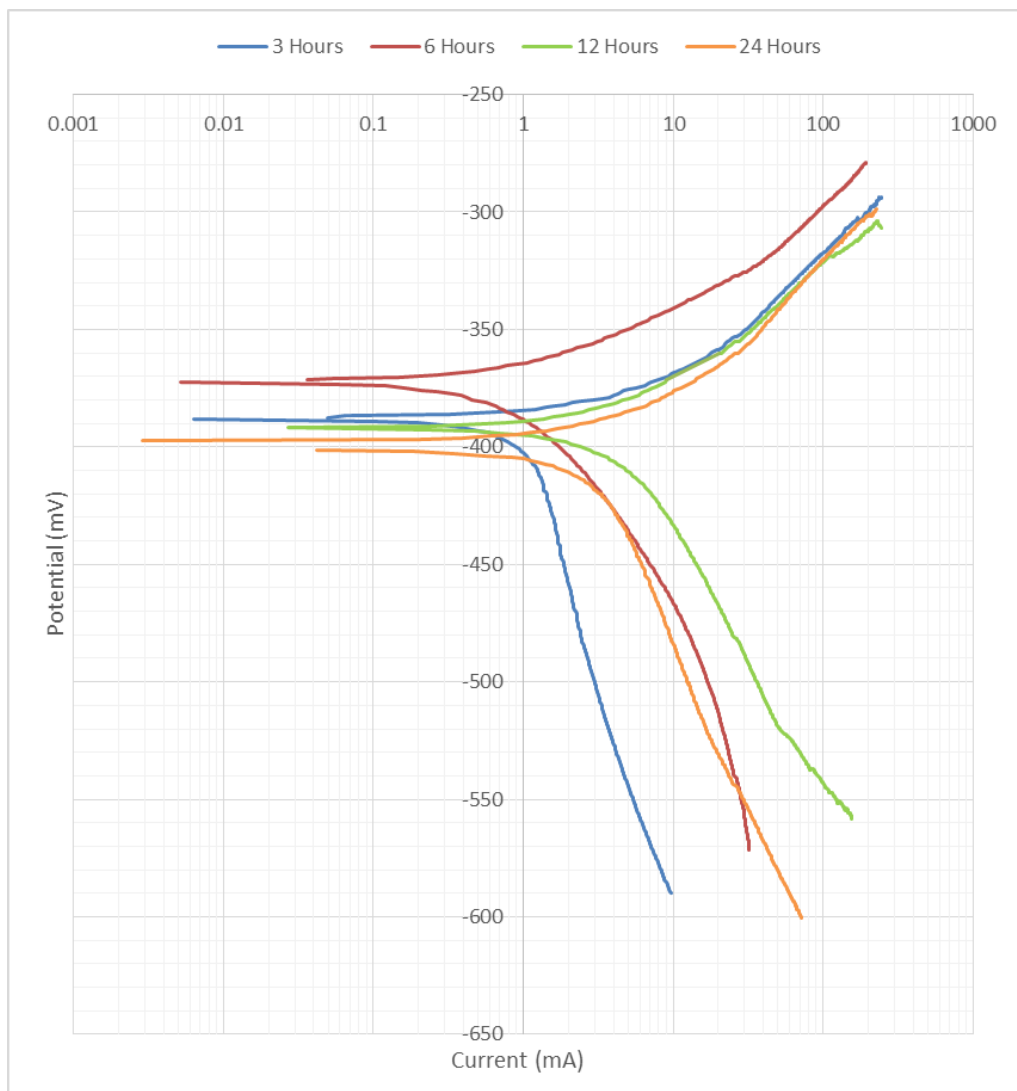
Figure 5.22 Comparison between anodic and cathodic polarisation tests performed in 4M HCl solution with 0.05wt.% PA after four different exposure times (3-24 hours) at 80°C.

Exposure Time (Hours)	β_a (mV/decade)	β_c (mV/decade)	Stern-Geary Coefficient
3	35	210	13.0
6	35	130	12.0
12	40	130	13.3
24	40	160	13.9

Table 5.2 Anodic and cathodic Tafel constants (β_a and β_c) and the calculated Stern-Geary coefficient for three different exposure times to 4M HCl containing 0.05wt.% PA.

5.3.4 Variation in Solution Corrosivity found from LPR Measurements

Linear Polarisation Resistance (LPR) measurements were performed on samples every 15 minutes over the 3 hour test duration. As discussed in Section 2.2.4 care should be taken when applying Stern-Geary coefficients to calculate the corrosion rate. Therefore in order to eliminate these issues and still provide an appreciation as to how the solution corrosivity varies over the duration of each test the reciprocal of the charge transfer resistances ($1/R_{ct}$) is plotted instead. The reciprocal of the charge transfer resistance is used as electrochemical theory shows that it is proportional to the corrosion rate [158]. Figure 5.23 shows how the reciprocal of the charge transfer resistances ($1/R_{ct}$) varies over the duration of 3 hour tests performed at a range of fixed HCl concentrations (4-4×10^{-4}M). The average value from two tests is shown and the scatter bands represent the maximum and minimum values measured at that time.

Despite the aforementioned problems, in order to allow a direct comparison with the mass loss results the reciprocal of the charge transfer resistance must be converted into a corrosion rate. The Stern-Geary coefficient shown in Table 5.1 was used to calculate the corrosion rates using the polarisation resistance value found from the LPR measurements. This is discussed in more detail in Section 4.5. The variation in corrosion rate over the 3 hour test for 4M to 4×10^{-4}M HCl solutions containing 0.05wt.% PA are shown in Figure 5.24.
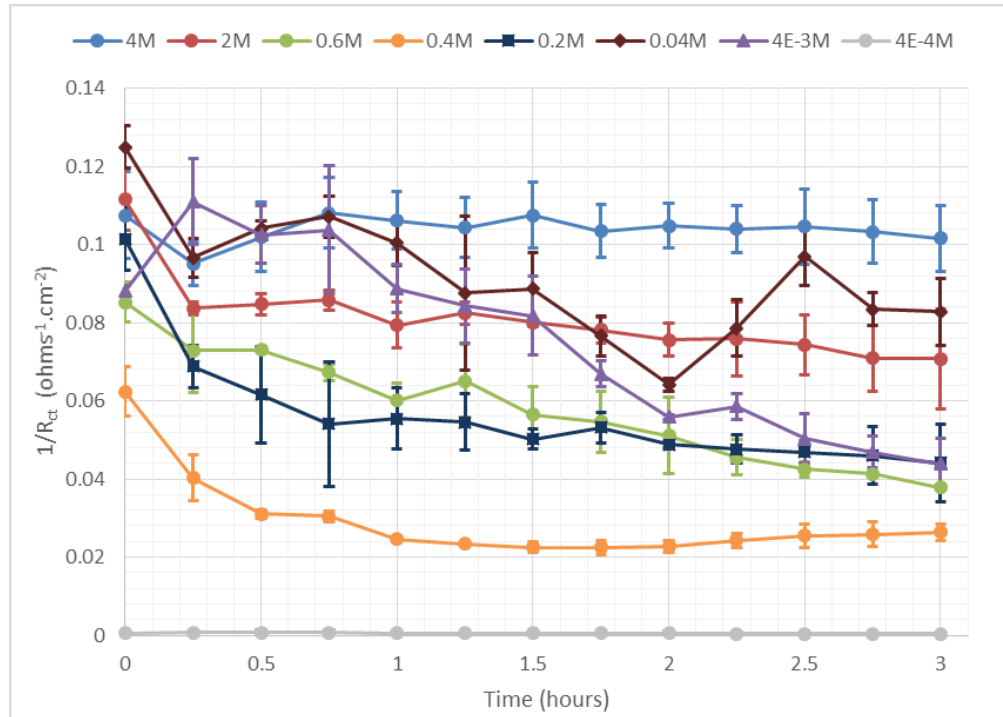
Figure 5.23 The reciprocal of the charge transfer resistances (1/R_{ct}) measured using HS80 exposed to different HCl concentrations (diluted using 4M NaCl brine), containing 0.05wt.% PA at 80°C for 3 hours. The scatter bands represent the maximum and minimum values measured in separate tests.
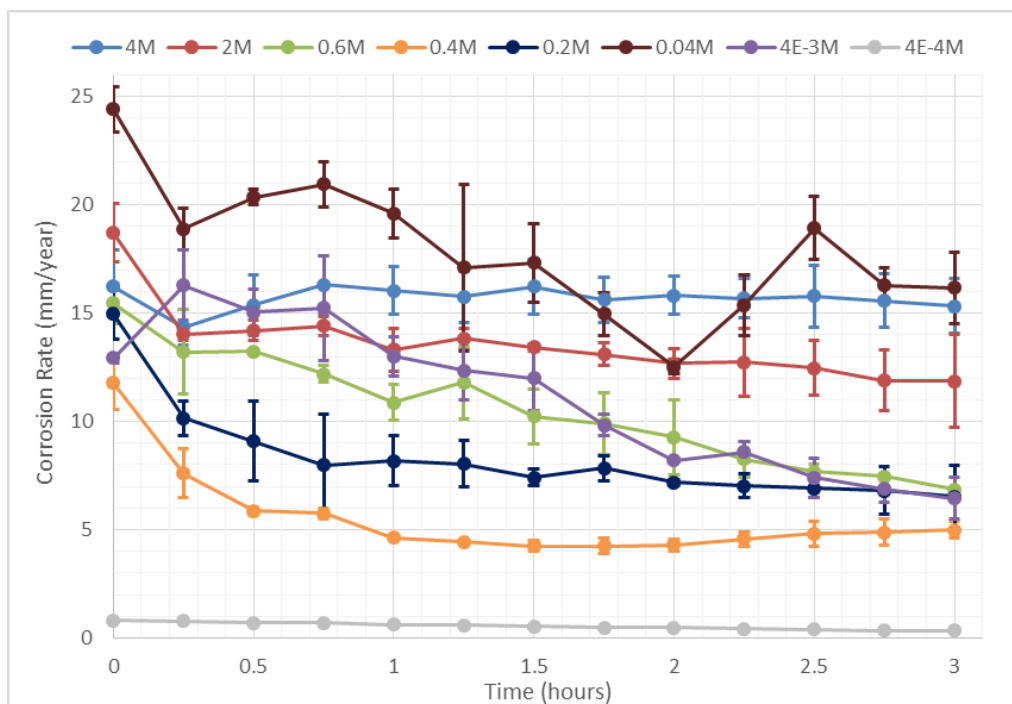
Figure 5.24 Corrosion rates over 3 hour exposure times to different HCl concentrations (diluted using 4M NaCl brine), containing 0.05wt.% PA at 80°C. The scatter bands represent the maximum and minimum values measured in separate tests

5.3.5 Dilution Tests

In order to understand how the corrosivity of the solution varies over the duration of the flowback process a new test methodology was developed. LPR measurements were performed every 5 minutes over the duration of the 18 hour dilution tests. A sample was placed in a beaker containing 4M HCl (with 0.05wt.% PA) which was then diluted with 4M NaCl brine (full test methodology is provided in Section 4.5.3). As discussed in Section 4.5.3.1, a dilution rate of between 10-20ml/min best replicates the flowback profile observed in the field. The dilution test was therefore performed at a dilution rate of 10ml/min. As discussed in Section 2.2.4 there are difficulties in calculating the corrosion rate in a solution of changing chemistry (due to the variations in the Stern-Geary coefficient). Therefore Figure 5.25 shows the reciprocal of the charge transfer resistance over the duration of the dilution test.
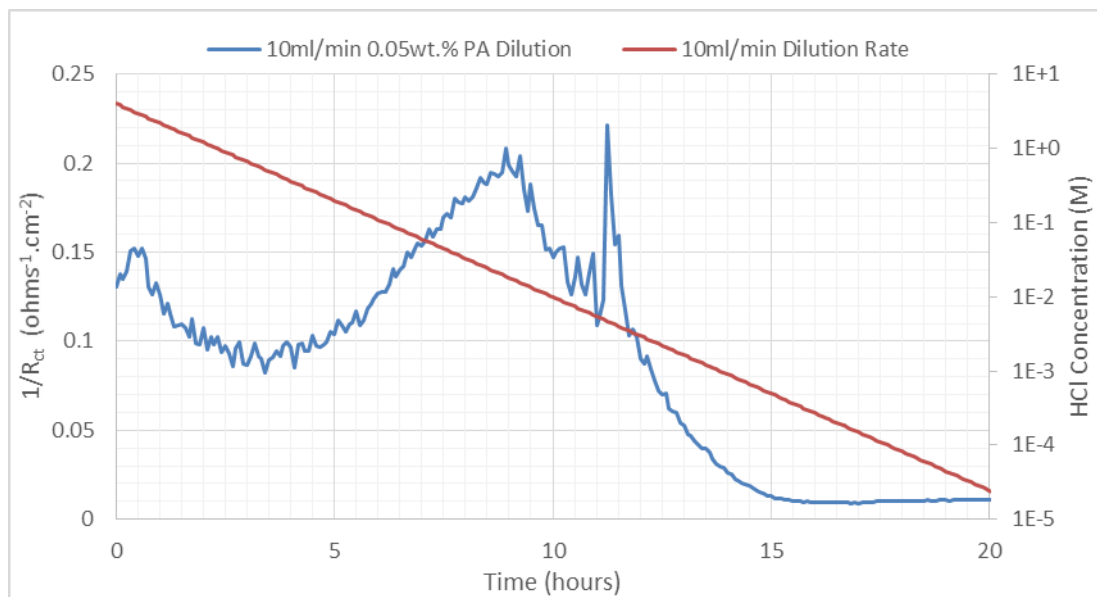
Figure 5.25 The reciprocal of the charge transfer resistances ($1/R_{ct}$) found over the duration of the 10ml/min dilution test. The dilution test was performed on HS80 steel placed in 4M HCl (containing 0.05wt.% PA) and diluted with 4M NaCl brine at a rate of 10ml/min at 80°C. The HCl concentration is displayed on the secondary axis.

5.3.5.1 Calculating the Corrosion Rate

Unlike the previous electrochemical tests, the dilution tests involve measuring the corrosivity of a solution with a constantly changing chemistry. The corrosion rates presented in Section 5.3.4 are calculated by applying the

Stern-Geary coefficient found at the end of each test. It was found that as the HCl concentration of the solution is varied from 4M to 4×10^{-4}M the Stern-Geary coefficient can potentially range from between 11.1-19.9. This variation makes it difficult to apply a single Stern-Geary coefficient to the dilution tests where the solution chemistry changes through the entire test. In order to represent this variation in the Stern-Geary coefficient Figure 5.26 shows the corrosion rate when three different Stern-Geary coefficients are applied.
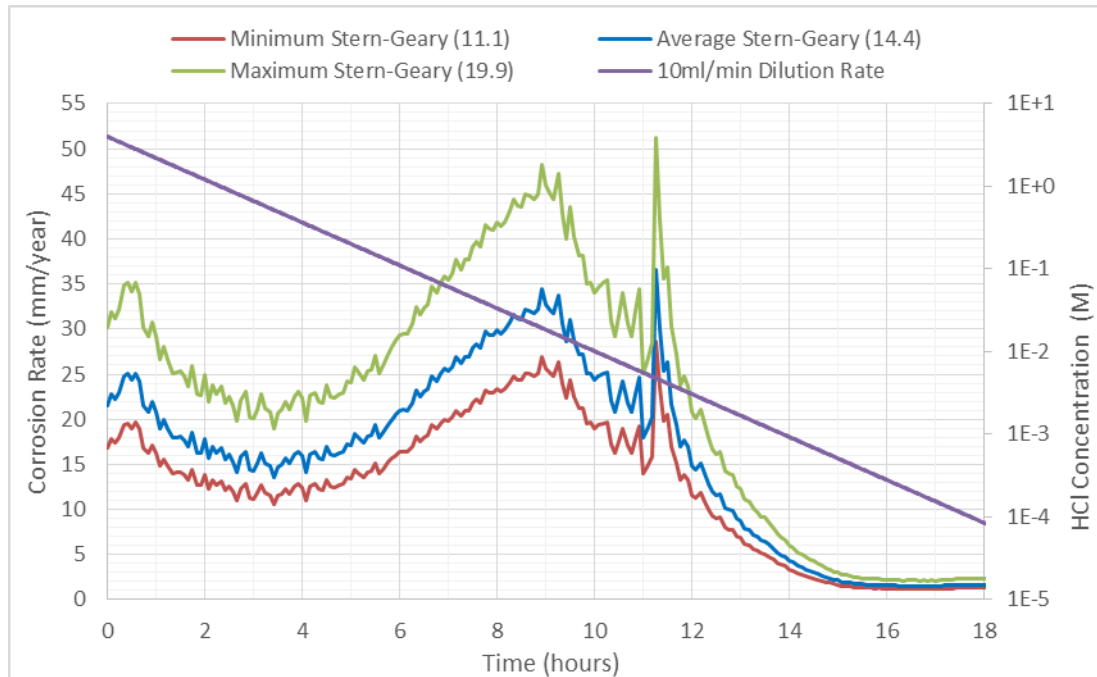
Figure 5.26 Calculated corrosion rates when the minimum possible (11.1), maximum possible (19.9) and average (14.4) Stern-Geary coefficients found from the fixed concentration tests were applied. Tests were performed on HS80 samples placed in 4M HCl (containing 0.05wt.% PA) diluted with 4M NaCl brine at a rate of 10ml/min at 80°C. The HCl concentration is displayed on the secondary axis.

The Stern-Geary coefficients used to calculate the three corrosion rate dilution profiles shown in Figure 5.26 are as follows.

1. **An average value of 14.4.** This is the average of the values found from fixed HCl concentrations of 4, 0.4, 0.04, 4×10^{-3} and 4×10^{-4}M. The average Stern-Geary coefficient of all HCl concentrations tested is 14.4. The average of all HCl concentrations was not used as this gives too much weight to the higher HCl concentrations (>0.04M) as more Stern-Geary coefficients were measured at these molarities.

2. **A minimum value of 11.1.** This is the smallest possible Stern-Geary coefficient measured in a solution with a HCl concentration of 0.2M.

This value was found from all of the polarisation tests performed at the full range of HCl concentrations.

3. **A maximum value of 19.9.** This is the largest possible Stern-Geary coefficient measured in a solution with a HCl concentration of 0.04M. Again, this value was found from all of the polarisation tests performed at the full range of HCl concentrations.

5.4 Electrochemistry Limitations

5.4.1 Introduction

As discussed in Section 5.2, there are several benefits to using electrochemistry instead of mass loss tests to monitor the corrosion rate. The dilution tests presented in Section 5.3.5 are able to characterise the complete dilution of HCl observed during the flowback process and measure the corrosion rate throughout the entire dilution process. However there are still several limitations to using the closed vessel dilution tests to understand the flowback process.

5.4.2 Hydrochloric Acid and Propargyl Alcohol Spending

The primary limitation of the dilution test performed in a 1L beaker is that the steel sample is in contact with the entire volume of HCl and PA throughout the test. This raises questions over the concentration of HCl and PA in the beaker at any given time as it is unknown how much acid and inhibitor has reacted at that point in the dilution test.

The main benefit of the dilution test is the ability to dilute the molarity of the solution at a known rate and therefore be able to calculate both the HCl and PA concentrations of the solution at any given time. However the problem of potential HCl and PA spending casts doubts over the validity of these calculated HCl and PA concentrations.

5.4.3 Propargyl Alcohol Reactions at 80°C

NMR work performed by Schlumberger [159] looked at how the PA reacts with the hydrochloric acid over time. The results showed that the PA did not significantly react with the HCl at room temperature. However the results

showed that at 80°C the PA reacts to form a large range of molecules. The ability of these different molecules to inhibit the corrosion rate on the carbon steel sample is unknown and may lead to an increase or a decrease in inhibitor efficiency over the duration of long term tests [85, 122].

This was supported by work performed by Aramaki and Fujioka [122] who studied the inhibition abilities of PA and the intermediate acetylenic derivatives formed in the reaction between PA and the HCl (this is discussed in detail in Section 2.4.2). It was found that a thicker inhibitor film formed on the steel at elevated temperatures. The formation of this thicker film can be attributed to an increased rate of the intermediate reaction providing more intermediate acetylenic derivatives which can be polymerised to form the protective film. Therefore heating the solution for significant periods of time leads to the PA breaking down into these intermediate products. Frenier, Growcock and Lopp [83] similarly found that temperature was an important factor in the intermediate step for acetylenic alcohol inhibitors. Although PA was not studied (another acetylenic alcohol, octynol was used instead) a similar trend between increasing temperature and inhibitor protectiveness was observed. At lower temperatures it was hypothesised that a secondary product is being formed at a slower rate hence resulting in a decrease in inhibitor protectiveness.

These previous studies raise further doubts over the validity of the calculated PA concentration in the solution at any given point in the dilution test. This is especially the case towards the end of the dilution test as any remaining PA in the solution will have been heated at 80°C for up to 20 hours. Although the intermediate reaction is a vital step in the PA forming a protective inhibitor film, for the purposes of this work it is vital that this reaction is minimised until the sample comes into contact with the test solution. In order to understand how the PA efficiency varies over the dilution profile the reaction of the PA to form the intermediate acetylenic derivatives should be minimised.

5.4.4 Solution Contamination

A significant limitation is the build-up of iron ions in the 1L solution as the carbon steel sample reacts with the HCl. This contamination can be seen in the laboratory as the solution begins to change colour less than an hour into

the dilution test. Ideally there would be no build-up of iron as it not known what effect this contamination may have upon the inhibitor behaviour.

5.4.5 Rationale for a New Test Methodology

It is clear that if any strong conclusions are to be drawn from the dilution tests and the peaks in corrosion rate are to be effectively explained then the discussed limitations must be addressed. The dilution tests are useful as they provide much more data regarding the flowback process than the 3 hour fixed HCl concentration tests. However, there are still several problems with the methodology that must be first addressed if the relationship between the PA and HCl throughout the flowback process is to be fully understood. This understanding can only be achieved if the solution chemistry is known at all times in the dilution test and this can only be accomplished through the development of a new test methodology that solves the problems outlined.

Chapter 6 The Corrosivity of the Flowback Fluid

6.1 Introduction

Very little research has been conducted to assess the corrosivity of the flowback fluid and understand how corrosive solutions with greatly diluted HCl concentrations might be in the field. Solutions designed to replicate those encountered during flowback were analysed using the methodologies commonly used to test the corrosivity of the injected HCl (primarily mass loss tests at fixed HCl concentrations). This chapter presents the corrosion rates of a wide range of different molarity HCl solutions containing a range of PA concentrations.

Almost all acidizing research performed previously has studied the corrosivity of high molarity HCl solutions containing high concentrations of acidizing inhibitors. Tests performed in these very low pH (<0) solutions containing various inhibitor packages (as discussed in Section 3.3.2) provide greatly reduced corrosion rates and very high inhibitor efficiencies. This chapter discusses the efficiency of the PA at greatly reduced molarities and inhibitor concentrations. Results from a range of different mass loss and electrochemistry tests are discussed and compared. Using these previously established test methodologies limits the extent to which the flowback process can be understood. In order to attempt to more accurately replicate the flowback process the results of a new dilution test are discussed and compared to those found from the 3 hour fixed HCl concentration tests.

6.2 Corrosion Rates Found from Mass Loss Tests

Despite the limitations previously discussed, the understanding gained from the mass loss tests and 3 hour electrochemistry tests should not be understated. The results are important for validating the corrosion rates observed in the dilution tests and also give an initial understanding as to how the inhibitor efficiency decreases as both the HCl concentration of the solution is varied along with the PA concentration.

6.2.1 Propargyl Alcohol Efficiency

An understanding as to how the PA efficiency changes as both the PA and the HCl concentration are reduced is vital if the corrosivity of the flowback fluid is to be understood. The PA is designed to protect the steel tubulars during the injection process, where high concentrations of PA (0.05wt.% PA) are injected with high molarity HCl (concentrations of 4M and above). When considering the corrosivity of the flowback fluid it is vital to understand how the inhibitor efficiency decreases as the PA and HCl are reduced to concentrations much lower than the values encountered in the injected acid.

6.2.1.1 Efficiency at a range of HCl Concentrations

The first tests performed were mass loss tests at a PA concentration typically used during acid injection in the field (0.05wt.% PA). The 4M HCl was diluted with 4M NaCl brine to give a range of different HCl molarities in an attempt to understand how the corrosivity of the flowback fluid varies as the HCl concentration reduces over the flowback process (Figure 5.4). The inhibitor efficiency for these different HCl solutions (all containing 0.05wt.% PA relative to the HCl content) was calculated using the corrosion rates found at each HCl concentration when no inhibitor was present (Figure 5.2). The efficiency (E) was calculated using the mass loss results in the presence and absence of inhibitor (W_i and W_0 respectively), as shown in Equation 6.1 [99].

$$E = \frac{W_0 - W_i}{W_0} \times 100 \qquad (6.1)$$

The efficiency of each HCl molarity (from 4M to 4×10^{-4}M) at a PA concentration of 0.05wt.% is shown in Figure 6.1. Figure 6.1 shows that at a high PA concentration of 0.05wt.% the inhibitor efficiency varies greatly with the HCl concentration of the solution. When the solution contains 4M HCl the PA efficiency is very high (97.4%) and remains high even when the solution is diluted to 2M HCl (97.1%). The inhibitor efficiency then drops slightly once the HCl concentration is reduced by 85% to 0.6M (95.0%) and then again when the concentration of the solution is reduced 20 times to 0.2M (93.7%).
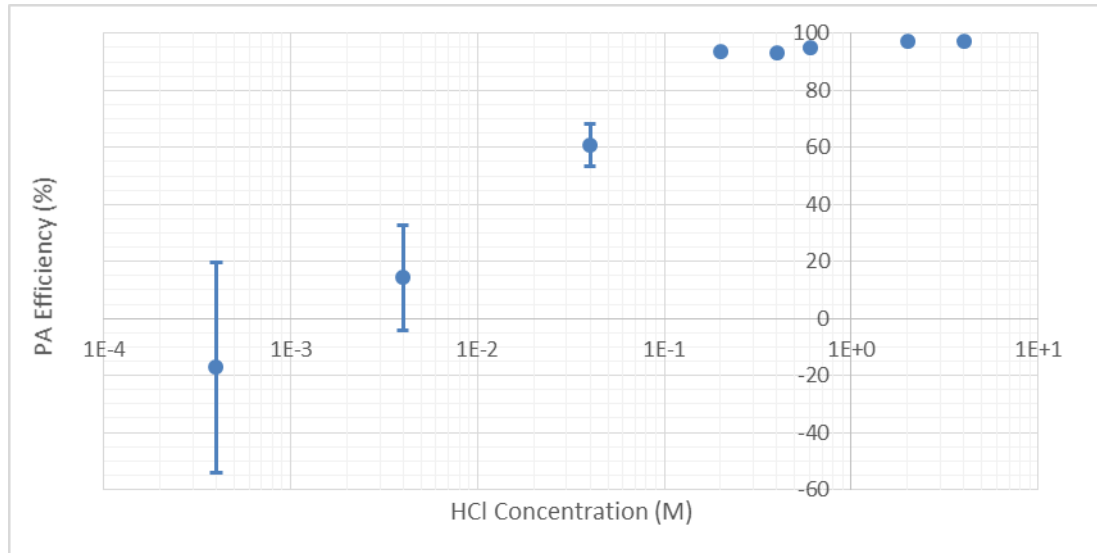
Figure 6.1 Inhibitor efficiency when 0.05wt.% PA is added to different HCl concentration solutions at 80°C. The scatter bands represent the maximum and minimum calculated efficiencies across all 3 hour mass loss tests in each environment. The HCl was diluted using 4M NaCl brine.

At HCl concentrations less than 0.2M the PA efficiency decreases significantly. The inhibitor efficiency drops to 54% when the solution molarity is reduced to 0.04M. At an HCl concentration of 4×10^{-3}M the efficiency decreases again to 14%. At the lowest HCl concentration of 4×10^{-4}M the corrosion rate is too low to produce reliable mass loss data, the PA volume is so small at this HCl molarity that it has no effect on reducing the corrosivity of the solution. This is highlighted by the negative efficiency value shown in Figure 6.1. The corrosion rate at this HCl concentration is too low and the mass loss over the 3 hours too small to provide reliable corrosion rate data.

At higher molarities the PA is able to reduce the corrosion rate significantly, being over 90% efficient at HCl concentrations above 0.2M. This is a reduction in corrosion rate from over 100mm/year to a value less than 8mm/year when the solution contains 0.2M HCl. It is important to note that although the acid concentration of the solution has been diluted 20 times the pH of the solution is still very low (a value less than 1). The PA is designed to inhibit high molarity HCl solutions with a very low pH so these high efficiencies are to be expected.

However once the HCl concentration in the solution is reduced to values below 0.2M the efficiency rapidly decreases with the solution molarity. The PA

concentration of the solution is always relative to the HCl concentration, therefore the PA is also being reduced proportionally as the HCl is diluted. This decrease in efficiency may be due to not enough inhibitor volume being present in the solution to form a protective film which is able to inhibit the relatively small amounts of HCl found in the lower molarity solutions.

6.2.1.2 Efficiency at Lower PA Concentrations

As previously discussed the PA concentration of the flowback fluid is always going to be significantly less than the concentration in the injected acid due to the inhibitor reacting with the steel tubulars and the formation during injection. Therefore it was vital to understand how the inhibitor efficiency changes as the PA concentration is reduced to values which are likely to be present in the flowback fluid. The efficiency of these lower PA concentrations are shown in Figure 6.2. Again the different PA concentrations were tested at a range of HCl molarities and the PA concentration was always kept relative to the HCl concentration of the solution.
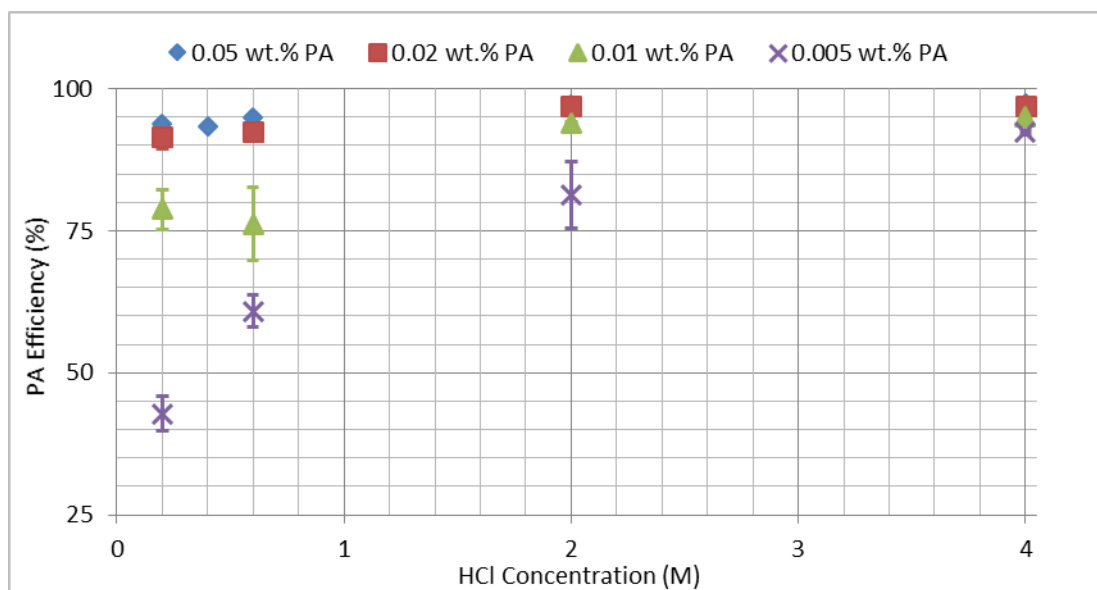
Figure 6.2 Inhibitor efficiencies when a range of PA concentrations are added to a range of different HCl concentrations at 80°C. The scatter bands represent the maximum and minimum calculated efficiencies across all 3 hour mass loss tests in each environment. The HCl was diluted with 4M NaCl brine.

The efficiencies in Figure 6.2 highlight several important points regarding the ability of the PA to inhibit the flowback fluid-

1. The PA is over 90% efficient at all HCl molarities when the concentration is above 0.02wt.%.

2. The PA is over 90% efficient at concentrations as low as 5×10^{-3}wt.% (10 times less than the injected concentration) provided that the HCl concentration is 4M.

3. At all HCl concentrations the inhibitor efficiency increases as the PA concentration increases.

4. At lower PA concentrations (0.01wt.% and 5×10^{-3}wt.%) the inhibitor efficiency reduces significantly at HCl concentrations less than 2M.

5. The inhibitor efficiency is at its lowest (42%) when the PA and HCl concentrations are also at their lowest values (5×10^{-3}wt.% and 0.2M respectively).

This raises doubts over the ability of the PA to effectively inhibit the solution which flows back following an acid job once the HCl and PA concentration of the flowback fluid is significantly reduced. Figure 6.2 highlights the ability of the PA to inhibit high strength injected HCl solutions, displaying over 90% efficiency for 4M solutions even when the PA concentration is 10 times less than typical injection concentrations. However, the PA efficiency drastically reduces at the low molarity and low PA concentrations tested. And it is these low PA and low HCl solutions which are intended to most accurately replicate the solution encountered once production restarts following an acid job. The results highlight the potential corrosion problems which may be caused by the flowback fluid in the field. Figure 6.2 suggests that the PA efficiency decreases as the solution pH increases (as the HCl concentration decreases). It is thought that the PA is catalysed by the high H^+ concentration of low pH solutions [122]. The lowest acid molarity shown in Figure 6.2 is 0.2M, 20 times less than the concentration of the injected acid. Although the molarity of the solution has been reduced significantly the pH of the solution is still incredibly low (below 1). The relationship between the HCl concentration and the PA efficiency is discussed in further detail in Section 8.2.7.

6.2.2 Effect of PA and HCl on the Steel Surface

Additional post-test analysis was performed on samples exposed to 4M HCl for 3 hours. A comparison is provided between samples that were exposed to

HCl both with and without the addition of 0.05wt.% PA and X-ray diffraction (XRD) was used to analyse these samples.

6.2.2.1 Corrosion Products on the Steel Surface

HS80 samples were exposed to HCl both with and without 0.05wt.% PA. XRD was then used to analyse the steel surface and a comparison between the data for each sample is shown in Figure 6.3.
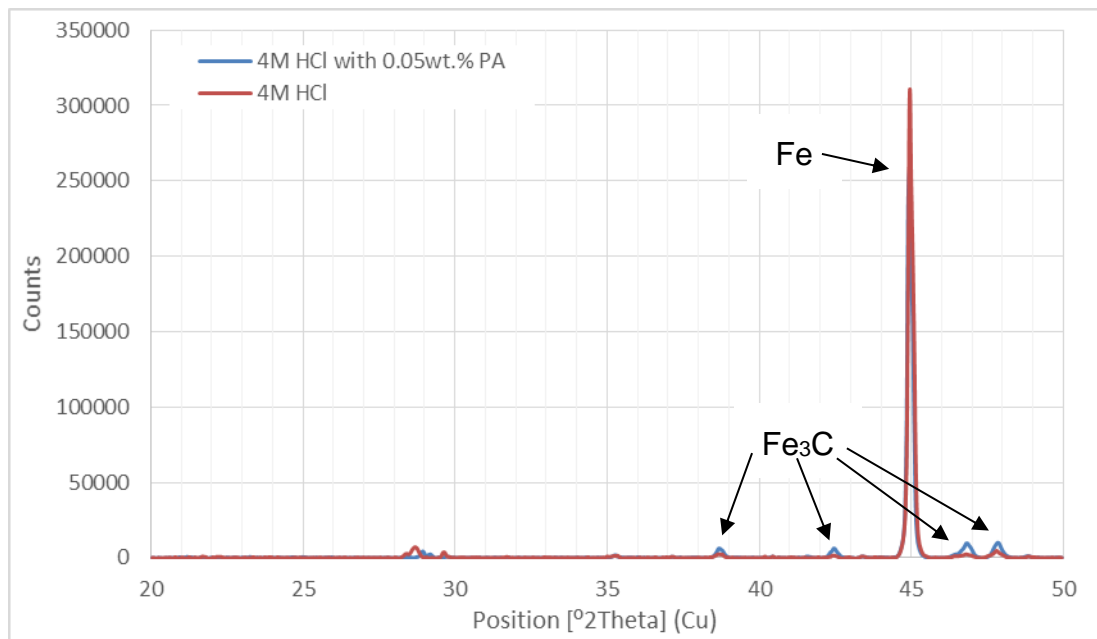
Figure 6.3 Comparison between the XRD patterns for HS80 samples exposed to 4M HCl for 3 hours when no inhibitor and when 0.05wt.% PA was added to the HCl.

The XRD patterns shows interesting peaks for the HS80 after being exposed to 4M HCl both with and without the addition of PA. The large peak at 45 represents iron (Fe) and the smaller peaks at ~39, 42, 47 and 48 indicates that iron carbide/cementite (Fe_3C) is present. The lack of iron carbide peaks in the test without PA suggests that there is more preferential dilution occurring when PA is added to the HCl. The HS80 has a ferrite/pearlite microstructure, with a pearlite phase which is composed of alternating ferrite-cementite (Fe_3C) layers [151]. The XRD results shown in Figure 6.3 suggest that when PA is added to the HCl the ferrite is being preferentially dissolved, leaving more of the pearlite (indicated by the measured increase in Fe_3C on the steel surface). This appears to be further supported by the SEM images (Figure 5.9-5.11) which appear to show some preferential dissolution of the

ferrite. The lack of cementite detected when the sample was exposed to uninhibited HCl suggests that there is no preferential dissolution and the entire surface is being corroded uniformly.

6.2.2.2 Effect of Exposure Time on the Surface Roughness of the HS80

In order to understand the effect of exposure time on the HS80, samples were exposed to 4M HCl (containing 0.05wt.% PA) for between 3 and 24 hours. Figure 6.4 shows the change in surface roughness of the sample as the exposure time to 4M HCl (containing 0.05wt.% PA) increases. The surface roughness, as defined by the American Society of Mechanical Engineers [160], is the average of the profile height deviations from the average surface line. The surface roughness was analysed across each of the three 3x3mm areas for each 10mm sample (discussed in Section 4.6.1). Figure 6.4 shows the average roughness found from the three scanned lines and the scatter bands represent the maximum and minimum roughness found from the three scans.
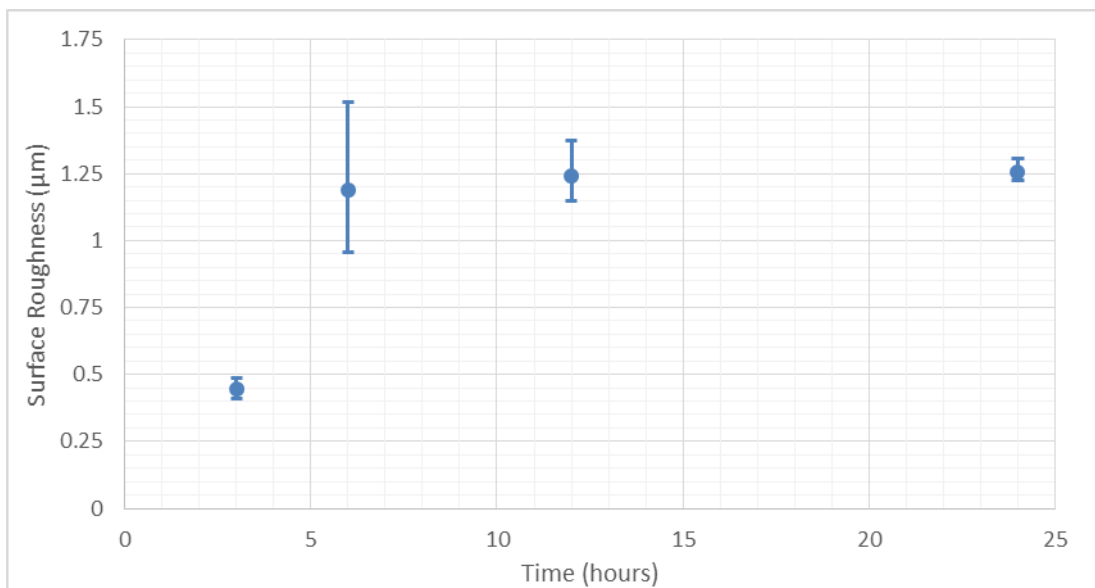
Figure 6.4 Variation in sample roughness as the HS80 is exposed to 4M HCl (containing 0.05wt.%) for different periods of time. The average roughness value calculated from three different areas is shown and the scatter bands represent the maximum and minimum calculated roughness values.

Figure 6.4 shows that there is very little variation in surface roughness as exposure time to the 4M HCl increases. There is a noticeable increase in

surface roughness (from ~0.4μm to ~1.2μm) when the exposure time was increased from 3 to 6 hours. The surface roughness then averages at around 1.2μm for exposure times between 6-24 hours.

The lack of change in surface roughness is validated by previous studies into the effect of HCl on surface roughness by Barmatov, et al. [151]. It was found that exposing a HS80 carbon steel sample to 4M HCl at 80⁰C for 3 hours actually resulted in a decrease in surface roughness. This was the case for all surface finishes tested included the least rough surface of P1200 (the same finish applied to the samples used for all tests presented in this Thesis). The decrease in roughness was attributed to the preferential dissolution of protruding cavities and peaks; resulting in a smoother surface [151].
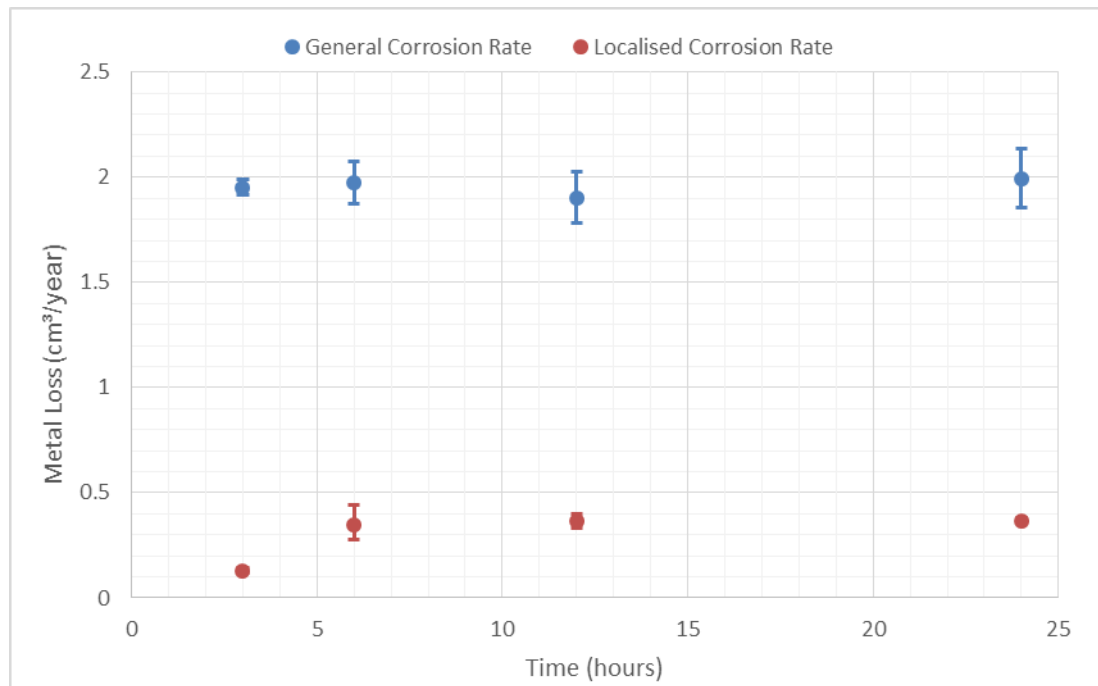
Figure 6.5 Comparison between total metal volume loss due to the general corrosion of the sample and the total volume loss due to localised corrosion of the sample. The scatter bands represent the maximum and minimum calculated metal losses across all tests in each environment.

Although Figure 6.3 suggests some preferential dissolution of the ferrite phase, the surface roughness of the sample does not change significantly as the exposure time increases. This suggests that despite some preferential dissolution, general corrosion is the most significant mechanism for mass loss. This is validated by Figure 6.5, which compares the total metal volume loss

due to the general corrosion of the sample and the total volume loss due to localised corrosion (the average surface roughness multiplied by the sample area). The metal loss due to general corrosion is approximately 15 times higher than the localised metal loss when the sample is exposed to the 4M HCl (containing 0.05wt.% PA) for 3 hours. For longer exposure times (6-24 hours) the localised metal loss becomes more significant but is still approximately 5 times less than the general corrosion rate.

6.2.3 Acceptable Corrosion Rates during the Flowback Process from Mass Loss Data

It is vital to understand how the inhibitor efficiency changes as the concentrations of HCl and PA change over the flowback process. However, it is of equal importance to monitor how the corrosion rate changes at each acid and inhibitor concentration as this is how the corrosion rates of acid jobs are quantified in the field. In the field the criteria for inhibitor selection is always to ensure that the corrosion rate remains below a specified value. Therefore an understanding of how the corrosion rate varies as the PA and HCl concentrations decrease during flowback is vital.

A typical industry standard for the acceptable level of corrosion during an acid job is less than 0.05 lb/ft^2 for conventional tubulars and less than 0.02lb/ft^2 for coiled tubing [5, 85, 161]. As the production tubing through which the flowback will typically travel is similar in metallurgy and role to the coiled tubing the lower acceptable corrosion rate of 0.02lb/ft^2 will be used as the acceptable corrosion rate for this discussion. The acceptable metal loss of 0.02lb/ ft^2 is over the duration of the acid job. This makes a direct comparison difficult as the contact time between the tubular and the injected acid can vary greatly as the injection rate, acid volume and subsequently the contact time is different for each acid job. If a typical exposure time of 3 hours is used then an acceptable corrosion rate in terms of mm/year can be calculated for the two values mentioned [6]. Firstly the value is multiplied by a conversion factor of 4,882 to convert the corrosion rate from lb/ft^2 to g/m^3. The value is then divided by the exposure time expressed in days (3 hours is equal to 0.125 days). Finally a second conversion factor is applied and the value is divided by 21.6 to convert from g/m^2/day to mm/year. This then gives the following acceptable corrosion rates throughout the entire acid job for each tubing class [161].

- 90mm/year for conventional tubulars (0.05 lb/ft^2)

- 36mm/year for coiled tubing (0.02 lb/ft^2)

Figure 6.6 shows the corrosion rates at each acid molarity for the different inhibitor concentrations. The acceptable corrosion rate of 36mm/year is shown to highlight acid and inhibitor concentrations which do not meet the acceptable corrosion rate.
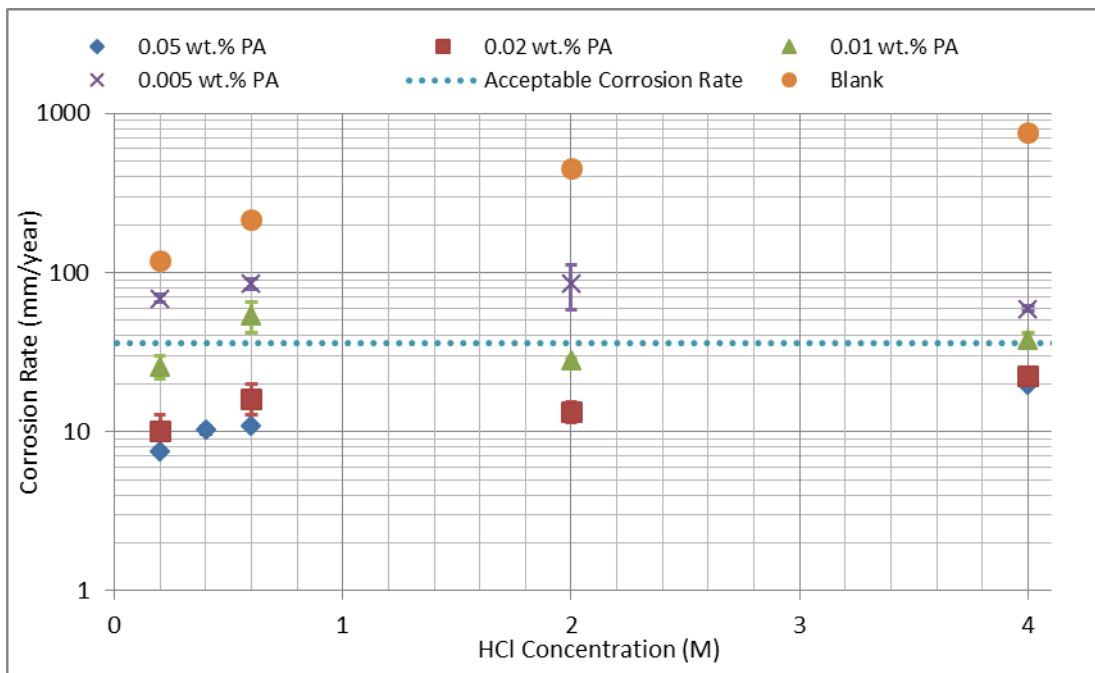
Figure 6.6 Corrosion rates when four PA concentrations are tested at a range of different HCl concentrations at 80°C. The scatter bands represent the maximum and minimum corrosion rates across all 3 hour mass loss tests in each environment. The HCl was diluted with 4M NaCl brine. Corrosion rates from blank (no inhibitor) tests are also shown. The acceptable corrosion rate in the field is shown.

Figure 6.6 highlights the importance of understanding how both the HCl molarity and the PA concentration of the solution can affect the corrosivity of the flowback fluid. PA concentrations above 0.02wt.% gave acceptable corrosion rates at all HCl concentrations tested. A PA concentration of 5x10^{-3}wt.% failed to give an acceptable corrosion rate at all molarities tested. An inhibitor concentration of 0.01wt.% PA gives acceptable corrosion rates at two HCl molarities (0.2M and 2M) but fails to do so when tested in 0.6M and 4M solution.

The corrosion rates observed in Figure 6.6 show that a complex relationship exists between the HCl and PA concentration of the solution. The results

provide an initial understanding as to how the corrosivity of the flowback fluid can change as the HCl and PA concentrations are varied. An unacceptable corrosion rate is observed in 6 of the 16 mass loss tests performed, all of which were at PA concentrations less than those encountered during injection. The blank corrosion rate measurements were above the acceptable corrosion rate for all HCl concentrations tested. At all HCl and PA concentrations tested the corrosion rate was reduced compared to the blank tests.

How the corrosion rate changes with changing HCl molarity is different for each of the PA concentrations tested. At a PA concentration of 0.05wt.% the corrosivity of the solution decreases with HCl concentration. When the PA concentration is 0.02wt.% (2.5 times less), the highest corrosion rate is again observed at the highest HCl concentration (4M). The corrosion rate again decreases when the molarity is halved to 2M, before it increases again at a molarity of 0.6M. It then produces the lowest corrosion rate at the lowest molarity of 0.2M.

When the PA concentration is reduced once again (to 0.01wt.% PA), a similar trend (as 0.02wt.% PA) is observed. Again, the corrosion rate reduces as the HCl molarity is reduced from 4M to 2M. A reduction in HCl concentration from 2M to 0.6M then produces an increase in corrosion rate. However unlike at 0.02wt.% PA, the corrosion rate at this molarity is higher than at 4M. A reduction in HCl concentration to 0.2M again sees the corrosion rate fall below the acceptable value. At the lowest PA concentration of $5x10^{-3}$wt.% (ten times less than a typical injection concentration) the corrosivity of the solution is again at its highest when the molarity of the solution is 0.6M. At this PA concentration the lowest corrosion rate is observed at the highest molarity (4M).

The PA volume in the solution varies with each HCl concentration (shown in Table 4.2), therefore the results from Figure 6.6 suggest a complicated relationship exists between the inhibitor volume and the molarity of the solution. Figure 6.7 shows how the corrosion rate changes with the inhibitor volume at the three PA concentrations less than 0.05wt.% PA. These are the PA concentrations intended to replicate the flowback fluid.
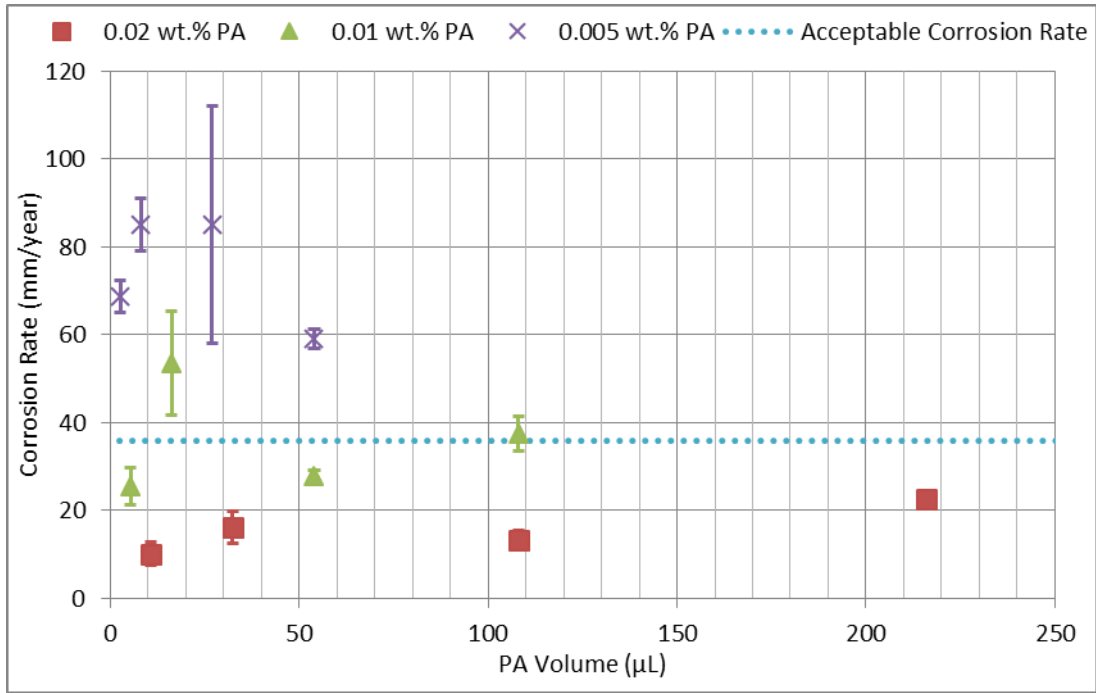
Figure 6.7 Corrosion rates from 3 hour mass loss tests (at 80°C) plotted as a function of the PA volume present in each solution for the three lowest PA concentrations tested. The scatter bands represent the maximum and minimum corrosion rates across all 3 hour mass loss tests in each environment. The HCl was diluted with 4M NaCl brine.

From Figure 6.7 it is clear that the corrosion rate is not directly related to the PA volume of the solution. The corrosivity of a solution must therefore be dependent upon both the HCl concentration of the solution and the inhibitor volume present in the solution. This is highlighted most clearly at a PA concentration of 0.01wt.% which shows the corrosion rate decreasing with PA volume (at 2M HCl) before increasing again (at 0.6M HCl) and then producing the lowest corrosion rate at the lowest PA volume (0.2M HCl).

Figure 6.7 further highlights the complexity of the relationship between the PA concentration and the HCl concentration of the solution. In order to understand this relationship further mass loss tests were performed at a greater range of HCl concentrations.

6.2.3.1 Further Mass Loss Tests at HCl Concentrations Less than 0.2M

The relationship between the PA concentration and the HCl molarity of the solution is vital if the corrosion rates associated with the flowback process are to be fully understood. The results shown in Figure 6.6 show that the two

lowest inhibitor concentrations (0.01 wt.% and 5x10-3 wt.% PA) are the most corrosive when the acid molarity is reduced significantly. The highest PA concentration of 0.05wt.% was shown to decrease in corrosivity as the molarity of the solution is reduced.

It was reasoned that by focusing on a single inhibitor concentration (0.05wt.%) and measuring the corrosivity of solutions containing less than 0.2M, a greater understanding of the relationship between the HCl and PA could be obtained. Mass loss tests were repeated with the HCl concentration reduced by a factor of 10 starting at 4M and decreasing to $4x10^{-4}$M. The results of these tests are plotted with the previous results (shown in Figure 6.6) on Figure 6.8 along with the acceptable corrosion rate (36mm/year). The corrosion rates found from uninhibited HCl solutions are provided for comparison.
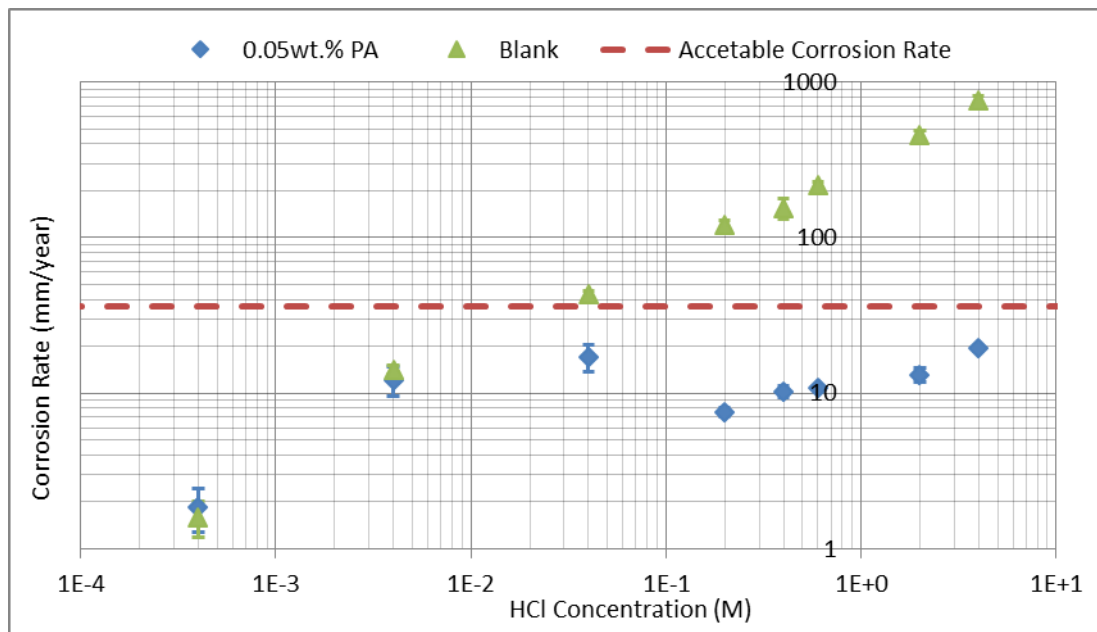
Figure 6.8 Corrosion rates from mass loss coupons at a range of different molarity HCl solutions, the scatter bands represent the maximum and minimum corrosion rates across all 3 hour mass loss tests in each environment. A comparison is made between tests containing no inhibitor and 0.05wt.% PA. Tests were performed for 3 hours at 80°C and the HCl was diluted with 4M NaCl brine. The acceptable corrosion rate is also shown.

Figure 6.8 once again highlights the complex relationship between the PA and the HCl concentration of the solution. The tests performed at lower molarities show that an inhibitor concentration of 0.05wt.% PA is sufficient to maintain

corrosion rates below the acceptable value (36mm/year) for all molarities tested. At HCl concentrations between 4M and 0.2M the corrosion rate reduces with decreasing HCl concentration. A further decrease in solution molarity, to 0.04M, produces a corrosion rate of 17mm/year, only 2mm/year less than the 4M solution, despite its molarity being 100 times less. The solution containing 4×10^{-3}M HCl is less corrosive (12mm/year) than the solution containing 0.04M (17mm/year). However this solution is still more corrosive than the solution containing 0.6M despite having a HCl concentration 150 times lower. Once the solution contains a HCl concentration of 4×10^{-4}M the corrosion rate returns to levels which would be associated with normal production.

Figure 6.8 shows that the PA is still offering some protection to the steel until it is diluted to a HCl concentration of 4×10^{-3}M. This suggests that in order for the PA to be an effective inhibitor it requires a minimum PA or HCl concentration to be maintained. It is vital to note that the PA concentration is always relative to the HCl in the solution, meaning that the PA volume is constantly decreasing as the molarity is reduced. This is in order to accurately replicate what is seen during the flowback process as the inhibitor concentration will always be relative to the HCl concentration of the flowback fluid. This suggests that a minimum PA volume is required to maintain the protective inhibitor film. However, as discussed in Section 3.2.3, it has been proposed that the PA polymerisation reaction is catalysed by H^+ [122], therefore the lack of inhibition may be due to the lack of hydrogen ions in the most dilute HCl solutions (less than 4×10^{-3}M).

6.2.3.2 Effect of Aqueous Salts on the Corrosivity of the Flowback Fluid

As discussed in Section 3.2.1.3, the presence of aqueous salts can affect the corrosivity of HCl containing solutions. It has been shown by several authors [110-112] that the addition of NaCl increases the activity coefficient of a solution containing HCl. This is of particular importance when considering the solutions intended to replicate flowback fluids that were tested in this work. In order to understand how the addition of NaCl affects the corrosion rate it is necessary to understand the relationship between the HCl concentration of the solution and the measured corrosion rate. The effect of NaCl addition and temperature on the activity coefficient of H^+ is shown in Figure 6.9.
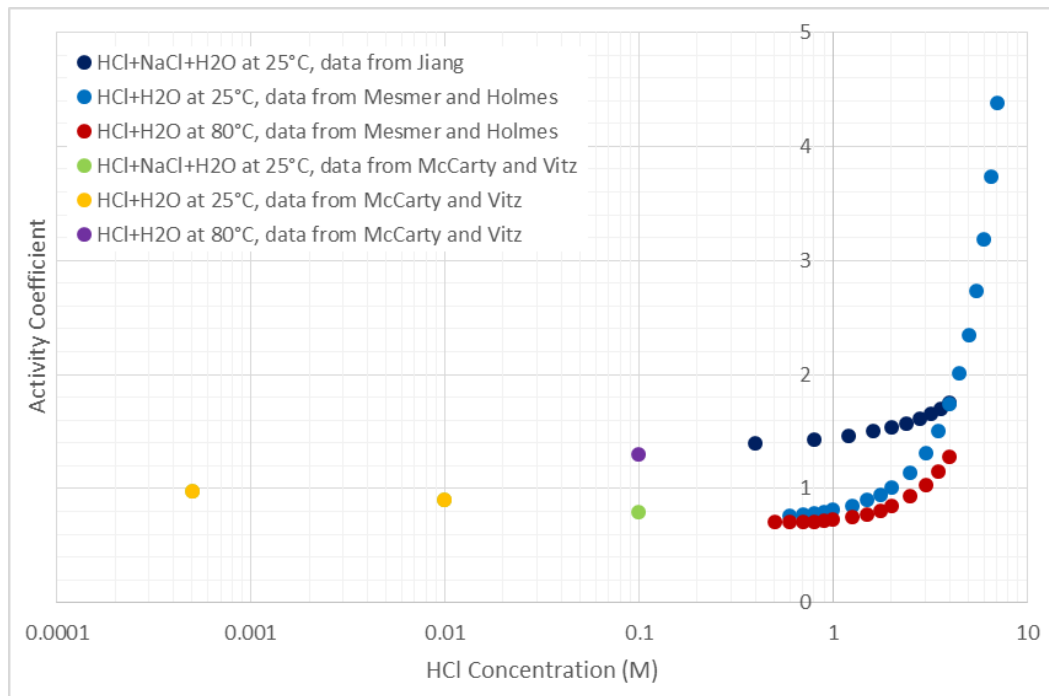
Figure 6.9 Activity coefficient values for a range of HCl concentrations at temperatures of 25ºC and 80ºC. Data is compared from studies performed by Jiang [162], Mesmer and Holmes [163] and McCarty and Vitz [111].

Results are presented from several studies [111, 162, 163] and highlight the changing activity coefficients at a range of different HCl concentrations and temperatures. The most important comparison is between the work performed by Jiang [162] and the data provided by Mesmer and Holmes [163]. The results compare the activity coefficients found for a HCl-H_2O system and a HCl-NaCl-H_2O system where the molar concentration was maintained at 4M/L (both studies were performed at 25ºC). Figure 6.9 shows that the addition of NaCl results in increased H^+ activity therefore producing a lower pH than the HCl-H_2O system. This highlights the difficulty in quantifying the pH of the flowback fluid. Therefore any reference to pH throughout this work is merely an approximation calculated based upon the H^+ concentration of the solution and is not the true pH.

6.2.4 Change in Solution Corrosivity over Time

One of the main limitations of the mass loss methodology is that from a 3 hour test only the average corrosion rate is known over the duration of the test. Mass loss tests can be increased or reduced in duration but not without potential issues arising. The test duration has to be long enough so that

enough mass is lost from the coupon to allow a reliable corrosion rate to be calculated. Longer exposure times also raise questions regarding the spending of the acid and inhibitor over time which in turn casts doubts upon the reliability of any corrosion rates calculated from these longer duration mass loss tests.

6.2.4.1 Varying the Exposure Time of Mass Loss Coupons in 4M HCl

Despite the limitations discussed above the exposure time was varied in order to attempt to understand how the corrosivity of the solution changes over time. Firstly coupons were placed in 4M HCl containing 0.05wt.% PA for exposure times ranging from 0.5 hours to 24 hours. The results of these tests are shown in Figure 5.7 and highlight several important points when considering the exposure time of mass loss coupons to 4M HCl (containing 0.05wt.% PA).

1. The difficulty in exposing mass loss coupons to solutions for durations less than 3 hours is highlighted by the scatter bands at these exposure times.

2. For exposure times greater than 3 hours the corrosion rate calculated from the mass loss does not change significantly regardless of if the coupon is exposed for 3 hours or 24 hours.

3. If the exposure time is reduced from 3 hours to 1 hour then the corrosion rate appears to rise significantly from 20mm/year to 26mm/year.

4. If the exposure time is reduced even further to 0.5 hours then the corrosion rate again increases to 30mm/year. This value is 1.5 times higher than the corrosion rate found from a three hour exposure.

The increase in corrosion rate at this lower exposure time may be due to the increased error in the measurements associated with shorter exposure times. The increase may however be due to the way the PA inhibits corrosion on the carbon steel sample. As previously discussed in Section 3.2.3 the PA is a film forming inhibitor [45], if the film takes a significant amount of time to form then the initial corrosion rate may be significantly higher than the values calculated from extended duration tests (longer than 3 hours).

6.2.4.2 Varying the Exposure Time of Mass Loss Coupons in Different HCl Molarities

The results from Figure 5.7 suggest that the corrosion rate may change over the first 3 hours of the test. With that in mind mass loss tests were repeated in different molarity solutions (again all containing 0.05wt.% PA relative to the HCl content of the solution) at shorter exposure times of 0.5 and 1 hour (Figure 5.6). Figure 6.10 shows the corrosion rate plotted as a function of the HCl concentration in order to compare the results found at the three different exposure times.
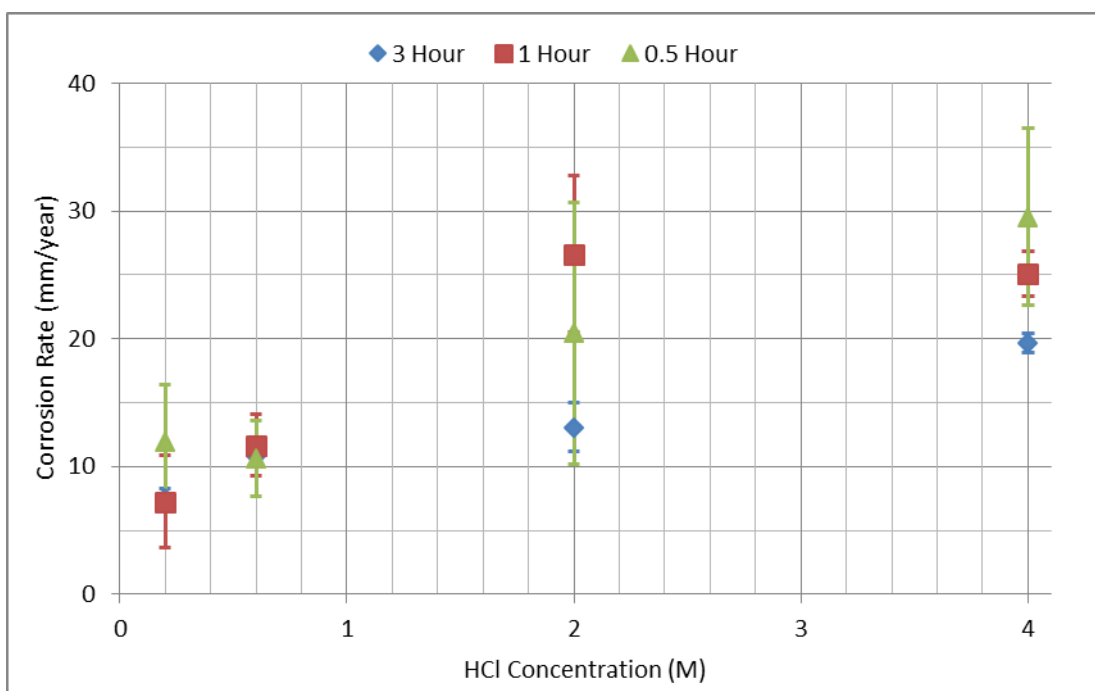
Figure 6.10 Corrosion rates when coupons were placed in different molarity HCl solutions all containing 0.05wt.% PA for three different exposure times (0.5-3 hours) at 80°C. The scatter bands represent the maximum and minimum corrosion rates across all mass loss tests in each environment. The HCl was diluted with 4M NaCl brine.

Figure 6.10 shows that very little information can be gained from performing short duration mass loss tests. All exposure times display a similar trend; corrosion rate increases with HCl concentration. The 3 hour tests provide the most repeatable mass loss results. A larger range of corrosion rates were measured at shorter exposure times (especially 0.5 hours) than the 3 hour tests. This suggests that the short term mass loss tests are not viable for exposure times less than 3 hours. Therefore mass loss tests should be performed for a minimum exposure time of 3 hours and this methodology is

not suitable for understanding how the corrosion rate changes with exposure time.

6.3 Solution Corrosivity found from Electrochemical Tests

Mass loss coupons are unsuitable for understanding how the corrosion rate changes over time. Therefore it was vital to implement electrochemistry in order to understand how the corrosion rate changes over the duration of the test. Initial electrochemistry tests involved exposing HS80 electrochemistry samples to different molarity solutions for 3 hours. LPR measurements were performed at the start and after every 0.25 hours meaning that each test provided 13 measurements throughout the 3 hour exposure (full methodology is discussed in Section 4.5).

6.3.1 3 Hour Electrochemistry at Different HCl Concentrations

Figure 6.11 shows the average corrosion rates measured over 3 hours when samples were placed in all HCl solutions tested, all containing 0.05wt.% PA (relative to the HCl content of the solution). Despite the limitations of applying a Stern-Geary coefficient (as discussed in Section 2.2.4) the corrosion rate has been calculated for each of the HCl concentrations tested in order to compare this value to the acceptable corrosion rate (discussed in Section 6.2.3). The average corrosion rate over the duration of each test is plotted and the scatter bands represent the minimum and maximum corrosion rates measured throughout the duration of the 3 hour test compared to the acceptable corrosion rate. As discussed in Section 2.1.4, the Stern-Geary coefficient measured at each individual HCl concentration has been used to calculate each corrosion rate. Figure 5.22 highlights how the corrosion rates change over the duration of the 3 hour tests and these results, along with Figure 6.11 highlight several interesting trends. At a HCl concentration of 4M the corrosion rate shows very little change over time. The corrosion rate varies between 14.4mm/year and 16.3mm/year over the duration of the test. A range of less than 2mm/year. Figure 6.12 shows the calculated average corrosion rates from each of the 3 hour fixed concentration tests. However, unlike Figure 6.11, the scatter bands represent the standard deviation of the corrosion rates measured over the duration of the 3 hour test.
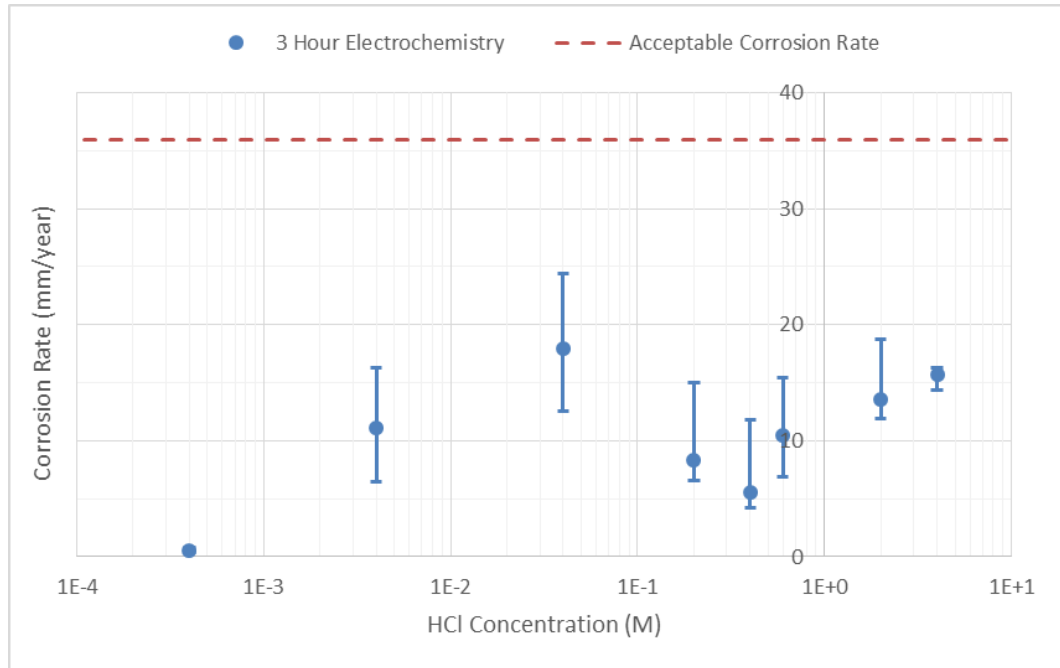
Figure 6.11 Average corrosion rates over 3 hour electrochemistry tests performed in a range of different molarity HCl solutions at 80°C, all containing 0.05wt.% PA and diluted with 4M NaCl brine. The acceptable corrosion rate is also shown. The scatter bands represent the maximum and minimum corrosion rates measured over the duration of each 3 hour test.
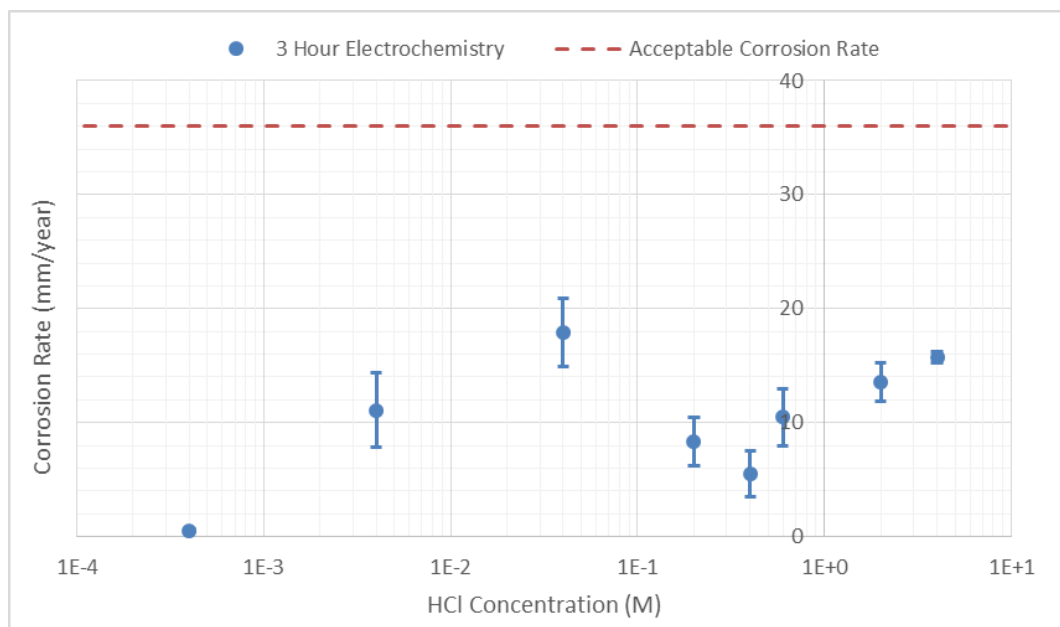
Figure 6.12 Average corrosion rates over 3 hour electrochemistry tests performed in a range of different molarity HCl solutions at 80°C, all containing 0.05wt.% PA and diluted with 4M NaCl brine. The acceptable corrosion rate is also shown. The scatter bands represent the standard deviation from the 13 corrosion rates measured over the duration of each 3 hour test.

At molarities less than 4M the corrosion rate tends to decrease over the duration of the test (Figure 5.24). For all solutions containing less than 4M HCl, the corrosion rate is at its highest value in the first 0.25 hours of the test. The corrosion rate is highest when the solution contains 0.04M of hydrochloric acid, 100 times less than the concentration of the injected HCl. At the lowest HCl concentration of 4×10^{-4}M the corrosion rate remains below 1mm/year throughout the entire test and decreases from 0.8mm/year to 0.4mm/year over the 3 hour test.

The points outlined above agree with the mechanisms of inhibition of the PA inhibitor. As discussed in Section 3.2.3.1 the PA polymerises to form an initial protective film which is then maintained by the PA in the solution over time. The 4M HCl solution maintains a very similar corrosion rate over the duration of the 3 hour test. This may be due to there being a large volume of PA in the solution (the PA volume is relative to the solution molarity) which is able to form the protective film in a very short time. This would result in the corrosion rate remaining at the same value throughout the entire 3 hour test as a protective PA film has formed almost instantaneously on the steel sample. At the lower molarities less inhibitor is in the solution, and as a result it may take longer to fully form the protective film on the steel sample. This may explain the decreasing corrosion rate as the inhibitor forms an ever more protective film over the duration of these tests. Alternatively, the relationship may be explained by the amount of HCl in the solution and the corrosivity of the solution decreasing over time. The 4M solution shows no decrease in corrosion rate over the 3 hour test unlike the lower molarity solutions which tend to decrease over time. The spending of HCl over time may explain why the lower molarity solutions become less corrosive over the 3 hour tests. This would suggest that the 4M HCl contains enough HCl to maintain a high corrosion rate over the entire test and the reaction of the HCl with the steel is not significant enough to reduce the corrosivity of the solution with time. Using this test methodology, it is not possible to definitively say which is the most likely explanation as the sample is exposed to the entire volume of HCl and PA throughout the entire test.

6.3.2 Statistical Difference between Electrochemical Tests

Figure 6.11 and 6.12 raise doubts over the statistical difference between the electrochemistry data. There appears to be very little variance between the

corrosion rates measured at different HCl concentrations. This is emphasised when comparing the scatter bands (which show the maximum and minimum measured corrosion rates) on Figure 6.11. There is overlap between these scatter bands for all HCl concentrations tested apart from the test performed at $4x10^{-4}$M. However, if the data is compared using Figure 6.12 (which show the standard deviation as the scatter bands) the difference in corrosion rate between each HCl concentration appears to be more significant.

In order to quantify the difference between the data sets statistical methods must be employed. One-way analysis of variance (ANOVA) can be used to determine if the means of several groups are all equal. It can be applied to any number of data sets greater than 2 meaning that it can be used to compare the electrochemistry data from all HCl concentrations tested (4M– $4x10^{-4}$M) or can instead be used to compare smaller samples of interest (e.g. 0.6M–0.2M). ANOVA is used to test whether samples in all groups are drawn from populations with the same mean values [164, 165]. If this is not found to be true then the data sets can be said to be statistically different. This allows statements to be made regarding the difference between the solution corrosivity measured across each of the different HCl concentrations. ANOVA compares the statistical variance of data sets by comparing two different variance values. The first variance is calculated among the means of the data sets. The second variance is found from each sample. If the variance between the group means is higher than the variance of the samples then this means that the group means are not drawn from populations with the same mean value and the data is therefore statistically different. Further detailed explanation of the ANOVA calculations is beyond the scope of this work and is widely available in published literature [164-167].

Table 6.1 compares the ratio of the variance calculated among the means to the variance within the samples value (F) with a critical value (F_{crit}) for a range of different HCl concentrations. The critical value is the number that the test statistic must exceed to reject the test. The critical value is found from tables available in literature [168, 169] and is based upon the number of datasets, the total number of test samples (in this case a maximum of 8 different HCl concentrations and a maximum of 104 individual corrosion rate measurements) and the desired value of statistical significance. A statistical significance of between 1-5% is typically used in studies [170]. A statistical significance of 1% was chosen (as shown in Table 6.1) as this gives the

highest critical value. If the calculated variance (F) is higher than the critical value (F_{crit}) then there is strong evidence that the data sets are statistically different [164].

Sample Size	HCl Concentration Range (M)	Calculated Variance (F)	Critical Value (1% significance)
8	4 - 4×10^{-4}	**80.8**	2.8
7	4 - 4×10^{-3}	**41.0**	3.0
6	2 - 4×10^{-3}	**35.6**	3.3
5	0.6 - 4×10^{-3}	**37.0**	3.6
4	2 - 0.2	**31.4**	4.2
3	4 - 0.6	**26.5**	5.2
2	2 - 0.6	**12.7**	7.8

Table 6.1 The lowest calculated variance for each different sample size. The HCl concentration range over which the lowest variance was calculated for each sample size is shown along with the critical value required for a 1% significance. A calculated variance higher than the critical value shows strong evidence that the expected values in the HCl range differ.

The variance was calculated for each possible sample size (2-8) and the HCl concentration range with the smallest variance are shown in Table 6.1. For all HCl concentrations the calculated variance was found to be significantly higher than the critical value for a 1% significance. Therefore it can be concluded that there is strong evidence that the corrosion rates measured in each data set differ. Therefore there is a variation in solution corrosivity at all tested HCl concentrations as the HCl is diluted from 4M to 4×10^{-4}M.

6.4 Comparison between Mass Loss and Electrochemistry

In order to fully understand the corrosivity of the solution that flows back following an acid job it is vital that both weight loss and electrochemistry are used to complement each other. Through comparisons between the two techniques and using the weight loss to validate the electrochemistry the corrosivity of the flowback fluid can be best characterised.

6.4.1 Comparison between Different HCl Concentrations

Figure 6.13 shows a comparison between the corrosion rates found from the 3 hour electrochemistry and the 3 hour mass loss tests at a range of HCl concentrations (all containing 0.05wt.% PA). Figure 6.13 shows that the relationship between the HCl concentration and the corrosion rate of the HS80 sample follows the same trend when both test methodologies are used. Excellent agreement is seen at almost all HCl concentrations with both the weight loss and electrochemistry results producing very similar corrosion rates at the majority of HCl concentrations tested. A discrepancy between the corrosion rates is observed at only two HCl concentrations; 4M and 0.4M. At both concentrations the electrochemistry underestimates the corrosion rate by approximately 4mm/year. The reason for this discrepancy is not immediately clear and difficult to explain.
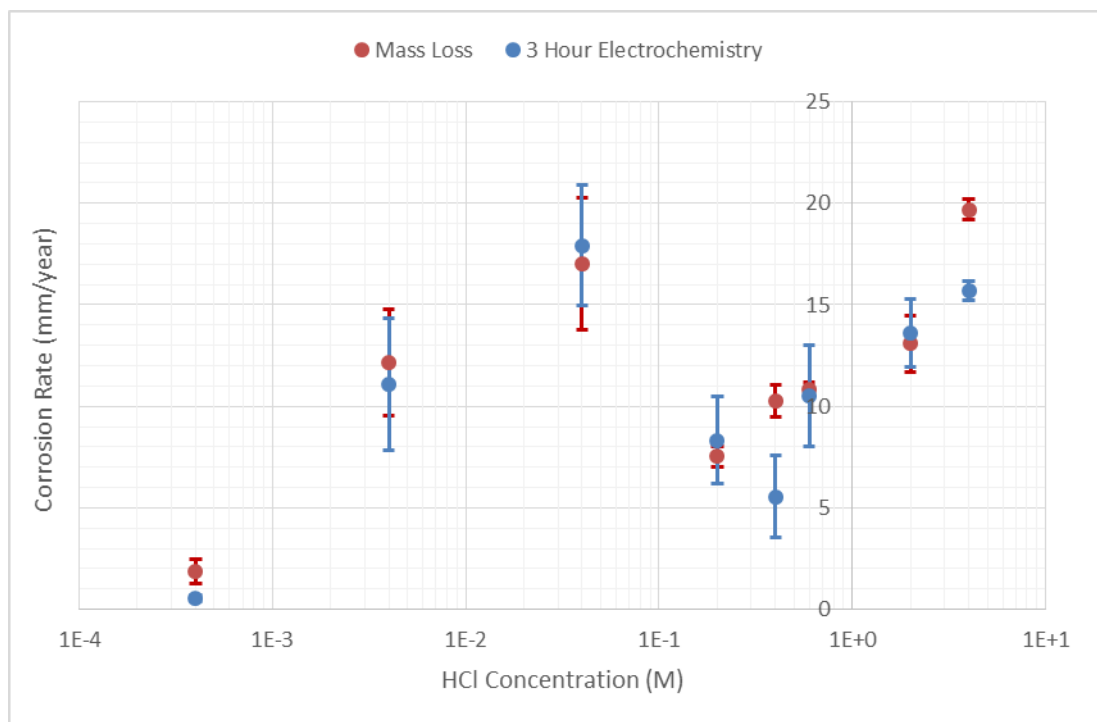
Figure 6.13 Comparison between the corrosion rates calculated from mass loss tests and the average corrosion rate over 3 hour electrochemistry tests when samples were placed in solutions containing between 4M and 4×10^{-4}M of HCl diluted with 4M NaCl brine. The mass loss scatter bands represent the maximum and minimum calculated corrosion rates across all 3 hour mass loss tests in each environment. The electrochemistry scatter bands represent the standard deviation from the 13 corrosion rates measured over the duration of each 3 hour test. All tests were performed for 3 hours at 80°C.

6.5 Corrosion Rates found from 1L Vessel Dilution Tests

The results outlined in the previous chapter are important for understanding how the corrosion rate changes in lower molarity solutions. The 3 hour mass loss and electrochemistry highlight just how corrosive solutions containing small amounts of HCl can be if there is not enough PA present in the solution. However in order to understand the molarity and PA concentration at which the corrosion rate begins to increase, a new dilution test methodology was developed (full methodology provided in Section 4.5.3).

6.5.1 1L Vessel Dilution Test Corrosion Rates

The results of the dilution test starting at 4M HCl (containing 0.05wt.% PA) and diluted with 4M NaCl brine at a rate of 10ml/min are shown in Figure 5.26. In order to understand how the corrosion rate changes as the molarity of the solution is diluted, the time has been converted to the molarity of the solution at that point in the test in Figure 6.14.
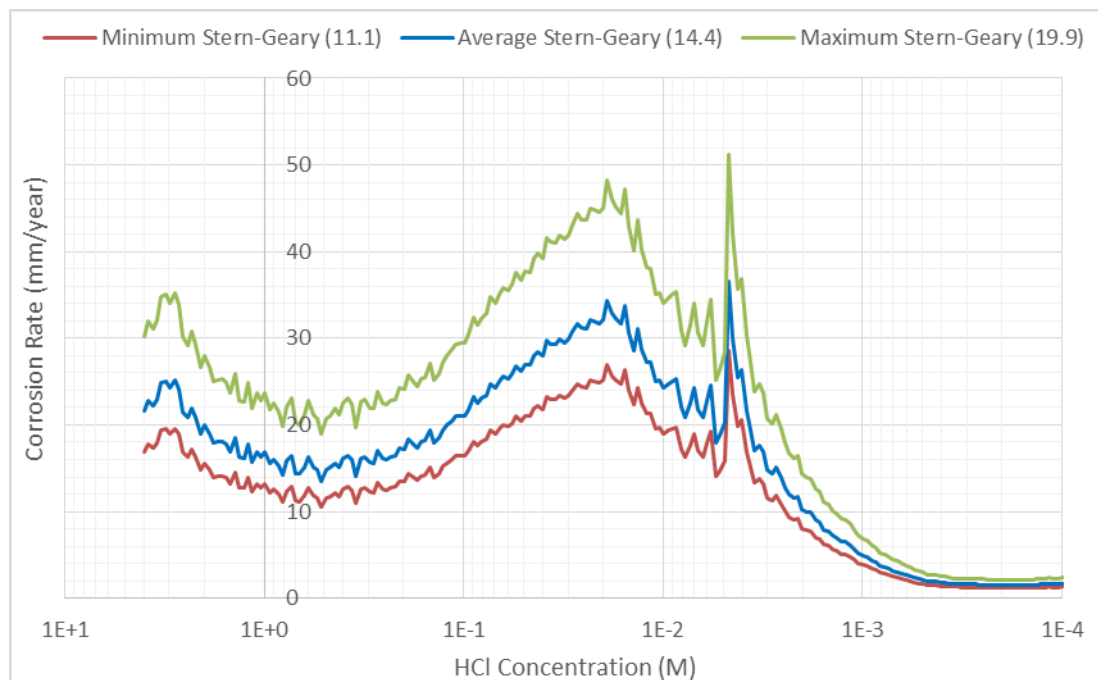
Figure 6.14 Calculated corrosion rates when the minimum possible (11.1), maximum possible (19.9) and average (14.4) Stern-Geary coefficients found from the fixed concentration tests were applied. Tests were performed on HS80 samples placed in 4M HCl (containing 0.05wt.% PA) diluted with 4M NaCl brine at a rate of 10ml/min at 80°C. The time has been converted to the HCl concentration.

Despite the limitations of applying a Stern-Geary coefficient the reciprocal of the charge transfer resistance has been converted to the corrosion rate using three values; the maximum (19.9), minimum (11.1) and average (14.4) Stern-Geary coefficients (the reason for applying these values is discussed in Section 5.3.5.1). The corrosion rates shown in Figure 6.14 further highlight the complex relationship observed in the fixed HCl concentration tests between the HCl concentration of the solution and the corrosion rate at low HCl molarities. From Figure 6.14 it is clear that the solution is most corrosive when the HCl concentration is less than 0.04M, 100 times less than the starting HCl concentration of 4M. The solution does not return to the pre-acid job corrosion rates until the HCl concentration is diluted to less than 0.001M (approximately 15 hours into the dilution test). Figure 6.14 suggests that two clear peaks in corrosion rate occur during the test; the first at a HCl concentration of 0.02M and the second at 5×10^{-3}M.

6.5.2 Comparison between 1L Vessel Dilution Test and Mass Loss Corrosion Rates

A direct comparison between the dilution test results (Figure 6.14) and the mass loss results (Figure 6.8) is provided in Figure 6.15. Figure 6.15 shows that a similar trend is observed between the corrosion rate and decreasing HCl concentration of the solution when both the dilution test and the weight loss methodology is used.

- A corrosion rate of approximately 20mm/year is observed in both tests when the solution contains 4M HCl (provided the average Stern-Geary coefficient is applied).
- The corrosion rate then decreases as the HCl concentration is reduced from 4M to 0.2M (5 hours into the dilution test). The corrosion rate measured in the dilution test is higher (for all applied Stern-Geary coefficients) than the mass loss tests.
- In both tests the corrosion rate increases as the solution is diluted to less than 0.2M before decreasing again once the solution contains less than 4×10^{-3}M HCl.
- The corrosion rate returns to normal pre-acid job values once the solution has been diluted to 4×10^{-4}M HCl (15 hours into the dilution test).
- The 3 hour mass loss tests fail to fully capture the first peak observed in the dilution test and failed to identify the second peak.
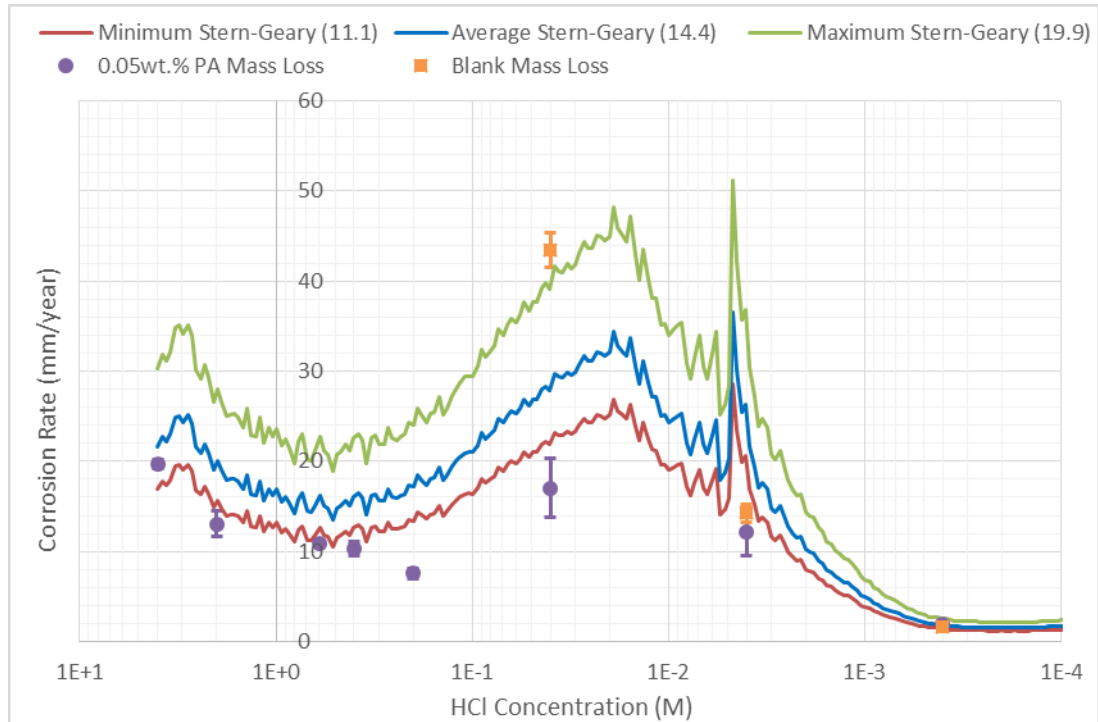
Figure 6.15 Corrosion rate measurements when 4M HCl (containing 0.05wt.% PA) is diluted with 4M NaCl brine at a rate of 10ml/min. Corrosion rates from 3 hour mass loss tests (blank and containing 0.05wt.% PA) are shown for comparison. The mass loss scatter bands represent the maximum and minimum calculated corrosion rates across all 3 hour mass loss tests in each environment. The corrosion rate has been plotted as a function of the HCl concentration of the solution at that point in the test.

The second peak appears to coincide with the point at which the PA stops offering the steel protection from the HCl. This is indicated by the mass loss results which are the same regardless of whether or not PA is added to the solution at a HCl concentration of less than 4×10^{-3}M. Unfortunately the HCl and PA concentration are not known at his point in the dilution test as it is unknown at what rate the HCl and PA have reacted over the duration of the test.

6.5.3 Comparison between the Dilution Test and 3 Hour Electrochemistry Corrosion Rates

The solution corrosivity found from the dilution test can also be compared to those found from the 3 hour fixed HCl concentration electrochemistry tests. Figure 6.13 shows that the corrosion rates found from 3 hour mass loss and electrochemistry are very similar. As a result the comparison between the dilution test and 3 hour electrochemistry (Figure 6.16) shows a very similar

trend to Figure 6.15. Again the solution corrosivity is represented by the reciprocal of the charge transfer resistance (in order to limit the issues with applying Stern-Geary coefficients that have been discussed extensively). The measured corrosivity in the dilution test is noticeably higher than the 3 hour electrochemistry tests. Like the mass loss tests, the 3 hour electrochemistry tests fail to fully capture either of the peaks in solution corrosivity observed in the dilution test.
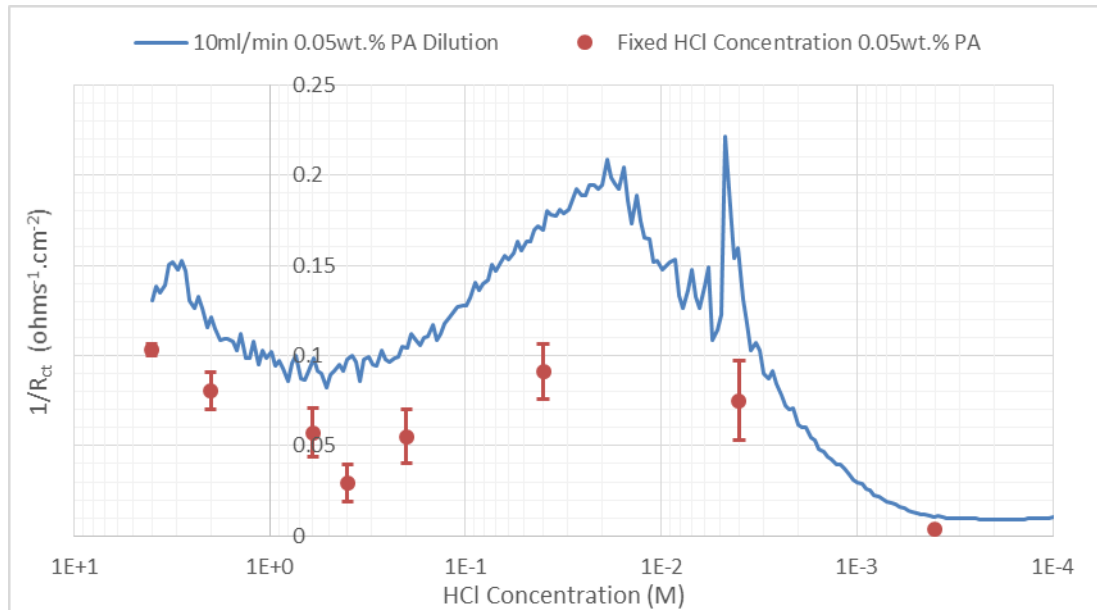
Figure 6.16 Reciprocal of the charge transfer resistance ($1/R_{ct}$) measurements when 4M HCl (containing 0.05wt.% PA) is diluted at a rate of 10ml/min with 4M NaCl brine. Average values from 3 hour fixed HCl concentration tests are shown for comparison and the scatter bands represent the standard deviation from the 13 corrosion rates measured over the duration of each 3 hour test. All tests were performed at 80°C.

6.5.4 Variation in Corrosion Rate as a Function of HCl Concentration

Different methodologies have been employed to study the flowback fluid. It is important to compare the results from each test and compare the solution corrosivity at each of the different HCl concentrations tested. Figure 6.17 compares the reciprocal of the charge transfer resistance ($1/R_{ct}$) values found from 3 hour electrochemical tests performed in fixed HCl concentration solutions and the 10ml/min dilution test.

The reciprocal of the charge transfer resistance is compared in order to eliminate the issues which arise from having to use Stern-Geary coefficients to calculate the corrosion rate. As discussed in Section 2.2.4 there are several problems which can be encountered when using Stern-Geary coefficients, in particular the variation in the Stern-Geary coefficient over the course of the dilution test and also the ambiguity in choosing the anodic and cathodic Tafel slopes. Therefore the reciprocal of the charge transfer resistance can be used to compare the results from the two test methodologies.
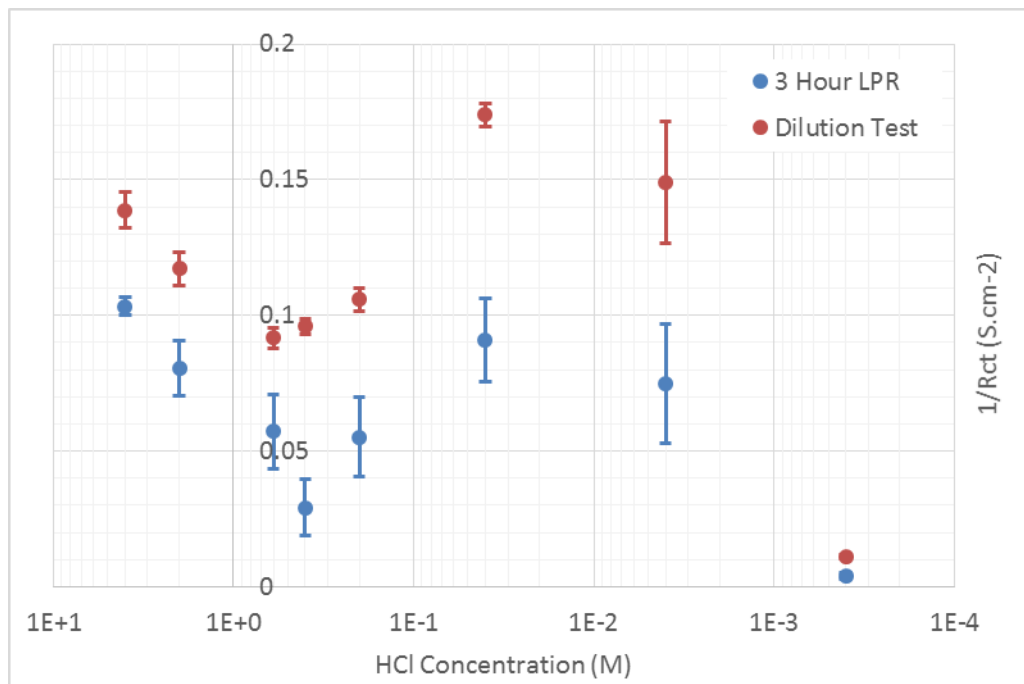
Figure 6.17 The average values for the reciprocal of the charge transfer resistances (1/R_{ct}) from the fixed concentration tests and the 10ml/min dilution test. The 3 hour test scatter bands represent the standard deviation calculated from all measurements made at that concentration. The dilution test scatter bands represent the standard deviation from the five nearest HCl concentrations at which measurements were taken.

The 3 hour electrochemical data shows the average reciprocal of the charge transfer resistances (1/R_{ct}) found from multiple measurements taken over the duration of two separate 3 hour tests. The scatter bands show the standard deviation from this average value. The dilution test results show the average value calculated from five LPR measurements taken at each of the HCl concentrations tested in the fixed concentration tests (ranging from 4M to 4x10^{-4}M). As the HCl concentration is constantly changing over the duration of the dilution test the measurement which was taken at the closest HCl

concentration is used along with the two previous and two following LPR measurements. This is not possible for the 4M HCl comparison as the dilution test starts at this concentration, therefore the first five measured values are used for this concentration. The range of HCl concentrations this includes from the dilution tests for each of the fixed HCl concentrations is provided in Table 6.2. The average reciprocal of the charge transfer resistance ($1/R_{ct}$) for each HCl concentration is also provided in Table 6.2.

HCl Concentration (M)	Fixed HCl Tests	10ml/min Dilution Tests	
	Average $1/R_{ct}$ (S.cm^{-2})	HCl Concentration Range (M)	Average $1/R_{ct}$ (S.cm^{-2})
4	0.1034	4 - 3.27	0.1387
2	0.0805	2.20 - 1.80	0.1173
0.6	0.0573	0.66 - 0.54	0.0916
0.4	0.0292	0.44 - 0.36	0.096
0.2	0.0552	0.22 - 0.18	0.1059
0.04	0.091	0.044 - 0.036	0.1738
0.004	0.0748	0.0044 - 0.0036	0.149
0.0004	0.0039	0.00044 - 0.00036	0.0111

Table 6.2 Comparison between the average reciprocal of the charge transfer resistances ($1/R_{ct}$) from the fixed concentration tests and the 10ml/min dilution test. The average reciprocal of the charge transfer resistance ($1/R_{ct}$) is calculated from five values over the HCl concentration shown.

The results shown in Figure 6.17 show a similar trend exists when the HCl concentration is varied. There is however a clear difference between the values of the average reciprocal of the charge transfer resistance when each of the test methodologies are used. Due to the limitations of the dilution test (discussed in Section 5.4) it is not possible to provide a reason for this discrepancy as the true HCl and PA concentrations of the solution throughout the dilution test are not known. Therefore the difference in the values may be due to the limitations of the closed beaker dilution test methodology.

6.6 Comparison with Literature

As discussed in Section 3.3 and 3.4 almost all of the previous acidizing corrosion research has focused on the corrosivity of the injected acids. The corrosivity of a large range of different acids and inhibitor packages have been researched at a range of acid and inhibitor concentrations and chemistries. However the injected acids are always high strength (pH<0) and always contain a high concentration of inhibitor. The aim of this work is to understand how the corrosivity of the injected acid changes once production resumes following an acid job. This makes a comparison between the low molarity HCl solutions (≤4M) tested in this work and the high strength HCl solutions discussed in literature (≥4M) difficult.

The majority of the tests performed were intended to help understand the corrosivity of the flowback fluid. Therefore only a small number of tests were performed at concentrations designed to replicate acid injection in the field (4M HCl with 0.05wt.% PA) however this does make a comparison between these tests and those found in literature possible.

In the literature, a small number of tests have been performed in spent acid, designed to replicate the fluid that flows back following an acid job. Due to the large number of experimental variables, a comparison cannot be made between the corrosivity of the flowback fluid characterised in literature and those found from the tests performed. Instead, the ability to characterise the flowback process achieved by previous studies and the newly developed dilution tests (Section 5.3.5) is compared.

6.6.1 Injection Strength HCl and Propargyl Alcohol Comparison

Tests were performed at several HCl concentrations without inhibitor present. Unfortunately it is difficult to compare these corrosion rates to values found in literature due to the nature of the previously performed studies. As outlined in Section 3.3 almost all of the previous studies have focused on the ability of high concentrations of inhibitors to reduce the corrosivity of high molarity injection strength acids. Therefore the blank data available tends to be at a fixed high HCl concentration and these studies not provide any indication as to how the corrosion rate varies with decreasing acid concentration. The few publications which do study different strength HCl solutions are not suitable

for comparison with this work due to significant differences in temperature [91, 171].

Acetylenic alcoholics (particularly PA) have long been known to be effective at inhibiting strong acids [45]. Unfortunately (as discussed in Section 3.3) most of the previous research work has looked at the ability of newly developed inhibitors (or inhibitor packages) to inhibit the corrosion caused by the injected acid. As a result very few studies have looked at the efficiency of just PA.

Unfortunately the comparison with literature is further limited by the large number of variables used in testing. The acid composition and strength used in previous studies varies and is typically HCl or HF (or a mixture of the two) at different concentrations. Tests are also performed at a range of temperatures and pressures. Many tests are performed at temperatures between 60°C and 80°C [5, 13, 64, 68, 71, 78, 88, 90, 98-101] but many studies have also included tests performed at significantly lower temperatures (25-40°C) [13, 88-93, 103]. Tests have also been performed at temperatures above 100°C and pressures higher than 1 atmosphere in order to better simulate well conditions [13, 93-96].

A range of different tubing grade steels have also been studied, including active and passive materials. A large number of different steels are typically found downhole, hence the large number of different grade steels that have been studied previously. For example, in one study alone over 30 different steels were tested; ranging from carbon steels to duplex stainless steels [13]. The exposure time can also vary significantly between each study, with mass loss coupons exposed for anywhere between 0.5 hours [93] and 72 hours [13].

Due to the large number of potential experimental variables comparison between the literature and the results presented in Section 5.1 is difficult. The only work which is directly comparable is that performed by Barmatov, Hughes and Nagl [5]. Mass loss tests were performed in 4M HCl at 80°C for an exposure time of 3 hours. A range of steels and inhibitors were tested but crucially the corrosion rate of HS80 at a range of PA concentrations was tested. Unfortunately, from the data presented it is not clear exactly what propargyl alcohol concentrations were tested and what the corrosion rates at

each of these PA concentrations was found to be. However, Barmatov, Hughes and Nagl state that a PA concentration of 11mM (0.061wt.% PA) was required to reach a plateau in corrosion rate [5]. This plateau is equal to a corrosion rate of 0.01lb/ft^3/3hr (18mm/year). Figure 6.18 shows a comparison between this value and the corrosion rates obtained from mass loss tests at a range of PA concentrations (presented in Section 5.1).
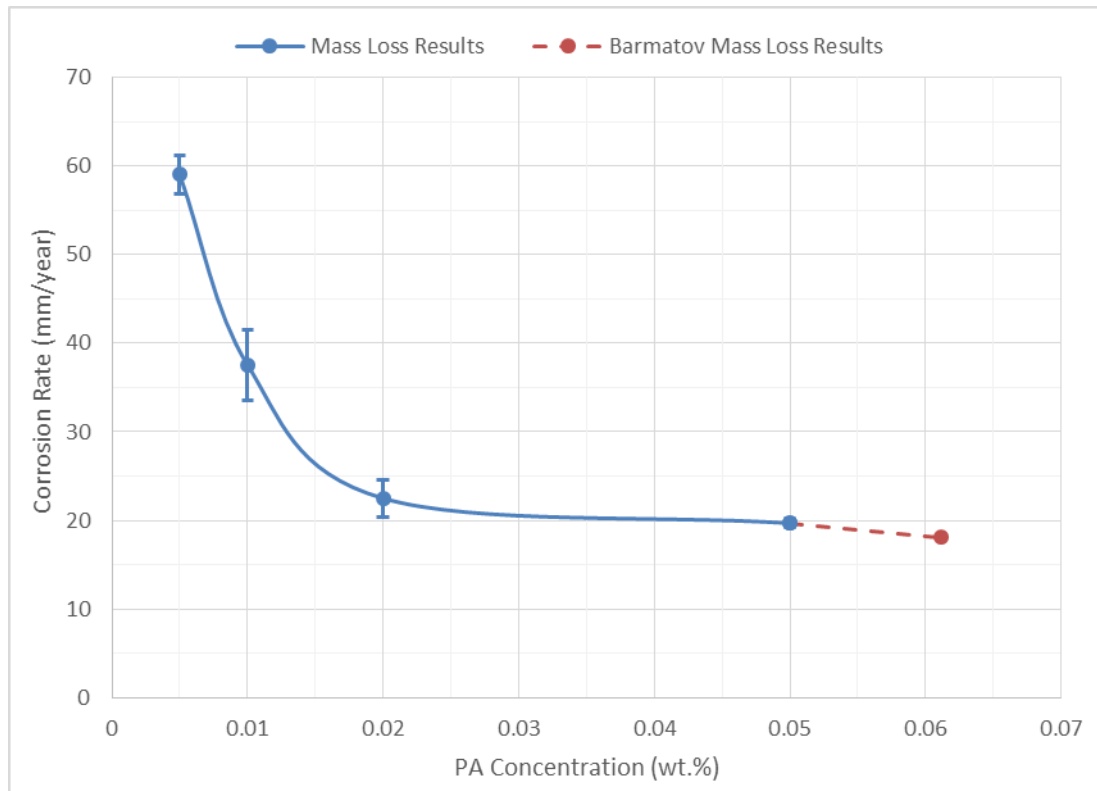
Figure 6.18 Corrosion rates found from HS80 mass loss tests performed in 4M HCl at 80°C at a range of PA concentrations, the mass loss scatter bands represent the maximum and minimum calculated corrosion rates across all 3 hour mass loss tests in each environment. A corrosion rate measurement from Barmatov, Hughes and Nagl [5] is shown for comparison.

Unfortunately only a single corrosion rate value can be obtained from the work performed by Barmatov, Hughes and Nagl [5]. This limits the comparison between the mass loss tests presented in this work and the value shown in Figure 6.18. The corrosion rate found by Barmatov, Hughes and Nagl [5] was at a slightly higher inhibitor concentration than the values tested in this work. This corrosion rate has been plotted on Figure 6.18 and a trend line added to allow a better visual comparison between both data sets. It is clear that the

corrosivity at this slightly higher PA concentration follows the trend of the mass loss results found from this work.

6.6.1.1 PA Efficiency

The efficiency of PA at a range of inhibitor concentrations has been studied. Funkhouser [96] looked at the efficiency of different PA concentrations in 4M HCl. The work tested the ability of PA to inhibit the corrosion on a general purpose mild steel (grade SAE 1010-1015) in autoclaves at temperatures of 120°C and pressures of 212kPa. A direct comparison between the PA efficiencies provided by Funkhouser [96] and those values calculated in this work is further complicated by the lack of individual data points provided (Funkhouser [96] provides only the trend line). The trend found by Funkhouser [96] has been replicated in Figure 6.19 in order to allow a comparison with the inhibitor efficiencies found in this work.
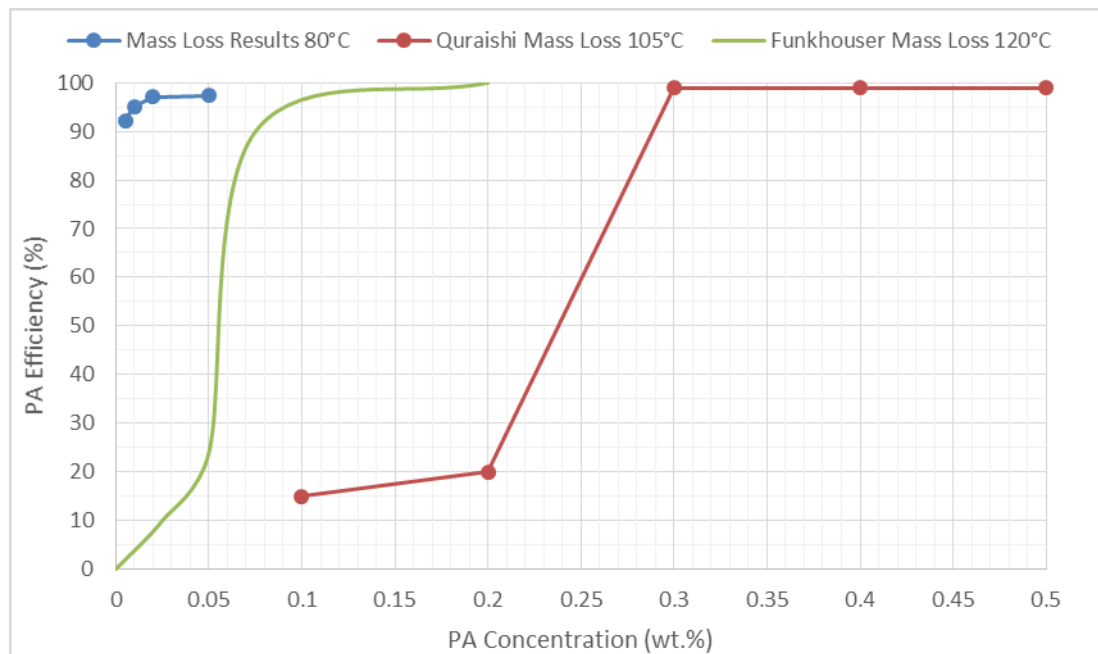
Figure 6.19 Inhibitor efficiency at a range of different PA concentrations added to 4M HCl. Results from mass loss tests performed with HS80 steel at 80°C are compared to efficiencies found at 120°C using SAE 110 steel found by Funkhouser [96]. Efficiencies found by Quaraishi and Jamal [93] at 105°C with mild steel are also shown.

The comparison between PA efficiencies shown in Figure 6.19 highlights the difficulty in comparing results performed at different temperatures and on different grade steels. Funkhouser [96] found that a PA concentration as high as 0.08wt.% was required in order for the PA to be over 90% efficient. The mass loss tests, presented in Section 5.1, found that a PA concentration 16 times less (5×10^{-3}wt.%) was still over 90% efficient.

The difference in efficiencies is likely due to the variations between the test methodologies. An exposure time of 3 hours and a temperature of 80°C was used in this work. This temperature was chosen as it meant that coupons could be exposed to the acid for a significant length of time (in order to provide reliable mass loss measurements) without substantial volumes of acid evaporating over the duration of the test. The chosen temperature and exposure time also allow a direct comparison with the work of Barmatov et al. [5, 85], who performed similar tests on similar tubing grade steels.

Funkhouser [96] placed mass loss samples in 120°C HCl for 24 hours (8 times longer than this work). The higher temperature, longer exposure time and the fact that different grade steels were tested may all be potential reasons for the difference in efficiency. Quaraishi and Jamal [93] performed similar mass loss tests to understand how the efficiency of the PA varies as the concentration is increased. Tests were performed using mild steel (the specific steel grade is not provided) mass loss coupons at a temperature of 105°C. The vessel was not pressurised, instead a condenser was used along with a short exposure time of 0.5 hours. A comparison between the efficiencies calculated from the mass loss tests (shown in Section 5.1) and those calculated by Quaraishi and Jamal [93] is shown in Figure 6.19.

Again, Quaraishi and Jamal [93] found that in order for the inhibitor to be over 90% efficient, much higher PA concentrations are required. There are several differences between the test methodology used in this work and that used by Quaraishi and Jamal [93]. Different grade steels and exposure times were used, but more importantly the tests were performed at different temperatures.

Both Funkhouser [96] and Quaraishi and Jamal [93] performed mass loss tests at a higher temperature than the results presented in this work and both

found that much higher PA concentrations were required in order to be over 90% efficient. The difference in inhibitor efficiency is likely due to the PA efficiency decreasing at higher temperatures and pressures. Acetylinic alcohols (such as PA) function well at temperatures below 100°C, at higher temperatures the inhibition must be improved through the addition of intensifiers [172]. Due to the decrease in PA efficiency at these higher temperatures a comparison cannot be made between this work and the previous studies.

Many factors can affect the inhibitor efficiency, including but not limited to the temperature and the exposure time [46]. The flow velocity of the solution is also important as it can physically remove protective inhibitor films [114, 116]. Figure 6.19 highlights the difficulty in comparing inhibitor efficiencies when different test parameters are used. This is due to the large number of factors which may affect the performance of the inhibitor (temperature, concentration, compatibility and solubility considerations) [117]. The results compared in Figure 6.19 are all performed using different grade steels at different pressures and temperatures and for a range of exposure times. This results in the PA efficiency varying greatly between each study therefore making a direct comparison incredibly difficult. Due to the range of different conditions used in previous tests (the temperature difference especially), an experimental methodology which allows a direct comparison with all previous studies is not possible.

6.6.2 Spent Acid Corrosivity

As discussed in Section 3.3.3, several attempts have been made to simulate the flowback fluid by placing mass loss coupons (cut from a range of different steel grades) in spent acid. Morgenthaler, Rhodes and Wheaton [7] attempted to replicate spent acid in the laboratory by adding different amounts of mineral slurry (containing illite clay, bentonite clay and silica) to different concentrations of HCl and HF. The acid concentrations tested were diluted twofold and fourfold from the injection concentrations (15% HCl and 1.5% HF). Tests were performed on S13Cr, 22Cr and N-80. Although tests were performed on N80, a tubing grade steel similar to HS80, a comparison between the corrosion rates found in this study and the N-80 samples tested by Morgenthaler, Rhodes and Wheaton [7] is not possible. Unfortunately there are too many differences between the HCl solutions tested in this work and

those tested by Morgenthaler, Rhodes and Wheaton [7]; the temperature, acid composition (due to the addition of HF) and exposure time are all different. Most crucially it is not possible to compare the inhibitors used in both tests. Morgenthaler, Rhodes and Wheaton [7] tested three inhibitors provided by service companies, unfortunately this is the only information provided. Although it is likely that these inhibitors are acetylenic alcohols (possibly even a derivative of PA) a direct comparison with the corrosion rates found in this work (with the addition of PA) is not possible.

It should however be noted that Morgenthaler, Rhodes and Wheaton [7] reached similar conclusions regarding the corrosivity of the spent acid. They found that spent HCl is highly corrosive to low-alloy steels, agreeing with the results of the tests performed at HCl concentrations designed to replicate flowback fluids.

Similar limitations to those already discussed apply when comparing the results of this work to the flowback tests performed by Hernandez et al [13]. A range of carbon steel and stainless steel coupons were exposed to fresh and spent acid solutions at a range of temperatures (4°C-135°C). The fresh acid was specified as a mixture of acetic, hydrochloric and hydrofluoric containing an unspecified acidizing inhibitor (further experimental details are discussed in Section 3.3.3). The spent acid was produced by passing this acid mixture (containing no inhibitor) through a column containing mineral particles found in the formation they were attempting to study.

Again, a direct comparison with the results found from this work is not possible due to the large number of variables. However, Figure 6.20 shows the potential corrosivity of the flowback fluid observed in this work and several other studies [7, 13]. Due to the large number of variables in each study, the results shown in Figure 6.20 are all from tests performed on carbon steels and at temperatures as close to 80°C as possible (ranging from 80-99°C). Figure 6.20 compares the range of corrosion rates recorded on carbon steel samples placed in flowback fluids found from this work and several previous studies. The temperature and carbon steel grade are shown in Figure 6.20.

Figure 6.20 highlights not only the potential corrosivity of the flowback fluid, but also the potential range of corrosion rates depending upon the composition of the flowback fluid. The maximum corrosion rates shown in Figure 6.20 were all measured when the flowback fluid either contained no or very low concentrations of inhibitor. Predictably, the lowest corrosion rates (<10mm/year) observed in the work performed by Morgenthaler, Rhodes and Wheaton [7] were measured in spent acid solutions which contained acidizing inhibitors (the inhibitor name and concentration is not provided).
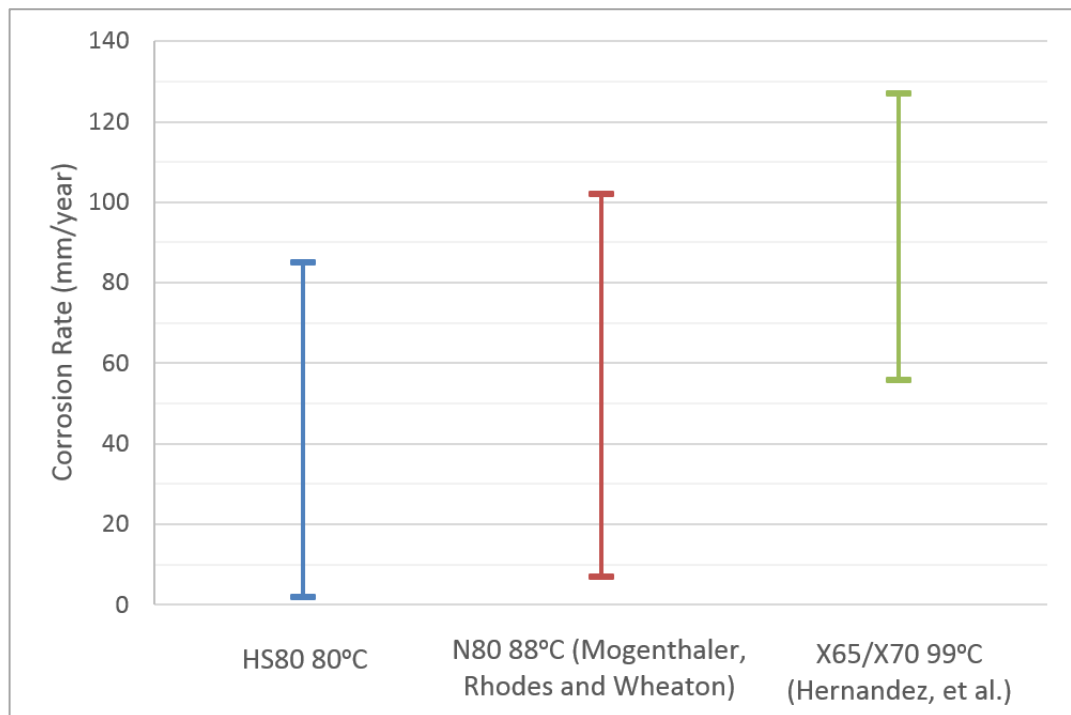
Figure 6.20 Comparison between the minimum and maximum corrosion rates observed in flowback fluids studied in this work and in previous studies by Morgenthaler, Rhodes and Wheaton [7] and Hernandez, et al. [13]. All corrosion rates are calculated from mass loss tests using different grade carbon steels at temperatures between 80-99ºC.

Al-Mutairi et al. [15] concluded that spent acid is highly acidic by monitoring acid fracturing treatments in the field. In one well, the flowback fluid was found to have a maximum HCl concentration of 21.2wt% (5.7M). Figure 3.15 shows how the Fe concentration of the flowback fluid from this well changes with the HCl concentration. Again, the results shown in Figure 3.15 indicate how corrosive the flowback fluid can be in the field. The total iron concentration is directly related to the corrosion of the tubulars as the formation was found to contain almost no iron. Unfortunately a comparison between Figure 3.15 and

the flowback corrosion profile found from dilution tests (Figure 5.26) is not possible. Again there are too many unknowns from the flowback profile shown in Figure 3.15; the most important of which is the flowrate from the well. Without knowing the production rate it is not possible to convert the iron in the flowback fluid (mg/L) to a corrosion rate (mm/year). It is also unknown how much of the iron in the acid is due to the reaction with the steel tubulars during injection. Any iron which is dissolved during injection will be produced in the flowback fluid once production restarts. Therefore it cannot be said that the total iron concentration shown in Figure 3.15 is due to the corrosivity of the flowback fluid.

Figure 3.15 highlights that the HCl concentration peaks approximately 30 minutes into the flowback profile reaching a high HCl concentration (16 wt.%) before drastically reducing to contain no HCl within approximately 10 minutes. This produces a spike in the total iron concentration of the solution before dropping to zero as the HCl concentration decreases. The corrosivity of the flowback fluid is expected to gradually decrease over the duration of the flowback [14], however this is not the case in Figure 3.15. This may be due to the production rate being high and the injected acid volume being low. This would result in the entire quantity of injected acid being produced in a relatively short time (as seen in Figure 3.15).

The flowback profiles provided by Al-Mutairi et al. [15] show the difficulty in replicating flowback accurately. Although general assumptions can be made about the flowback fluid i.e. the pH increases over the course of the flowback, each acid job will have a different flowback profile based on a range of different factors. These factors include, but are not limited to; the type and strength of the injected acid, geology of the formation, production rate and the bottom hole static temperature (BHST). In order to replicate all of the different potential variables a test methodology would be required in which the full flowback process can be replicated in a single test. Ideally this new test methodology should allow the concentration of a range of variables (e.g. acid, inhibitor, calcium, carbon dioxide) to be controlled throughout the test. This would provide a much better representation than the standard 3 hour mass loss tests in a solution of fixed chemistry.

Chapter 7 Flow Cell Design and Results

7.1 Flow Cell Design

The weight loss, 3 hour electrochemistry and dilution test results suggest that a complex relationship exists between the HCl and PA concentration of the flowback fluid. As discussed in Section 5.4 there are several limitations to the closed vessel test methodologies which must be overcome if the corrosivity of the flowback fluid is to be fully understood.

7.1.1 New Test Methodology Objectives

The aims of the new methodology should be to overcome the limitations outlined in Section 5.4.

- The steel sample must always be in contact with 'fresh' solution. This solution must contain a known HCl and PA concentration which has not been in contact with the steel previously. This provides a laboratory technique which is able to simulate the dilution of acid encountered during flowback from an acid job in a controlled and repeatable manner.
- The PA must not be heated with the HCl throughout the entire duration of the dilution test. It should only be heated prior to coming into contact with the steel sample. This eliminates the problem of the PA reacting to form unwanted products when heated to 80°C.
- Ideally the new test methodology should also eliminate the problem of the build-up of unwanted contaminants in the test solution. This allows the solution chemistry to be calculated throughout the duration of the dilution test which in turn allows more definitive conclusions to be drawn regarding the corrosivity of the flowback fluid. This can be solved by ensuring the sample is always in contact with fresh solution and any reacted solution is removed from being in contact with the sample.

7.1.2 Flow Cell Rationale

All of the aforementioned criteria can be met by the use of a flow cell through which a changing molarity solution is pumped. The use of a flow cell containing a steel sample and integrated electrochemistry has the benefit that fresh solution can be pumped into the cell. This solution comes into contact with the steel sample before then exiting the cell. This ensures that the sample is always in contact with fresh solution which has not seen the steel sample

prior to that point in the test. Due to the solution being able to exit the cell, once it has come into contact with the steel sample, the problem of contamination is eliminated (as any reacted solution is immediately removed from the flow cell).

Finally, the solution can be stored at room temperature throughout the duration of the test as the use of a flow cell means that it only needs to be heated prior to entering the cell. The desired temperature of 80°C can still be achieved by placing the flow cell in a water bath and allowing the solution to reach the desired temperature prior to entering the cell.

7.1.3 Flow Cell Development and Integration with Electrochemistry

Based on the criteria discussed in Section 7.1.1 a custom flow cell was developed. Due to the flow cell having to withstand strong hydrochloric acid at high temperatures the flow cell was manufactured from highly acid resistant polyethylene.
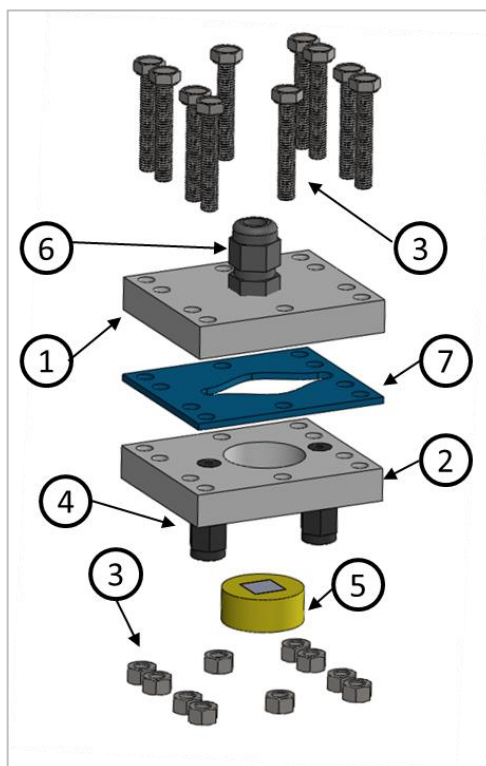
Figure 7.1 Exploded view of the flow cell. Each component has been numbered and is discussed in the text.

Figure 7.1 shows a diagram of the flow cell. The flow cell consists of a polyethylene top (1) and bottom piece (2) which is held together with 10 M6 nuts and bolts (3). The inlet and outlet ports are located in the base piece of the flow cell (4). The carbon steel sample (5) is flush mounted into the base of the cell. The sample was sealed into the base piece using a non-conducting acid resistant resin with strong edge retention (in order to prevent crevice corrosion). Prior to mounting the steel sample in resin an electrochemical connection was produced by soldering a wire to the back of sample. A combined reference and counter electrode is positioned directly opposite the steel sample. This was inserted through a cable gland (6) which was mounted into the top piece of the cell. A custom 2mm thick laser cut gasket (7) was manufactured from Viton FKM and used to separate the top and bottom piece of the flow cell. The fully assembled cell can be seen in Figure 7.2.

7.1.3.1 Flow Cell Electrochemistry

As mentioned previously the flow cell was designed to accommodate a 1 cm^2 carbon steel sample, a platinum counter electrode and a 4M Ag/AgCl reference electrode. Through the integration of a three-electrode cell, real-time electrochemical measurements can be performed to determine how the corrosion rate of the steel sample changes during flow-back.
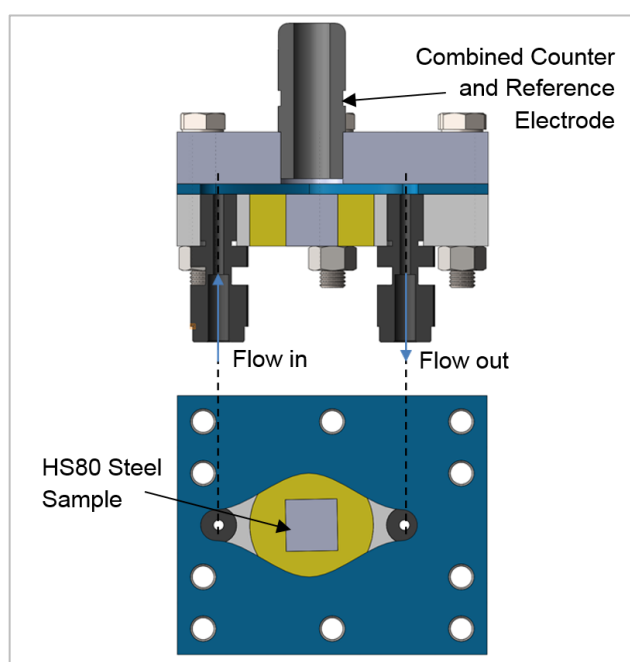
Figure 7.2 Cross-section through the flow cell indicating the position of the combined reference/counter electrode and the sample in relation to the gasket.

The platinum counter electrode and Ag/AgCl reference electrode were both flush mounted into the top of the cell directly opposite the carbon steel sample. Several publications [173, 174] have shown that positioning the working electrode directly opposite the reference and counter electrodes improves electrochemical measurements (through limiting both the electrochemical noise and the effect of solution resistance). Figure 7.2 shows the positioning of the combined counter and reference electrode relative to the steel sample.

7.1.3.2 Selection of Gasket Geometry

The fluid flow in the system is intended to be laminar (the Reynolds number calculations for the flow cell are provided in Section 7.1.4.3), however regions of reversed fluid motion (or eddies) can develop as the flow channel expands. It is therefore vital that the formation of any eddies within the system is prevented through the choice of an appropriate gasket geometry. Failure to understand the behaviour of fluid flow within the cell would result in a poorly designed cell which fails to simulate the 'once-through' process occurring within the field.

In order to meet the criteria outlined in Section 7.1.1 it is vital to ensure that once any 'fresh' solution has passed over the steel surface it then exits the flow cell quickly. A study by Pike et al. [175] focused on the evaluation of a number of central flow cell channel designs for biosensor applications. The flow cell gasket used the most efficient geometry found from this study. The geometry was termed the iCell and it was found to be best able to delay the onset of eddy development towards higher velocities.

The gasket geometry chosen for the flow cell was a scaled up version of this iCell geometry developed by Pike et al. [175]. The iCell geometry is specified via the 3rd order polynomial shown in Equation 7.1.

$$y = (C_1 x^3 + C_2 x^2 + C_3 x + 0.5) \quad (0 \le x \le 9) \tag{7.1}$$

Equation 7.1 provides a quarter of the profile using the local x and y co-ordinate positions (in mm). The equations used to calculate C_1, C_2 and C_3 using two size constraints (a and b) are provided in Equation 7.2-7.4. The size

constraints (*a* and *b*) were chosen based upon the gasket size and were set at 18mm and 12mm respectively.

$$C_1 = -\left(\frac{2b}{a^3}\right) \tag{7.2}$$

$$C_2 = \frac{3b}{a^2} \tag{7.3}$$

$$C_3 = 0 \tag{7.4}$$

The quarter curve obtained using Equation 7.1 was reflected about the vertical and horizontal planes. This provided the final flow cell geometry shown in Figure 7.3. It is important to note that the purpose of the flow through the cell was to replicate the dilution of acid seen during flowback following an acidizing procedure. The intention of the cell is not to replicate the actual flow regime encountered once production resumes in the field.
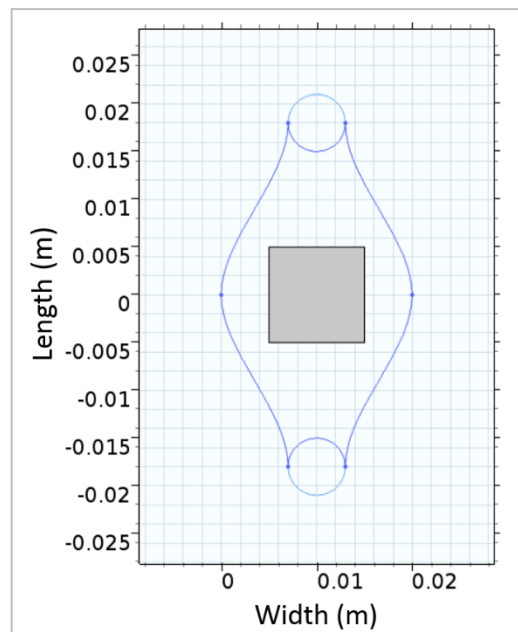
Figure 7.3 Geometry of gasket specified for the flow cell based on the iCell shape proposed by Pike et al. [175] – the square indicates the size and position of the 1cm^2 carbon steel sample within the cell.

7.1.4 Numerical and Experimental Validation of Flow Cell

It was important to validate the proposed design of the flow cell prior to performing any electrochemical experiments. A computational and experimental approach were used in order to understand the depletion of H^+ ions and accumulation of Fe^{2+} ions within the cell and help validate the outlined criteria (Section 7.1.1).

7.1.4.1 Producing the Mesh

A geometric model was built with the flow domain comprising of 460,000 elements. The constructed geometry was built to replicate the proposed flow cell and can be seen in Figure 7.4.
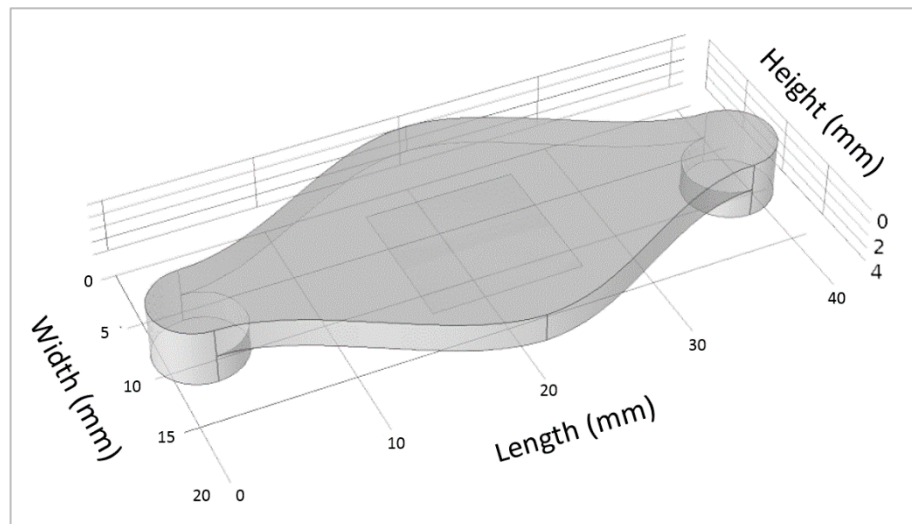
Figure 7.4 3D geometry of the flow cell within COMSOL Multiphysics.

In order to adequately resolve the concentration gradients (as a result of the simulated corrosion process) a distributed boundary layer mesh was implemented at the wall of the steel sample. Full details of the mesh sizes used in the flow cell simulation are included in Table 7.1. Figure 7.5 shows the final produced mesh.

	Mesh Location	**Element Size**
Flow cell surface (minus the steel sample)		Extra fine $(4.2 \times 10^{-5} - 9.8 \times 10^{-4})$
Steel sample		Extremely fine $(5.6 \times 10^{-6} - 4 \times 10^{-4})$
Boundary between the sample and the flow cell base		Extremely fine $(5.6 \times 10^{-6} - 1 \times 10^{-5})$
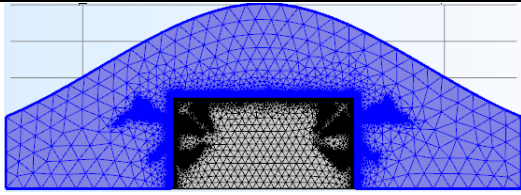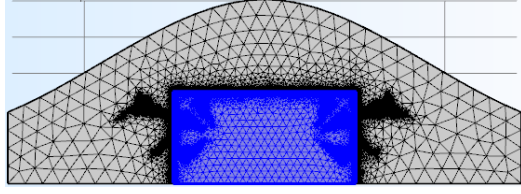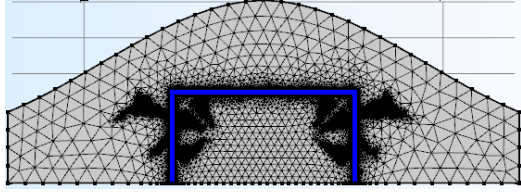
Table 7.1 Description of the mesh sizes used in the COMSOL model. The location of each mesh that was applied is shown in blue. The element size range is provided for each of the three mesh sizes.
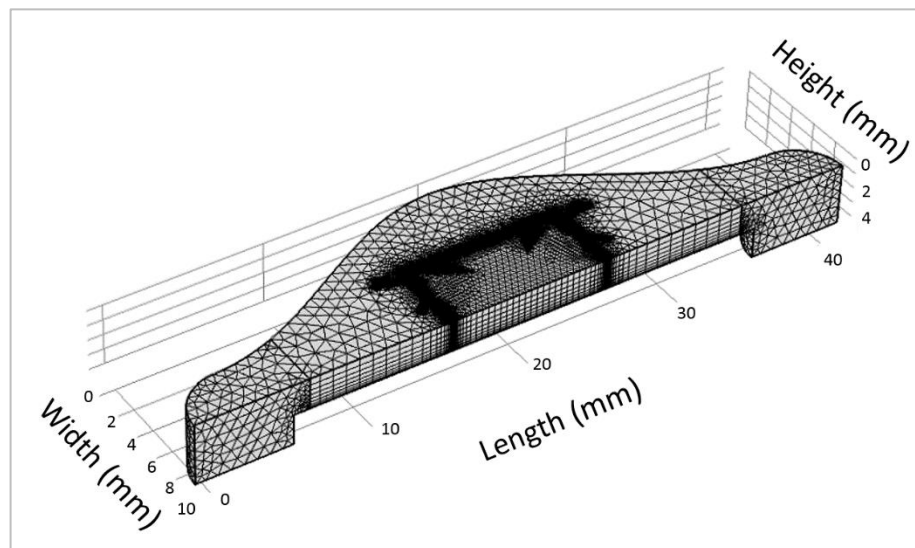
Figure 7.5 Axisymmetric model showing the distributed mesh applied across the sample in order to adequately resolve the concentration gradient in the boundary layer.

7.1.4.2 Setup of Numerical Model and Input Parameters

COMSOL Multiphysics was used to study the flow behaviour of the proposed cell. The standard time-dependant advection-diffusion equation for an incompressible flow (Equation 7.5) was used. Where c is the concentration, t

is time, D is the diffusion coefficient, $\boldsymbol{u}$ is velocity field; and ∇ is the del operator.

$$\frac{dc}{dt} = D\nabla^2 c - \boldsymbol{u} \cdot \nabla \boldsymbol{c} \tag{7.5}$$

The first step was to establish the velocity field by solving the steady state Navier-Stokes equation for an incompressible fluid under laminar conditions (Equation 7.6 and 7.7), calculated from the fluid density (ρ), the fluid pressure (p) and the coefficient of dynamic viscosity (μ).

$$\rho\boldsymbol{u} \times \nabla\boldsymbol{u} = -\nabla p + \mu\nabla^2\boldsymbol{u} \tag{7.6}$$

$$\nabla \times \boldsymbol{u} = 0 \tag{7.7}$$

The physical properties of the fluid were defined based on the concentration of the acid travelling through the cell. The values used in the simulation were based on those recorded in a study by Barmatov, et al. [85]. It should be noted that a symmetry boundary condition was used, as highlighted by the axisymmetric model (Figure 7.5), in order to reduce the computational effort.

An appropriate set of boundary conditions were applied in order to allow the steady state flow equations to be solved. Based on the previous work by Pike et al. [175], the boundary condition at the inlet was set to match the volumetric flow rate being studied (between 1-25ml/min) and at the outlet of the flow cell a pressure boundary condition (0 Pa) was set. Finally along the walls of the flow cell a no-slip boundary condition was applied. Table 7.2 provides the full details of the physical properties and the calculations used to determine the density and viscosity. In order to find values for the mixed solution the density and viscosity were proportionally ratioed. They were calculated based on density values of 1044.6kg/m^3 and 1205.6kg/m^3, and viscosity values of 3.475x10^{-4} Pa.s and 3.54x10^{-4} Pa.s for the 4M HCl and 4M NaCl solutions, respectively [176].

Initial concentrations of species were based on molarity values ranging from 4M to 4×10^{-4}M. Table 7.2 shows the molarities entering the cell and the concentrations of the following species; H^+, Cl^-, Na^+ and OH^-. The static mass loss tests (Section 5.1) were used to provide the corrosion rate used to model the Fe^{2+} and H^+ flux. For every 1mm/year of corrosion, it was calculated that 5.165×10^{-5}mol/m²/s flux of Fe^{2+} from the surface and 1.033×10^{-4}mol/m²/s flux of H^+ into the surface should be applied. The finite element method within COMSOL Multiphysics was used to solve the equations.

Property Name/Symbol	Value	Description
K_{H2O}	1×10^{-8} mol²/m⁶	Water dissociation constant
$k_{H2O, b}$	1×10^7 m³/(s·mol)	Backward rate constant for dissociation of water
D_{cH}	9.312×10^{-9} m²/s	Diffusion coefficient of hydrogen ions [177]
D_{cFe}	0.72×10^{-9} m²/s	Diffusion coefficient of iron ions [177]
D_{cCl}	2.032×10^{-9} m²/s	Diffusion coefficient of chloride ions [177]
D_{cOH}	5.26×10^{-9} m²/s	Diffusion coefficient of hydroxide ions [177]
D_{cNa}	1.334×10^{-9} m²/s	Diffusion coefficient of sodium ions [177]

Table 7.2 Chemical and physical properties of acid/brine mixture defined for the flow cell at 80ºC.

7.1.4.3 Numerical Model Flow Rate Results

The Reynolds number (R_e) was calculated at the highest flow rate to be simulated (25ml/min) to ensure that the flow through the cell is always laminar. The flow rate was converted from ml/min to m/s by converting the flow rate into m³/s and then dividing by the area of the cross section of the gasket at its widest point (2mm x 20mm). Equation 7.8 was used to calculate the Reynolds number of a HCl solution and a 4M NaCl solution [178]. The diameter at the widest point of the gasket (L) was used as this will give the largest possible

Reynolds number. The density (ρ) and viscosity (μ) of both 4M HCl and 4M NaCl brine were used to calculate the Reynolds number. The values used in the calculations and the calculated Reynolds numbers are shown in Table 7.3.

$$R_e = \frac{\rho V L}{\mu}$$
(7.8)

	Unit	Symbol	4M HCl	4M NaCl Brine
Density	kg/m3	ρ	1044.6	1205.6
Viscosity	Pa.s	μ	3.475×10^{-3}	3.54×10^{-3}
Diameter	m	L	0.02	0.02
Velocity (ml/min)	ml/min	V	25	25
Velocity (m/s)	m/s		0.010425	0.010425
Reynolds number			**627**	**710**

Table 7.3 Values used to calculate the Reynolds number for a 4M HCl and a 4M NaCl solution through the flow cell at a flowrate of 25ml/min. The calculated Reynolds number for each fluid at this flowrate are also provided.

Table 7.3 shows that the Reynolds number is less than 2,000 regardless of whether 4M HCl or 4M NaCl is pumped through the flow cell at a rate of 25ml/min. This indicates that the flow through the cell is laminar at all experimental and computational conditions discussed in this thesis [178]. The upper limits of flow within the cell were determined by analysing the velocity field at a range of flow rates through the cell. Figure 7.6-7.8 show the simulation results for a range of flow rates (1ml/min to 25ml/min.) The left-hand image in Figure 7.6-7.10 indicates the velocity field for each of the three different flow rates. The velocity profile across the leading edge, trailing edge and centre of the steel sample (1mm away from the surface) is provided in the right-hand image. This allows regions within the cell where flow across the sample is non-uniform, recirculating or stagnant to be identified. The location of the carbon steel sample relative to the gasket are shown in each of the images on the left. The velocity field is constant over the sample at a flowrate of 10ml/min. The velocity profile across the leading edge of the sample becomes less uniform as the flow rate is increased from 1ml/min to 25ml/min.

Based upon the profiles shown in Figure 7.6-7.8 the upper flow rate through the cell is thought to be between 10 and 25ml/min. It should again be emphasised that the flow through the cell is in no way intended to replicate the flow observed in the field. The aim of the cell is to provide a methodology for exposing a steel sample to a solution with a constantly changing chemistry. Therefore laminar flow through the cell is required to ensure uniform, non-circulating flow through the cell rather than the turbulent (high Reynolds number flow) that would be encountered once production restarts in the field.
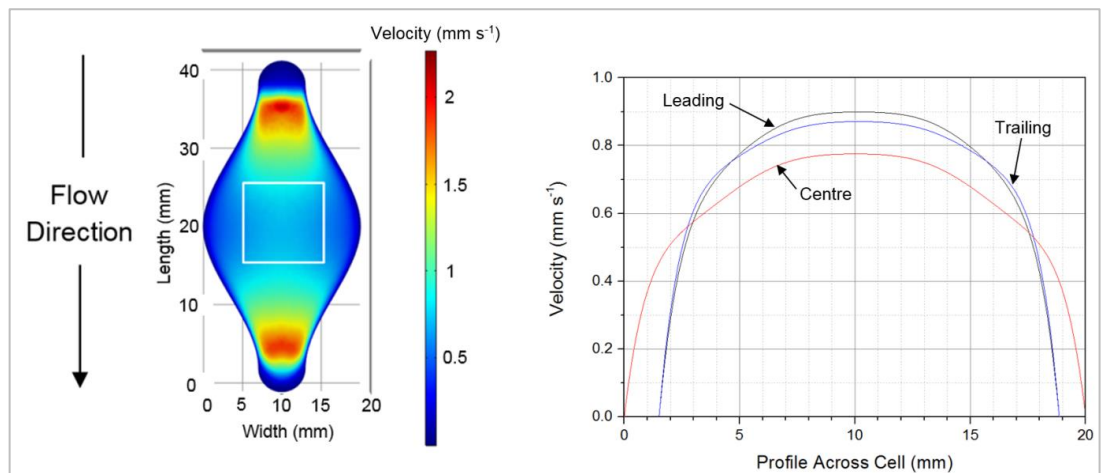
Figure 7.6 Computational results showing the velocity fields (left) and the velocity profiles across the leading edge (black), trailing edge (blue) and centre (red) of the steel sample (right) at a flow velocity of 1ml/min.
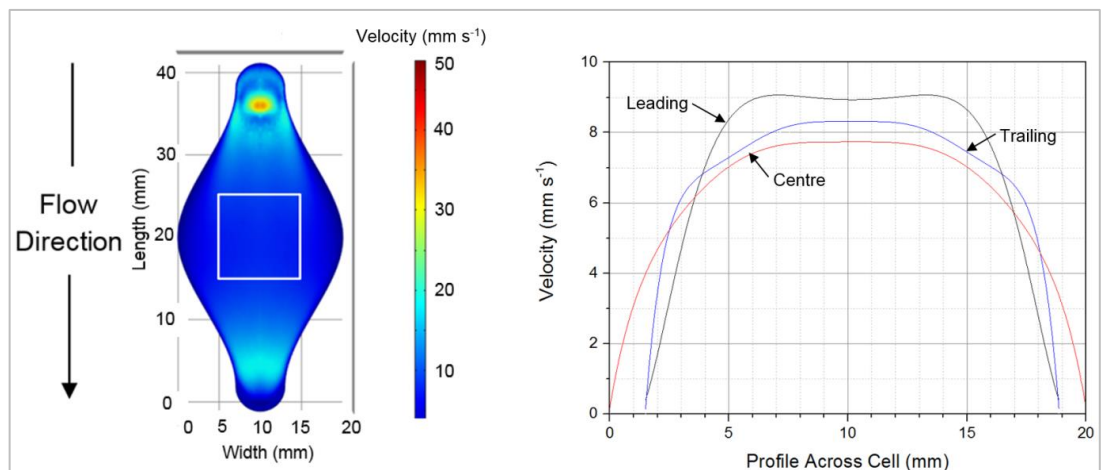
Figure 7.7 Computational results showing the velocity fields (left) and the velocity profiles across the leading edge (black), trailing edge (blue) and centre (red) of the sample (right) at a flow velocity of 10ml/min.
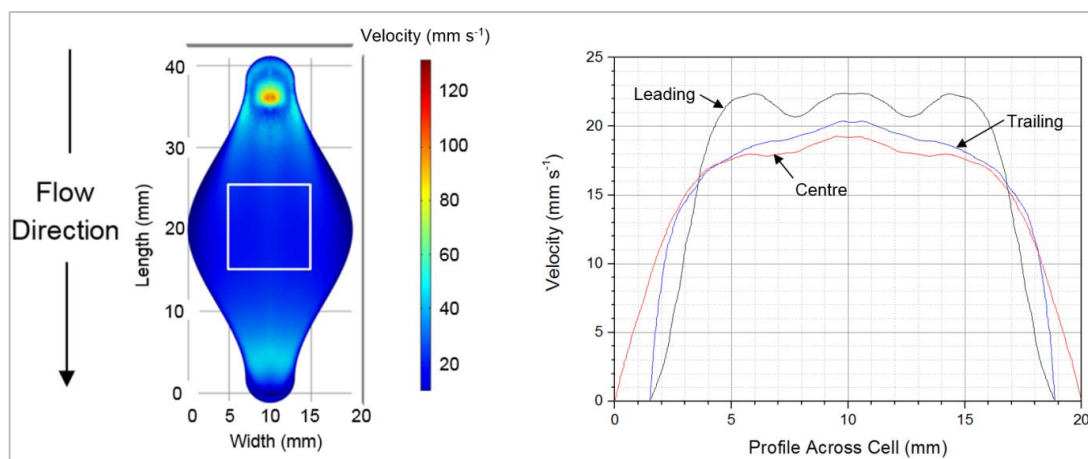
Figure 7.8 Computational results showing the velocity fields in (left) and the velocity profiles across the leading edge (black), trailing edge (blue) and centre (red) of the sample (right) at a flow velocity of 25ml/min.

7.1.4.4 Numerical Model Corrosion Simulation Results

It was vital to validate that there was not an accumulation of Fe^{2+} ions in the cell as the steel sample was corroded by the HCl solution. Any such build-up of Fe^{2+} ions would influence the electrochemical measurements and would result in the flow cell not meeting the outlined criteria (Section 7.1.1). After the steady state flow equations were solved, the advection-diffusion process was solved subject to the determined velocity field for the inlet. The inlet flow rate was set at 1, 2.5, 5 and 10ml/min, and the diffusion coefficients specified previously (Table 7.2) were used. The concentration of HCl entering the cell was varied to match the HCl concentrations ($4-4\times10^{-4}$M) used in the fixed concentration tests (shown in Table 4.1). A positive flux of Fe^{2+} ions and a negative flux of H^+ ions was specified for the surface representing the carbon steel sample. This flux corresponded to a corrosion rate of 1,000mm/year which represents a realistic worst case scenario at an acid concentration of 4M and temperature of 80°C [85]. All other cell walls were constrained to zero flux.

Figure 7.9 and 7.10 provide an example of the surface concentration maps for H^+ and Fe^{2+} produced using the numerical model at the lowest flowrate of 1ml/min. Images are shown for this flowrate as this resulted in the largest accumulation of H^+ and Fe^{2+} ions in the cell. These images depict the concentration of H^+ and Fe^{2+} ions across the surface of the steel sample within the flow cell at the highest acid concentration of 4M (the corrosion rate is 1,000mm/year). The images show that even at this extreme scenario it is clear

that the reacted acid and produced Fe^{2+} ions do not accumulate within the cell. Figure 7.10 also shows that the variation in H^+ across the steel sample is minimal.
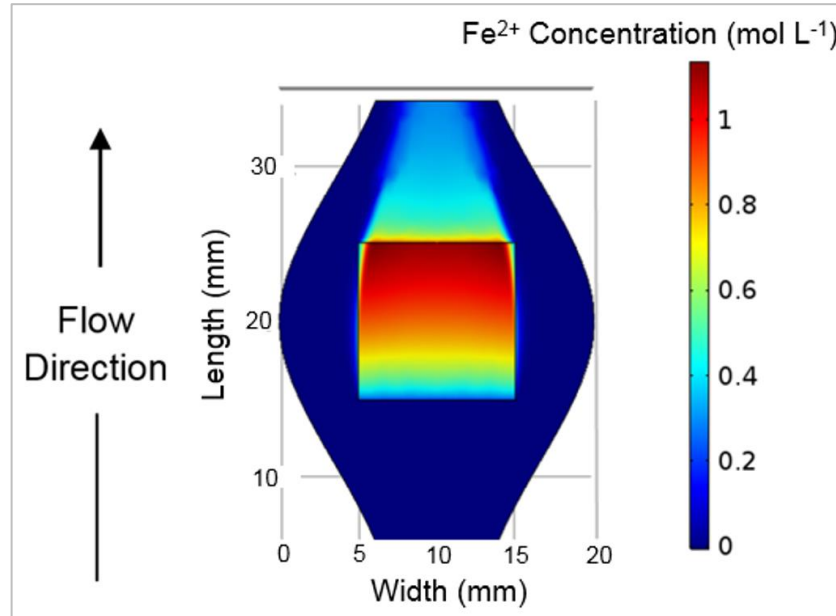
Figure 7.9 Concentration maps for Fe^{2+} at the base of the flow cell where the steel sample is positioned for an inlet flow rate of 1ml/min, HCl concentration of 4M and a defined corrosion rate of 1,000mm/year.
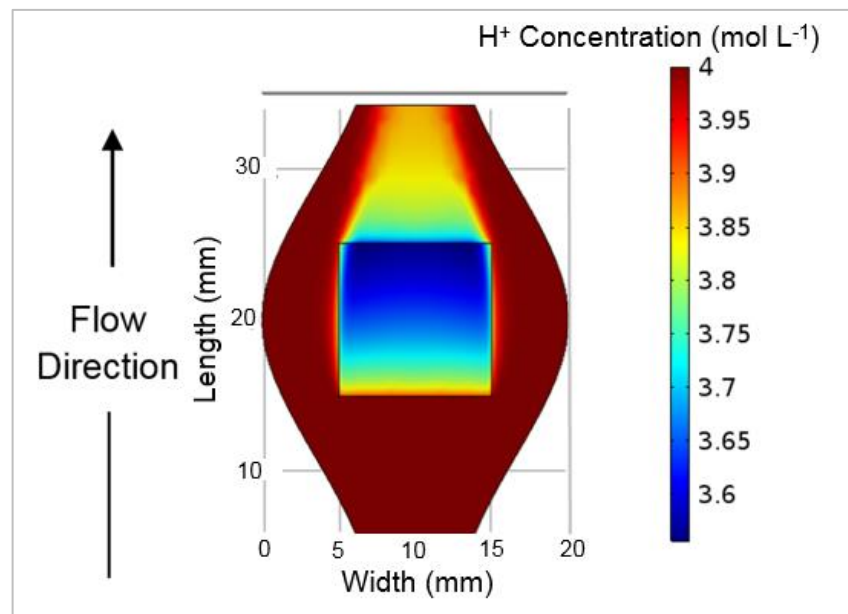
Figure 7.10 Concentration maps for H^+ at the base of the flow cell where the steel sample is positioned for an inlet flow rate of 1ml/min, HCl concentration of 4M and a defined corrosion rate of 1,000mm/year.

In all simulations performed over acid inlet concentrations of 4M to 4×10^{-4}M, a steady state response was achieved within the cell and no accumulation of reacted HCl or Fe^{2+} was observed. This meets the outlined criteria that there should be no accumulation of reacted solution in the cell.

7.1.4.5 Experimental Validation of Flow through the Cell

In order to compliment the flow modelling work discussed in the previous section and further validate the flow through the cell, experiments were performed using a clear Perspex flow cell. Water was pumped through the cell and allowed to fill the gasket. Blue dye was then pumped through the cell at a flow rate of 10ml/min in order to ensure that all of the water evacuated the cell. Figure 7.11 shows the dye being pumped into the cell at a rate of 10ml/min. Water was then pumped through the cell to flush the blue dye from the cell. If the dye was not able to flush the water from the cell (or vice versa), this would suggest that stagnation points or eddies exist. This would be an indication that either the flow rate through the cell is too high or the gasket geometry is not suitable.
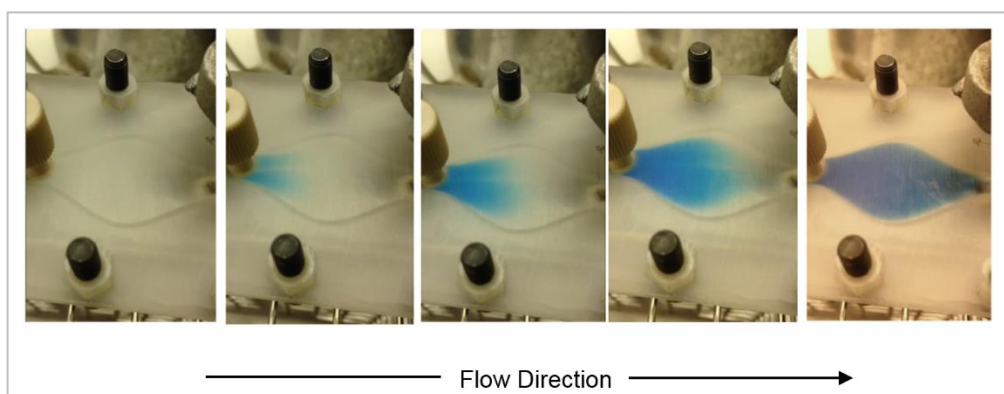
Figure 7.11 Tracer experiment performed using a Perspex flow cell. Blue dye was pumped through the cell at a rate of 10ml/min to show no stagnation points exist. The flow of the dye through the cell is shown in each subsequent image from left to right.

Figure 7.11 shows that the flow through the cell is as expected. The water is flushed from the cell by the blue dye with no noticeable stagnation points or recirculation at a flow rate of 10ml/min. The same was observed when water was used to flush the blue dye from the cell. This further validates the CFD results shown in Figure 7.7 at a flowrate of 10ml/min.

7.1.5 Development of Acidizing System and Temperature Control

7.1.5.1 Description of Complete Setup

Once the design and validation of the flow cell was complete, it was integrated into a system capable of simulating acidizing flow-back. The test methodology was based on the previous dilution test discussed in Section 4.5.3, but with the flow cell integrated into the setup.
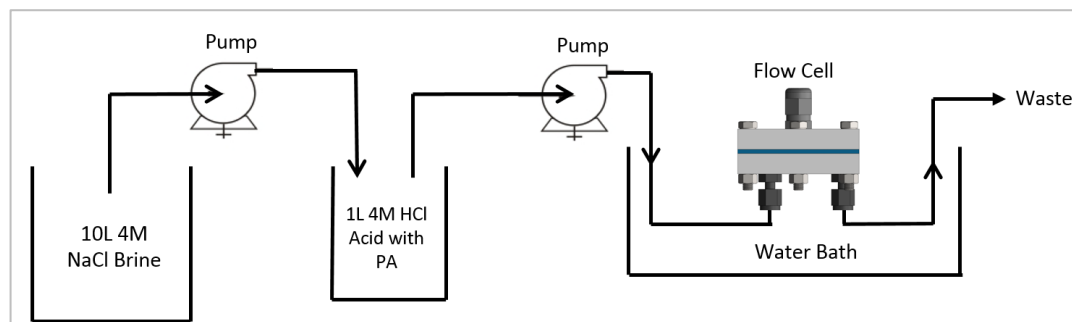
Figure 7.12 Schematic of complete acidizing experimental setup.

A schematic representation of the flow cell dilution test is provided in Figure 7.12. The test consists of 1L of 4M HCl (containing a known PA concentration) being diluted with 10L of 4M NaCl solution. A peristaltic pump is used to dilute the 4M HCl with the 4M NaCl solution, meanwhile an identical peristaltic pump is used to transfer solution from the 1L vessel through the flow cell and into a waste container at an identical flow rate. This maintains a constant solution volume of 1L. Acid resistant Tygon tubing was used to transfer all solutions to and from the flow cell. A water bath (discussed in greater detail in the following section) is used to control the temperature of the solution entering the flow cell.

7.1.5.2 Temperature Control within the Flow Cell

A water bath was used to regulate the temperature within the flow cell. Once the acid/brine mixture leaves the 1L vessel at room temperature, it travels through 50cm of Tygon tubing which is immersed in the water bath. In addition, the flow cell is also immersed in the water bath to ensure no temperature drop occurs whilst the solution is flowing through the cell.
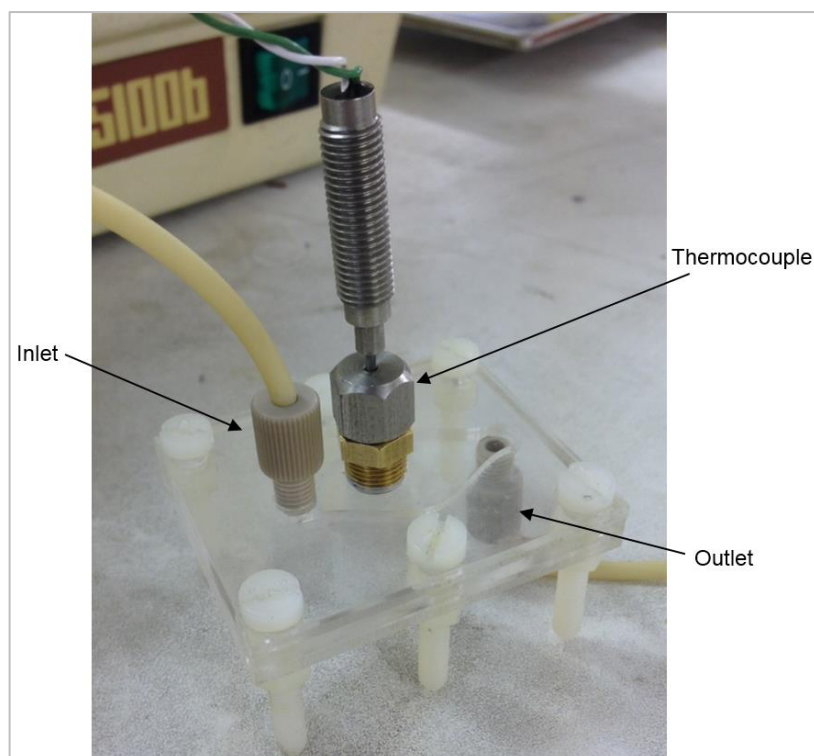
Figure 7.13 Custom flow cell built to measure the temperature of the solution flowing through the cell.

The application of the water bath was validated using a customised cell integrated with a thermocouple. The custom flow cell, shown in Figure 7.13, allowed a thermocouple to be in contact with the solution flowing through the cell. The temperature of the solution in the flow cell could then be measured.

It was found that by placing the inlet on the top of the cell that the last 5cm of tubing was not emerged in the water bath. This resulted in the solution being pumped through tubing that is not submerged in the water bath prior to entering the cell. This meant that the solution in the cell dropped below the desired temperate of 80°C. The flow cell was therefore redesigned with both the inlet and outlet on the base of the flow cell. The redesigned flow cell is shown placed in the water bath in Figure 7.14.

By placing the inlet on the base of the cell it was found that a temperature of up to 80°C could reliably be reached by controlling the temperature of the water bath to 5°C above the desired temperature. It was found that if the solution passed through 50cm of Tygon tubing, which was immersed in the

water bath, this was sufficient to ensure the solution was at 80°C as it passed through the cell.
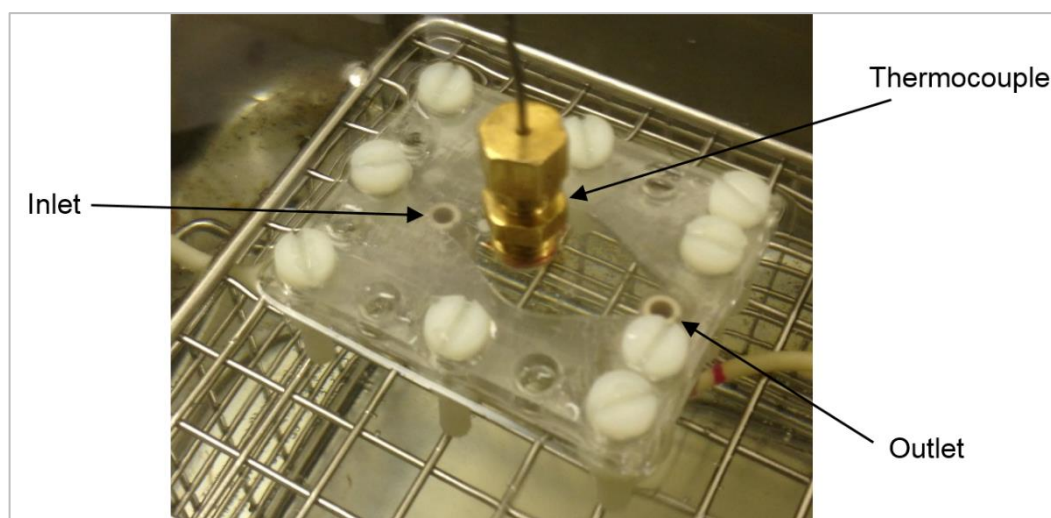
Figure 7.14 Redesigned custom flow cell designed to measure the temperature of the solution flowing through the cell. The cell has been redesigned with both the inlet and outlet on the base of the cell.

7.1.5.3 Control of Dilution Rates

As the new methodology allows the acid to be diluted in the same way as the previous methodology (as discussed in Section 4.5.3) the dilution rate can be set to model the dilution seen in the field. Equation 4.6 can be applied to the flow cell dilution tests as it still expresses the solution molarity at a given point in the flow cell dilution test for a specified flowrate. It is however important to note that the range of dilution rates is limited by the flow through the cell. As discussed previously in order to ensure that there is no stagnation or recirculation in the flow cell the upper limit of flow is between 10-25ml/min. Therefore if the statement that all spent acid is evacuated from the cell is to be made the dilution rate is limited to a maximum value within this range.

7.1.6 Meeting the Outlined Criteria

The criteria outlined in Section 7.1.1 are now met as the following is true for the new test methodology-

1. The steel sample is always in contact with 'fresh' solution. This solution now contains a known HCl and PA concentration and has not been in contact with the steel sample prior to this point.

2. The PA is no longer heated with the HCl throughout the entire duration of the dilution test. It is now only heated prior to coming into contact with the steel sample.

3. The new test methodology now eliminates the problem of solution contamination. Computational fluid dynamics analysis has shown that all reaction products are evacuated from the cell and there is no stagnation in the flow cell.

7.2 Flow Cell Results

7.2.1 Introduction

Once the flow cell had been designed, and the flow and temperature through the cell validated, it was used to try and understand the corrosivity of the flowback fluid through a range of tests. It was hoped that by repeating the dilution tests performed previously (presented in Section 5.3.5) using the new set-up a greater understanding of the flowback process could be gained. This chapter highlights the quality of the electrochemical data obtainable from the cell before presenting the results from a range of different dilution tests.

7.2.2 Flow Cell Results and LPR Measurements

The quality of the electrochemical data achievable from the cell and ensuring a high level of repeatability were the first step when performing experiments with the flow cell. The dilution test performed previously (Figure 5.25) was the first test to be performed. 1L of 4M HCl (containing 0.05wt.% PA) was diluted with 4M NaCl brine at a rate of 10ml/min (following the methodology outlined in Section 7.1.5). The variation in the OCP over the duration of the dilution test is shown in Figure 7.15.

LPR measurements were performed every 5 minutes with the OCP being recorded between each measurement. Due to the frequency of the measurements each working electrode was polarised to a potential (±10mV) considerably less than the ASTM recommended value of ±30mV from the OCP [179]. This was in order to minimise the effect of performing repeat measurements on the sample. The values of the reciprocal of the charge transfer resistance ($1/R_{ct}$) shown in Figure 7.19 were calculated from the LPR measurements. As discussed previously the reciprocal of the charge transfer

resistance is plotted as it eliminates the issues with applying the correct Stern-Geary coefficient but it is still proportional to the corrosion rate [158]. Figures 7.16-7.18 show example LPR measurements taken 1, 7 and 14 hours into the test.
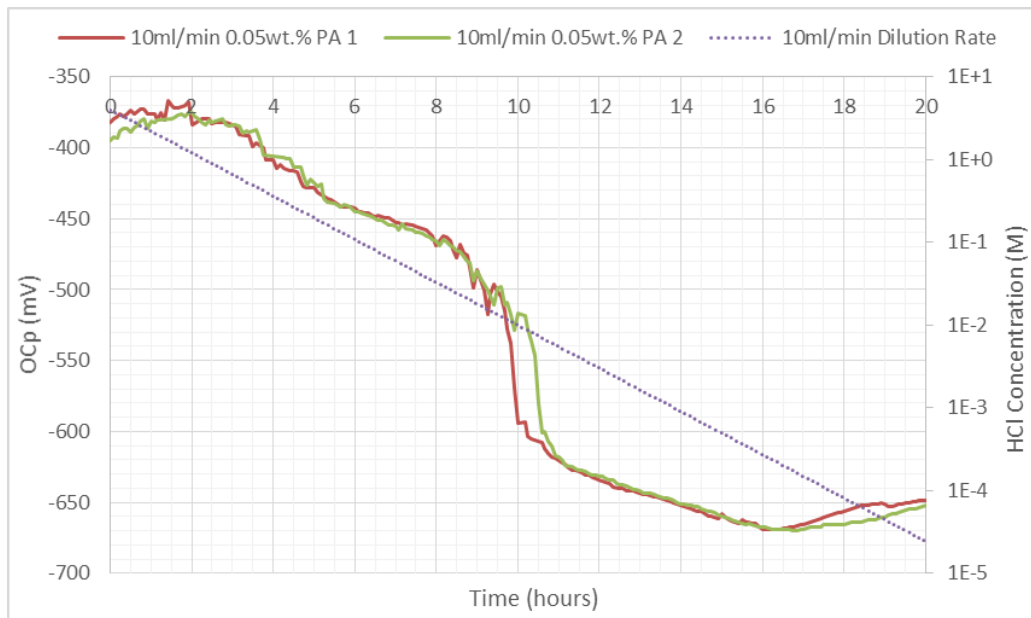
Figure 7.15 OCP during two dilution tests starting at 4M HCl containing 0.05wt.% PA and diluted with 4M NaCl brine at a rate of 10ml/min at 80°C. The HCl concentration is shown on the secondary axis.
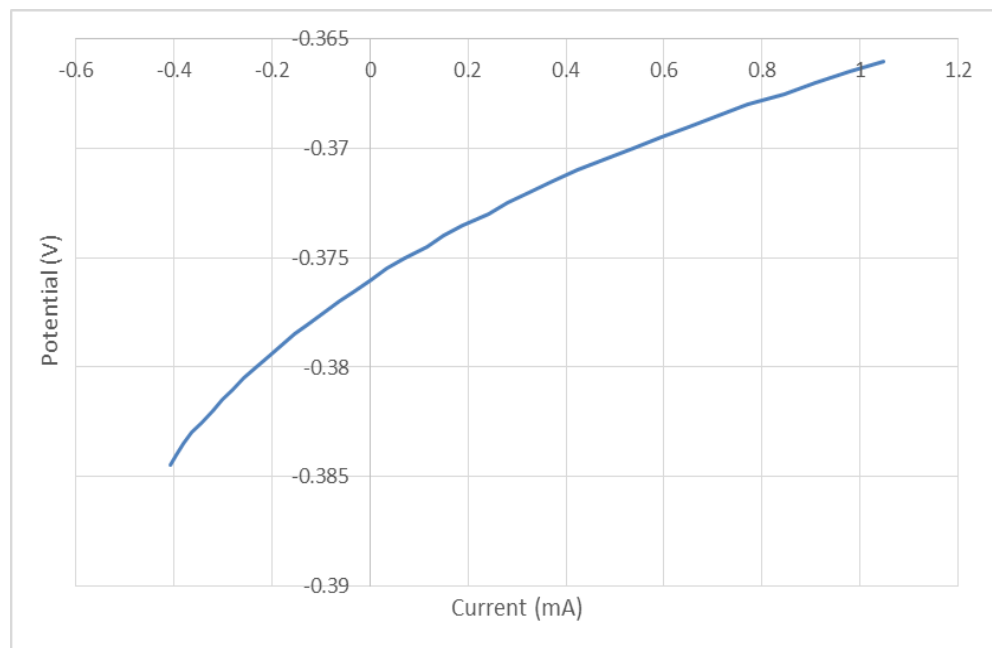
Figure 7.16 Example LPR measurement taken 1 hour into the dilution test performed at 80°C. The HCl concentration in the flow cell is approximately 2M HCl.
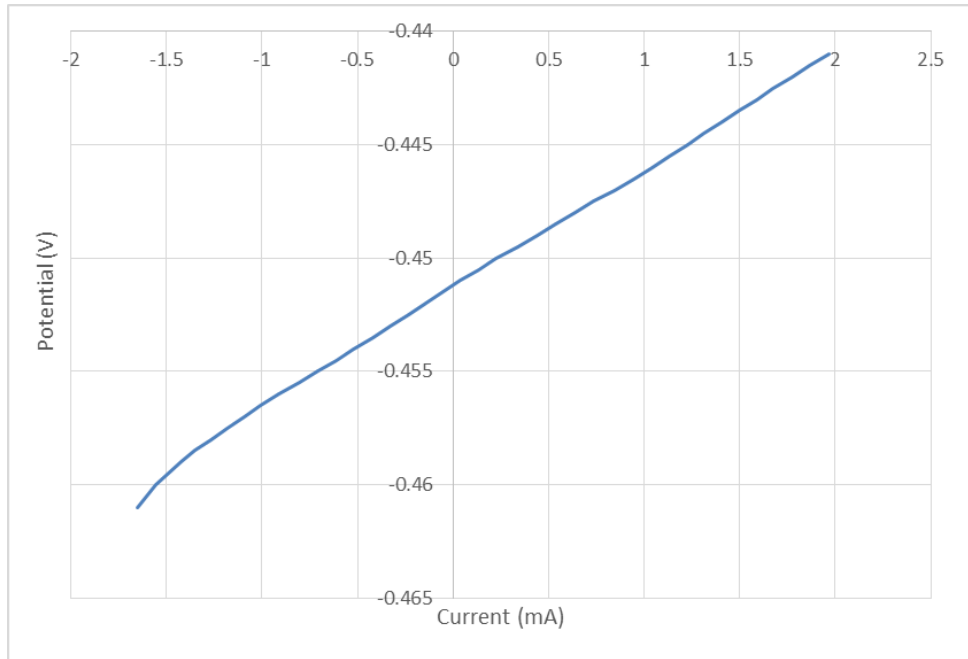
Figure 7.17 Example LPR measurement taken 7 hours into the dilution test performed at 80°C. The HCl concentration in the flow cell is approximately 0.04M HCl.
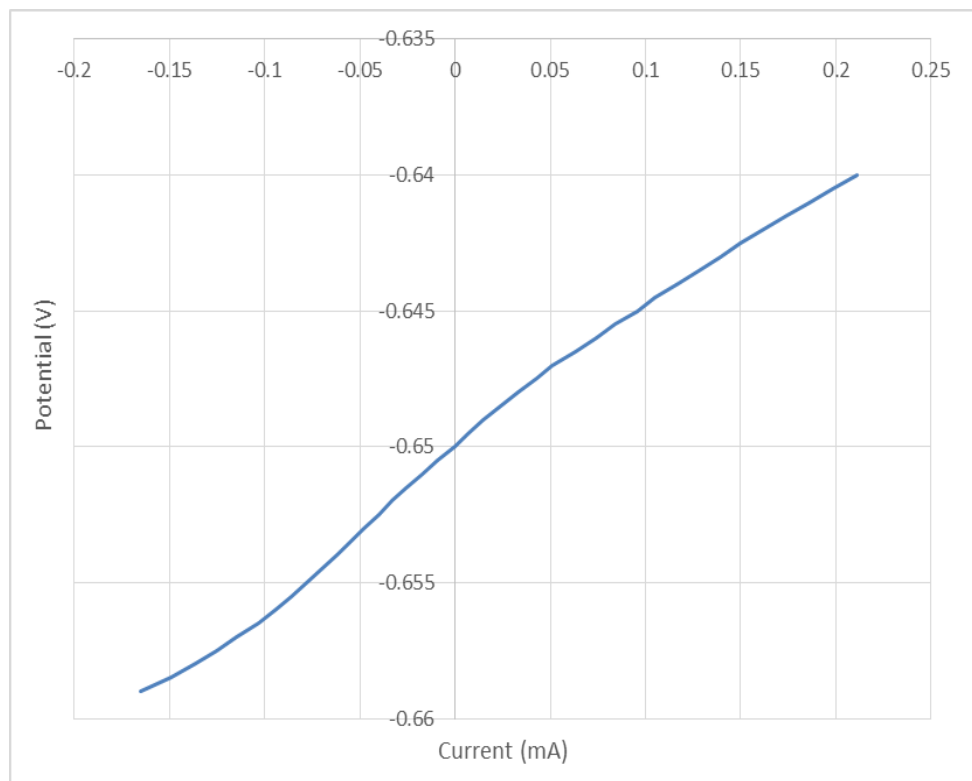
Figure 7.18 Example LPR measurement taken 11 hours into the dilution test performed at 80°C. The HCl concentration in the flow cell is approximately $8x10^{-4}$M HCl.
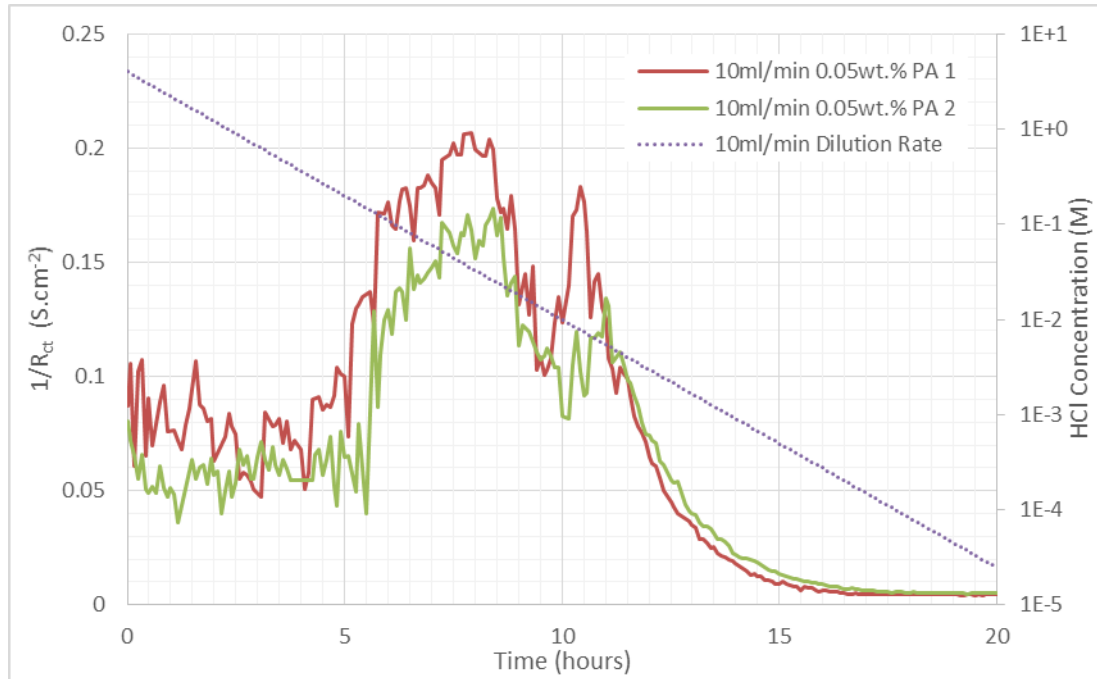
Figure 7.19 Reciprocal of the charge transfer resistance ($1/R_{ct}$) from two dilution tests starting at 4M HCl containing 0.05wt.% PA and diluted with 4M NaCl brine at a rate of 10ml/min at 80°C. The HCl concentration is shown on the secondary axis.

The change in the reciprocal of the charge transfer resistance ($1/R_{ct}$, calculated from the LPR measurements) over the duration of two separate entire dilution tests is shown in Figure 7.19. The HCl concentration of the solution is shown on the secondary axis.

As discussed extensively throughout the thesis there are many issues with calculating the corrosion rate using Stern-Geary coefficients in a solution of changing chemistry. Despite these issues it is important to attempt to quantify the corrosion rates found from the dilution tests. Table 5.2 shows the variation in Stern-Geary coefficient as the HCl concentration of the solution is reduced, found from the 3 hour tests. As discussed in Section 5.3.5 the Stern-Geary coefficient was found to have a minimum possible value of 11.1 and a maximum possible value of 19.9 with an average of 14.4. Figure 7.20 shows the corrosion rate of the dilution test solution if an average value of 14.4 is applied. The issues associated with applying an average Stern-Geary coefficient to a solution with a constantly changing chemistry are discussed in Section 2.2.4 and Figure 8.5 shows the effect of applying the minimum and maximum measured Stern-Geary coefficients (11.1 and 19.9 respectively).
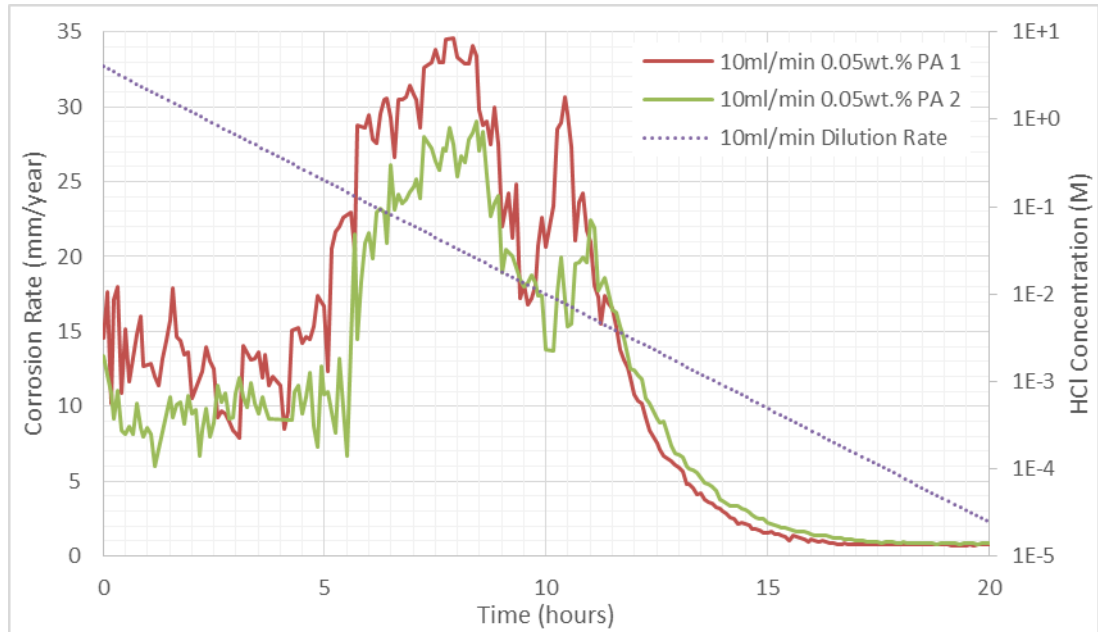
Figure 7.20 Corrosion rate from two dilution tests starting at 4M HCl containing 0.05wt.% PA and diluted with 4M NaCl brine at a rate of 10ml/min at 80°C. An average Stern-Geary coefficient of 14.4 was used to calculate the corrosion rate. The HCl concentration is shown on the secondary axis.

7.2.3 Variation of the Initial Hydrochloric Acid Concentration

The results from the dilution tests (Figure 7.20) raise several important questions regarding the corrosivity of the flowback fluid and how the corrosion rate varies as the acid concentration decreases throughout the dilution process. In order to further understand this the dilution test was repeated with different starting HCl concentrations of 0.4M and 0.04M (both containing 0.05wt.% PA relative to the HCl concentration of the solution).

Figure 7.21-7.22 shows the variation in the OCP over the duration of both dilution tests and the reciprocal of the charge transfer resistance ($1/R_{ct}$), found from the LPR measurements.
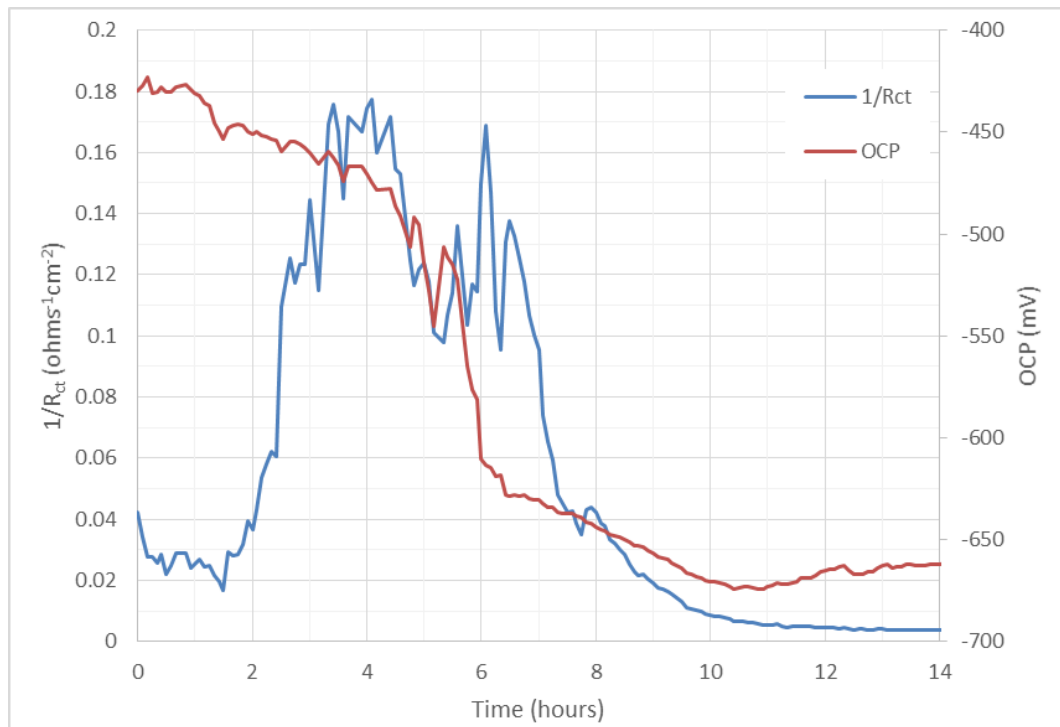
Figure 7.21 Reciprocal of the charge transfer resistance (1/R_{ct}) measured during a dilution test with a starting concentration of 0.4M HCl containing 0.05wt.% PA and diluted with 4M NaCl brine at a rate of 10ml/min, at 80°C. The OCP is shown on the secondary axis.
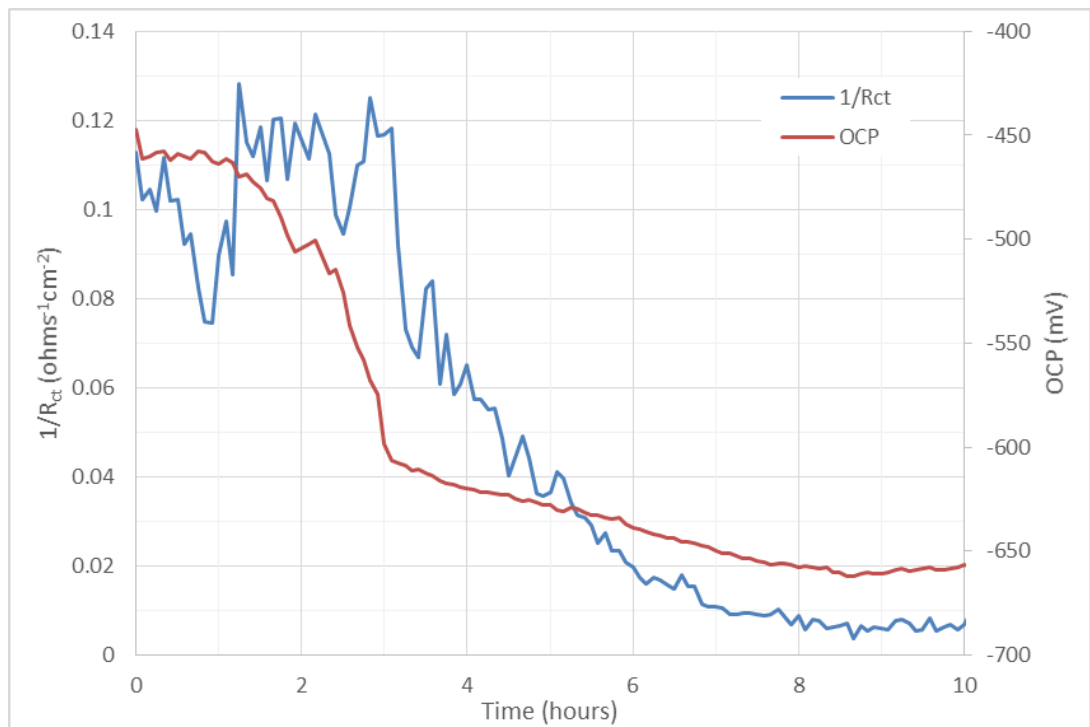
Figure 7.22 Reciprocal of the charge transfer resistance (1/R_{ct}) measured during a dilution test with a starting concentration of 0.04M HCl containing 0.05wt.% PA and diluted with 4M NaCl brine at a rate of 10ml/min, at 80°C. The OCP is shown on the secondary axis.

7.2.4 Varying the Inhibitor Concentration

In order to understand how the initial PA concentration effects the corrosivity of the flowback fluid dilution tests were performed at starting PA concentrations higher (0.25wt.%) and lower (0.01wt.%) than the previous experiments. Table 7.4 shows the PA concentrations and the corresponding inhibitor volume added to 1L of 4M HCl at the start of each test. The OCP and $1/R_{ct}$ found from dilution tests performed at starting inhibitor concentrations of 0.01wt.% and 0.25wt.% PA are presented in Figure 7.23 and 7.24 respectively.

PA Concentration (wt.%)	PA Volume (mL)
0.01	0.11
0.05	0.54
0.25	2.7

Table 7.4 The three different inhibitor concentrations tested and the corresponding inhibitor volume added to 1L of 4M HCl.
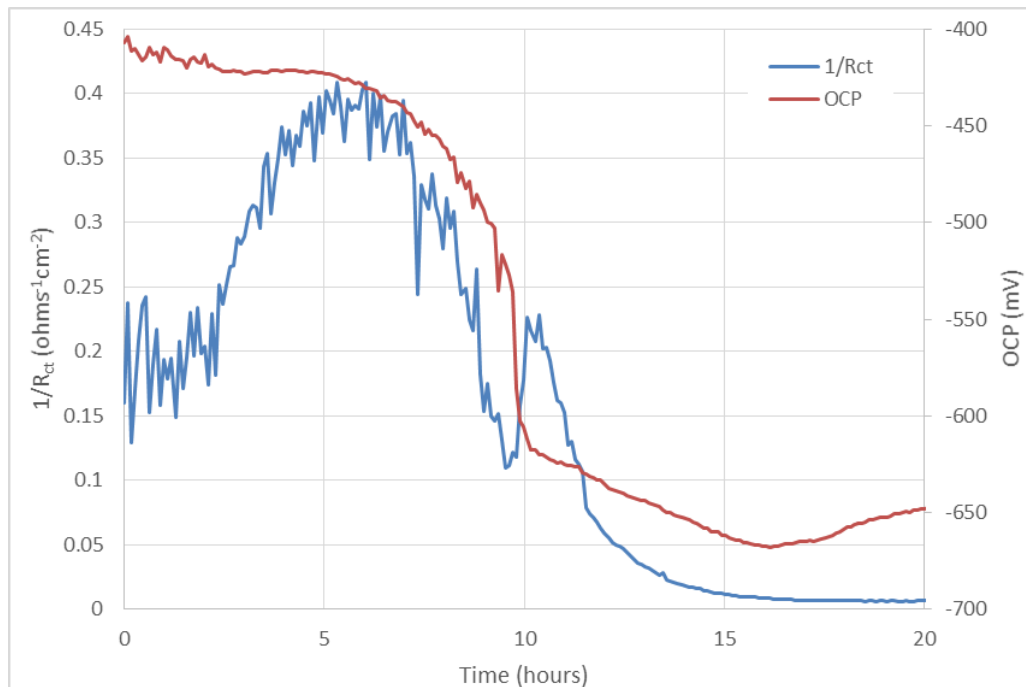
Figure 7.23 Reciprocal of the charge transfer resistance ($1/R_{ct}$) measured during a dilution test containing 0.01wt.% PA and diluted with 4M NaCl brine at a rate of 10ml/min, at 80°C with a starting concentration of 4M HCl. The OCP is shown on the secondary axis.
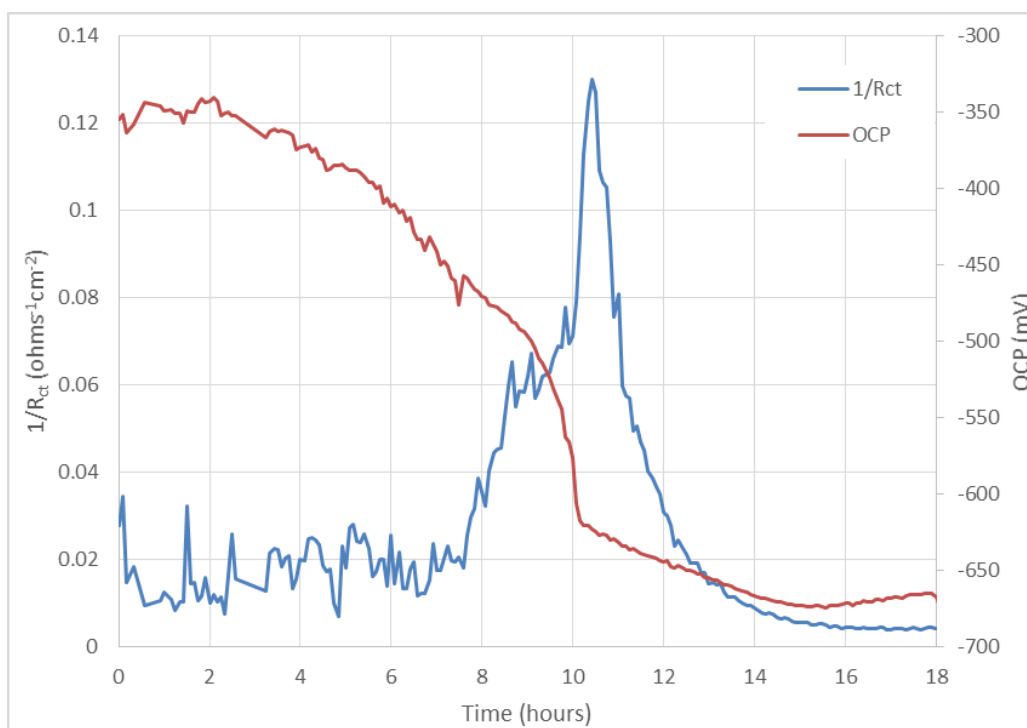
Figure 7.24 Reciprocal of the charge transfer resistance (1/R_{ct}) measured during a dilution test containing 0.25wt.% PA and diluted with 4M NaCl brine at a rate of 10ml/min, at 80°C with a starting concentration of 4M HCl. The OCP is shown on the secondary axis.

7.2.5 Varying the Flow Rate

All dilution tests previously presented have been at the same flow rate of 10ml/min in order to allow for a direct comparison between the different tests performed. However, it was also important to see how varying the flow rate affected the measured corrosivity of the flowback fluid.

As discussed in Section 7.1.4 the upper limit of the flow cell is between 10-25ml/min. A dilution test was performed at 5ml/min (well below the upper limit of flow) to help understand how a slower dilution rate affects the measured corrosion rates. A further test was performed at a faster dilution rate of 15ml/min, despite this flowrate being potentially larger than the upper limit of flow through the cell, to gain an understanding as to how this effects the measured corrosion rate. The OCP and 1/R_{ct} found from the 5ml/min and 15ml/min dilution tests are presented in Figure 7.25 and 7.26 respectively.
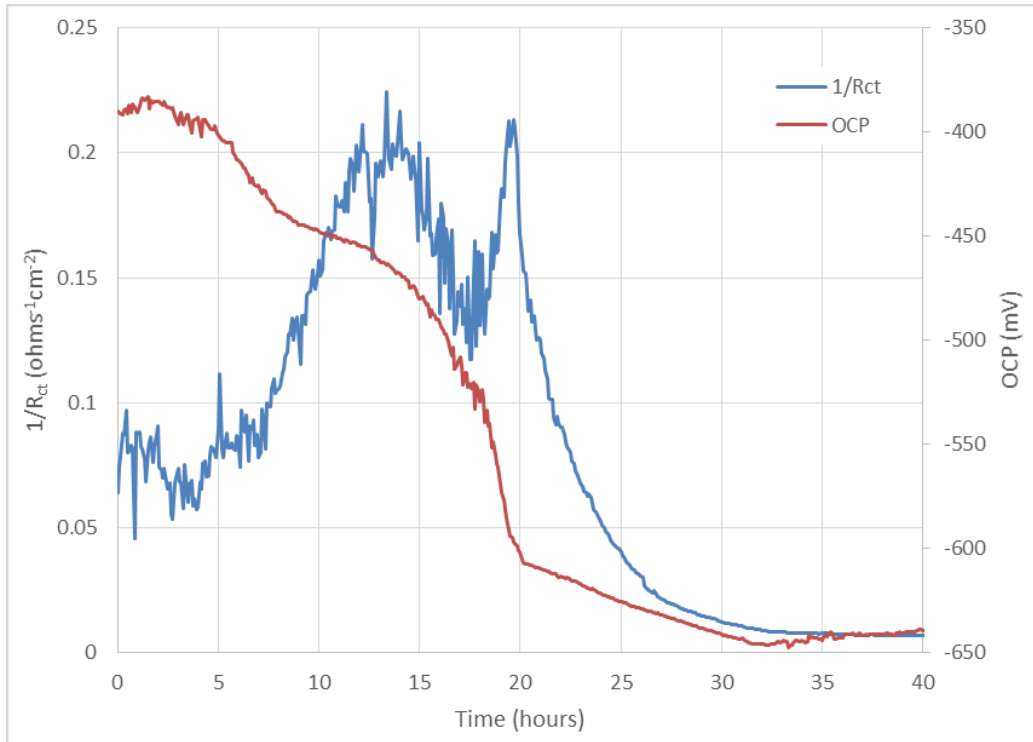
Figure 7.25 Reciprocal of the charge transfer resistance (1/R_{ct}) measured during a dilution test containing 0.05wt.% PA and diluted with 4M NaCl brine at a rate of 5ml/min, at 80°C with a starting concentration of 4M HCl. The OCP is shown on the secondary axis.
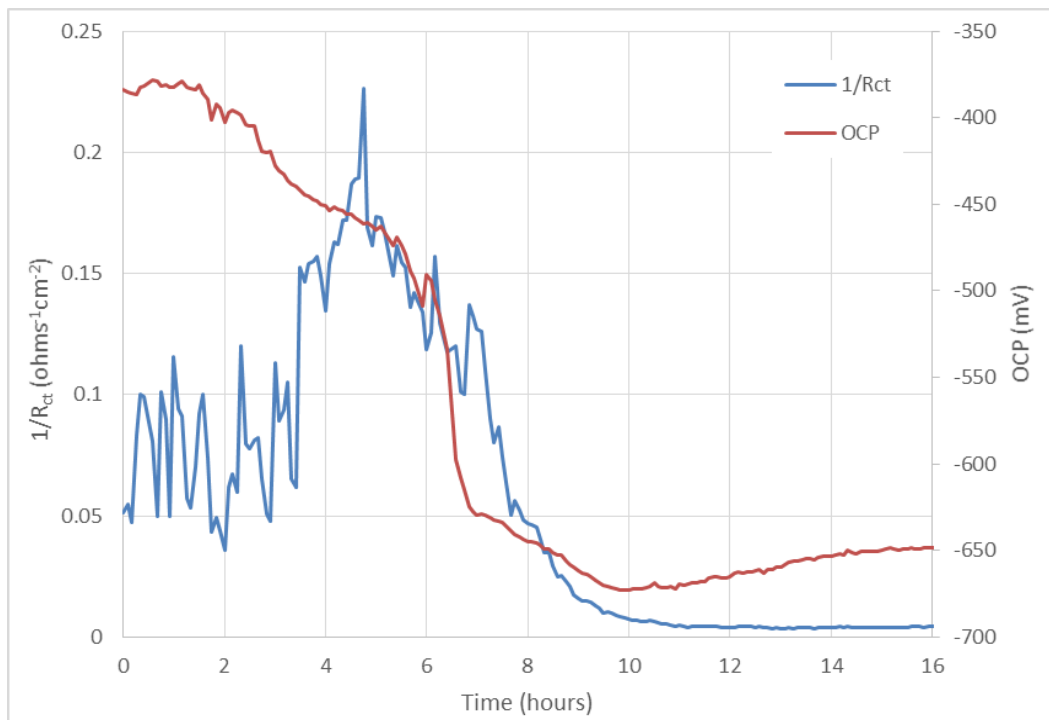
Figure 7.26 Reciprocal of the charge transfer resistance (1/R_{ct}) measured during a dilution test containing 0.05wt.% PA and diluted with 4M NaCl brine at a rate of 15ml/min, at 80°C with a starting concentration of 4M HCl. The OCP is shown on the secondary axis.

7.2.6 Further Flow Cell Tests

Several additional tests were performed in an attempt to gain a greater understanding of the corrosivity of the flowback process and in particular the relationship between the HCl and PA concentration of the solution.

7.2.6.1 Reverse Dilution Test

The standard dilution test was performed in reverse. A 4M NaCl solution was initially pumped through the flow cell which was then diluted with 4M HCl (containing 0.05wt.% PA) at a rate of 10ml/min. The brine was diluted with 4M HCl for 7 hours (the HCl concentration of the solution reached 3.92M). The OCP and $1/R_{ct}$ found from the reverse dilution test are shown in Figure 7.27.
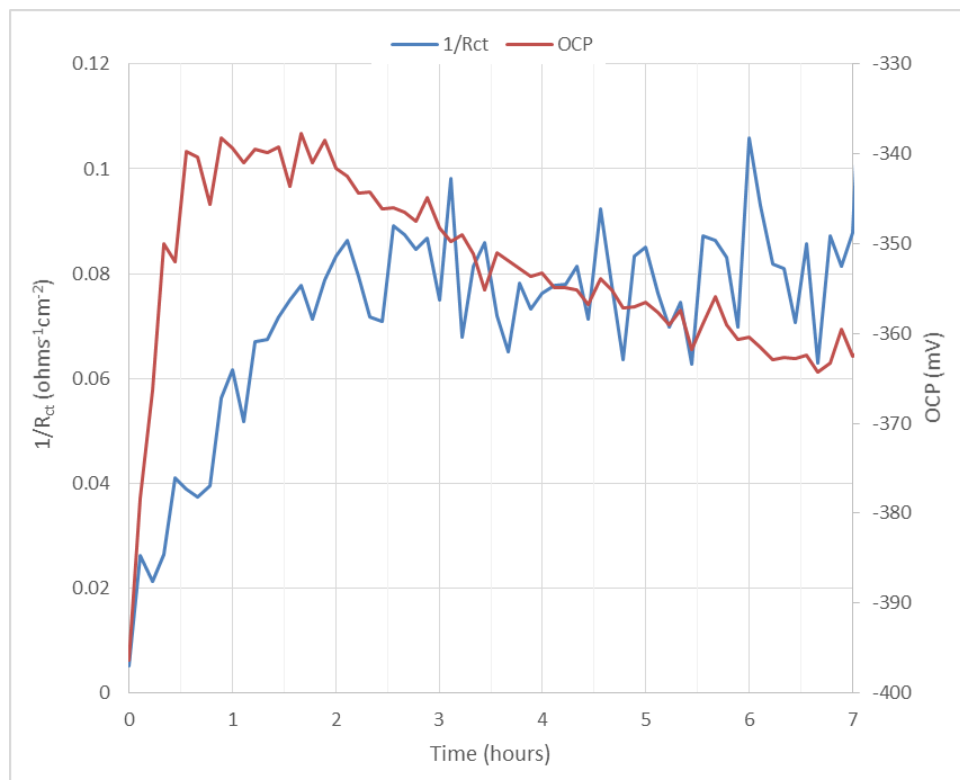
Figure 7.27 Reciprocal of the charge transfer resistance ($1/R_{ct}$) measured during a reverse dilution test starting with 4M NaCl brine and diluted with 4M HCl containing 0.05wt.% PA, at 80°C. The OCP is shown on the secondary axis.

7.2.6.2 Redosing Experiments

Figure 7.19 suggests that the corrosion rate begins to increase once the PA concentration drops below a HCl concentration of 0.3M. This HCl

concentration corresponds to a PA concentration of ~3×10^{-3}wt.%. Therefore a further dilution test was performed where the PA was re-dosed before it could drop below this critical concentration. A PA concentration of 5×10^{-3}wt.% was chosen as the point at which the PA would be re-dosed. This was in order to ensure that the PA always remains above the critical concentration of 3×10^{-3}wt.%.

The dilution test was repeated at 10ml/min with a starting PA concentration of 0.05wt.% (540µL of PA). However when the concentration was diluted to 5×10^{-3}wt.%, (after 3.85 hours), the concentration was re-dosed back to 0.05wt.% by adding 486µL of PA (the PA concentration throughout the test is shown in Figure 7.28). The dilution test was then allowed to proceed. The OCP and $1/R_{ct}$ found from this dilution test are shown in Figure 7.29.
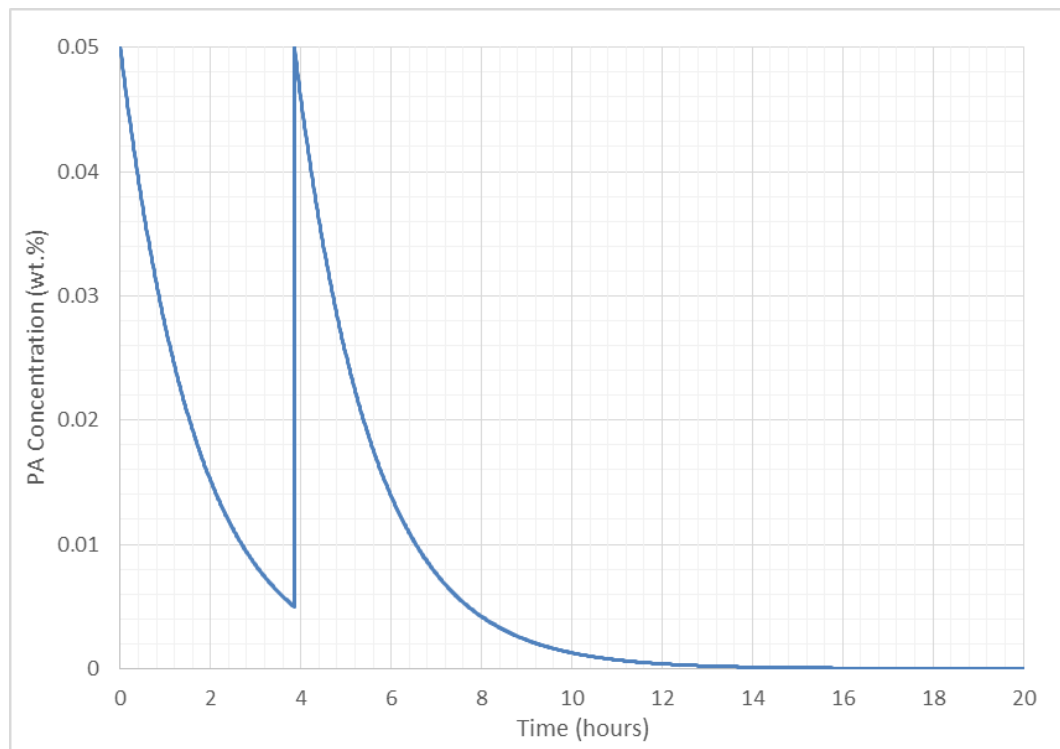
Figure 7.28 Variation in PA concentration throughout the redosing experiments.
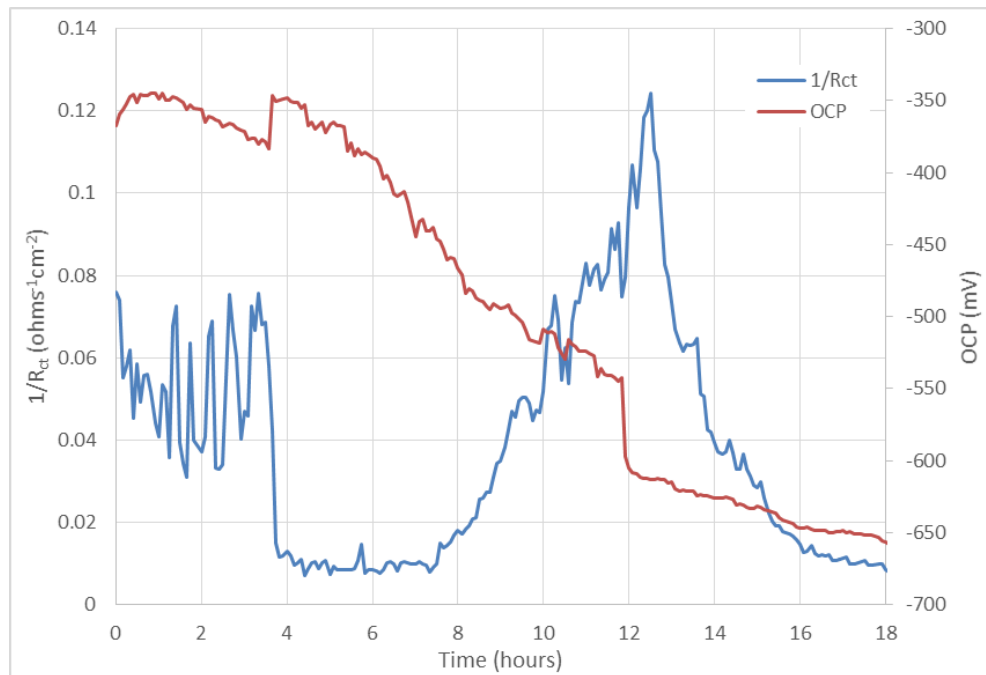
Figure 7.29 Reciprocal of the charge transfer resistance ($1/R_{ct}$) measured during a dilution test starting with 4M HCl (with 0.05wt.% PA) at 80°C and diluted with 4M NaCl brine at a rate of 10ml/min. The PA concentration was diluted to 5×10^{-3}wt.% before being redosed to 0.05wt.%. The OCP is shown on the secondary axis.

7.2.6.3 Surface Area Changes over Dilution Test

In order to understand how the sample surface area changes over the duration of the dilution test samples were removed at 10 points over a dilution test performed at 10ml/min with a starting HCl concentration of 4M with 0.05wt.% PA (this test methodology is discussed in Section 4.5.3). An NPFLEX interferometer was used to measure the true surface area of each sample (the full methodology is provided in Section 4.6.1).

The times at which samples were removed, the HCl concentration in the solution at this point and the surface area of the sample (expressed as a true surface area and a percentage increase) are shown in Table 7.5. The surface area increase (%) over the course of the dilution test is shown in Figure 7.30. The average surface area from two separate samples is shown in Figure 7.30 and the scatter bands represent the maximum and minimum surface area found from the two tests.
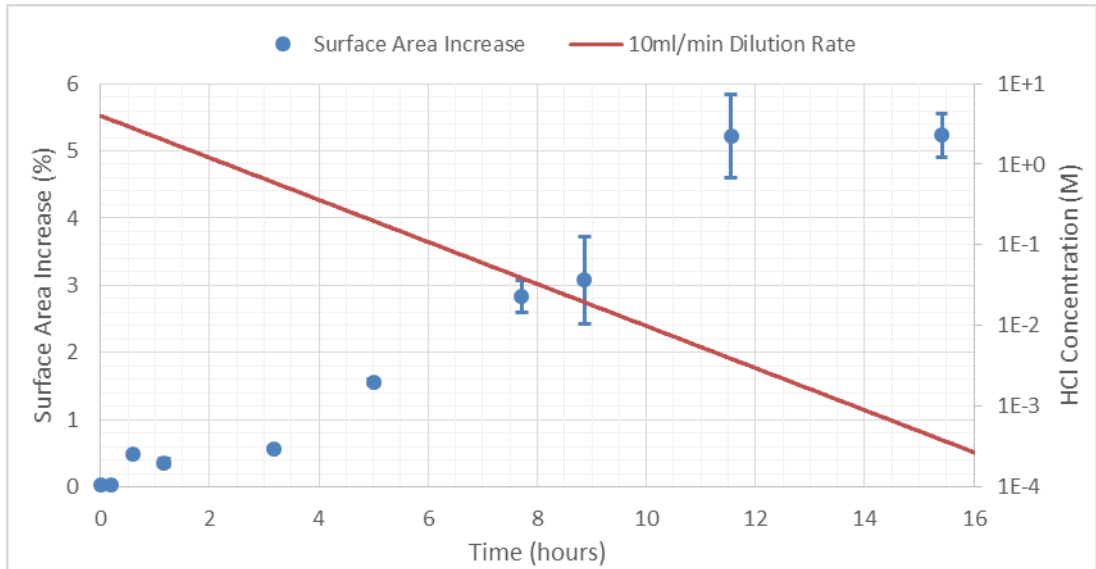
Figure 7.30 Surface area increase of the sample over the duration of the dilution test at 80°C, the scatter bands represent the maximum and minimum calculated surface area increase. The HCl concentration started at 4M (with 0.05wt.% PA) and is shown on the secondary axis. The HCl was diluted with 4M NaCl brine at a rate of 10ml/min.

Time (hours)	HCl Concentration (M)	Average True Surface Area (cm²)	Average Surface Area Increase (%)
0.2	3.6	1.0003	0.03
0.6	2.8	1.0048	0.48
1.2	2	1.0037	0.37
3.2	0.6	1.0058	0.58
5	0.2	1.016	1.6
7.7	0.04	1.028	2.8
8.9	0.02	1.031	3.1
11.6	4×10^{-3}	1.052	5.2
15.4	4×10^{-4}	1.052	5.2

Table 7.5 Times at which samples were removed throughout the dilution test. The HCl concentration at this time in the 10ml/min dilution test is shown along with the average true surface area of the samples and the percentage increase in surface area.

Chapter 8 Discussion of the Flow Cell Benefits and Critical PA Concentration

8.1 Benefits of the Flow Cell

8.1.1 Introduction

The results presented in Chapter 7 highlight the benefit of using the flow cell dilution tests to characterise the full flowback process following an acid job. There are several benefits to using the new test methodology, not only in terms of the experimental results acquired, but also in the amount of experimental time and resources saved. The results from the flow cell tests, presented in Section 7.2, would be virtually impossible to achieve using a pre-existing test methodology and key observations regarding the critical HCl and PA concentrations would be missed. This chapter outlines the benefits of using the flow cell over the existing test methodologies and compares the corrosion rate data acquired from each test.

8.1.2 The Full Dilution Profile and Flow Cell Repeatability

The most obvious benefit of the flow cell is its ability to replicate the full dilution process and provide large amounts of data regarding the corrosivity of the solution from each test. The flow cell tests are also the most representative of what is seen in the field. As discussed in Section 1.2.2 the flowback fluid from an acid job initially can contain a significant amount of hydrochloric acid which is then gradually diluted as more of the formation brine and spent acid is produced [6]. This scenario is much better replicated by the flow cell dilution tests (where the solution chemistry is constantly changing) than the closed vessel tests (where the sample is in contact with a solution of fixed acid molarity and inhibitor concentration).

8.1.2.1 Quality of Flow Cell Electrochemistry

Figure 7.16-7.18 shows three example LPRs taken throughout the dilution test at a range of HCl concentrations. The quality of the LPR measurements show that the positioning of the reference and counter electrode, opposite the working electrode, provides high quality electrochemical data at all HCl concentrations in the dilution test.

8.1.2.2 Flow Cell Repeatability

In order to test the repeatability of the data the flow cell was used in two separate tests to dilute 4M HCl (containing 0.05wt.% PA) at a rate of 10ml/min. The reciprocal of the charge transfer resistances ($1/R_{ct}$) measured are shown in Figure 7.19, the reason for plotting the reciprocal of the charge transfer resistance rather than the corrosion rate has been discussed extensively throughout the thesis (Section 5.3.5 and 6.5.4). In order to see how the corrosivity changes as the solution is diluted in each of the two tests the time has been converted to the HCl concentration at that point in the dilution test. The HCl concentration (C_t) was calculated at any time (t) in the dilution test using Equation 4.6. This comparison between the two sets of data is presented in Figure 8.1 and the average value calculated from the two tests is shown.
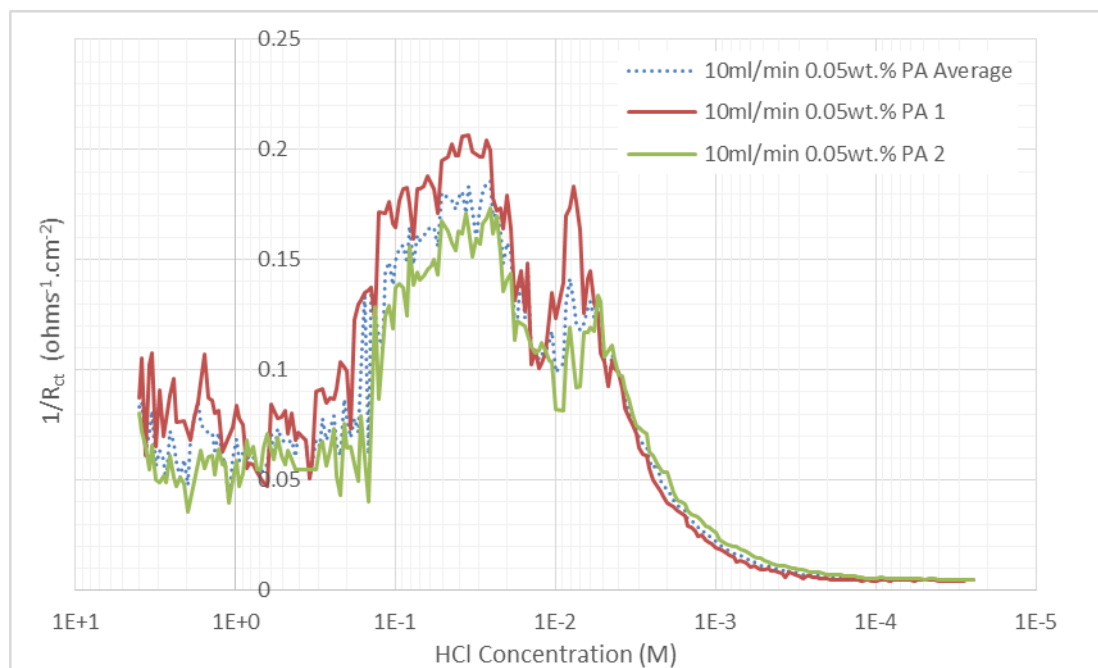
Figure 8.1 Comparison between two dilution tests starting at 4M HCl (containing 0.05wt.% PA) at 80°C and diluted with 4M NaCl brine at a rate of 10ml/min. The time has been converted to the HCl concentration.

In order to further compare the two data sets shown in Figure 8.1, the percentage difference between the reciprocal of the charge transfer resistances ($1/R_{ct}$) was compared. The percentage difference gives the deviation of two values (V_1 and V_2) from the mean corrosion rate as a percentage and was calculated using Equation 8.1 [180].

$$\text{Percentage Difference (\%)} = \frac{(V_1 - V_2)}{(V_1 + V_2) \times 0.5} \qquad (8.1)$$
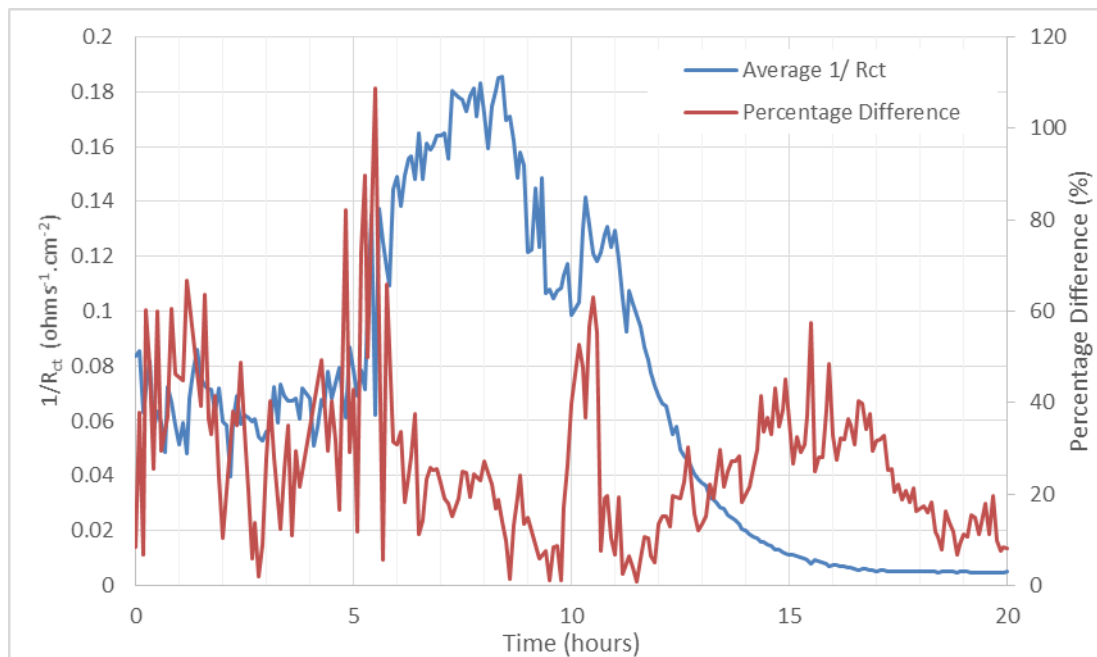
Figure 8.2 The average reciprocal of the charge transfer resistances (1/R_{ct}) and the percentage difference for both of the 10ml/min flow cell dilution tests.

Figure 8.2 allows the difference between the two data sets to be compared as a function of the percentage difference between the two values. It is clear that the percentage error varies greatly over the duration of the dilution test and there are four points at which the percentage error is above 50%.

1. For the initial portion of the dilution test (~1-4 hours) the percentage error is approximately 50%. This initial difference is difficult to explain but it may be due to differences in the inhibitor film protectiveness. Due to the nature of the tests (high concentration HCl at high temperatures) the corrosion behaviour can vary significantly between each individual test.

2. The highest percentage error occurs at the point at which the corrosion rate in the dilution test begins to increase (~5 hours). This large percentage error is due to the peak in corrosion rate beginning at slightly different HCl concentrations in each of the dilution tests. This results in a large percentage error as the corrosion rate is much higher for the test which begins to peak first. It should be noted that despite

the large percentage difference seen in Figure 8.2 the difference in the HCl concentration at which the first peak begins is minimal.

3. A significant error occurs when the HCl concentration reaches 0.01M (~10 hours), coinciding with the second peak in corrosion rate. This is due to the magnitude of the second peak being more significant in one of the tests. It should be noted that the second peak is clearly present in both repeats however the magnitude of the peak is different for both tests.

4. At the end of the dilution test the error is over 30% (after ~13 hours into the test). However, although the percentage difference is significant the actual corrosion rate value varies between ~1-1.5mm/year.

8.1.2.3 Flow Cell Dilution Test Comparisons

LPR data has been collected using three different experimental methodologies, the fixed concentration tests, the closed vessel dilution tests and the flow cell dilution tests. As discussed in Section 6.5.4, it is important to compare the solution corrosivity found at each of the different HCl concentrations tested using each methodology.

The reciprocal of the charge transfer resistance ($1/R_{ct}$) values found from 3 hour electrochemical tests performed in fixed concentration solutions and each of the 10ml/min dilution tests are compared in Figure 8.3. Figure 8.3 shows the average value found from multiple measurements taken over the duration of two separate 3 hour fixed HCl concentration tests. The dilution test results show the average value calculated from five LPR measurements taken at each of the HCl concentrations tested. Table 6.2 shows the HCl range over which the values have been taken (further details are provided in Section 6.5.4).

Figure 8.3 suggests that a similar trend is observed as the HCl concentration of the solution is reduced regardless of which of the three test methodologies is used to measure the solution corrosivity. The values found from the flow cell dilution test show much better agreement with the fixed concentration tests than the closed vessel dilution tests. The only significant difference between the flow cell results and the fixed concentration tests is observed at HCl concentrations of 0.4M and 0.04M. The reason for the difference at these two HCl concentrations is not fully understood. However there are several

important differences in the test methodologies which may contribute to the difference at each HCl concentration.
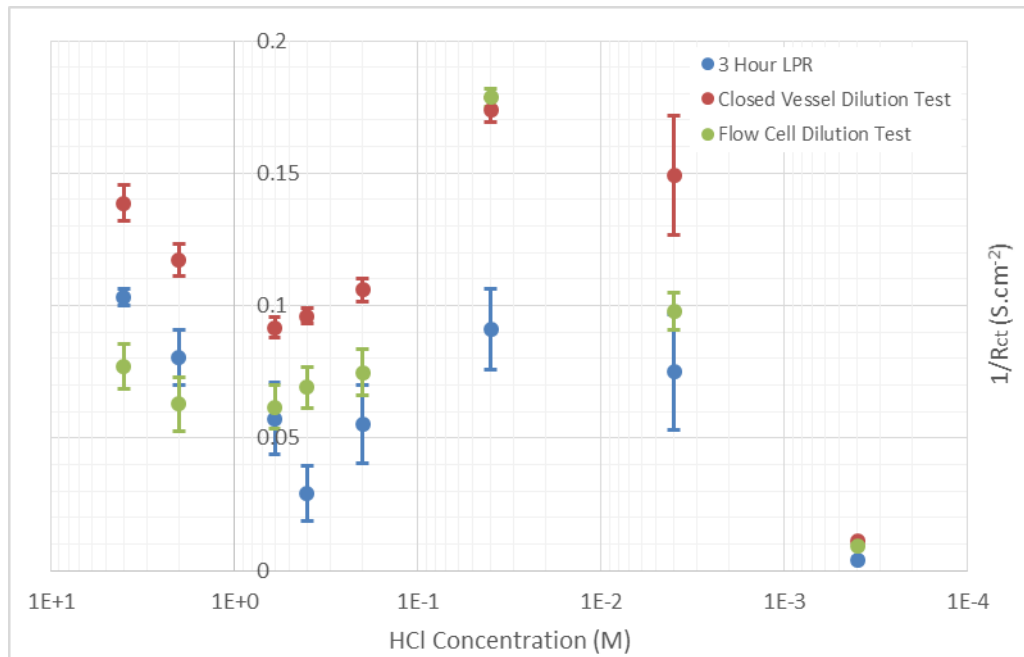
Figure 8.3 The average values for the reciprocal of the charge transfer resistance ($1/R_{ct}$) from the fixed concentration tests and the 10ml/min closed vessel and flow cell dilution tests. The 3 hour test scatter bands represent the standard deviation calculated from all measurements made at that concentration. The dilution test scatter bands represent the standard deviation from the five nearest HCl concentrations at which measurements were taken.

In the flow cell tests, once the HCl concentration has been diluted to 0.4M, the steel has already been in contact with a solution containing between 4M-0.4M (with a PA concentration of between 0.05-0.005wt.%). The results of all tests performed showed that the corrosivity of the solution in the flow cell tests does not start to increase until the PA concentration of the solution is less than 0.005wt.%. Therefore it could be hypothesised that at this point in the dilution test the steel is the most protected relative to the HCl concentration of the solution. The sample has been exposed to a high PA concentration for ~4 hours allowing a protective inhibitor film to develop. This point in the dilution test is then the lowest HCl concentration at which the PA concentration of the solution is still high enough to maintain the protective film. This could possibly explain the low solution corrosivity seen in Figure 8.3.

The difference observed at a HCl concentration of 0.04M is much more difficult to explain. At this concentration both dilution tests measured a significantly higher solution corrosivity than the fixed concentration tests. This suggests that the difference is due to the difference in test methodologies. The increase may be due to the sample already having been exposed to a high concentration of HCl for approximately 8 hours in both of the dilution tests prior to this increase. It is unknown what effect this may have had upon the steel sample compared to the polished sample used in the fixed concentration test.

Despite these differences it is clear that the results of the flow cell dilution tests show much more agreement with the fixed concentration closed vessel tests than those performed in the closed vessel. The use of the flow cell eliminates the issue of HCl and PA spending and this is likely to be the reason for the better agreement with the results of the fixed concentration tests.

8.1.2.4 Repeatability at Different Flow Rates

The dilution test was performed at two additional flow rates of 5ml/min and 15ml/min (Figures 7.25 and 7.26 respectively) to see what effect the dilution rate and flow rate through the cell has upon the solution corrosivity measured throughout the dilution test. In order to allow a direct comparison between the different dilution rates the time has been converted to the HCl concentration at that point in the test in Figure 8.4. It should be noted that the flow regime remains laminar at all flow rates tested with the Reynolds number increasing from 142 to 426 as the flow rate is increased from 5ml/min to 15ml/min (for a 4M HCl solution).

Figure 8.4 shows that similar flowback profiles are observed at a range of different flow rates. Despite the flow rate through the cell changing significantly a similar trend is seen as the HCl is diluted throughout all three tests. All three dilution rates measure a very similar solution corrosivity profile and all peak and then decrease again at very similar HCl concentrations.

The main difference between the different flow rates is the presence and magnitude of the second peak. At the fastest dilution rate of 15ml/min the second peak is not as clearly defined as in the tests at the slower flow rates (5ml/min and 10ml/min). This may be due to the solution being diluted at a

rate that is too fast to fully capture the entire dilution process to the same extent as the tests performed at 5ml/min and 10ml/min. This further suggests that tests should be performed at a maximum dilution rate of 10ml/min, in order for the full dilution process to be captured.
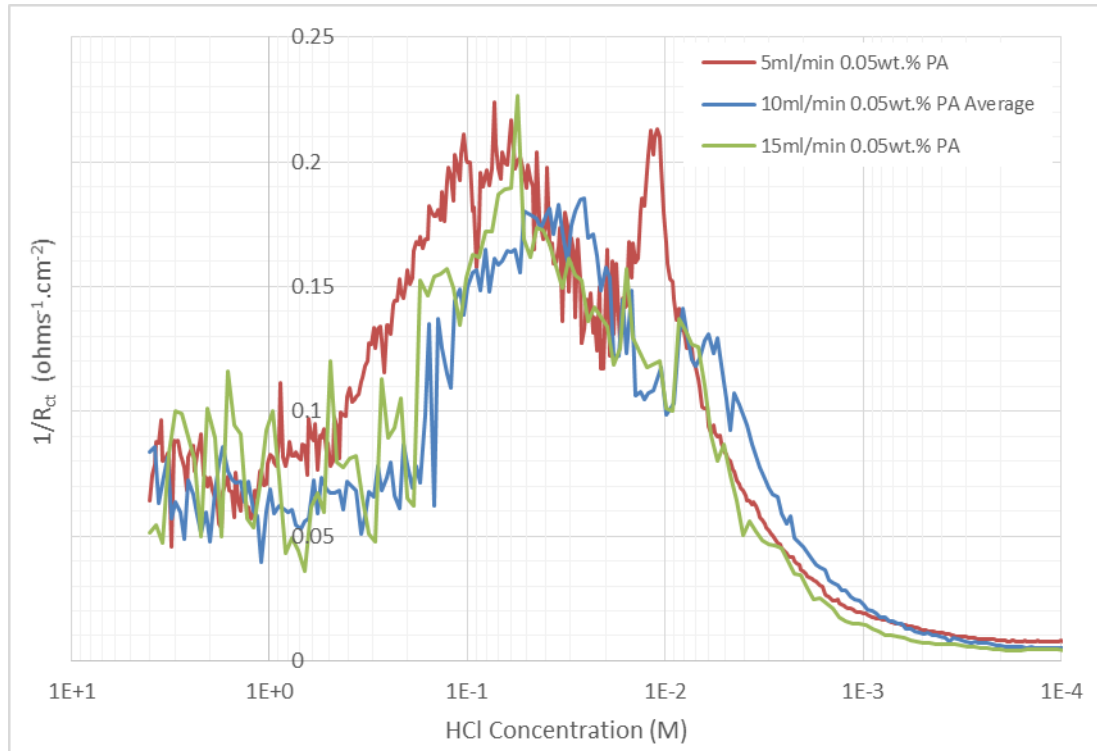
Figure 8.4 Comparison between the reciprocal of the charge transfer resistances ($1/R_{ct}$) found from dilution tests performed at 80°C where 4M HCl (containing 0.05wt.% PA) was diluted with 4M NaCl brine at a rate of 5, 10 and 15ml/min. The time has been converted to the HCl concentration.

8.1.3 Flow Cell Benefits over Standard Mass Loss Tests and 3 Hour Electrochemistry

The most commonly used technique for measuring the corrosion rates associated with strong HCl solutions is to use mass loss coupons in 3 hour tests. Electrochemistry is also used but crucially all tests are performed in solutions at a fixed HCl and inhibitor concentration. These short term tests are sufficient for testing the corrosivity of injected HCl, where the solution is always at a fixed HCl and inhibitor concentration. However when attempting to characterise flowback (where the solution composition is constantly changing) there are many limitations to using these existing test methodologies.

8.1.3.1 Reduced Number of Tests and Costs

The solution chemistry of the fluid that flows back following an acid job is constantly changing. In order to replicate this using fixed concentration closed vessel tests an incredibly large number of tests would be required. This would represent a large number of laboratory hours plus significant material costs. The dilution tests using the flow cell require just 1L of HCl and each dilution profile can be achieved from a single 18 hour test.

8.1.3.2 Ability to Characterise the Full Dilution Profile

As mentioned above, in order to fully characterise the dilution process a significant number of tests would be required to capture the entire dilution process. Mass loss tests were performed for 8 different molarities at a PA concentration of 0.05wt.%. This represents 16 (due to repeats) 3 hour mass loss tests (plus all solution and sample preparation times). Therefore the new test methodology provides a larger number of corrosion rates over the duration of the dilution process whilst requiring significantly less testing time and materials.

The comparison between the dilution profiles found from each of the two methodologies is shown in Figure 8.5. In order to compare the dilution tests to the mass loss tests the corrosion rate throughout the dilution test must be calculated. Figure 8.5 shows the corrosion rates calculated when an average (14.4), maximum (19.9) and minimum (11.1) Stern-Geary coefficient was used to calculate the corrosion rate. The mass loss corrosion rates have been plotted on Figure 8.5 at the point in which the solution in the dilution test is at that acid molarity. Table 8.1 shows the time at which the dilution test solution reaches each of the 8 acid molarities.

Figure 8.5 highlights that there are several benefits to using the flow cell dilution tests rather than the mass loss tests; primarily that the mass loss tests fail to capture the full dilution process. The mass loss test performed at 0.04M (7.7 hours) captures the increase in corrosion rate from the previous mass loss test at 0.2M (5 hours). However the mass loss results are unable to provide the exact HCl concentration at which the corrosion rate starts to increase.

HCl Concentration (M)	Time in Dilution Test (hours)
4	0
2	1.16
0.6	3.18
0.4	3.86
0.2	5.01
0.04	7.71
4×10^{-3}	11.55
4×10^{-4}	15.41

Table 8.1 The time at which each HCl concentration is reached in the 10ml/min dilution test.
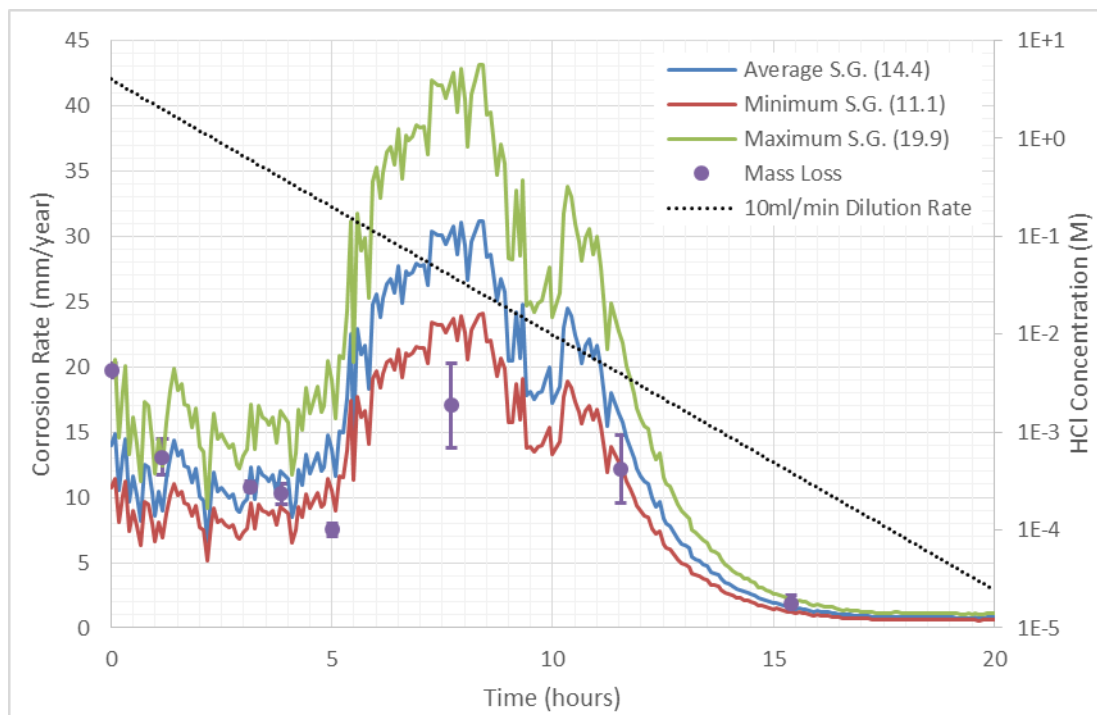
Figure 8.5 Comparison between the corrosion rates measured in the dilution test compared to those found from mass loss tests (mass loss scatter bands represent the maximum and minimum calculated corrosion rates across all 3 hour mass loss tests in each environment). The dilution test corrosion rates shown are calculated using the minimum (11.1), maximum (19.9) and average (14.4) Stern-Geary coefficients found from the fixed concentration tests. All tests were performed at 80°C. The HCl concentration is shown on the secondary axis.

The mass loss tests performed at the lowest two HCl concentrations of 4×10^{-3} and 4×10^{-4}M show a decrease in corrosion rate from the solution containing 0.04M. This same trend is observed in the flow cell dilution test. The corrosion rate found from the mass loss test at 0.04M is significantly less than the corrosion rates found from the dilution test at a concentration of 0.04M. Figure 8.5 shows the dilution test corrosion rate when the lowest and highest measured Stern-Geary coefficients (from 3 hour fixed concentration tests) were applied. This difference in solution corrosivity is observed, when compared to the mass loss results, regardless of which Stern-Geary coefficient is applied. There is still a discrepancy between the mass loss corrosion rate and the dilution test at a HCl concentration of 0.04M even when the lowest measured Stern-Geary coefficient is applied. Potential reasons for this difference are discussed in Section 8.1.3.3. The mass loss tests also fail to characterise the second peak in corrosion rate (at a time of 10.5 hours into the dilution test). Again, the potential explanation for this second peak is discussed in detail in Section 8.1.3.3.

In addition to the 3 hour mass loss tests, 3 hour electrochemistry tests were performed at the same range of HCl concentrations (all containing 0.05wt.% PA). The average reciprocal of the charge transfer resistance found from these tests has been compared to the flow cell dilution test results. Table 8.1 shows the times at which each of the 3 hour tests have been plotted on Figure 8.6. By comparing the reciprocal of the charge transfer resistance the issues which arise from having to use Tafel slope values to calculate the corrosion rate are eliminated (discussed in Section 2.2.4).

The 3 hour electrochemistry tests fail to capture the full dilution process. Figure 8.6 shows a similar trend to the comparison with the mass loss results (Figure 8.5). Tests performed at 0.04M (7.7 hours) once again capture the increase in solution corrosivity from the previous 3 hour electrochemistry test (0.2M). However the 3 hour tests are unable to find the exact molarity at which the corrosion rate starts to increase (the first peak).

The reciprocal of the charge transfer resistances ($1/R_{ct}$) from each of the two test methodologies (Figure 8.6) show high levels of agreeability other than at HCl concentrations of 0.4M and 0.04M. The reciprocal of the charge transfer resistances ($1/R_{ct}$) found from the 3 hour fixed electrochemistry tests is

significantly less than the corrosion rates found from the dilution test at this solution molarity. Again, potential reasons for this discrepancy are discussed in Section 8.1.3.3. Once again, the 3 hour electrochemistry results fail to characterise the second peak in corrosion rate (at a time of 10.5 hours into the dilution test).
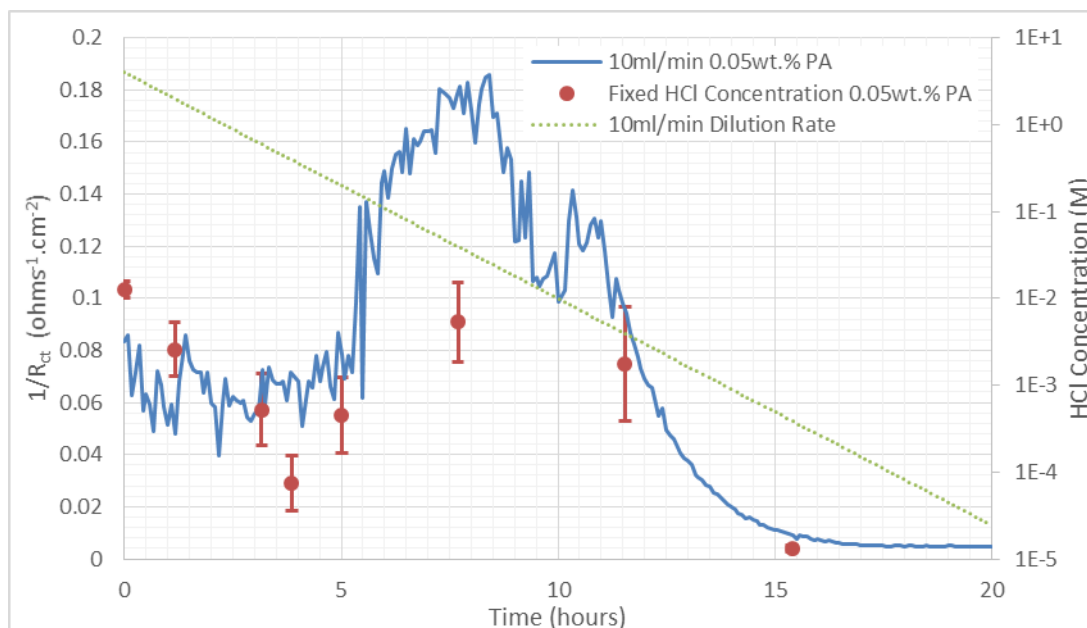
Figure 8.6 Comparison between the average reciprocal of the charge transfer resistances ($1/R_{ct}$) from the fixed HCl concentration tests and the average value calculated from the 10ml/min flow cell dilution tests. The fixed HCl tests standard deviation is calculated from all measurements made at that concentration. All tests were performed at 80°C. The HCl concentration is shown on the secondary axis.

The corrosion rates found from each of the three different test methodologies are compared in Figure 8.7. In order to compare the electrochemistry data to the mass loss data it must be converted to a corrosion rate. This raises difficulties regarding which Stern-Geary value should be used to calculate this corrosion rate.

Figure 8.7 shows three dilution test corrosion rates calculated using the maximum (19.9), minimum (11.1) and average (14.4) calculated Stern-Geary coefficients. The corrosion rates for each of the fixed concentration tests are calculated using the Stern-Geary coefficients found from the polarisation tests performed at the end of each individual test.
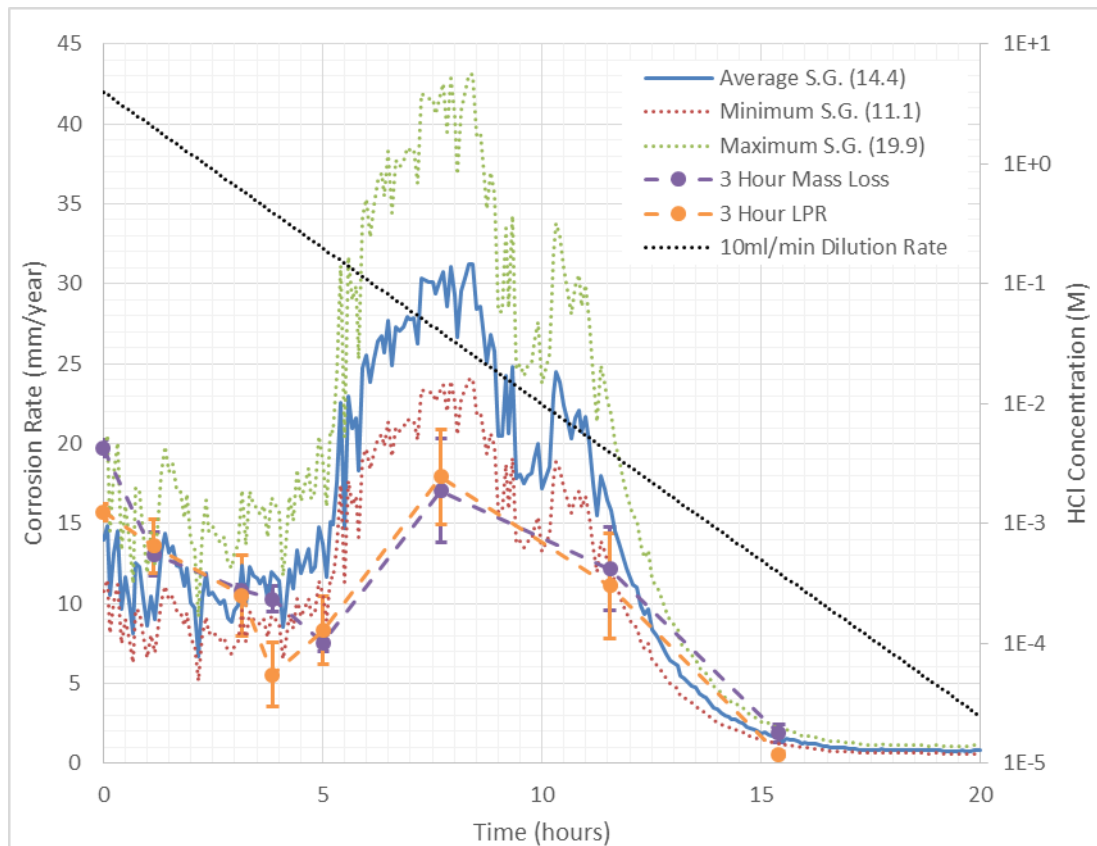
Figure 8.7 Comparison between the corrosion rates from the fixed HCl concentration tests (mass loss and LPR) and the average value calculated from the two 10ml/min flow cell dilution tests. The corrosion rates shown for the dilution tests are calculated using the minimum (11.1), maximum (19.9) and average (14.4) Stern-Geary coefficients found from the fixed concentration tests. All tests were performed at 80°C. The HCl concentration is shown on the secondary axis.

By finding the total area under each of the three flow cell dilution profiles and the dashed lines connecting the results from the fixed concentration tests (on Figure 8.7) the total metal loss over the first 15.4 hours of the test can be compared. This value can them be divided by the total test length (15.4 hours) to find the average corrosion rate for the three different test methodologies. These results are presented in Table 8.2.

The results shown in Table 8.2 highlight the difference between the total metal loss calculated over a full dilution process if each of the three test methodologies are used. Over the 15.4 hour test if the mass loss tests are used to estimate the metal loss it will be underestimated by 6.5μm compared to the flow cell dilution test (when the average Stern-Geary coefficient is applied). This means that the total metal loss is underestimated by ~24%

when compared to the value found from the dilution tests. If the 3 hour electrochemistry tests are used to estimate the metal loss over the 15.4 hour test it will be underestimated by 7.4µm. This equates to a total metal loss that is underestimated by ~28% when compared to the dilution tests. If the maximum Stern-Geary coefficient is applied then the mass loss and 3 hour LPR tests underestimate the total metal loss by as much as 45% and 48% respectively.

	3 Hour Mass Loss	3 Hour LPR	Flow Cell Dilution Test		
			Min S.G. (11.1)	Average S.G. (14.4)	Max S.G. (19.9)
Total metal loss over 15.4 Hours (µm)	20.20	19.22	20.55	26.66	36.84
Average corrosion rate (mm/year)	11.50	10.94	11.59	15.03	20.77

Table 8.2 Comparison between the total metal loss and average corrosion rates calculated from the mass loss, fixed concentration 3 hour LPR and dilution test methodologies. The metal loss has been calculated for the dilution test when the maximum, average and minimum Stern-Geary coefficient has been applied.

The average corrosion rate over the full flowback profile is therefore significantly less when the mass loss and 3 hour electrochemistry results are used to estimate the corrosivity of the flowback fluid. For both the mass loss and 3 hour electrochemistry results, the average corrosion rate is underestimated by approximately 5mm/year over the full dilution process when the average Stern-Geary coefficient is applied. Even when the minimum Stern-Geary coefficient is applied the average corrosion rate calculated using the flow cell is still slightly higher than the mass loss and 3 hour LPR tests.

8.1.3.3 Understanding the Difference in Corrosion Rate

Figure 8.3 and 8.4 shows that the corrosion rates found from the mass loss and 3 hour electrochemistry tests show excellent agreement with the dilution test corrosion rates apart from when the solution contains 0.4M or 0.04M HCl.

Crucially it is at a HCl concentration of 0.04M that the dilution test produces the highest corrosion rates. The corrosion rate found from both of the 3 hour methodologies is approximately half the corrosion rate seen when the solution in the dilution test is at the same molarity. This is the main reason for the large underestimation in total metal loss (Table 8.2) and there are several potential explanations for the discrepancy.

The most significant difference between the test methodologies is that the fixed concentration tests require the steel sample to be in contact with the solution for 3 hours. In the flow cell test the solution is constantly being replenished. This means that the acid and inhibitor in contact with the sample are not spending over time like in the 3 hour test. It is therefore difficult to directly compare the mass loss and 3 hour electrochemistry corrosion rates with those measured in the dilution test. This is due to the differences in test methodologies and the rate of HCl and PA spending not being known over the duration of the 3 hour tests.

The difference in corrosion rate when the solution contains 0.04M can be explained by three main differences between the test methodologies.

1. In the 3 hour tests the volume of PA in the solution is sufficient to form a protective film on the sample at the start of the test which then results in a lower corrosion rate. In the dilution test the entire volume of PA is not available to the sample at the start of the test due to the sample being in constant contact with fresh solution.

2. The lower corrosion rate may also be due also to the small amount of HCl present in the mass loss test reacting with the larger steel surface area (compared to the flow cell tests) and becoming less corrosive towards the end of the test. Figure 5.24 shows that the corrosion rate does decrease significantly over the 3 hour electrochemistry test; from 24mm/year to 16mm/year. However the maximum corrosion rate in the 3 hour test is still significantly less than the 34mm/year corrosion rate calculated from the dilution test.

3. When the peak occurs in the dilution test the sample has already been exposed to a corrosion rate of over 10mm/year for nearly 8 hours. It is unknown what effect this may have upon the sample. Figure 8.8 shows the increase in sample surface area over the duration of the dilution test is minimal. The surface area of the sample has increased by ~3%

once the solution concentration reaches 0.04M in the dilution test. This suggests that the higher corrosion rate is not due to an increase in sample surface area.
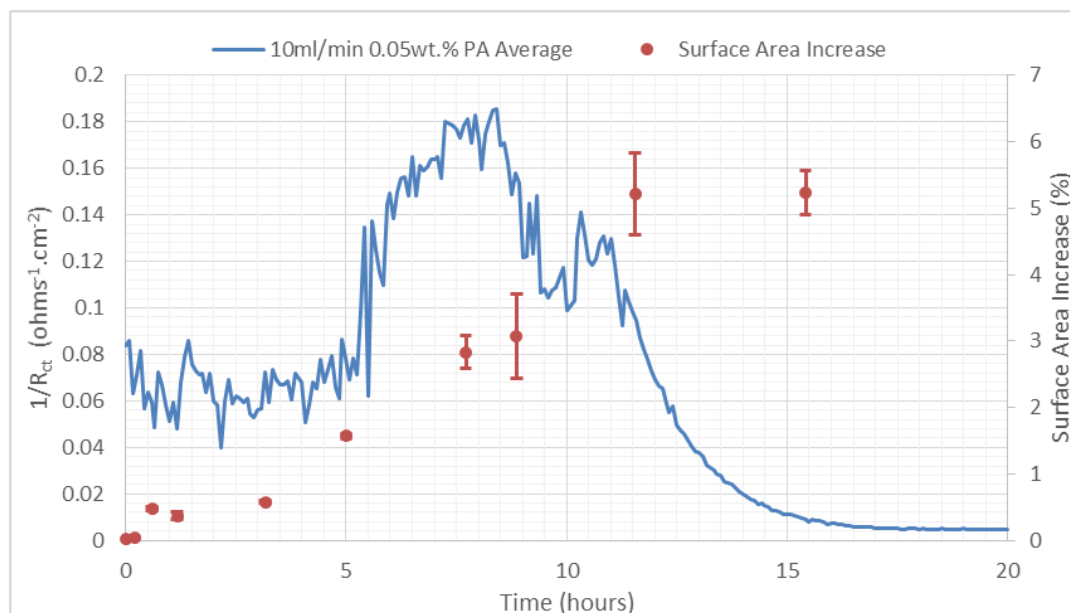
Figure 8.8 The average reciprocal of the charge transfer resistances ($1/R_{ct}$) from multiple flow cell tests when 4M HCl (with 0.05wt.% PA) is diluted with 4M NaCl brine at a rate of 10ml/min at 80°C. The surface area increase of the sample over the duration of the dilution test is shown on the secondary axis.

It is very difficult to give a definitive reason for the difference in corrosion rates measured using the two techniques. This is due to the difference in the test methodologies; specifically the fact that the dilution test is always in contact with HCl and PA which has not yet seen the sample (fresh solution). The same cannot be said about the 3 hour tests where the sample is exposed to the entire volume of HCl and PA throughout the entire test. The PA is a film forming inhibitor which requires an initial high concentration of PA to form the protective film (discussed in Section 3.2.3). A much lower concentration of inhibitor is then required to maintain the film. It may be the case that the inhibitor volume is sufficient in the 3 hour tests to provide this required initial volume of inhibitor to form the film and then maintain it with the remaining PA. It can also be argued that in the dilution test the initial solution which flows through the cell contains the highest PA volume which is then diluted over time as the HCl molarity is reduced. This should be able to form a protective

inhibitor film which should be sustained by the smaller volumes of PA in the diluted HCl solutions.

Due to the fundamental differences in the test methodologies it is unclear which of the aforementioned reasons is the cause of the discrepancy. This further highlights the benefit of the flow cell methodology and the ability to know both the exact inhibitor and HCl volumes in contact with the sample at all times throughout the test.

8.1.4 Flow Cell Comparison with the Standard Dilution Test

It is possible to replicate the full dilution process without the use of the flow cell. The original dilution test methodology outlined in Section 4.5.3 allows the corrosion rate of a steel sample to be measured throughout an entire dilution profile. The results of the standard dilution test at 10ml/min are compared with the flow cell results at the same dilution rate in Figure 8.9.
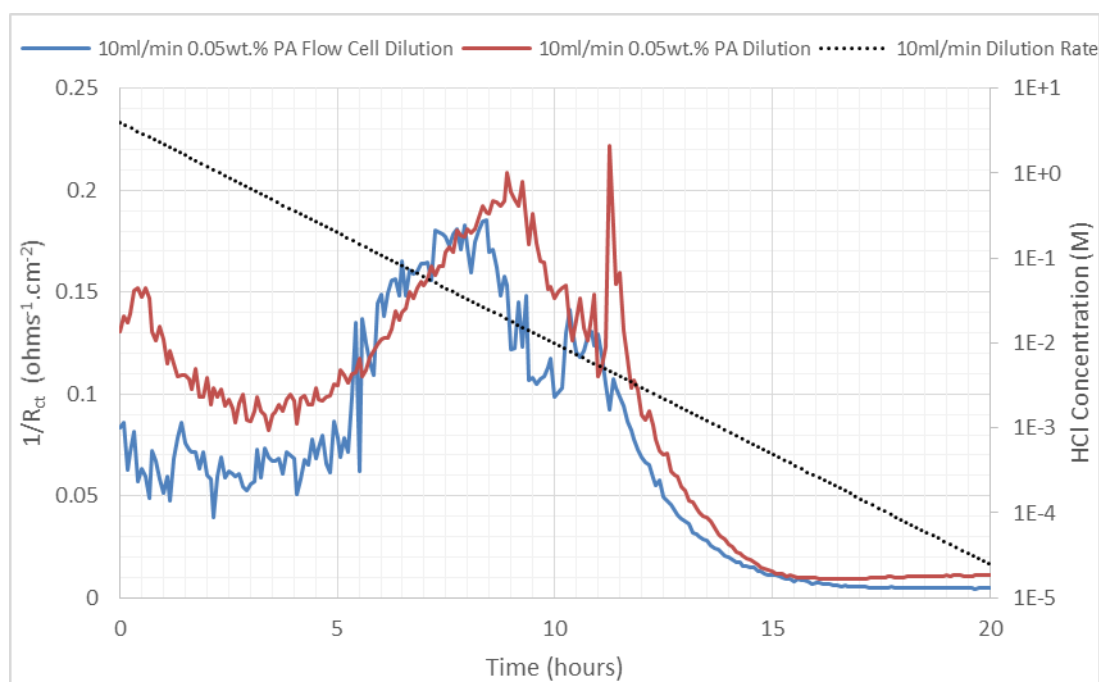
Figure 8.9 Comparison between the average reciprocal of the charge transfer resistance ($1/R_{ct}$) measured in the flow cell dilution test compared to those found from the standard dilution test. 4M HCl (containing 0.05wt.% PA) was diluted with 4M NaCl brine at a rate of 10ml/min at 80°C in both tests. The HCl concentration is shown on the secondary axis.

Figure 8.10 shows the comparison between the two tests when the time has been converted to the HCl concentration at that point in both tests. Figure 8.9 and 8.10 show that the original dilution test is able to capture the full dilution profile and measure similar corrosion rates to the dilution tests using the flow cell. The corrosion rates measured as the HCl concentration is diluted are very similar throughout both tests. The corrosion rate begins to increase in both tests when the HCl concentration reaches 0.5M.
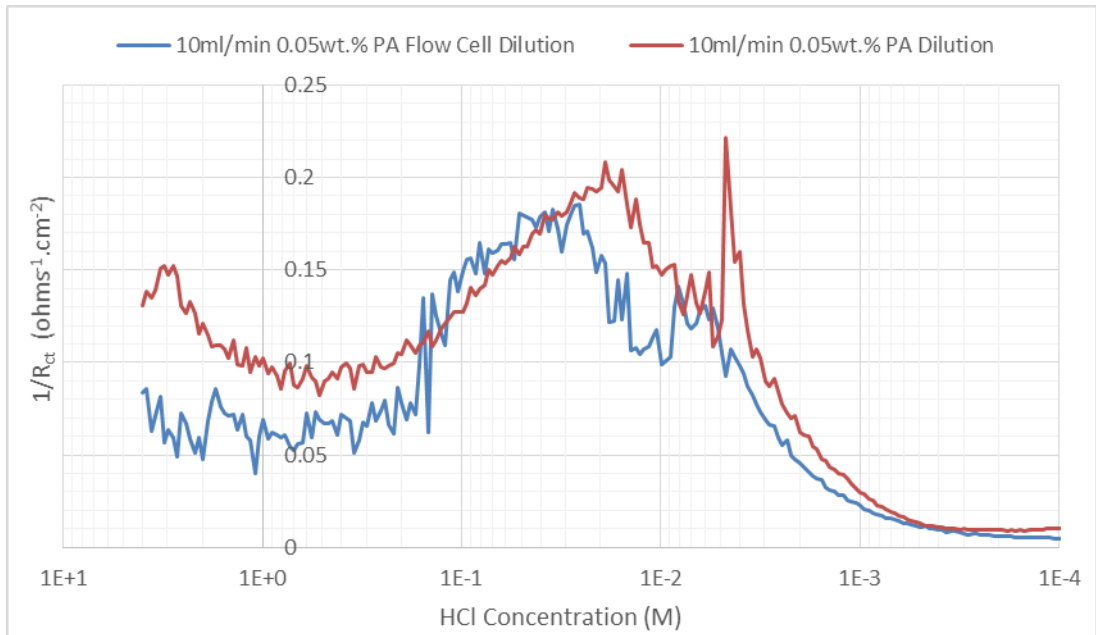
Figure 8.10 Comparison between the average reciprocal of the charge transfer resistances (1/R_{ct}) measured in the flow cell dilution test compared to those found from the standard dilution test. The time has been converted to the HCl concentration at that point in the dilution test. 4M HCl (containing 0.05wt.% PA) was diluted with 4M NaCl brine at a rate of 10ml/min at 80°C in both tests.

The first peak reaches a similar maximum solution corrosivity in both tests. The standard dilution test reaches this maximum corrosivity at a HCl concentration of 0.02M while the flow cell dilution test reaches this maximum when the HCl concentration is 0.04M. The standard dilution test peaks for a second time at a HCl concentration of 5×10^{-3}M. Whilst the flow cell dilution test peaks for a second time at a slightly higher HCl concentration (8×10^{-3}M). Both methodologies show that the corrosion rate does not return to pre-acidizing corrosion rates until the HCl concentration is less than 1×10^{-3}M.

The two test methodologies produce very similar corrosion rates over the duration of the dilution tests. Both tests exhibit peaks at similar HCl molarities and measure similar corrosion rates at these peaks. There are however several key limitations to the standard dilution test methodology.

8.1.4.1 Advantages of using the Flow Cell over the Standard Dilution

As discussed in Section 7.1.1 there were several reasons for developing the flow cell. The most important of which was that the flow cell allowed the HCl and PA concentration of the solution to be known at all times in the dilution test. Prior to performing the flow cell tests it was unknown if the peaks seen in the standard dilution test would be seen in the flow cell tests.

Prior to validating the results with the flow cell tests it could not be said with any degree of confidence that the two peaks are genuine phenomena associated with the dilution process. Due to the sample being in contact with the entire volume of PA and HCl from the start of the test, the peaks in corrosion rate could be explained by the full volume of PA being available to react with the sample from the start of the test. The peak could then be said to occur when the inhibitor has all reacted with the steel sample (or with the HCl itself) and enough inhibitor is not present to maintain the protective film. The second peak is more difficult to explain using this rationale but could potentially be explained by the remnants of the protective PA film being removed from the sample.

In order to validate the peaks in corrosion rate observed in the standard dilution test it was vital that a test methodology was developed where the sample is always in contact with fresh solution. By observing the peaks again in the flow cell tests it disproves the argument that they are caused by a lack of PA due to reactions with the HCl and steel sample earlier in the dilution test. Herein lies the key benefit of the flow cell dilution tests over the standard dilution test; the ability to quantify the critical PA and HCl concentration at which the peaks occur.

8.1.5 Characterisation of the Entire Flowback Process

No attempt has been made to model the entire flowback process in previous work. No research has been conducted into how the corrosivity of the solution

changes with decreasing acid and inhibitor concentrations as the solution flows back. As discussed earlier a limited number of previous studies have been performed at acid concentrations that are considerably lower than the injected strength acids. Therefore an understanding as to how the corrosivity changes as the solution molarity decreases (i.e. the flowback from an acid job) cannot be gained from the previous research work. This means that the closed vessel dilution test methodology (discussed in Section 4.5.3), despite its limitations, is the first test of its kind to attempt the replicate the changing solution chemistry encountered during flowback. The use of the flow cell further improves the understanding of the flowback process that can be achieved through laboratory testing.

8.1.5.1 Flow Cell Dilution Tests

The benefits of using the flow cell over the standard dilution test can be outlined as follows.

- The steel sample is always in contact with 'fresh' solution. The HCl and PA concentration of the solution are always known as it has not been in contact with the steel prior to this point. This more accurately replicates the situation encountered during acid flowback in the field.
- The PA is not heated with the HCl throughout the entire duration of the dilution test and is only heated prior to entering the flow cell. This eliminates the problem of any unwanted PA reactions prior to the solution entering the flow cell.
- The problem of solution contamination is eliminated as the sample is always in contact with fresh solution. Any reacted solution is removed from the cell and pumped to a waste container.

8.2 Understanding the Critical PA and HCl Concentrations

8.2.1 Introduction

The results of the 3 hour mass loss and electrochemistry tests (Chapter 5) show a complicated relationship exists between the HCl and the PA concentration of the solution. The dilution test results, both with and without the flow cell (Section 5.3.5 and Section 7.2 respectively), only further emphasise the complexity of this relationship. The flow cell was designed to allow the HCl and PA concentration to be known at all times in the dilution test. It was hoped that by performing a range of different tests using this newly

developed test methodology the relationship between the HCl and PA concentrations could be better understood.

Each of the additional tests performed, at a range of starting PA and HCl concentrations, are analysed in turn. An attempt is made to explain the two peaks seen in the dilution tests and identify the critical PA and HCl concentrations associated with these peaks in corrosion rate.

8.2.2 Defining the Two Peaks

It is important to first analyse the dilution test performed in the flow cell at a starting concentration of 4M (with 0.05wt.% PA) and diluted at a rate of 10ml/min and define what is meant by the two peaks. Figure 8.11 shows how the corrosion rate changes as the HCl concentration of the solution is diluted. The start of the peak is defined as the point at which the corrosivity of the solution starts to increase and the end of the peak is the point at which the corrosion rate reaches a maximum value before starting to decrease again. The start and end of each peak are shown on Figure 8.11.
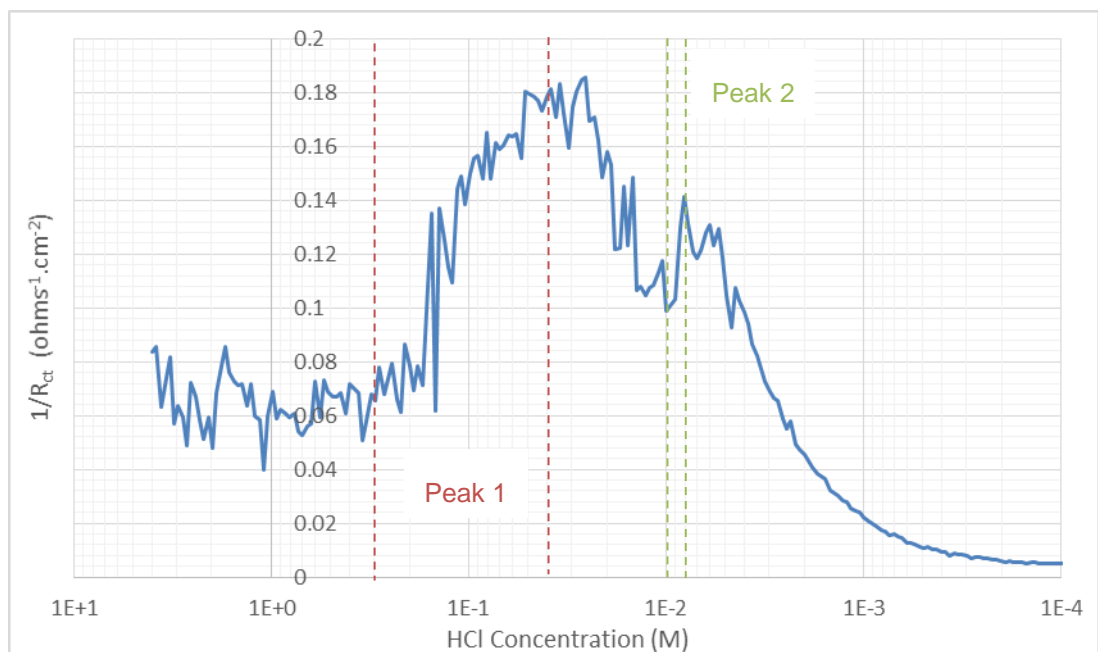
Figure 8.11 Average reciprocal of the charge transfer resistances ($1/R_{ct}$) calculated from both flow cell dilution tests starting at 4M HCl (containing 0.05wt.% PA) and diluted with 4M NaCl brine at a rate of 10ml/min at 80°C. The time has been converted to the HCl concentration. The two peaks in corrosion rate are highlighted.

Table 8.3 shows the HCl concentrations at which the two peaks identified in Figure 8.11 start and reach a maximum corrosion rate. The PA concentration of the solution is diluted at the same rate as the HCl. Table 8.3 shows each of the PA concentrations calculated from each of the HCl concentrations.

	Peak 1		Peak 2	
	Start	Maximum	Start	Maximum
HCl Concentration (M)	0.3	0.04	0.01	8×10^{-3}
PA Concentration (wt.%)	3×10^{-3}	5×10^{-4}	1.3×10^{-4}	1×10^{-4}

Table 8.3 HCl and PA concentrations at which the two peaks in corrosion rate start and reach a maximum value when the 4M HCl, containing 0.05wt.% PA is diluted at 10ml/min.

8.2.3 Further Flow Cell Tests at 10ml/min

In order to help better understand the peaks a variety of tests were performed using the flow cell. There are three main variables which can be changed in the flow cell dilution tests.

1. Dilution Rate
2. Starting PA concentration
3. Starting HCl concentration

8.2.3.1 Varying the Flow Rate

The effect of varying the dilution rate has been discussed in Section 8.1.2 and Figure 8.2 shows that a similar trend is observed regardless of the dilution rate. However the intensity of the second peak appears to vary at each flow rate. Figure 8.2 shows that the intensity of the second peak is highest at the slowest flowrate of 5ml/min (35mm/year). It then decreases in intensity as the flow rate is increased to 10ml/min (30mm/year) and 15ml/min (23mm/year). Potential explanations for this and the nature of the second peak are discussed in Section 8.2.7.

8.2.3.2 Varying the Starting HCl Concentration

The starting HCl concentration was varied and the results are presented in Section 7.2.3. It was hoped that by a direct comparison of these tests it would

be possible to identify the HCl concentrations at which point each of the peaks starts and reaches a maximum value. Dilution tests were performed at a flow rate of 10ml/min at a range of different starting HCl concentrations all of which contained 0.05wt.% PA relative to the HCl concentration. These dilution tests were performed at starting HCl concentrations of 0.4M and 0.04M and the solution corrosivity measured throughout these tests are shown in Figure 7.21-7.22. A comparison between these tests and the dilution test starting at 4M is shown in Figure 8.12. The time has been converted to the HCl concentration at that time in the dilution test.
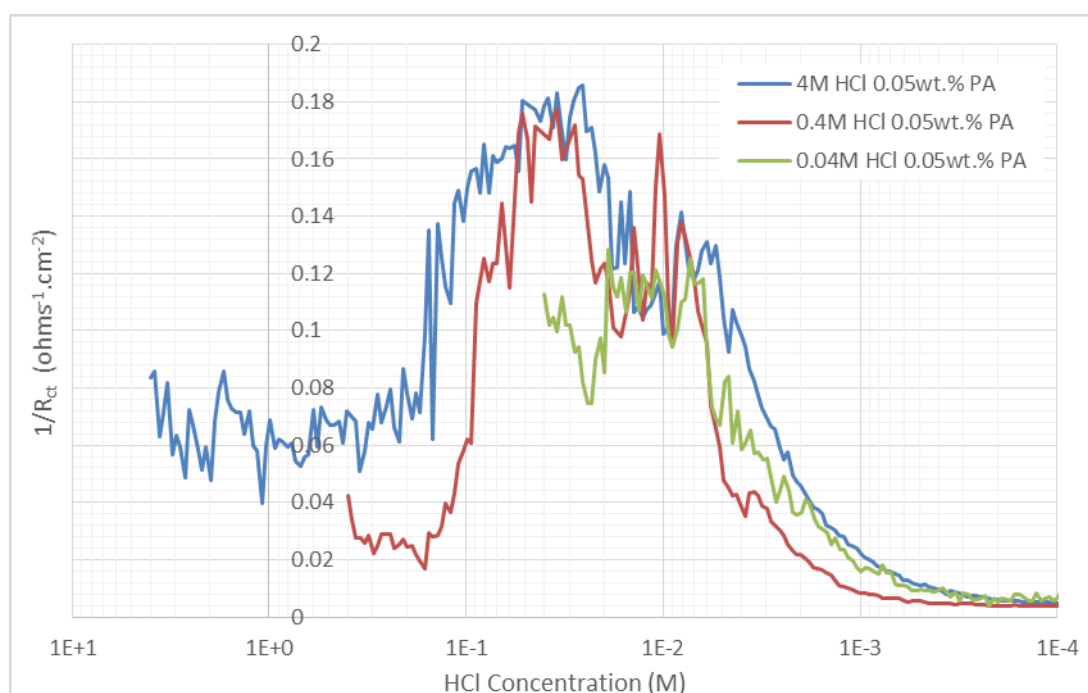
Figure 8.12 Reciprocal of the charge transfer resistances ($1/R_{ct}$) from the flow cell dilution tests starting at a range of HCl concentrations, 4M-0.04M (all containing 0.05wt.% PA), at 80°C and diluted with 4M NaCl brine at a rate of 10ml/min. All results have been plotted as a function of the HCl concentration at that time in the dilution test.

Figure 8.12 shows a direct comparison between all of the dilution tests starting at different HCl concentrations. It is clear that all tests follow a very similar trend and it appears that they all peak at similar HCl values. However in order to more clearly compare the peaks a direct comparison between the dilution test starting at 4M and each of the tests starting at lower HCl concentrations is made in Figure 8.13 and 8.14. The peaks observed at these lower starting HCl concentrations are highlighted.
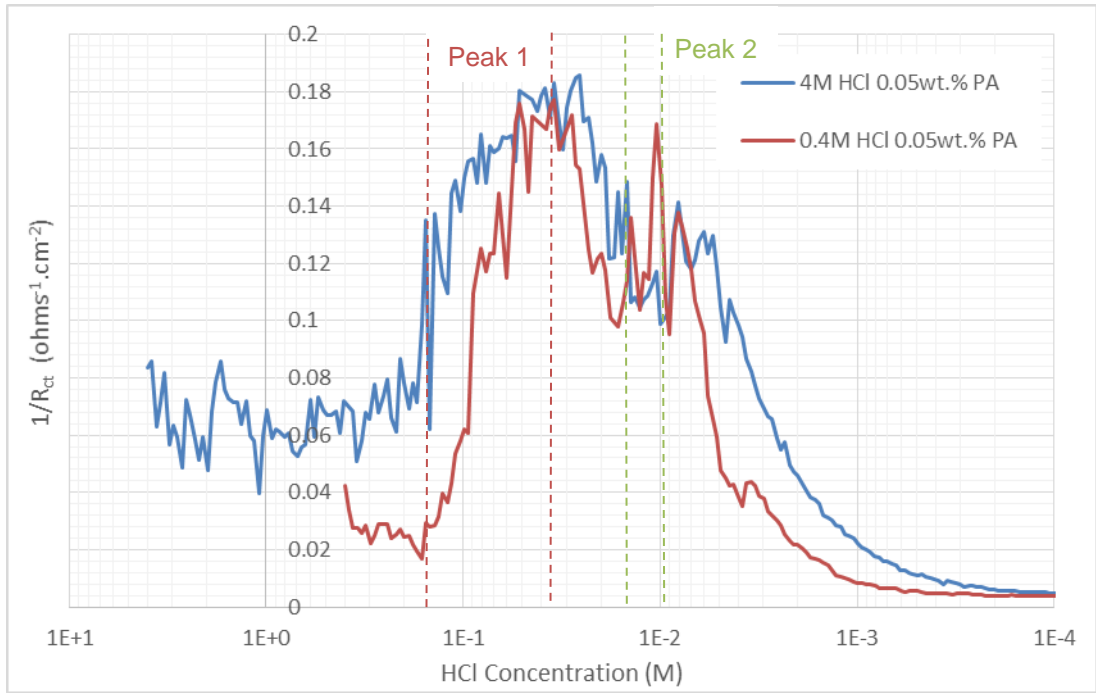
Figure 8.13 Reciprocal of the charge transfer resistances ($1/R_{ct}$) from the flow cell dilution tests starting at 4M and 0.4M HCl (both containing 0.05wt.% PA) and diluted with 4M NaCl brine at a rate of 10ml/min at 80°C. The two peaks observed in the 0.4M dilution test are highlighted.
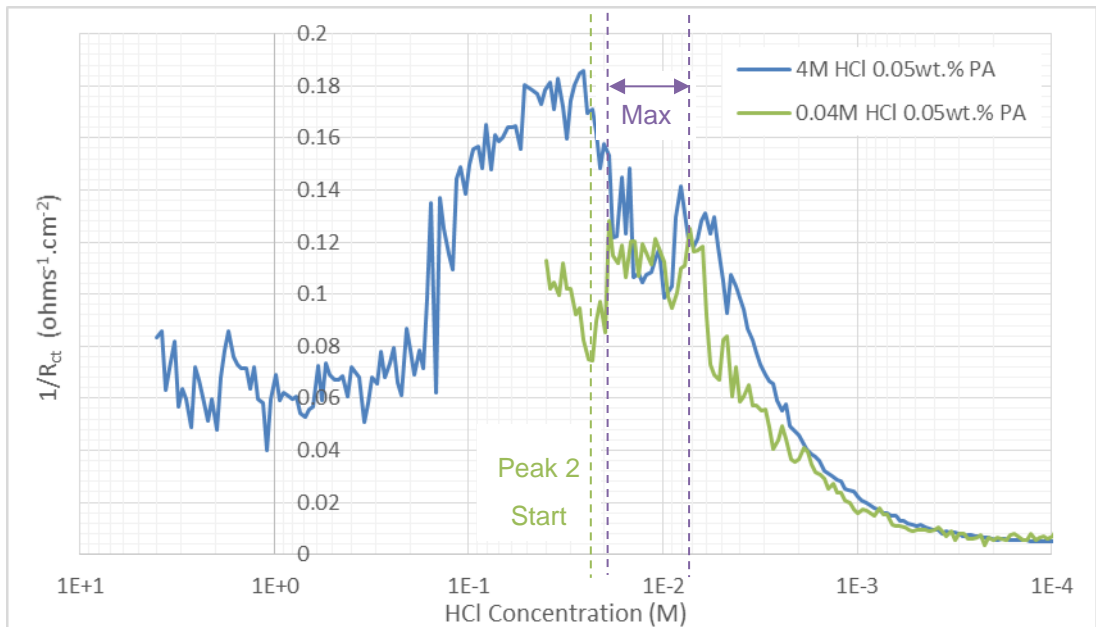
Figure 8.14 Reciprocal of the charge transfer resistances ($1/R_{ct}$) from the flow cell dilution tests starting at 4M and 0.04M HCl (both containing 0.05wt.% PA) and diluted with 4M NaCl brine at a rate of 10ml/min at 80°C. The single peak observed in the 0.04M dilution test is highlighted.

The comparison between the different starting HCl concentrations helps to further understand the peaks in corrosion rate. The 0.4M starting concentration is the only other test to characterise both peaks. A starting HCl concentration of 0.04M fails to fully characterise the first peak as the starting HCl concentration is too low. The second peak is also difficult to characterise as it is not clear where the peak in corrosion rate occurs. The region in which it appears to occur is between a HCl concentration of 0.02M and 7×10^{-3}M. This range is shown on Figure 8.14.

The HCl concentrations for the start and maximum values of each of the two peaks in all three tests are shown in Table 8.4. All values shown in all tables are given to 1 significant figure.

Dilution Test Starting HCl Concentration (M)	Peak 1 HCl Conc. (M)		Peak 2 HCl Conc. (M)	
	Start	Maximum	Start	Maximum
4	0.3	0.04	0.01	8×10^{-3}
0.4	0.2	0.04	0.02	$0.02 - 7 \times 10^{-3}$
0.04	-	-	0.01	7×10^{-3}

Table 8.4 HCl concentrations at which the two peaks in corrosion rate start and end when the dilution test starting HCl concentration is varied. All tests contained 0.05wt.% PA and were diluted with 4M NaCl brine at a rate of 10ml/min.

8.2.3.3 Varying the PA Concentration

Figure 8.12 suggests that changing the starting HCl concentration of the dilution tests has little impact upon the start and end HCl concentrations of the peaks. In all tests the PA concentration was kept constant (0.05wt.%) relative to the HCl concentration of the solution. Further dilution tests were performed at a starting HCl concentration of 4M and diluted at a rate of 10ml/min. The PA concentration was decreased 5 times to 0.01wt.% and the corrosivity of the solution over the dilution test is shown in Figure 7.23. A further test was performed at a PA concentration of 0.25wt.% (5 times higher than the original dilution test) and the corrosivity over the duration of the dilution test shown in Figure 7.24.

8.2.3.4 Relationship between the Corrosion Rate and H⁺ Concentration

Figure 8.15 shows a comparison between each different starting PA concentration (0.01, 0.05 and 0.25wt.%). All tests were performed at a starting HCl concentration of 4M and were diluted with 4M NaCl brine at a rate of 10ml/min. The time has been converted to the HCl concentration at that point in each of the dilution tests. The PA concentration at which the first peak starts is also shown on Figure 8.15.
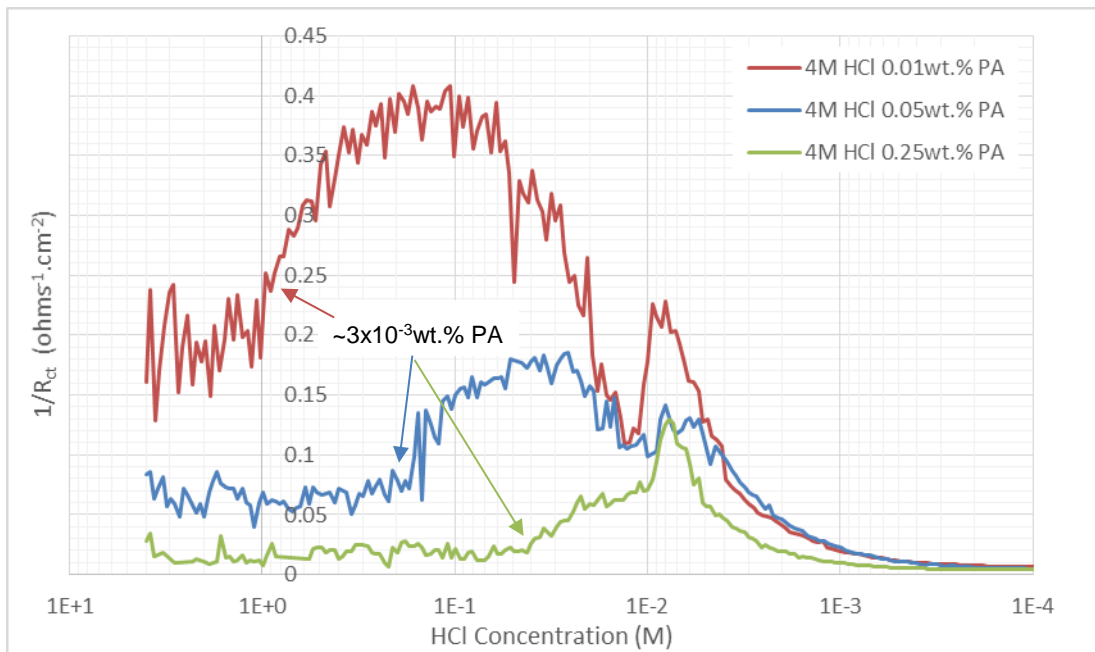
Figure 8.15 Reciprocal of the charge transfer resistances ($1/R_{ct}$) from the flow cell dilution tests starting at 4M at a range of different PA concentrations and diluted with 4M NaCl brine at 80°C. The time has been converted to the HCl concentration at that point in the dilution test. The approximate PA concentration of the solution is shown when the first peaks reaches a maximum value in all three tests.

The location of the two peaks when the starting PA concentration is 0.01wt.% and 0.25wt.% are shown on Figure 8.16 and 8.17 respectively. The time has been converted to the HCl concentration at that point in the dilution test.

The HCl concentrations at which each of the peaks starts and reaches a maximum value, at each of the three different PA concentrations tested are provided in Table 8.5. Unfortunately it is unclear from Figure 8.17 at what HCl concentration the first peak reaches a maximum value and when the second peak starts.
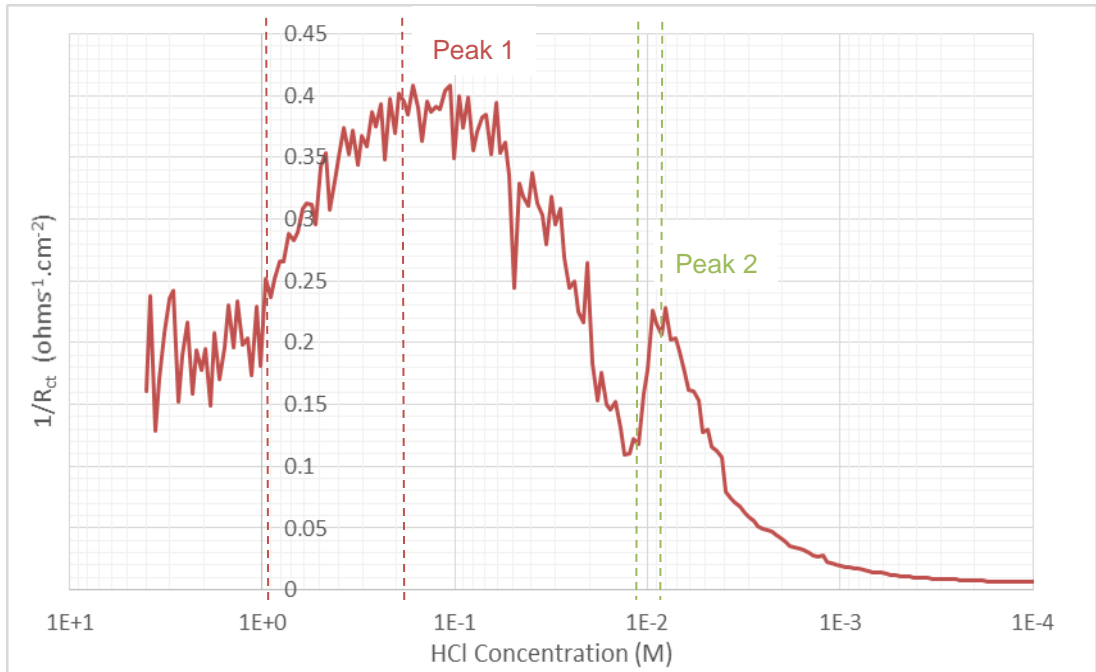
Figure 8.16 Reciprocal of the charge transfer resistances (1/R_{ct}) from the flow cell dilution tests starting at 4M HCl containing 0.01wt.% PA and diluted with 4M NaCl brine at a rate of 10ml/min at 80°C. The two peaks observed in the dilution test are highlighted.
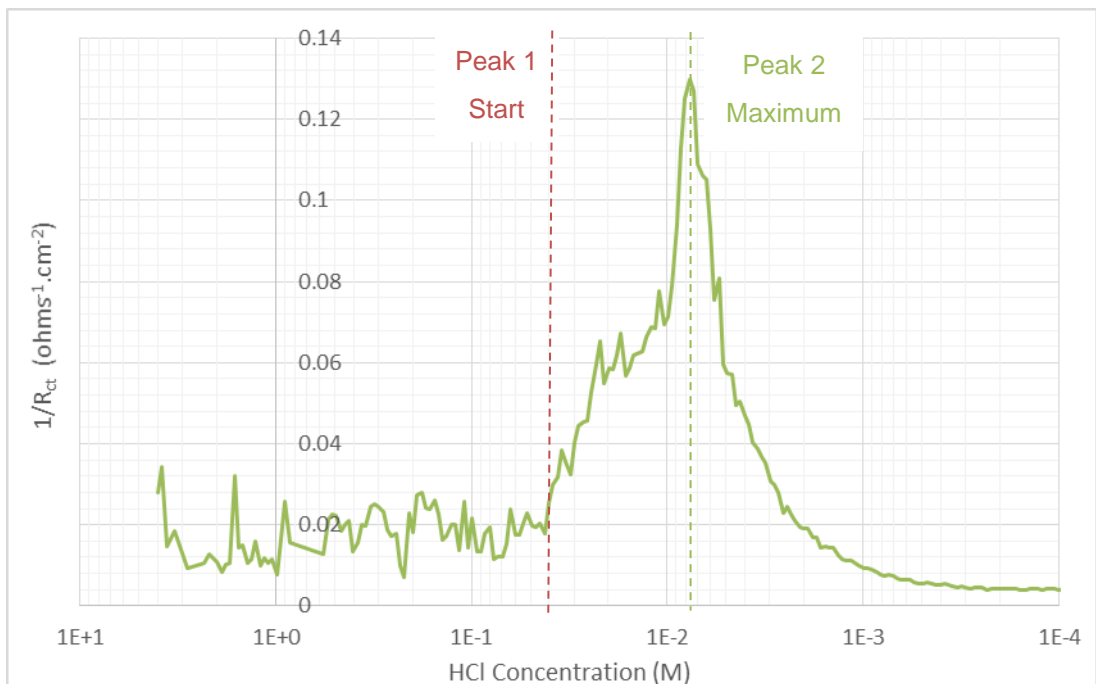
Figure 8.17 Reciprocal of the charge transfer resistances (1/R_{ct}) from the flow cell dilution tests starting at 4M HCl containing 0.25wt.% PA and diluted with 4M NaCl brine at a rate of 10ml/min at 80°C. The two peaks observed in the dilution test are highlighted.

Dilution Test PA Concentration (wt.%)	Peak 1 HCl Conc. (M)		Peak 2 HCl Conc. (M)	
	Start	Maximum	Start	Maximum
0.25	0.04	-	-	8×10^{-3}
0.05	0.3	0.04	0.01	8×10^{-3}
0.01	1	0.2	0.01	8×10^{-3}

Table 8.5 HCl concentrations at which the two peaks in corrosion rate start and end when the PA concentration is varied. All tests started at 4M HCl and were diluted with 4M NaCl brine at a rate of 10ml/min.

The HCl concentration of the solution can be used to estimate the pH of the solution. The number of moles of hydrogen ions (H^+) of the solution is equal to the HCl molarity of the solution throughout the test. Therefore Equation 8.2 [111] can be used to approximate the pH at each of the molarities shown in Table 8.5. The approximate pH values are calculated in Table 8.6 and presented to 2 significant figures.

$$pH = -\log(H^+) \tag{8.2}$$

It should however be noted that this is not the true pH of the solution (especially at the higher HCl molarities) due to the increased activity coefficient of the HCl due to the addition of the NaCl brine [110-112]. The complex relationship between the H^+ and the NaCl concentration of the flowback fluid means that calculating the true pH is very difficult (as discussed in Section 3.2.1.3). Consequently, the pH values presented in this chapter are intended to provide an indication as to the variation of H^+ concentration on a log scale. This in turn produces an approximation as to the extent of the pH variation over the test by assuming ideal solution chemistry and behaviour. As discussed previously, the values calculated using Equation 8.2 better represents the true pH as the HCl concentration reduces throughout the dilution test [111]. It is vital to stress that the pH values provided are not the true pH, merely an approximation based on the H^+ concentration of the solution. Unfortunately, due to the very low pH of the solution, a standard pH meter is not suitable for measuring the actual solution pH.

Dilution Test PA Concentration (wt.%)	Peak 1 pH		Peak 2 pH	
	Start	Maximum	Start	Maximum
0.25	1.4	-	-	2.1
0.05	0.52	1.4	2.0	2.1
0.01	0.0	0.70	2.0	2.1

Table 8.6 Approximate solution pH at which the two peaks in corrosion rate start and end when the PA concentration is varied. All tests started at 4M HCl and were diluted with 4M NaCl brine at a rate of 10ml/min.

The HCl concentrations shown in Table 8.5 and the approximate pH values in Table 8.6 show that the first peak occurs at a different HCl concentration for each of the starting PA concentrations tested. At the lowest PA concentration (0.01wt.%) the solution corrosivity starts to increase approximately 2 hours into the dilution test, at a pH of ~0 (1M HCl). If the PA concentration is increased 5 fold (0.05wt.%) then the first peak in corrosion rate occurs 5 hours into the dilution test at an approximate pH of ~0.52 (0.3M HCl). A further 5 times increase in PA concentration, to 0.25wt.%, further delays the peak in corrosion rate which occurs approximately 7 hours into the dilution test. The pH at this point in the dilution test is ~1.4 (0.04M HCl).

The second peak highlighted on Figures 8.8, 8.13 and 8.14 and the values shown in Table 8.5 and 8.6 suggest that this peak is related to the pH of the solution. At the lowest PA concentration (0.01wt.%) the second peak in corrosivity begins at a pH of ~2 (0.01M) and reaches a maximum value at ~2.1 (8×10^{-3}M). An increase in PA concentration (to 0.05wt.%) results in the second peak also starting at a pH of ~2 (0.01M) which then again reaches a maximum corrosion rate at pH ~2.1 (8×10^{-3}M). The highest PA concentration (0.25wt.%) reaches a maximum value at pH ~2.1 (8×10^{-3}M). This suggests that the second peak is related to the H^+ concentration (expressed as the approximate pH) of the solution. At the three PA concentrations tested the peak starts at a pH of approximately 2 and the maximum corrosion rate occurs at pH ~2.1 in all tests.

8.2.3.5 Relationship between the Corrosion Rate and PA Concentration

Figure 8.18 shows the comparison between the tests with different starting PA concentrations if the time is converted to the PA concentration of the solution at that time in the dilution test. The location of the two peaks are the same as those shown in Figure 8.16 and 8.17. The PA concentration of the solution is always relative to the HCl concentration of the solution allowing the PA concentration at any point in the dilution test to be found using Equation 4.6 and substituting the initial PA concentration into the equation rather than the initial HCl concentration (C_0).
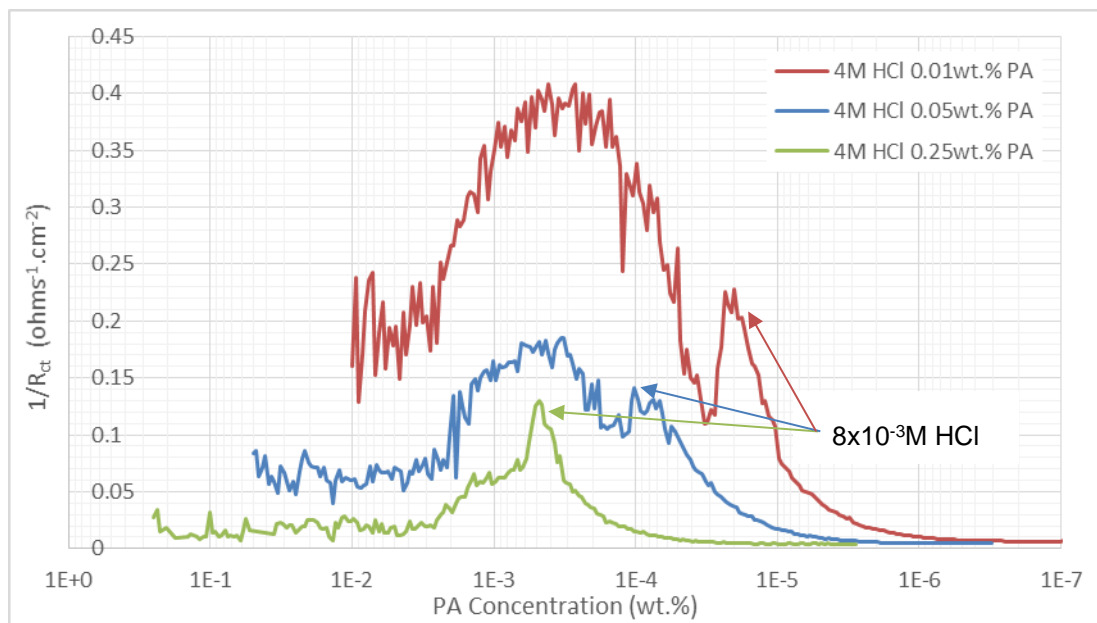

Figure 8.18 Reciprocal of the charge transfer resistances ($1/R_{ct}$) from the flow cell dilution tests starting at 4M HCl at a range of different PA concentrations at 80°C. The HCl was diluted with 4M NaCl brine at a rate of 10ml/min. The time has been converted to the PA concentration at that point in the dilution test. The HCl concentration of the solution is shown when each of the second peaks reaches a maximum value.

The PA concentrations shown in Table 8.7 suggests that the first peak occurs at similar PA concentrations for each of the three different concentrations tested. The lowest PA concentration (0.01wt.%) starts to increase once the PA concentration reaches 2×10^{-3}wt.%. If the PA concentration is increased 5 times (0.05wt.%) then the first peak in corrosion rate occurs once the PA concentration reaches 4×10^{-3}wt.%. A further 5 fold increase in PA concentration (to 0.25wt.%) results in the first peak starting at 3×10^{-3}wt.%. The maximum corrosion rate observed from the first peak in corrosion rate in the

0.01 and 0.05wt.% tests also occurs at similar PA concentrations (it is not clear at what point the first peak reaches a maximum value and the second peak starts at a PA concentration of 0.25wt.%). The peak occurs at 4×10^{-4} and 5×10^{-4}wt.% as the initial PA concentration is increased from 0.01 to 0.05wt.%. The range of PA concentrations over which the peak starts is from 2×10^{-3} to 4×10^{-3}wt.% and the range over which it reaches a maximum is from 4×10^{-4} to 5×10^{-4}wt.%. The small range over which this peak occurs and reaches a maximum suggests that this peak in corrosion rate is controlled by the PA concentration of the solution.

Dilution Test PA Concentration (wt.%)	Peak 1 PA Conc. (wt.%)		Peak 2 PA Conc. (wt.%)	
	Start	Maximum	Start	Maximum
0.25	3×10^{-3}	-	-	5×10^{-4}
0.05	4×10^{-3}	5×10^{-4}	2×10^{-4}	1×10^{-4}
0.01	2×10^{-3}	4×10^{-4}	3×10^{-5}	2×10^{-5}

Table 8.7 PA concentrations at which the two peaks in corrosion rate start and end when the dilution test starting PA concentration is varied. All tests contained 0.05wt.% PA and were diluted at 10ml/min.

The second peak highlighted on Figures 8.16-8.18 and the values shown in Table 8.7 suggest that this peak is not related to the PA concentration of the solution. At the lowest PA concentration (0.01wt.%) the second peak starts at a PA concentration of 3×10^{-5}wt.% and reaches a maximum value at 2×10^{-5}wt.%. An increase in PA concentration (to 0.05wt.%) results in the second peak starting at a PA concentration of 2×10^{-4}wt.% which then reaches a maximum corrosion rate at 1×10^{-4}wt.%.

At the highest starting PA concentration (0.25wt.%) it is unclear at what concentration the second peak starts before then reaching a maximum value once the solution reaches a PA concentration of 5×10^{-4}wt.%. This suggests that the second peak is not related to the PA concentration of the solution. The range at which the second peak starts is between 1×10^{-3} and 3×10^{-5}wt.%. Whilst the range of PA concentrations over which the maximum corrosion rate occurs is between 5×10^{-4} and 2×10^{-5}wt.%.

8.2.4 Redosing Propargyl Alcohol

The results from the dilution tests performed at different starting PA concentrations suggest that once the solution reaches a critical PA concentration the first peak in corrosion rate occurs. This is followed by a second peak which is due to the solution reaching a critical H^+ concentration. In order to further test this theory a dilution test was repeated at 10ml/min with starting concentrations of 4M HCl and 0.05wt.% PA. However in this test the inhibitor was redosed back to 0.05wt.% once the PA concentration had been diluted to 5×10^{-3}wt.%. In the standard dilution test the first peak had started at a PA concentration of 4×10^{-3}wt.%, so it was decided to redose the PA just before it was diluted to this concentration.

The change in solution corrosivity measured over the duration of this test is shown in Figure 7.29. The time has been converted to the HCl concentration and the PA concentration at that point in the dilution test and these results are shown in Figure 8.19 and 8.20 respectively. The peaks have been highlighted on each of these figures and a comparison between the peaks seen when the PA is redosed and when it is not redosed is provided in Table 8.8 (as a function of HCl concentration) and Table 8.9 (as a function of PA concentration).
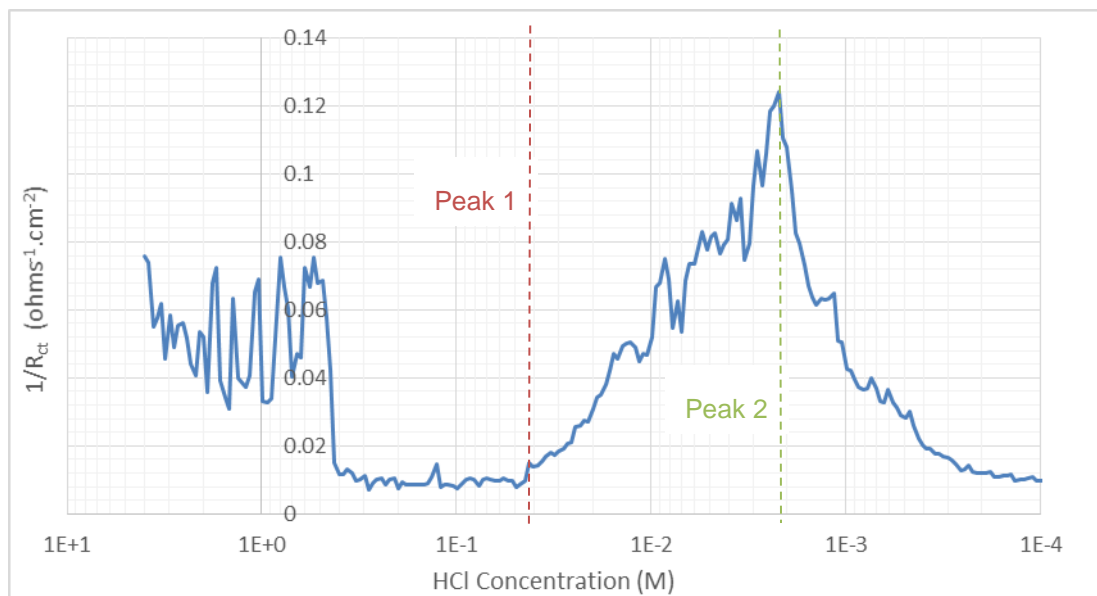
Figure 8.19 Corrosion rates from the flow cell dilution tests starting at 4M HCl containing 0.05wt.% PA (redosed at 5×10^{-3}wt.%) and diluted with 4M NaCl brine at a rate of 10ml/min at 80°C. The time has been converted to the HCl concentration at that point in the dilution test. The peaks observed in the dilution test are highlighted.
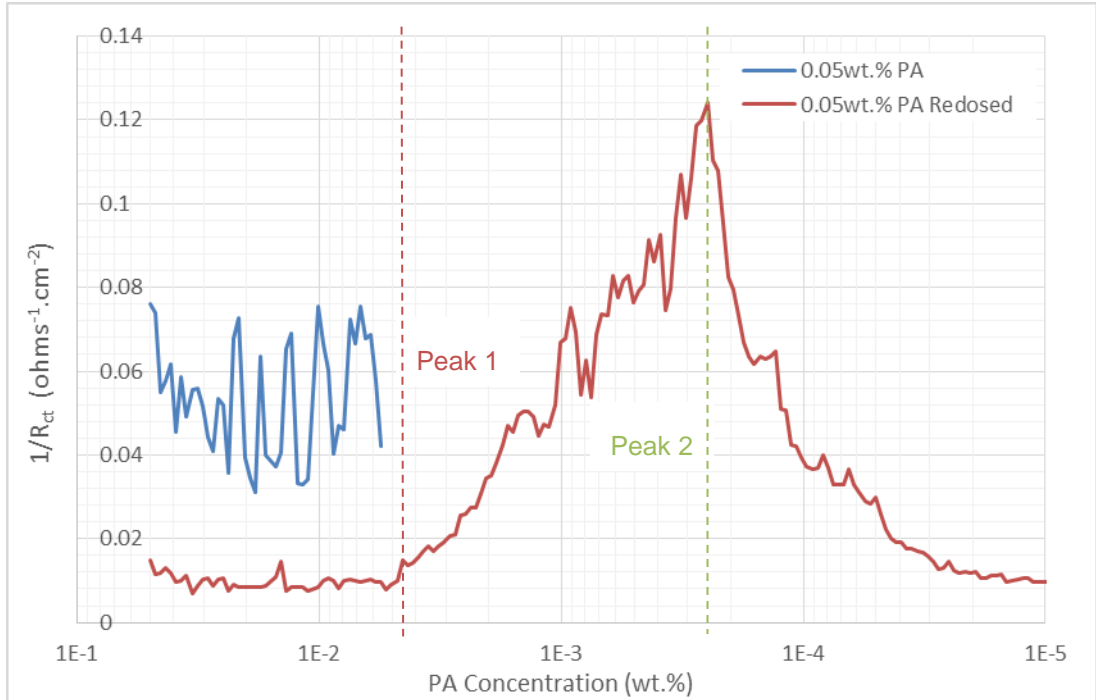
Figure 8.20 Corrosion rates from the flow cell dilution tests starting at 4M containing 0.05wt.% PA (corrosion rate is shown in blue) and diluted at a rate of 10ml/min at 80°C. The PA was then redosed once it reached a concentration of 5×10^{-3}wt.% (corrosion rate after redosing is shown in red). The time has been converted to the PA concentration.

Dilution Test PA Concentration (wt.%)	Peak 1 HCl Conc. (M)		Peak 2 HCl Conc. (M)	
	Start	Maximum	Start	Maximum
0.05	0.3	0.04	0.01	8×10^{-3}
0.05 and redosed	0.05	-	-	2×10^{-3}

Table 8.8 HCl concentrations at which the two peaks in corrosion rate start and end when PA both is and is not redosed at 5×10^{-3}wt.%. Both tests started at 0.05wt.% PA and were diluted with 4M NaCl brine at a rate of 10ml/min.

The peaks observed in Figure 8.19 and 8.20 are difficult to interpret. It is clear the corrosion rate begins to increase once the HCl concentration has been diluted to 0.05M (pH ~1.3 and 5×10^{-3}wt.% PA). This is therefore the start of the first peak in corrosion rate. However it is then difficult to clearly state at what point in the test the first peak reaches a maximum and the second peak starts.

Dilution Test PA Concentration (wt.%)	Peak 1 PA Conc. (wt.%)		Peak 2 PA Conc. (wt.%)	
	Start	Maximum	Start	Maximum
0.05	4×10^{-3}	5×10^{-4}	2×10^{-4}	1×10^{-4}
0.05 and redosed	5×10^{-3}	-	-	3×10^{-4}

Table 8.9 PA concentrations at which the two peaks in corrosion rate start and end when PA both is and is not redosed at 5×10^{-3}wt.%. Both tests started at 0.05wt.% PA and were diluted with 4M NaCl brine at a rate of 10ml/min.

There is then a peak in solution corrosivity at a HCl concentration of 2×10^{-3}M (pH ~2.7 and 3×10^{-4}wt.% PA) before the corrosion rate begins to decrease to acceptable pre-acid job corrosivity. It can be assumed that this is the maximum corrosion rate from the second peak as in all previous tests the solution corrosivity returns to a value similar to that found when the solution consists entirety of 4M NaCl brine.

The results of the redosing test show that the corrosion rate begins to increase at a PA concentration of 5×10^{-3}wt.% (the start of the first peak) regardless of the PA being redosed. The redosing of the PA does nothing to prevent the corrosion rate increasing, it merely delays the start until the critical PA concentration is reached. This is further evidence that the first peak in corrosion rate is due to a lack of PA in the solution. Table 8.10 compares the PA concentrations at which the first peak starts and reaches a maximum value for all tests performed (with different PA concentrations). It is clear from Table 8.10 that the corrosion rate in the dilution test starts to increase once the PA concentration reaches between 3×10^{-3} and 5×10^{-3}wt.% PA. Increasing the PA concentration or redosing PA both fail to prevent the corrosion rate from increasing once this critical PA concentration is reached.

As previously discussed the second peak appears to be controlled by the H$^+$ concentration of the solution. Table 8.10 also compares the HCl concentration at which the second peak starts and reaches a maximum value in all dilution tests. Table 8.10 suggests that when the PA is redosed the second peak occurs later in the dilution test once the solution reaches a lower H$^+$ concentration. At all three inhibitor concentrations tested the second peak

reached a maximum value at a HCl concentration of 8×10^{-3}M. By redosing the inhibitor the maximum value is not observed until the HCl concentration is diluted to 2×10^{-3}M, a slightly lower value than the tests in which the PA was not redosed.

Dilution Test PA Concentration (wt.%)	Peak 1 PA Conc. (wt.%)		Peak 2 HCl Conc. (M)	
	Start	Maximum	Start	Maximum
0.25	3×10^{-3}	-	-	8×10^{-3}
0.05	4×10^{-3}	5×10^{-4}	0.01	8×10^{-3}
0.05 redosed	5×10^{-3}	-	-	2×10^{-3}
0.01	2×10^{-3}	4×10^{-4}	0.01	8×10^{-3}

Table 8.10 PA concentrations at which the first peak in corrosion rate starts and reaches a maximum and the HCl concentration at which the second peak in corrosion rate starts and reaches a maximum when the dilution test PA concentration is varied. All tests started with 4M HCl were diluted with 4M NaCl brine at a rate of 10ml/min.

8.2.5 Reverse Dilution Test

It was hoped that by performing a reverse dilution test a greater understanding of the relationship between the HCl and the PA could be gained. This involved performing a dilution test starting with 4M NaCl brine which was diluted with 4M HCl (containing 0.05wt.% PA). The 4M NaCl brine was diluted with 4M HCl at a rate of 10ml/min for 7 hours and the HCl concentration of the solution reached 3.92M. Figure 7.27 shows the solution corrosivity over the duration of the reverse dilution test. Figure 8.21 shows the comparison between the standard and the reverse dilution test and highlights how the reverse test fails to characterise the HCl concentrations at which the corrosion rate increases in the standard dilution test.

The results in Figure 8.21 show that the corrosion rate increases as the 4M HCl concentration of the solution increases. The main limitation of the reverse dilution test is that it fails to characterise the very low HCl concentrations at which the peaks in corrosion rate are observed in the standard dilution test. In the reverse dilution test the first corrosion rate measured is when the solution

contains entirely 4M NaCl, the second corrosion rate is measured when the solution contains ~0.2M HCl. This means that the reverse dilution test completely fails to characterise HCl concentrations less than ~0.2M.
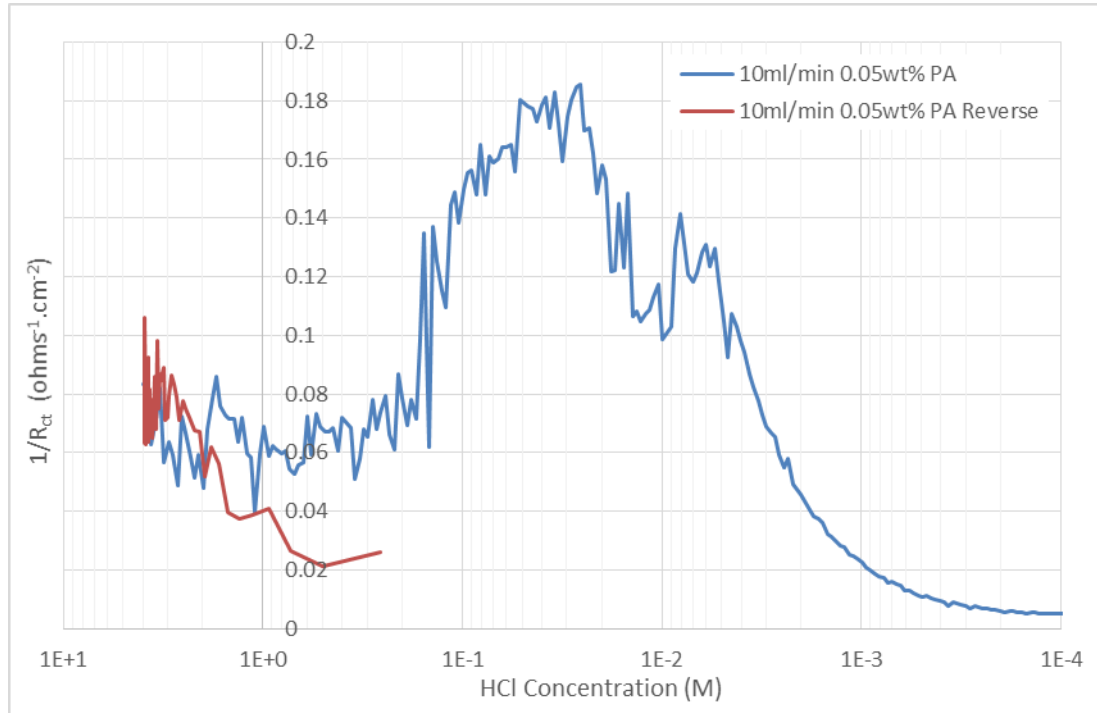
Figure 8.21 Comparison between the standard dilution test (4M HCl containing 0.05wt.% PA diluted with 4M NaCl brine) and the reverse dilution test (4M NaCl diluted with 4M HCl containing 0.05wt.% PA). Both tests were performed at 80°C. The time has been converted to the HCl concentration.

The reverse dilution test results are much easier to explain than those found from the standard dilution test. The corrosion rate increases as the HCl concentration of the solution increases. However the test is clearly not representative of what is seen in the field due to flowback following an acid job.

The intention of the test was instead to help understand the results observed in previous tests. Unfortunately the results provide very little additional information in terms of explaining the relationship observed previously. In order for the reverse dilution test to characterise the low HCl concentrations the dilution speed would have to be reduced to very low values. This is likely to cause problems with fluid stagnation in the flow cell.

8.2.6 Explaining the Critical PA Concentration

The results presented in Section 8.2.3 suggest that the first increase in corrosion rate occurs when the PA concentration of the solution reaches a critical value. Regardless of the starting PA or HCl concentration the corrosion rate of the steel sample starts to increase once this critical PA concentration is reached. Redosing the PA does not prevent the corrosion rate increasing, it merely delays the increase until the PA is diluted to this critical concentration.

The explanation for this increase in corrosion rate is likely due to how the PA protects the steel sample. The inhibitor forms a protective film on the surface of the sample [70, 75, 83, 117-119]. The results from the dilution tests suggest that the film protectiveness decreases as the HCl and PA concentration of the solution decreases. This indicates that a minimum volume of PA is required to maintain the protectiveness of the film and inhibit the corrosion rate of the sample.

The increase in corrosion rate being caused by the PA concentration falling below a critical concentration is supported by the observations of both Barmatov et al. [76] and Growcock and Frenier et al. [123]. If the bulk solution contains insufficient inhibitor it can lead to degradation of the polymerisable film [76] and the inhibitor should be kept above this critical concentration if a protective inhibitor film is to be maintained [123]. Therefore the polymeric inhibitor film on the steel surface is in equilibrium with the bulk solution concentration, with the film constantly degrading and being replenished by the PA in the solution. Once there is an insufficient quantity of polymerisable inhibitor to repair the polymer film, the critical inhibitor concentration has been reached. Therefore the polymer film will thin and degrade causing the corrosion rate to increase. This is supported by the work of Poling [132] who found that thinner PA films lead to a decrease in inhibitor protection.

The results of the flow cell tests suggest that a minimum PA concentration of between 3×10^{-3} and 5×10^{-3} wt.% is required to maintain the protective inhibitor film. The increase in corrosion rate at PA concentrations below this value suggests that this is the minimum amount of inhibitor required to maintain the film at these experimental conditions.

8.2.7 Explaining the Critical HCl Concentration

The results from the flow cell dilution tests suggest that the corrosion rate increases once the HCl concentration reaches a low enough value. Initially this seems illogical as a lower HCl concentration means less H^+ ions are present in the solution and as a result the corrosion rate should decrease.

In order to explain the increase in corrosion rate the inhibiting mechanism of the PA must be considered. As discussed previously the PA is catalysed by H^+, this suggests that the PA functions better in low pH solutions [122]. The second increase in corrosion rate could therefore be due to the H^+ concentration of the solution no longer being high enough to catalyse the intermediate reaction of the PA required in order for the polymer film to be able to form on the steel surface (as discussed in Section 3.2.3). This is further validated by the inhibitor mechanism proposed by Poling [132]; that the evolution of hydrogen (a result of the acid corrosion reaction) is necessary for the final polymerisation step.

8.2.7.1 Comparison with Blank Mass Loss Results

Prior to reaching this critical H^+ concentration the protective PA film has degraded significantly due to a lack of PA in the solution (required to maintain the protective film). However the flow cell test results suggest that the PA is still offering some protection to the steel, although the film has degraded significantly, until a critical H^+ concentration is reached. Once the approximate pH of the solution increases to a value of between ~1.7-2, the PA film no longer offers any protection to the steel from the HCl in the flowback fluid. This is highlighted by the corrosion rates shown in Figure 8.22; where the 3 hour mass loss tests (with and without PA) are compared to the dilution test results.

Figure 8.22 suggests that the PA is still offering some protection to the steel at an approximate pH of 1.4. This is shown by the lower corrosivity of the solution containing 0.05wt.% PA than to the blank mass loss test performed at this pH. Once the pH of the solution increases to approximately 2.4 the corrosivity of the solution is the same in the mass loss tests with and without PA present. Therefore at this pH the PA is no longer offering any protection to the steel from the HCl in the solution.
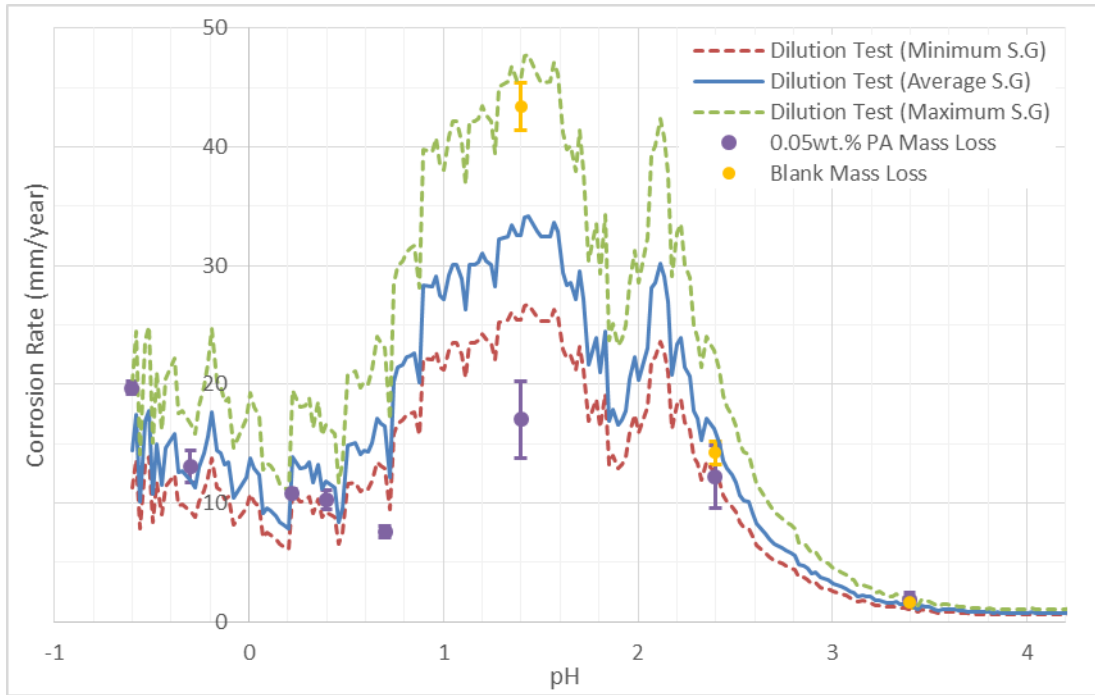
Figure 8.22 Comparison between the standard dilution test (4M HCl containing 0.05wt.% PA) and the 3 hour mass loss tests (both with and without 0.05wt.% PA). The calculated corrosion rates shown are for when the minimum (11.1), maximum (19.9) and average (14.4) Stern-Geary coefficients found from the fixed concentration tests were applied. All tests were performed at 80°C. The time has been converted to the approximate pH of the solution.

This is further highlighted by the inhibitor efficiencies shown in Figure 6.1. The PA has an efficiency of over 90% for all HCl concentrations above 0.2M (a pH<~0.7) tested in 3 hour mass loss experiments. The inhibitor efficiency then decreases to approximately 60% as the HCl concentration is further reduced to 0.04M (pH ~1.4). At HCl concentrations less than 4×10^{-3}M (pH>~2.4), the inhibitor efficiencies indicate that the PA is no longer offering any protection to the steel. This is further evidence that the ability of the PA to protect the steel decreases with increasing pH. It should again be emphasised that the pH provided are not the true values, they are merely an approximation based upon the HCl concentration of the solution and are intended to give an approximation as to how the pH affects the corrosion behaviour.

8.2.7.2 Comparison with the OCP

The outlined theory is further validated by the OCP measurements taken throughout the dilution test. In all dilution tests performed (at all starting PA concentrations and dilution rates) the second peak in solution corrosivity

coincides with a significant decrease in OCP. Figure 8.23 shows how the OCP and the solution corrosivity vary throughout the duration of the flow cell dilution test starting with 4M HCl (containing 0.05wt.% PA).
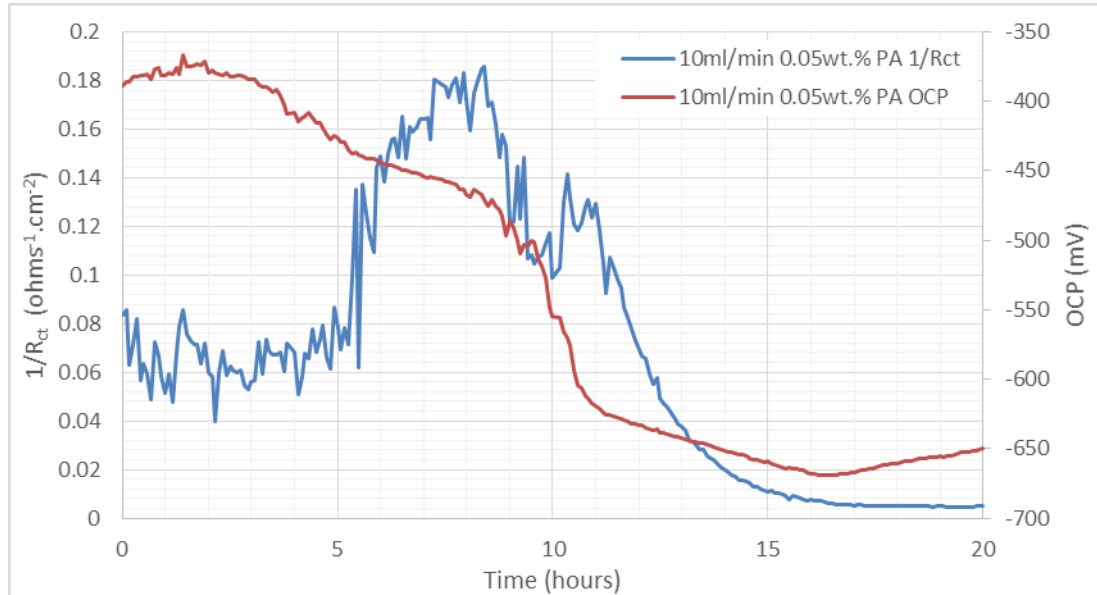
Figure 8.23 Comparison between the corrosion rate and OCP throughout a dilution test starting with 4M HCl and containing 0.05wt.% PA at 80°C. The HCl was diluted with 4M NaCl brine at a rate of 10ml/min.

The decrease in OCP suggests that prior to this point the PA is predominantly retarding the anodic corrosion reaction of the mild steel [181]. The decrease in OCP by over 100mV suggests a breakdown/thinning of the PA film which in turn results in an increase in the anodic corrosion reaction. The decrease in OCP at a time of 10 hours in Figure 8.23 coincides directly with an increase in the corrosion rate. At this point it is hypothesised that desorption of the PA has occurred (predominantly from the anodic sites on the steel surface). The result of this being that the corrosion rates observed at this point in the test (once the solution pH increases above a value of ~2) are similar values to those observed in tests containing no PA (this is highlighted in Figure 8.22).

Figure 8.24 further highlights the relationship between the HCl concentration and the drop in OCP observed in all of the dilution tests performed. In all of the different starting PA concentration tests (bar the redosing experiment) the OCP drops at the same HCl concentration (~0.01M). However, when the PA is redosed the drop in OCP is delayed slightly. The reason for this drop in OCP occurring at a lower HCl concentration is difficult to explain. However, it

should be noted that the difference in HCl concentrations is minimal, with the drop in OCP occurring at 3×10^{-3}M compared to a HCl concentration of 0.01M for all other tests. If the HCl concentration is used to calculate the approximate pH then the drop in OCP occurs in the pH range ~2-2.5 for all tests performed.
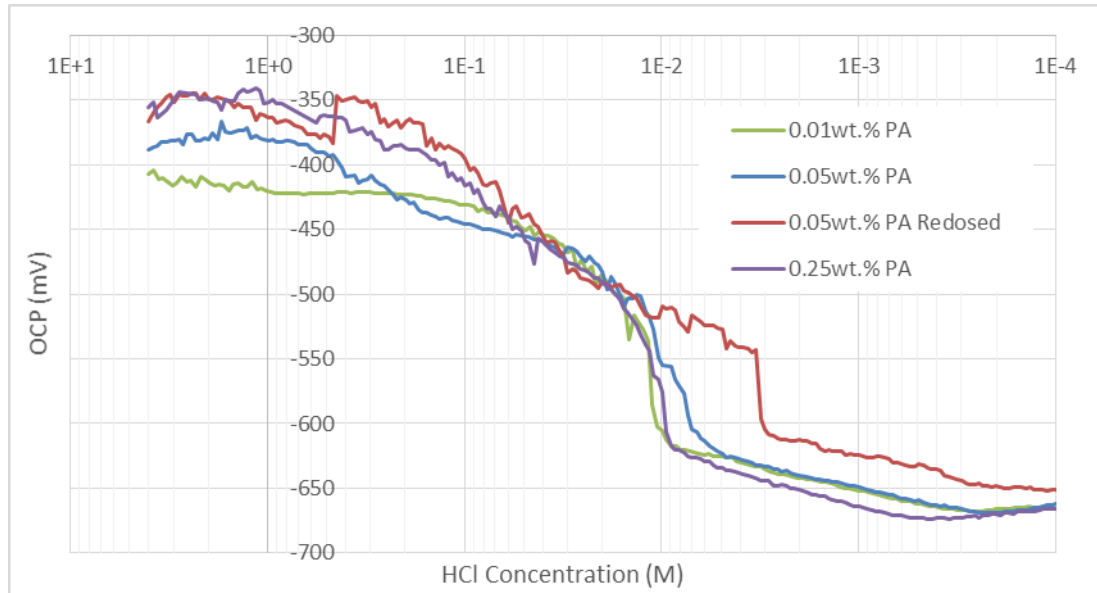
Figure 8.24 OCP measurements for a range of dilution tests plotted as a function of the HCl concentration of the solution in the flow cell. All tests started with a HCl concentration of 4M with a range of different PA concentrations. The HCl was diluted with 4M NaCl brine at a rate of 10ml/min in all tests.

8.2.7.3 The Inhibitor Film Behaviour throughout the Dilution Test

Figure 8.25 shows the hypothesised PA film on the steel surface throughout the duration of the dilution tests. The average corrosion rate is calculated from two tests starting with 4M HCl (containing 0.05wt.% PA) and diluted with 4M NaCl brine at a rate of 10ml/min. An average Stern-Geary value of 14.4 has been used to calculate the corrosion rate (the limitations of applying this average value have been discussed extensively throughout the thesis). Figure 8.25 is labelled with schematics intended to highlight the hypothesised PA film at different points in the test.

It has been proposed (in Section 8.2.6) that for the first 5 hours of the test the PA is able to establish a protective film and the PA concentration in the solution is sufficient to maintain this film. A schematic of this well-established PA film is shown in Figure 8.25 for the first 5 hours. The film then begins to

thin as the PA concentration in the solution is no longer sufficient to maintain the film. This is represented by the thinner film shown in Figure 8.25. The corrosion rate then begins to decrease as the HCl concentration of the solution decreases, at this point in the test (~9 hours) the damaged PA film is still offering some protection to the steel. The second peak (occurring approximately 10 hours into the test) indicates that the PA is no longer providing any protection to the steel and any residual film that may have been present has either desorbed or is no longer able to offer any protection to the steel. The corrosion rates beyond this second peak match the uninhibited corrosion rates from 3 hour tests (as shown in Figure 8.25).
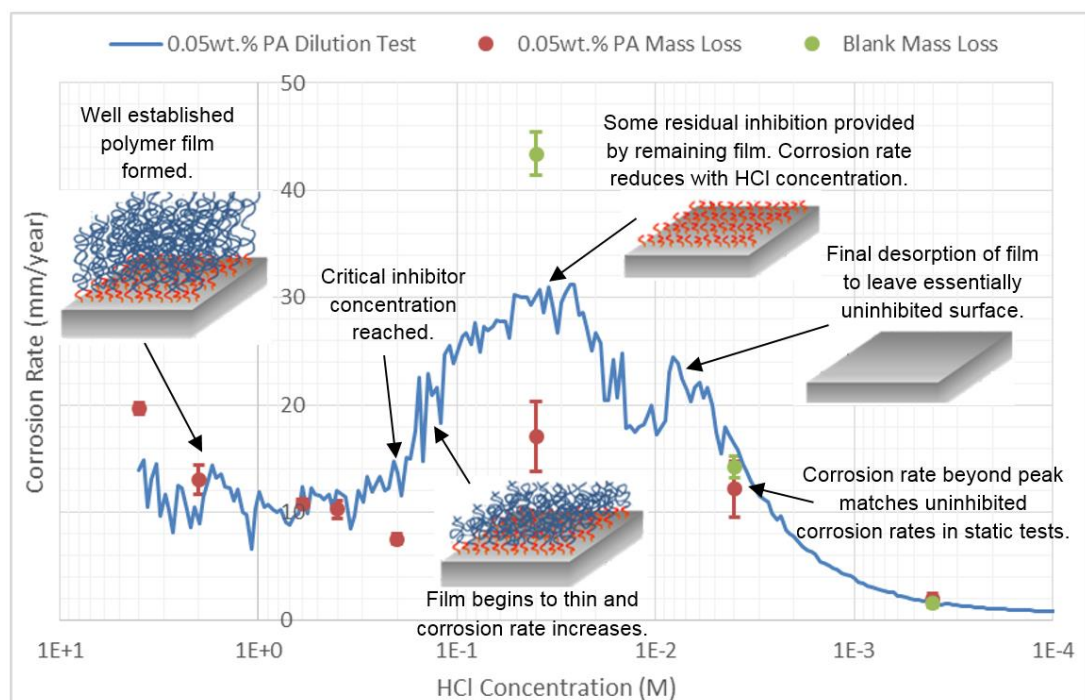
Figure 8.25 The proposed inhibitor film on the steel surface over the course of the dilution test. The graph shows the corrosion rate from a dilution test starting with 4M HCl and containing 0.05wt.% PA at 80°C. The HCl was diluted with 4M NaCl brine at a rate of 10ml/min. Corrosion rates from 3 hour mass loss experiments are also shown (blank tests and tests containing 0.05wt.% PA).

Chapter 9 Conclusions

The work presented is the first of its kind to attempt to replicate the entire flow back process following an acid job in the field. HCl containing PA inhibitor was diluted to values that are orders of magnitude lower than the injected HCl concentrations. It was found that if the PA was diluted at the same rate as the HCl then the flowback fluid can be more corrosive than the injected HCl. 3 hour mass loss tests (an established technique for measuring acidizing corrosion rates) showed the threat that the flowback fluid poses to well tubulars. The same trend was observed when a new test methodology was developed to model the entire acid dilution profile encountered during flowback in a single test. The conclusions have been divided into the development of the new flow cell test methodology and observations regarding the critical relationship between the HCl and the PA in the flowback fluid (found using the new methodology).

9.1 Flow Cell Test Methodology

A new test methodology was developed which allowed the threat posed to steel tubulars by the flowback from acid jobs to be quantified. This was achieved through the use of a continuous flow cell integrated with *in-situ* electrochemistry and capable of operating at temperatures of up to 80˚C. This allows a solution of changing chemistry to be pumped through the cell and the corrosion rate to be monitored throughout the entire flow-back process.

The results show that the methodology is able to help fully characterise the flow back process with the implementation of the correct Stern-Geary coefficient for the electrochemical data. Unlike previous methodologies, which would require a large number of tests, the new methodology is able to profile the full dilution process associated with acid flowback in a single test. This has significant cost and time saving implications.

Prior to developing the flow cell, dilution tests were performed in a 1L closed vessel containing 4M HCl (with PA) which was then diluted with 4M NaCl brine in order to model the acid dilution profile seen during flowback following an acid job. There were however several limitations to this test methodology, primarily due to the sample being in contact with the entire volume of PA and

HCl throughout the duration of the test. This led to issues with HCl and PA spending and meant that conclusions could not be drawn regarding the critical PA and HCl concentrations at which peaks in corrosion rate were observed. A flow cell was designed to eliminate these issues by ensuring that the sample is always in contact with fresh solution, with a known HCl and PA concentration.

The closed vessel dilution tests (Section 5.3.5) produced similar results to the flow cell dilution tests (Section 7.2.2) and allow both peaks in corrosion rate to be identified. However, without the flow cell validating these results it would be impossible to say that these peaks were actual phenomena related to the dilution tests or if the peaks were due to the test methodology used. It was only once the experiment had been repeated using the flow cell, and the same peaks observed, that the relationship between the solution corrosivity and the critical HCl and PA concentrations could be identified.

The flow cell corrosion rates highlighted that the low solution molarities encountered during flowback can be more corrosive than the injection strength HCl. The corrosion rates measured in the dilution tests were validated by the mass loss tests performed at a range of HCl concentrations (ranging from 4M to 4×10^{-4}M). The mass loss results showed excellent agreement with corrosion rates measured using the flow cell at all molarities except from at 0.04M HCl. The mass loss results provide further validation for the corrosion profile found using the flow cell.

9.2 The Relationship between HCl and PA

There are two main advantages of the flow cell test methodology that together allow the relationship between the HCl and PA to be understood. The first is that the full flowback process can be replicated in a single test. This allows the corrosion rate to be measured across the entire dilution profile. By performing traditional mass loss tests a large number of tests would be required in order to fully replicate the corrosion profile found from a single flow cell test. The second major benefit of the flow cell tests is that the sample is always in contact with fresh solution. As the acid and inhibitor have not reacted with the sample prior to being pumped through the cell, the exact concentration of the solution is known at all times. Therefore the dilution tests allow the exact acid

and inhibitor concentrations at which the corrosion rate peaks and returns to pre acid job rates to be found. This results in the flow cell providing information that is vital for understanding the corrosivity of the flowback fluid.

The dilution tests found that two clear peaks in corrosion rate exist as the HCl concentration of the solution is diluted. Tests were performed using the new flow cell at a range of starting HCl and PA concentrations in order to better quantify these peaks. It was found that the first peak in corrosion rate occurred once a critical PA concentration of 3×10^{-3} wt.% was reached. Increasing the starting PA concentration resulted in this peak occurring later in the dilution test once the PA had been diluted to this critical concentration. Redosing the PA also failed to eliminate the peak in corrosion rate. The peak was merely delayed until the PA concentration had been diluted to the critical value. The critical PA concentration is the point at which there is no longer enough PA in the solution to maintain the protective film which has previously established on the steel sample. This leads to the increase in corrosion rate observed in the dilution test.

A second peak was observed in the majority of the dilution tests performed. This peak was found to reach a maximum value once a critical pH of ~2 was reached. The peak occurred at this pH regardless of the starting PA concentration and it is thought to be the pH at which the PA is no longer able to form a protective film due to a lack of H^+ ions in the solution. When the solution pH is below this critical value the PA film is still offering some protection to the steel. It is only once the solution pH is above ~2 that the PA film no longer offers any corrosion protection to the sample.

The presence of this second peak is one of the most significant findings of the work. The relationship between propargyl alcohol and HCl is complicated and still not fully understood. As discussed in Section 3.2.3 it has been proposed that the low pH of the acid supports the surface catalysed polymerisation reaction of the propargyl alcohol [122]. However the exact nature of this relationship and how it effects the ability of the PA to polymerise and protect the steel surface is unknown. The results of this work have led to a much greater understanding as to how the H^+ concentration of the solution effects the PA. Using the new test methodology it is even possible to identify the

approximate pH at which the PA is no longer offering any protection to the steel surface.

Much of the previously published acidizing work has focused on the ability of inhibitors to protect steels from high strength acids that contain high inhibitor concentrations. This work is the first of its kind to study a range of different PA concentrations at a range of different HCl concentrations (ranging from injection strength acids to very dilute acid solutions encountered once production restarts). By studying the PA at these greatly reduced acid and inhibitor concentrations an understanding of the inhibitor can be gained that would not be possible by performing tests at conditions intended to replicate injection.

9.3 Relevance to Acid Jobs Performed in the Field

The flow cell can be used to more accurately replicate the fluid which flows back following an acid job. No two acid jobs are alike and a large number of different factors can alter the chemistry of the fluid which flows back following an acid job. The new test methodology can be used to model different flowback profiles from individual acid jobs (based on the formation geology, injected acid, injected inhibitor, etc.) in a single test. For example, the formation may be sandstone that contains very few carbonates; as a result the flowback fluid will initially contain a significant amount of unreacted acid which may then drastically decrease as normal production resumes. This would be difficult and time consuming to replicate using 3 hour mass loss tests at fixed acid concentrations. Using the flow cell however, a volume of high strength acid could be pumped through the cell before the HCl concentration of the solution is then drastically diluted to match the flowback profile observed in the field.

The work presented in this thesis has highlighted how corrosive the flowback fluid can potentially be, particularly at acid concentrations which in the field would not be considered a threat to the steel tubulars. Through the use of the new test methodology a full dilution profile can be tested in a single experiment. This allows individual acid jobs performed in the field to be simulated in a laboratory environment in a manner which is repeatable and

time and cost effective. Different grade steels, inhibitors and acids can all be varied in order to accurately replicate individual flowback profiles.

9.4 Additional Flow Cell Uses and Future Work

The ability to dilute the acid and inhibitor at a known rate is incredibly useful for understanding the critical inhibitor concentration required to maintain protective inhibitor films. It would be very time consuming to find this critical concentration using 3 hour mass loss tests but can be found relatively simply using the dilution test methodology. If the critical concentration was found using 3 hour mass loss tests a large number of tests at a range of concentrations would be required; representing significant time and cost implications. In contrast, several dilution tests, performed at a range of different starting inhibitor concentrations, will help to identify if there is a critical PA concentration at which the corrosion rate starts to increase. The flow cell can therefore be used to identify the minimum amount of inhibitor required to maintain a protective inhibitor film (during injection or flowback). This is particularly useful for testing newly developed inhibitors.

The dilution tests identified two clear peaks in the corrosivity of the flowback fluid. In order to better understand the second peak further experiments are required. The most vital of which is a redosing experiment performed just before the second peak occurs. If the corrosion rate still increases this would validate that the PA no longer inhibits the corrosion rate at very low HCl concentrations. The cell can also be used to study the film formation over the flowback profile. By systematically removing steel samples at points in the dilution test an evaluation of the inhibitor film and its ability to protect the steel tubulars can be obtained. This will allow an understanding of how the inhibitor film varies over the entire flowback process to be obtained.

The flow cell can also be used to more accurately replicate the flowback process by varying the solution chemistry to more accurately replicate flowback. One of the key benefits of the dilution test methodology is that it allows the solution chemistry to be progressively varied throughout the duration of the test. The work presented in this thesis has focused on the relationship between the acid and inhibitor. However there are several other important components of the produced fluid which change over the duration

of the flowback. The concentration of iron, calcium and carbon dioxide in the flowback fluid is a direct result of the acid reacting with the downhole scales and/or formation. The concentration of each is therefore going to change over the duration of the flowback process. This can be replicated using the dilution test methodology as the quantity of Ca and CO_2 of the solution can be controlled prior to it being pumped through the flow cell. The eventual end point of the work would be to perform a dilution test which accurately models the concentrations of iron, calcium and carbon dioxide in addition to the acid and inhibitor concentrations over the duration of an entire flowback profile.

Another advantage of the test methodology is that the solution can be sampled over the duration of the flowback profile. This would allow the solution to be analysed at various points over the test to analyse the inhibitor and any products that may have formed in different strength acid solutions.

9.4.1 In-situ Measurements of the Inhibitor Film

A future use of the flow cell could be to implement in-situ measurements of the inhibitor film over the duration of the dilution tests. Infared reflection spectroscopy (IRS) has been used extensively in previous studies to investigate the PA and its inhibition mechanism [87, 123, 124, 132, 182]. Unfortunately infared measurements are limited in their ability to characterise both the adsorption behaviour of PA and its reaction products on the surface of the steel. This limitation is due to the infrared measurements being ex-situ which means that the sample has to be removed from the solution (in the case of these experiments, the flowback fluid) and exposed to the air. An in-situ measurement, such as the one described by Aramaki and Fujioka [183], is required if the inhibitor reactions and products are to be fully understood. In the work surface-enhanced Rama scattering (SERS) spectroscopy was used to study the reaction product of PA on an iron covered silver electrode. In the work it was possible to study the iron surface using X-ray photoelectron spectroscopy (XPS) without exposing the sample to the air [183].

Through integrating this technique with the flow cell a much greater understanding of the mechanisms of PA can be gained. In-situ analysis of the inhibitor film over the course of a dilution test will provide information regarding the nature of the peaks observed in previous tests. It has been hypothesised that the initial peak occurs once the PA concentration in the solution is no

longer sufficient to repair the protective inhibitor film and that the second peak occurs when the film is no longer offering any protection to the steel. These hypotheses could potentially be validated by the results of the in-situ measurements.

9.4.2 Understanding the Corrosivity of the Injected Acid

Although the flow cell was initially designed to replicate the flowback from an acid job it can also be used to more accurately replicate the injection process. 3 hour mass loss tests are used to test the ability of inhibitors to protect steel tubulars from high strength injected acids. The steel sample is exposed to the entire volume of inhibitor and HCl from the start of the test. However in the field the tubing will be in contact with freshly pumped acid and inhibitor. This is important as most acidizing inhibitors are film forming acetylinic alcohols or derivatives of these. These inhibitors protect the steel by forming a protective film which then degrades and requires more inhibitor to maintain it. By performing mass loss tests the sample is exposed to the entire inhibitor volume from the start of the test. In the field, the tubing is only exposed to the inhibitor contained in the acid which is in contact with the tubing at that point. By exposing the sample to the entire volume of inhibitor this may be enough to form the protective inhibitor film in the laboratory tests but the same may not be observed in the field where the tubing is not exposed to such a high initial inhibitor concentration.

By using the flow cell to replicate the injection process the steel is always in contact with solution of known acid and inhibitor concentrations. The corrosion rate over the entire test can also be monitored unlike the 3 hour mass loss tests with just provide the average corrosion rate. This will give an understanding as to how long the inhibitor takes to form the protective film on the steel. An issue with the mass loss tests is the volume to surface area ratio between the acid and the steel. It is too costly and impractical to meet the ratio recommended by ASTM G31 [147]. By using the flow cell the sample is constantly in contact with fresh acid and inhibitor, eliminating the issues associated with meeting the minimum acid volume to sample surface area ratio.

List of References

1. Williams, B.B., J.L. Gidley, and R.S. Schechter, *Acidizing Fundamentals.* 1979: Henry L. Doherty Memorial Fund of AIME, Society of Petroleum Engineers of AIME.

2. Economides, M.J. and K.G. Nolte, *Reservoir stimulation.* 2000, Chichester, England; New York: Wiley.

3. Ali, S.A., L. Kalfayan, and C.T. Montgomery, *Acidizing.* SPE Monograph. Vol. 26. 2016: SPE.

4. Schechter, R.S., *Oil well stimulation.* 1992: Prentice Hall.

5. Barmatov, E., T. Hughes, and M. Nagl, *Performance of Organic Corrosion Inhibitors on Carbon Steels and High Alloys in 4M Hydrochloric Acid*, in *CORROSION*2015, NACE International: Dallas, Texas.

6. Valdes, A.V., A. ; Marcano, S. ; Boggio, C., *A Field Experience of Corrosion Inhibition During the Acid Fracturing of a Deep Oil Well Completed with 22 % Cr Duplex Steel* in *Corrosion -National Associaton of Corrosion Engineers Anual Conference*1993. p. 1096-1103.

7. Morgenthaler, L.N., P.R. Rhodes, and L.L. Wheaton, *Testing the Corrosivity of Spent HCl/HF Acid to 22 Cr and 13 Cr Stainless Steels*, in *International Symposium on Oilfield Chemistry*1997, Society of Petroleum Engineers: Houston, Texas.

8. Gdanski, R.D. and C.E. Shuchart, *Advanced Sandstone-Acidizing Designs With Improved Radial Models.* SPE Production & Facilities, 1998. **13**(4).

9. Hartman, R.L., et al., *Acid-Sensitive Aluminosilicates: Dissolution Kinetics and Fluid Selection for Matrix-Stimulation Treatments.* SPE Production & Operations, 2006. **21**(02).

10. Hayatdavoudi, A., A. Ghalambor, and V. Veludandi, *Application of a New Technique in Acid Flowback Analysis*, in *SPE Formation Damage Control Symposium*1996, Society of Petroleum Engineers: Lafayette, Louisiana.

11. Taylor, K.C. and H.A. Nasr-El-Din, *Flowback Analysis of Acid Stimulation of Seawater Injection Wells: Case Histories*, in *SPE International Symposium on Formation Damage Control*2000, Society of Petroleum Engineers: Lafayette, Louisiana.

12. Hashem, M.K., H.A. Nasr-El-Din, and J.A. Hopkins, *An Experience in Acidizing Sandstone Reservoirs: A Scientific Approach*, in *SPE Annual Technical Conference and Exhibition*1999, Society of Petroleum Engineers: Houston, Texas.

13. Hernandez, S., et al., *Materials and Corrosion Risk Mitigation Associated with Flowback of Acid Stimulation Fluids*, in *CORROSION 2017*2017, NACE International: New Orleans, Louisiana.

14. Huizinga, S. and W.E. Liek, *Corrosion Behavior of 13% Chromium Steel in Acid Stimulations.* CORROSION, 1994. **50**(7): p. 555-566.

15. Al-Mutairi, S.H., et al., *Corrosion Control during Acid Fracturing of Deep Gas Wells: Lab Studies and Field Cases*, in *SPE International Symposium on Oilfield Corrosion*2005, Society of Petroleum Engineers: Aberdeen, United Kingdom.

16. Moritis, G., *Coiled tubing use expands.* Oil & Gas Journal, 2011. **109**(26).

17. International, N., *International Measures of Prevention, Apllication, and Economics of Corrosion Technologies Study*, 2016, NACE International: Houston, Texas.

18. Davis, J.R., *Corrosion: Understanding the Basics.* 2000: ASM International.

19. Stansbury, E.E. and R.A. Buchanan, *Fundamentals of Electrochemical Corrosion.* 2000: ASM International.

20. Newman, J. and K.E. Thomas-Alyea, *Electrochemical systems.* 2012: John Wiley & Sons.

21. Noren, D.A. and M.A. Hoffman, *Clarifying the Butler–Volmer equation and related approximations for calculating activation losses in solid oxide fuel cell models.* Journal of Power Sources, 2005. **152**: p. 175-181.

22. Scully, J.R., *The Polarization Resistance Method for Determination of Instantaneous Corrosion Rates: A Review*, in *CORROSION 98*1998, NACE International: San Diego, California.

23. Tait, W.S., *An Introduction to Electrochemical Corrosion Testing for Practicing Engineers and Scientists.* 1994: PairODocs Publications.

24. Frankel, G.S., *Fundamentals of Corrosion Kinetics*, in *Active Protective Coatings: New-Generation Coatings for Metals*, A.E. Hughes, et al., Editors. 2016, Springer Netherlands: Dordrecht. p. 17-32.

25. Stern, M. and A.L. Geary, *Electrochemical Polarization: I . A Theoretical Analysis of the Shape of Polarization Curves.* Journal of The Electrochemical Society, 1957. **104**(1): p. 56-63.

26. Zwillinger, D., *CRC Standard Mathematical Tables and Formulae, 32nd Edition.* 2011: CRC Press.

27. Anaee, R.A.M. and M.H. Abdulmajeed, *Tribocorrosion*, in *Advances in Tribology*, P.H. Darji, Editor. 2016, InTech: Rijeka. p. Ch. 05.

28. ASTM, *Standard Reference Test Method for Making Potentiodynamic Anodic Polarization Measurements*, in *ASTM G5-14*2014, ASTM International: West Conshohocken, Pennsylvania.

29. Kelly, R.G., et al., *Electrochemical techniques in corrosion science and engineering.* 2002: CRC Press.

30. Kear, G. and F.C. Walsh, *The characteristics of a true Tafel slope.* Corrosion and materials, 2005. **30**(6): p. 51-55.

31. McCafferty, E., *Validation of corrosion rates measured by the Tafel extrapolation method.* Corrosion Science, 2005. **47**(12): p. 3202-3215.

32. McCafferty, E. and N. Hackerman, *Double layer capacitance of iron and corrosion inhibition with polymethylene diamines.* Journal of the Electrochemical Society, 1972. **119**(2): p. 146-154.

33. Marsh, G. and E. Schaschl, *The difference effect and the chunk effect.* Journal of the Electrochemical Society, 1960. **107**(12): p. 960-965.

34. Baboian, R., *Corrosion Tests and Standards: Application and Interpretation.* 2005: ASTM International.

35. Bosch, R.W., et al., *Electrochemical Frequency Modulation: A New Electrochemical Technique for Online Corrosion Monitoring.* CORROSION, 2001. **57**(1): p. 60-70.

36. Instruments, B.S. *Application Note 47 Corrosion current determination with mass transfer limitation.* 2013 [cited 2018 05/04/18]; Available from: http://www.bio-logic.net/wp-content/uploads/AN47-corrosion-current-with-mass-transfer-limitation.pdf.

37. Mackay, E.J., M.M. Jordan, and F. Torabi, *Predicting Brine Mixing Deep Within the Reservoir, and the Impact on Scale Control in Marginal and Deepwater Developments*, in *International Symposium and Exhibition on Formation Damage Control* 2002, Society of Petroleum Engineers: Lafayette, Louisiana.

38. Fontana, M.G., *Corrosion Engineering.* 3 ed. 1986, New York: McGraw-Hill.

39. Whitman, W.G. and R.P. Russell, *The Acid Corrosion of Metals. Effect of Oxygen and Velocity.* Industrial & Engineering Chemistry, 1925. **17**(4): p. 348-354.

40. Sastri, V.S., *Corrosion inhibitors: principles and applications.* 1998, Chichester: Wiley.

41. Jones, D.A., *Principles and Prevention of Corrosion.* 1996: Prentice Hall.

42. Garverick, L., *Corrosion in the Petrochemical Industry.* 1994: ASM International.

43. Hampel, C.A., *The encyclopedia of electrochemistry.* 1964, New York: Reinhold Pub. Corp.

44. Deshpande, P.P. and D. Sazou, *Corrosion protection of metals by intrinsically conducting polymers.* 2016: CRC Press.

45. Kelland, M.A., *Acid Stimulation*, in *Production Chemicals for the Oil and Gas Industry.* 2009, CRC Press.

46. Rostami, A., *Review and Evaluation of Corrosion Inhibitors Used in Well Stimulation*, in *SPE International Symposium on Oilfield Chemistry* 2009, Society of Petroleum Engineers: The Woodlands. Texas.

47. Knox, J.A., *Acidizing -- Past, Present, And Future*, in *Annual Technical Meeting* 1973, Petroleum Society of Canada: Edmonton, Canada.

48. King, G.E., *Acidizing Concepts - Matrix vs. Fracture Acidizing.* Journal of Petroleum Technology, 1986. **38**(5).

49. Yeager, V.J. and C.E. Shuchart, *Acidizing Gas Storage Wells*, in *SPE Eastern Regional Meeting* 1997, Society of Petroleum Engineers: Lexington, Kentucky.

50. Hendrickson, A.R., R.B. Rosene, and E.N. Alderman, *Acidizing: Fact And Fiction*, in *Annual Technical Meeting* 1971, Petroleum Society of Canada: Banff.

51. Tambini, M., *Beyond Acidizing and Fracturing*, in *SPE European Formation Damage Conference* 2003, Society of Petroleum Engineers: The Hague, Netherlands.

52. Bailey, D.E. and J.F. Wickham, *Sand Fracturing vs. Fracture Acidizing*, in *SPE Rocky Mountain Regional Meeting* 1984, Society of Petroleum Engineers: Casper, Wyoming.

53. Knox, J.A. and H.E. Ripley, *Fracture Acidizing In Carbonate Rock.* Journal of Canadian Petroleum Technology, 1979. **18**(4).

54. Gatewood, J.R., et al., *Predicting Results of Sandstone Acidizing.* Journal of Petroleum Technology, 1970. **22**(06).

55. Wang, Y., A.D. Hill, and R.S. Schechter, *The Optimum Injection Rate for Matrix Acidizing of Carbonate Formations*, in *SPE Annual Technical Conference and Exhibition*1993, Society of Petroleum Engineers: Houston, Texas.

56. Trehan, R., N.D. Jones, and J.A. Haney, *Acidizing Optimization: Monterey Shale, California*, in *SPE Western Regional Meeting*2012, Society of Petroleum Engineers: Bakersfield, California.

57. Smith, C.F., C.W. Crowe, and D.R. Wieland, *Fracture Acidizing In High Temperature Limestone*, in *SPE Deep Drilling and Production Symposium*1970, Society of Petroleum Engineers: Monahans, Texas.

58. Al-Harthy, S., et al., *Options for high temperature well stimulation.* Oilfield Review, 2008. **20**(4).

59. da Motta, E.P., et al., *Field Evaluation and Optimization of Matrix Acidizing Treatments*, in *SPE Production Operations Symposium*1997, Society of Petroleum Engineers: Oklahoma City, Oklahoma.

60. Aboud, R.S., et al., *Effective Matrix Acidizing in High-Temperature Environments*, in *SPE Annual Technical Conference and Exhibition*2007, Society of Petroleum Engineers: Anaheim, California.

61. McLeod, H.O., *Matrix Acidizing.* Journal of Petroleum Technology, 1984. **36**(12).

62. McLeod, H.O., Jr., L.B. Ledlow, and M.V. Till, *The Planning, Execution, and Evaluation of Acid Treatments in Sandstone Formations*, in *SPE Annual Technical Conference and Exhibition*1983, Society of Petroleum Engineers: San Francisco, California.

63. McLeod, H.O., *Significant Factors for Successful Matrix Acidizing*, in *SPE Centennial Symposium at New Mexico Tech*1989, Society of Petroleum Engineers: Socorro, New Mexico.

64. Popova, A., et al., *AC and DC study of the temperature effect on mild steel corrosion in acid media in the presence of benzimidazole derivatives.* Corrosion Science, 2003. **45**(1): p. 33-58.

65. Sitz, C., W.W. Frenier, and C.M. Vallejo, *Acid Corrosion Inhibitors with Improved Environmental Profiles*, in *SPE International Conference and Exhibition on Oilfield Corrosion*2012, Society of Petroleum Engineers: Aberdeen, UK.

66. Singh, A.K. and M.A. Quraishi, *Adsorption properties and inhibition of mild steel corrosion in hydrochloric acid solution by ceftobiprole.* Journal of Applied Electrochemistry, 2011. **41**(1): p. 7-18.

67. Finšgar, M. and J. Jackson, *Application of corrosion inhibitors for steels in acidic media for the oil and gas industry: A review.* Corrosion Science, 2014. **86**(0): p. 17-41.

68. Shank, R.A. and T.R. McCartney, *Comparative Study of Commercially Available Propargyl Alcohol-Free Corrosion Inhibitors for Hydrochloric Acid Systems*, 2013, NACE International.

69. Wang, H.L., H.B. Fan, and J.S. Zheng, *Corrosion inhibition of mild steel in hydrochloric acid solution by a mercapto-triazole compound.* Materials Chemistry and Physics, 2003. **77**(3): p. 655-661.

70. Frenier, W.W., Hill, D.G. and Jasinski, R, *Corrosion inhibitors for acid jobs.* Oilfield Review, 1989. **1**(2).

71. Seth, K., B.A. Evans, and A.D. Gabrysch, *Development and Testing of a Novel Corrosion Inhibitor Technology for Acid Corrosion*, in *SPE Middle East Oil and Gas Show and Conference*2011, Society of Petroleum Engineers: Manama, Bahrain.

72. Priya, A.R.S., V.S. Muralidharan, and A. Subramania, *Development of novel acidizing inhibitors for carbon steel corrosion in 15% boiling hydrochloric acid.* Corrosion, 2008. **64**(6): p. 541-552.

73. Crowe, C.W. and S.S. Minor, *Effect of Acid Corrosion Inhibitors On Matrix Stimulation Results.* Journal of Petroleum Technology, 1985. **37**(10): p. 1853-1860.

74. Okamoto, G., et al., *Effect of organic inhibitors on the polarization characteristics of mild steel in acid solution.* Corrosion Science, 1962. **2**(1): p. 21-27.

75. Jayaperumal, D., *Effects of alcohol-based inhibitors on corrosion of mild steel in hydrochloric acid.* Materials Chemistry and Physics, 2010. **119**(3): p. 478-484.

76. Barmatov, E., T. Hughes, and M. Nagl, *Efficiency of film-forming corrosion inhibitors in strong hydrochloric acid under laminar and turbulent flow conditions.* Corrosion Science, 2015. **92**: p. 85-94.

77. Cizek, A., *A History - Corrosion-Inhibitors used in Acidizing.* Materials Performance, 1994. **33**(1): p. 56-61.

78. Ali, S.A., et al., *Hydrophobic-tailed bicycloisoxazolidines: A comparative study of the newly synthesized compounds on the inhibition of mild steel corrosion in hydrochloric and sulfuric acid media.* Corrosion Science, 2008. **50**(3): p. 664-675.

79. Quaraishi, M.A., et al., *Inhibition of mild steel corrosion in presence of fatty acid imidazolines in hydrochloric acid.* Protection of Metals, 2008. **44**(1): p. 91-98.

80. Quraishi, M.A., S. Ahmad, and M.Q. Ansari, *Inhibition of steel corrosion by some new triazole derivatives in boiling hydrochloric acid.* British Corrosion Journal, 1997. **32**(4): p. 297-300.

81. Al-Taq, A.A., S.A. Ali, and H.A. Nasr-El-Din, *Inhibition Performance of a New Series of Mono-/Diamine-Based Corrosion Inhibitors for HCl Solutions.* SPE Journal, 2009. **14**(4): p. pp. 627-633.

82. Ali, S.A., M.T. Saeed, and S.U. Rahman, *The isoxazolidines: a new class of corrosion inhibitors of mild steel in acidic medium.* Corrosion Science, 2003. **45**(2): p. 253-266.

83. Frenier, W.W., F.B. Growcock, and V.R. Lopp, *Mechanisms of Corrosion Inhibitors Used in Acidizing Wells.* SPE Production Engineering, 1988. **3**(4): p. 584-590.

84. Pandya, N., S. Wadekar, and J. Cassidy, *An Optimized Emulsified Acid System for High-Temperature Applications*, 2013, Offshore Mediterranean Conference.

85. Barmatov, E., et al., *Research On Corrosion Inhibitors For Acid Stimulation*, in *Corrosion*2012, NACE International: Salt Lake City, UT.

86. Podobaev, N.I. and Y.G. Avdeev, *A Review of Acetylene Compounds as Inhibitors of Acid Corrosion of Iron.* Protection of Metals, 2004. **40**(1): p. 7-13.

87. Bartos, M., S.D. Kapusta, and N. Hackerman, *A Study of Polymerization of Propargyl Alcohol on Steel.* Journal of The Electrochemical Society, 1993. **140**(9): p. 2604-2605.

88. Yadav, M., S. Kumar, and P.N. Yadav, *Corrosion Inhibition of Tubing Steel during Acidization of Oil and Gas Wells.* Journal of Petroleum Engineering, 2013. **2013**: p. 9.

89. Lagrenée, M., et al., *Study of the mechanism and inhibiting efficiency of 3,5-bis(4-methylthiophenyl)-4H-1,2,4-triazole on mild steel corrosion in acidic media.* Corrosion Science, 2002. **44**(3): p. 573-588.

90. Zaafarany, I.A., *Corrosion Inhibition of Mild Steel in Hydrochloric Acid Solution using Cationic Surfactant Olyel-amido Derivatives.* International Journal of Electrochemical Science, 2013. **8**(7).

91. Ehteram A. Noor, A.H.A.-M., *Corrosion Behavior of Mild Steel in Hydrochloric Acid Solutions* Int. J. Electrochem. Sci., 2008. **3**: p. 806-818.

92. Quraishi, M.A., et al., *N-(Piperidinomethyl)-3- (pyridylidene)amino isatin: A new and effective acid corrosion inhibitor for mild steel.* Materials Chemistry and Physics, 2008. **112**(3): p. 1035-1039.

93. Quraishi, M.A. and D. Jamal, *Corrosion inhibition of N-80 steel and mild steel in 15% boiling hydrochloric acid by a triazole compound - SAHMT.* Materials Chemistry and Physics, 2001. **68**(1-3): p. 283-287.

94. Metcalf, S., J. Delorey, and S. Allen, *Coiled Tubing Acid Corrosion Protection: Laboratory vs. Field Performance*, in *SPE Asia Pacific Oil and Gas Conference and Exhibition*2003, Society of Petroleum Engineers: Jakarta, Indonesia.

95. Quraishi, M.A. and D. Jamal, *Dianils: New and Effective Corrosion Inhibitors for Oil-Well Steel (N-80) and Mild Steel in Boiling Hydrochloric Acid.* Corrosion, 2000. **56**(2): p. 156-160.

96. FUNKHOUSER, J.G., *Acid Corrosion Inhibition With Secondary Acetylenic Alcohols.* CORROSION, 1961. **17**(6): p. 283t-287t.

97. Sparr, M., *Influence of Test Conditions And Test Methods In the Evaluation of Corrosion Inhibitors Used In Pipelines-A Review*, 2011, NACE International.

98. Khadom, A.A., et al., *The effect of temperature and acid concentration on corrosion of low carbon steel in hydrochloric acid media.* American Journal of Applied Sciences, 2009. **6**(7): p. 1403-1409.

99. Singh, A.K. and M.A. Quraishi, *Effect of Cefazolin on the corrosion of mild steel in HCl solution.* Corrosion Science, 2010. **52**(1): p. 152-160.

100. Garber, J.D. and M. Kantour, *How high-alloy tubulars react in acidizing environments.* Petroleum Engineering International, 1984. **56**(8): p. 60-68.

101. Ali, S.A., et al., *The isoxazolidines: the effects of steric factor and hydrophobic chain length on the corrosion inhibition of mild steel in acidic medium.* Corrosion Science, 2005. **47**(11): p. 2659-2678.

102. Huizinga, S., *Passivation of Superduplex Stainless Steel after an Acidizing Treatment*, in *CORROSION 2001*2001, NACE International: Houston, Texas.

103. Tourabi, M., et al., *Electrochemical and XPS studies of the corrosion inhibition of carbon steel in hydrochloric acid pickling solutions by 3,5-bis(2-thienylmethyl)-4-amino-1,2,4-triazole.* Corrosion Science, 2013. **75**(0): p. 123-133.

104. Houston, S.J., *Formation waters in petroleum reservoirs : their controls and applications*, 2007, University of Leeds.

105. Collins, A.G., *Geochemistry of Oilfield Waters.* Developments in Petroleum Science, ed. A.G. Collins. Vol. Volume 1. 1975, Amsterdam, The Netherlands: Elsevier.

106. Harned, H.S. and N.J. Brumbaugh, *The activity coefficient of hydrochloric acid in aqueous salt solutions.* Journal of the American Chemical Society, 1922. **44**(12): p. 2729-2748.

107. Land, L., G. Macpherson, and L. Mack, *The geochemistry of saline formation waters, Miocene, offshore Louisiana.* Gulf Coast Association of Geological Societies, 1988. **38**: p. 503-511.

108. Warren, E.A. and P.C. Smalley, *North Sea Formation Waters Atlas.* 1994: Geological Society.

109. Carpenter, A.B., *Origin And Chemical Evolution Of Brines In Sedimentary Basins*, in *SPE Annual Fall Technical Conference and Exhibition*1978, Society of Petroleum Engineers: Houston, Texas.

110. Max, J.-J. and C. Chapados, *Infrared titration of aqueous NaOH by aqueous HCl.* Canadian Journal of Chemistry, 2000. **78**(1): p. 64-72.

111. McCarty, C.G. and E. Vitz, *pH Paradoxes: Demonstrating That It Is Not True That pH ≡ -log[H+].* Journal of Chemical Education, 2006. **83**(5): p. 752.

112. Lewis, G.N. and M. Randall, *Thermodynamics; Revised by Pitzer, KS; Brewer, L.* 2 ed. 1961, New York McGraw-Hill.

113. Mathur, P.B. and T. Vasudevan, *Reaction Rate Studies for the Corrosion of Metals in Acids—I, Iron in Mineral Acids.* CORROSION, 1982. **38**(3): p. 171-178.

114. Barmatov, E. and T.L. Hughes, *Effect of corrosion products and turbulent flow on inhibition efficiency of propargyl alcohol on AISI 1018 mild carbon steel in 4M hydrochloric acid.* Corrosion Science, 2017. **123**: p. 170-181.

115. Mazanek, A. and H. Bala, *The corrosion of iron in 0.5–8 M hydrochloric acid solutions.* Corrosion Science, 1988. **28**(5): p. 513-522.

116. Fink, J., *Oil Field Chemicals.* 2003: Elsevier Science.

117. Tedeschi, R.J., *Acetylenic Corrosion Inhibitors.* Corrosion, 1975. **31**(4): p. 130-134.

118. Trabanelli, G., et al., *Corrosion inhibition of carbon and low alloy steels in hot hydrochloric acid solutions.* British Corrosion Journal, 1992. **27**(3): p. 213-217.

119. Pati, B.B., et al., *Effect of Propargyl Alcohol on Corrosion and Hydrogenation of Steel in Hydrochloric Acid Solution.* Corrosion, 1990. **46**(5): p. 354-359.

120. Frenier, W.W., *Analytical Techniques Used for Identification and Quantification of Acid Corrosion Inhibitors*, in *Corrosion*1988, NACE: St-Louis, Missouri.

121. Foster, G.L., B.D. Oakes, and C.H. Kucera, *Acetylenic Corrosion Inhibitors.* Industrial & Engineering Chemistry, 1959. **51**(7): p. 825-828.

122. Aramaki, K. and E. Fujioka, *Spectroscopic Investigations on the Inhibition Mechanism of Propargyl Alcohol for Iron Corrosion in Hydrochloric Acid at Elevated Temperatures.* CORROSION, 1997. **53**(4): p. 319-326.

123. Growcock, F.B. and V.R. Lopp, *The inhibition of steel corrosion in hydrochloric acid with 3-phenyl-2-propyn-1-ol.* Corrosion Science, 1988. **28**(4): p. 397-410.

124. Growcock, F.B., V.R. Lopp, and R.J. Jasinski, *Corrosion Protection of Oilfield Steel with 1-Phenyl-2-Propyn-1-Ol.* Journal of The Electrochemical Society, 1988. **135**(4): p. 823-827.

125. Farafonov, V., M. Grovu, and C. Simionescu, *Electrochemical polymerization of acetylenic derivatives. I. Anionic polymerization of phenylacetylene and diphenyldiacetylene.* Journal of Polymer Science: Polymer Chemistry Edition, 1977. **15**(8): p. 2041-2042.

126. Avdeev, Y.G. and N.I. Podobaev, *The Role of Acrolein in the Inhibition of the Acid Corrosion of Iron with Propargyl Alcohol.* Protection of Metals, 2005. **41**(6): p. 592-596.

127. Heydari, M.R., Fatemeh Baghaei; Dadgarinezhad, Athareh, *Corrosion Inhibition Propargyl Alcohol on Low Alloy Cr Steel in 0.5 M H2SO4 in the Absence and Presence of Potassium Iodide.* Gazi University Journal of Science, 2011. **24**(3): p. 507.

128. Singh, D.D.N. and A.K. Dey, *Synergistic Effects of Inorganic and Organic Cations on Inhibitive Performance of Propargyl Alcohol on Steel Dissolution in Boiling Hydrochloric Acid Solution.* Corrosion, 1993. **49**(7): p. 594-600.

129. Funkhouser, G.P., et al., *Metal corrosion inhibitors, inhibited acid compositions and methods*, 2001, US 6192987 B1.

130. Cizek, A. and J.A. Hackerott, *Corrosion inhibitor*, 2003, WO2001079590 A3.

131. C.M.Menendez, J. M.Bojes, and J. Lerbscher, *Obtaining Batch Corrosion Inhibitor Film Thickness Measurements Using an Optical Profiler*, in *CORROSION*2010, NACE International: San Antonio, Texas.

132. Poling, G., *Infrared studies of protective films formed by acetylenic corrosion inhibitors.* Journal of The Electrochemical Society, 1967. **114**(12): p. 1209-1214.

133. Paty, B.B. and D.D.N. Singh, *Solvents Role on HCl-Induced Corrosion of Mild Steel: Its Control by Propargyl Alcohol and Metal Cations.* Corrosion, 1992. **48**(6).

134. Treseder, R.S. and R.N. Tuttle, *Corrosion control in oil and gas production.* 1998, Houston, Texas: NACE International.

135. Chang, F.F., et al., *Matrix Acidizing of Carbonate Reservoirs Using Organic Acids and Mixture of HCl and Organic Acids*, in *SPE Annual Technical Conference and Exhibition*2008, Society of Petroleum Engineers: Denver, Colorado.

136. Kalfayan, L.J., *Fracture Acidizing: History, Present State, and Future*, in *SPE Hydraulic Fracturing Technology Conference*2007, Society of Petroleum Engineers: College Station, Texas.

137. Singh, A.K. and M.A. Quraishi, *Inhibiting effects of 5-substituted isatin-based Mannich bases on the corrosion of mild steel in hydrochloric acid solution.* Journal of Applied Electrochemistry, 2010. **40**(7): p. 1293-1306.

138. Singh, A.K. and M.A. Quraishi, *Investigation of adsorption of isoniazid derivatives at mild steel/hydrochloric acid interface: Electrochemical and weight loss methods.* Materials Chemistry and Physics, 2010. **123**(2-3): p. 666-677.

139. Bartos, M. and N. Hackerman, *A Study of Inhibition Action of Propargyl Alcohol during Anodic Dissolution of Iron in Hydrochloric Acid.* Journal of The Electrochemical Society, 1992. **139**(12): p. 3428-3433.

140. King, G.E. *Acid Backflow.* 2009 23/06/14]; Available from: http://gekengineering.com/Downloads/Free_Downloads/Acid_Backflow.pdf.

141. Kalfayan, L., *Production Enhancement with Acid Stimulation (2nd Edition).* 2008, Tulsa, Oklahoma: PennWell.

142. Smith, C.F., C.W. Crowe, and T.J. Nolan, III, *Secondary Deposition of Iron Compounds Following Acidizing Treatments.* Journal of Petroleum Technology, 1969. **21**(9).

143. Taylor, K.C., H.A. Nasr-El-Din, and M.J. Al-Alawi, *Systematic Study of Iron Control Chemicals Used During Well Stimulation.* SPE Journal, 1999. **4**(1).

144. Crowe, C.W., *Prevention of Undesirable Precipitates from Acid Treating Fluids*, in *International Meeting on Petroleum Engineering*1986, Society of Petroleum Engineers: Beijing, China.

145. Dill, W. and P. Smolarchuk, *Iron Control In Fracturing And Acidizing Operations.* 1988. **27**(03).

146. Zhao, G.X., et al., *Formation Characteristic of CO2 Corrosion Product Layer of P110 Steel Investigated by SEM and Electrochemical Techniques.* Journal of Iron and Steel Research, International, 2009. **16**(4): p. 89-94.

147. ASTM, *Standard Practice for Laboratory Immersion Corrosion Testing of Metals*, in *ASTM G31-72*2004, ASTM International: West Conshohocken, Pennsylvania.

148. Pacheco, J.L., F.C. Ibrahim, and R.J. Franco, *Testing Requirements Of Corrosion Inhibitor Qualification For Pipeline Applications*, in *CORROSION*2010, NACE International: San Antonio, Texas.

149. Dugstad, A., Gulbrandsen, E. , Kvarekvål, J. , Nyborg, R. , Seiersten, M, *Corrosion testing in multiphase flow, challenges and limitations*, in *CORROSION*2006: San Diego, California.

150. Tenaris. *Material Specification HS-80.* 2014 [cited 2016 30.06.16]; Available from: http://www.tenaris.com/~/media/Files/ProductLiterature/OCTG/HS80_CoiledTubeDocs101909.ashx.

151. Barmatov, E., T. Hughes, and D. Eskin, *Effect of surface roughness on corrosion behaviour of low carbon steel in inhibited 4 M*

hydrochloric acid under laminar and turbulent flow conditions. Corrosion Science, 2015. **103**: p. 196-205.

152. Bhadeshia, H. and R. Honeycombe, *Steels - Microstructure and Properties*. 3 ed. 2006, Oxford, United Kingdom: Elsevier.

153. Scribner, L.L., *The measurement and correction of electrolyte resistance in electrochemical tests*. Vol. 1056. 1990: ASTM International.

154. Saliyan, V.R. and A.V. Adhikari, *Quinolin-5-ylmethylene-3-{[8-(trifluoromethyl)quinolin-4-yl]thio}propanohydrazide as an effective inhibitor of mild steel corrosion in HCl solution.* Corrosion Science, 2008. **50**(1): p. 55-61.

155. Sherif, E.-S.M., R.M. Erasmus, and J.D. Comins, *In situ Raman spectroscopy and electrochemical techniques for studying corrosion and corrosion inhibition of iron in sodium chloride solutions.* Electrochimica Acta, 2010. **55**(11): p. 3657-3663.

156. M.F, A. and R. R.G, *Corrosion of steel in ionic liquids.* Journal of Mining and Metallurgy. Section B: Metallurgy, 2003. **39**(1): p. 81-91.

157. Wabeke, R.L., *Air contaminants and industrial hygiene ventilation: A handbook of practical calculations, problems, and solutions*. 1998: CRC Press.

158. Nunez, M., *Prevention of metal corrosion: new research*. 2007, New York: Nova Publishers.

159. Hughes, T., *Conversation with Benjamin Pickles*, 11 September, 2015.

160. Engineers, T.A.S.o.M., *Surface Texture (Surface Roughness, Waviness, and Lay)*, in *ASME B46.1*2009, ASME: New York, NY.

161. Rae, P. and G.d. Lullo, *Matrix Acid Stimulation - A Review of the State-Of-The-Art*, in *SPE European Formation Damage Conference*2003, Society of Petroleum Engineers: The Hague, Netherlands.

162. Jiang, C., *Activity Coefficients of Hydrochloric Acid in Concentrated Electrolyte Solutions. 1. HCl + NaCl + H2O, HCl + LiCl + H2O, and HCl + BaCl2 + H2O at 298.15 K.* Journal of Chemical & Engineering Data, 1996. **41**(1): p. 113-116.

163. Mesmer, R.E. and H.F. Holmes, *pH, Definition and measurement at high temperatures.* Journal of Solution Chemistry, 1992. **21**(8): p. 725-744.

164. Walpole, R.E., et al., *Probability and statistics for engineers and scientists*. Vol. 5. 1993: Macmillan New York.

165. Miller Jr, R.G., *Beyond ANOVA: basics of applied statistics*. 1997: CRC press.

166. Girden, E.R., *ANOVA: Repeated measures*. 1992: Sage.

167. Cardinal, R.N. and M.R. Aitken, *ANOVA for the behavioral sciences researcher*. 2013: Psychology Press.

168. Statistics, P.D.o. *F critical values*. 2015 [cited 2018 15/03/18]; Available from: http://www.stat.purdue.edu/~jtroisi/STAT350Spring2015/tables/FTable.pdf.

169. Weathington, B.L., C.J. Cunningham, and D.J. Pittenger, *Understanding business research*. 2012: John Wiley & Sons.

170. Salkind, N.J., *Encyclopedia of measurement and statistics*. Vol. 1. 2007: Sage.

171. Osarolube, E., I. Owate, and N. Oforka, *Corrosion behaviour of mild and high carbon steels in various acidic media.* Scientific Research and Essay, 2008. **3**(6): p. 224-228.

172. Frenier, W.W., *Acidizing Fluids Used to Stimulate High Temperature Wells Can Be Inhibited Using Organic Chemicals*, in *SPE International Symposium on Oilfield Chemistry*1989, Society of Petroleum Engineers: Houston, Texas.

173. Taylor, D. and T.A. Nieman, *Effect of cell geometry on conductance measurements in flow cells.* Analytica Chimica Acta, 1984. **159**(0): p. 397-400.

174. Myland, J.C. and K.B. Oldham, *Uncompensated Resistance. 1. The Effect of Cell Geometry.* Analytical Chemistry, 2000. **72**(17): p. 3972-3980.

175. Pike, D., et al., *Flow Cell Design for Effective Biosensing.* Sensors, 2012. **13**(1): p. 58-70.

176. Nishikata, E., T. Ishii, and T. Ohta, *Viscosities of aqueous hydrochloric acid solutions, and densities and viscosities of aqueous hydroiodic acid solutions.* Journal of Chemical & Engineering Data, 1981. **26**(3): p. 254-256.

177. Nesic, S., et al., *Mechanistic Modeling for CO_2 Corrosion with Protective Iron Carbonate Films*, in *CORROSION*2001, NACE International: Houston, Texas.

178. Holland, F.A. and R. Bragg, *Fluid Flow for Chemical Engineers*, Elsevier, Editor. 1995, Elsevier.

179. ASTM, *Standard Test Method for Conducting Potentiodynamic Polarization Resistance Measurements*, in *ASTM G59-97*2014, ASTM International: West Conshohocken, Pennsylvania.

180. Cole, T.J. and D.G. Altman, *Statistics Notes: What is a percentage difference?* Bmj, 2017. **358**: p. j3663.

181. Heitz, E., R. Henkhaus, and A. Rahmel, *Corrosion Science: An Experimental Approach*. 1992, New York: Ellis Horwood.

182. Bockris, J.M. and B. Yang, *The mechanism of corrosion inhibition of iron in acid solution by acetylenic alcohols.* Journal of the Electrochemical Society, 1991. **138**(8): p. 2237-2252.

183. Aramaki, K. and E. Fujioka, *Surface-Enhanced Raman Scattering Spectroscopy Studies on the Inhibition Mechanism of Propargyl Alcohol for Iron Corrosion in Hydrochloric Acid.* CORROSION, 1996. **52**(2): p. 83-91.